PTEP

Prog. Theor. Exp. Phys. **2014**, 012D01 (149 pages)
DOI: 10.1093/ptep/ptt095

Vortices and other topological solitons in dense quark matter

Minoru Eto[1], Yuji Hirono[2,3,4], Muneto Nitta[5,*], and Shigehiro Yasui[6,†]

[1]*Department of Physics, Yamagata University, Kojirakawa 1-4-12, Yamagata, Yamagata 990-8560, Japan*
[2]*Department of Physics, University of Tokyo, Hongo 7-3-1, Bunkyo-ku, Tokyo 113-0033, Japan*
[3]*Theoretical Research Division, Nishina Center, RIKEN, Wako 351-0198, Japan*
[4]*Department of Physics, Sophia University, Tokyo 102-8554, Japan*
[5]*Department of Physics, and Research and Education Center for Natural Sciences, Keio University, Hiyoshi 4-1-1, Yokohama, Kanagawa 223-8521, Japan*
[6]*KEK Theory Center, Institute of Particle and Nuclear Studies, High Energy Accelerator Research Organization (KEK), 1-1 Oho, Tsukuba, Ibaraki 305-0801, Japan*
*E-mail: nitta@phys-h.keio.ac.jp

Received August 29, 2013; Accepted September 27, 2013; Published January 10, 2014

Dense quantum chromodynamic matter accommodates various kind of topological solitons such as vortices, domain walls, monopoles, kinks, boojums, and so on. In this review, we discuss various properties of topological solitons in dense quantum chromodynamics (QCD) and their phenomenological implications. Particular emphasis is placed on the topological solitons in the color–flavor-locked (CFL) phase, which exhibits both superfluidity and superconductivity. The properties of topological solitons are discussed in terms of effective field theories such as the Ginzburg–Landau theory, the chiral Lagrangian, or the Bogoliubov–de Gennes equation. The most fundamental string-like topological excitations in the CFL phase are non-Abelian vortices, which are 1/3 quantized superfluid vortices and color magnetic flux tubes. These vortices are created at a phase transition by the Kibble–Zurek mechanism or when the CFL phase is realized in compact stars, which rotate rapidly. The interaction between vortices is found to be repulsive and consequently a vortex lattice is formed in rotating CFL matter. Bosonic and fermionic zero-energy modes are trapped in the core of a non-Abelian vortex and propagate along it as gapless excitations. The former consists of translational zero modes (a Kelvin mode) with a quadratic dispersion and $\mathbb{C}P^2$ Nambu–Goldstone gapless modes with a linear dispersion, associated with the CFL symmetry spontaneously broken in the core of a vortex, while the latter is Majorana fermion zero modes belonging to the triplet of the symmetry remaining in the core of a vortex. The low-energy effective theory of the bosonic zero modes is constructed as a non-relativistic free complex scalar field and a relativistic $\mathbb{C}P^2$ model in 1+1 dimensions. The effects of strange quark mass, electromagnetic interactions, and non-perturbative quantum corrections are taken into account in the $\mathbb{C}P^2$ effective theory. Various topological objects associated with non-Abelian vortices are studied; colorful boojums at the CFL interface, the quantum color magnetic monopole confined by vortices, which supports the notion of quark–hadron duality, and Yang–Mills instantons inside a non-Abelian vortex as lumps are discussed. The interactions between a non-Abelian vortex and quasiparticles such as phonons, gluons, mesons, and photons are studied. As a consequence of the interaction with photons, a vortex lattice behaves as a cosmic polarizer. As a remarkable consequence of Majorana fermion zero modes, non-Abelian vortices are shown to behave as a novel kind of non-Abelian anyon. In the order parameters of

†These authors contributed equally to this work.

Funded by SCOAP[3]

chiral symmetry breaking, we discuss fractional and integer axial domain walls, Abelian and non-Abelian axial vortices, axial wall–vortex composites, and Skyrmions.

Subject Index B35, D30, D41, E32, I62

Contents

1. Introduction

Topological solitons are a subject of considerable interest in condensed matter physics [240]. Their properties have been studied extensively and it has been found that they play quite important roles phenomenologically. One such example is in superfluidity. Superfluidity emerges in a wide variety of physical systems such as helium superfluids [361] or ultracold atomic gases [273,274,354]. Superfluids are known to accommodate *quantized vortices* as topological solitons, which are important degrees of freedom to investigate the dynamics of superfluids [90,352,353,361]. The observation of quantized vortices has worked as the evidence of superfluidity for ultracold atomic gases such as Bose–Einstein condensates (BECs) [1] and Fermi gases in the BEC/Bardeen–Cooper–Schrieffer (BCS) crossover regime [390]. A rotating superfluid is threaded with numerous vortices and they form a vortex lattice. Vortices are also created at phase transitions by the Kibble–Zurek mechanism [169,203,388,389]. Superfluid vortices also play pivotal roles in quantum turbulence in superfluid helium and atomic BECs [267,351,353,357]. In lower dimensions, vortices are essential in Berezinskii–Kosterlitz–Thouless (BKT) transitions [49,50,212].

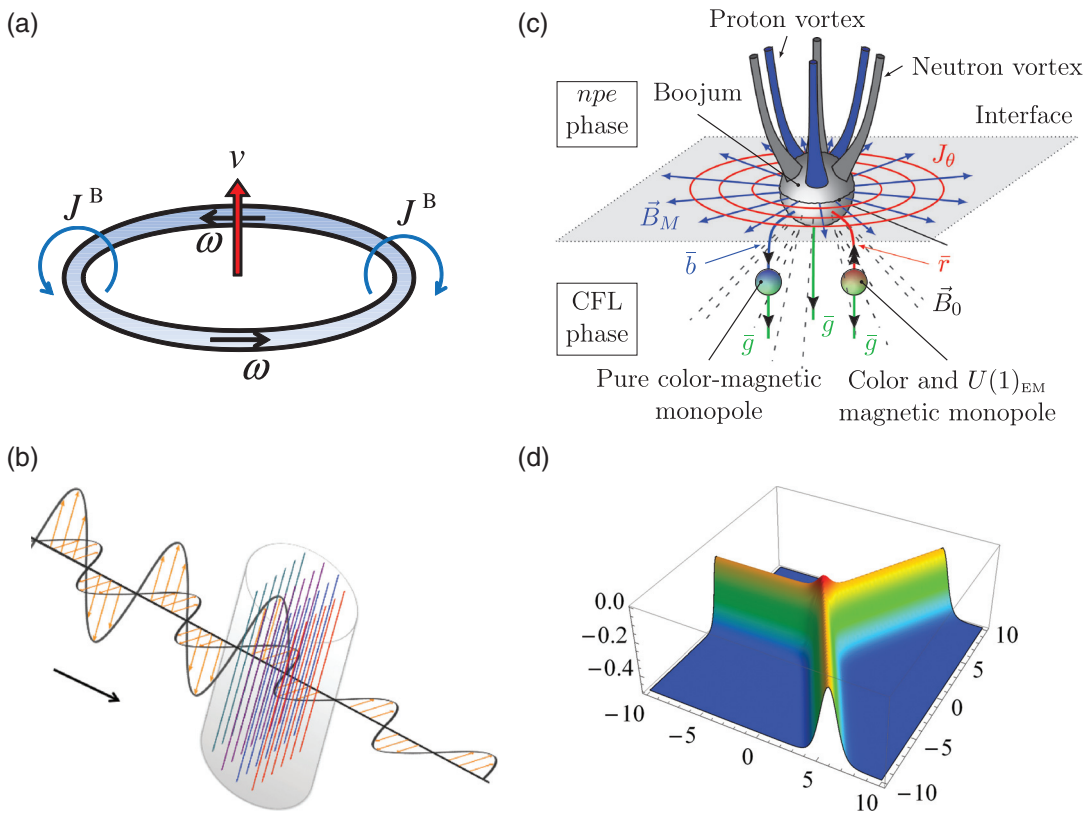

Fig. 1. Examples of topological solitons in dense QCD. For details, see the relevant sections. (a) Vortex ring (Sect. 4.2) (b) Vortex lattice and photons (Sect. 6.3) (c) Colorful boojum (Sect. 7) (d) Axial domain wall junction (Sect. 10.4)

Topological solitons also manifest themselves in the condensed matter physics of quantum chromodynamics (QCD), which is the theory of the strong interaction. The stability of topological solitons is closely related to the structure of the vacuum. QCD matter exhibits a rich variety of phases at finite temperatures and/or baryon densities [138]. Depending on the symmetry breaking patterns, QCD matter accommodates various kind of topological solitons (see Fig. 1 for some examples), some of which are listed in Table 1. Since topological solitons affect the bulk properties of the matter, it is important to investigate their basic properties and phenomenological implications. They could affect the properties of the matter created in heavy-ion collisions or the matter realized inside compact stars. Theoretical studies suggest that quark matter is expected to exhibit color superconductivity, triggered by quark–quark pairings, at high baryon densities and low temperatures [11,32,38,187,280]. It has been predicted in Refs. [11,12] that the ground state is the color–flavor-locked (CFL) phase at asymptotically high densities, in which the three light flavors (up, down, and strange) of quarks contribute symmetrically to the pairing. There are also various other phases, such as the two-flavor superconducting (2SC) phase [32], the kaon condensation (CFL+K) phase [47], the crystalline superconducting phase [22,72], and the magnetic CFL (MCFL) phase [117,121,122]. For reviews of the phase structure of QCD matter, see Refs. [6,13,138,279,283].

Among the various ground states of QCD matter, the CFL phase is an important phase, which is realized at asymptotically high densities where weak coupling theory is applicable and theoretically controlled calculations are possible. The CFL phase has an interesting property that it exhibits both superfluidity and superconductivity, because of the spontaneous breaking of the global $U(1)_{\rm B}$ baryon number symmetry and the local $SU(3)_{\rm C}$ color symmetry, respectively. As in superfluid helium, we

Table 1. Topological solitons in dense QCD. For each topological soliton, we have summarized the phase in which it appears, the relevant order parameter space, and relevant homotopy group. The types of topological solitons are classified into "defects" or "textures", denoted by D and T, respectively. The former are characterized by a map from the boundary $\partial\mathbf{R}^n \simeq S^{n-1}$ of space $\mathbf{R}^n$ to the order parameter space (OPS) and consequently by the homotopy group $\pi_{n-1}(\mathcal{M})$, while the latter are characterized by a map from the whole space $\mathbf{R}^n$ to the OPS and consequently by the homotopy group $\pi_n(\mathcal{M})$, where n counts the codimensions of the solitons. Confined monopole and trapped instanton imply a monopole and instanton inside a non-Abelian vortex, where the order parameter space is $\mathbb{C}P^2$. For vortons in the CFL+K phase, $U(1)_{\rm EM}$ symmetry is broken only inside a $U(1)_{\rm Y}$ vortex. The section in which each topological soliton is explained in this review is also indicated. Note that this table is not a complete list of topological solitons in dense QCD. "NA" is the abbreviation for "non-Abelian" and "YM" is that for "Yang–Mills". "relative" denotes a relative homotopy group [361].

Topological solitons	Phase	OPS $\mathcal{M}$	Type	Homotopy $\pi_n(\mathcal{M})$	Sect.
$U(1)_{\rm B}$ superfluid vortex	CFL	$U(1)_{\rm B}$	D	$\pi_1(\mathcal{M}) \simeq \mathbb{Z}$	3.1.1
NA semi-superfluid vortex	CFL	$U(3)_{\rm C-F+B}$	D	$\pi_1(\mathcal{M}) \simeq \mathbb{Z}$	3.3
confined monopole	CFL	$\mathbb{Z}_3$ (in $\mathbb{C}P^2$)	D	$\pi_0(\mathcal{M}) \simeq \mathbb{Z}_3$	5.4
trapped YM instanton	CFL	$\mathbb{C}P^2$	T	$\pi_2(\mathcal{M}) \simeq \mathbb{Z}$	5.5
$U(1)_{\rm A}$ axial vortex	CFL	$U(1)_{\rm A}$	D	$\pi_1(\mathcal{M}) \simeq \mathbb{Z}$	3.1.2
NA axial vortex	CFL	$U(3)_{\rm L-R+A}$	D	$\pi_1(\mathcal{M}) \simeq \mathbb{Z}$	10.3.2
$U(1)_{\rm A}$ integer axial wall	CFL	$U(1)_{\rm A}$	T	$\pi_1(\mathcal{M}) \simeq \mathbb{Z}$	10.1.2
$U(1)_{\rm A}$ fractional axial wall	CFL	$\mathbb{Z}_3$ in $U(1)_{\rm A}$	D	$\pi_0(\mathcal{M}) \simeq \mathbb{Z}_3$	10.1.1
Skyrmion (qualiton)	CFL	$U(3)_{\rm L-R+A}$	T	$\pi_3(\mathcal{M}) \simeq \mathbb{Z}$	10.7
boojum	CFL edge	$U(3)_{\rm C-F+B}$	D	relative	7
2SC domain wall	2SC	$U(1)_{\rm A}$	T	$\pi_1(\mathcal{M}) \simeq \mathbb{Z}$	11.1
$U(1)_{\rm Y}$ supercond. vortex	CFL+K	$U(1)_{\rm Y}$	D	$\pi_1(\mathcal{M}) \simeq \mathbb{Z}$	11.2
(drum) vorton	CFL+K	$U(1)_{\rm Y}$, $U(1)_{\rm EM}$	D	–	11.2
kaon domain wall	CFL+K	$U(1)_{\rm Y}$	T	$\pi_1(\mathcal{M}) \simeq \mathbb{Z}$	11.2

can expect the existence of topological vortices from consideration of the ground-state symmetry [128,183]. Vortices in the CFL phase will be created if the matter is rotated, as is observed in rotating superfluids in condensed matter systems. Thus, if the CFL phase is realized in the cores of dense stars, vortices are inevitably created since the stars rotate rapidly. The superfluid vortices discussed in Refs. [128,183] have integer winding numbers with respect to $U(1)_{\rm B}$ symmetry, and they are dynamically unstable, since they can decay into a set of vortices with lower energies. It was first pointed out by Balachandran, Digal, and Matsuura [35] that the stable vortices are so-called non-Abelian vortices, which are superfluid vortices as well as color magnetic flux tubes. Since they carry 1/3 quantized $U(1)_{\rm B}$ circulations, an integer $U(1)_{\rm B}$ vortex decays into three non-Abelian vortices with different color fluxes canceled in total [242]. The color magnetic flux tubes studied before [183] are non-topological and unstable, and have a color flux triple of a non-Abelian vortex. The properties of non-Abelian vortices have been studied using the Ginzburg–Landau (GL) theory [110,112,115,170,242,309,315] or in the Bogoliubov–de Gennes (BdG) equation [134,378]. A remarkable property of non-Abelian vortices is that both bosonic and fermionic zero energy modes are localized in the core of a non-Abelian vortex and propagate along it as gapless excitations. Bosonic zero modes are found in the GL theory; one is the Kelvin mode, which also appears in vortices in superfluids, and the other is the orientational zero modes, characterizing an orientation of a vortex in the internal space [110,242]. Both of them are Nambu–Goldstone modes; the Kelvin mode is associated with two translational symmetries transverse to the vortex, and the orientational modes are associated with the spontaneous symmetry breaking of the CFL symmetry $SU(3)_{\rm C+F}$ into its subgroup $[SU(2) \times U(1)]_{\rm C+F}$ inside the vortex core. There is only one Kelvin mode for each vortex

although two translational symmetries are spontaneously broken, because it has a quadratic dispersion and is a so-called type-II Nambu–Goldstone mode. The orientational zero modes have a linear dispersion and are so-called type-I Nambu–Goldstone modes. The low-energy effective field theory of Kelvin modes is a non-relativistic free complex field with the first order time derivative in the $1+1$ dimensional vortex world-sheet [207]. The low-energy effective field theory of the orientational zero modes is written as the relativistic $\mathbb{C}P^2$ model inside the $1+1$ dimensional vortex world-sheet, where $\mathbb{C}P^2 \simeq SU(3)/[SU(2) \times U(1)]$ is the target space spanned by the Nambu–Goldstone modes [110]. On the other hand, Majorana fermion zero modes belonging to a triplet of the core symmetry $SU(2)_{\rm C+F}$ have been found in the BdG equation and the low-energy effective theory in the $1+1$ dimensional vortex world-sheet has been derived [378]. The existence of these fermion zero modes is ensured by topology, which can be seen as the index theorem [134]. One remarkable consequence of the Majorana fermion zero modes is that non-Abelian vortices obey a novel kind of non-Abelian statistics [172,379] if they are parallel or are restricted to $2+1$ dimensions.

While $\mathbb{C}P^2$ zero modes appear as Nambu–Goldstone gapless (zero) modes in the $1+1$ dimensional vortex world-sheet, exactly speaking they have to be gapped (massive) because of the Coleman–Mermin–Wagner theorem [78,239], which prohibits Nambu–Goldstone modes in $1+1$ dimensions. This problem is solved once non-perturbative effects are taken into account in the $\mathbb{C}P^2$ vortex world-sheet theory. There appears a quantum mechanically induced potential in the $1+1$ dimensional $\mathbb{C}P^2$ model. As a consequence, there appear quantum magnetic monopoles confined by non-Abelian vortices [116,150]. They provide a partial proof of the quark–hadron duality. In the confining phase, quarks are confined and monopoles are conjectured to be condensed. As a dual of this, in the CFL phase, monopoles are confined and quarks are condensed. As another example of topological solitons inside a non-Abelian vortex world-sheet, we introduce Yang–Mills instantons, which stably exist inside a non-Abelian vortex as lumps or sigma model instantons in the $d = 1+1$ dimensional $\mathbb{C}P^2$ model in the vortex world-sheet.

The interactions between a vortex and quasiparticles can be treated as couplings between the $1+1$ dimensional vortex effective theory and fields propagating in the bulk. The $U(1)_{\rm B}$ phonon field can be mapped to a two-form field by a duality or the Hubbard–Stratonovich transformation. The interaction between a vortex and the $U(1)_{\rm B}$ phonons can be described as point particle interaction between a vortex and the two-form field [170], as is usually done for superfluid vortices or global cosmic strings. On the other hand, gluons can be dualized to non-Abelian two-form fields [314]. The interaction between a vortex and gluons can be described by the interaction between the orientational zero modes and the non-Abelian two-form fields. Since the $U(1)_{\rm EM}$ electromagnetic symmetry is embedded in the flavor $SU(3)_{\rm F}$ symmetry that acts on the $\mathbb{C}P^2$ model as an isometry, the interaction with the electromagnetic fields (photons) can be incorporated by the $U(1)_{\rm EM}$ gauged $\mathbb{C}P^2$ model, where the $U(1)_{\rm EM}$ field propagates in the bulk. This model is similar to Witten's superconducting strings [371], in which the $U(1)_{\rm EM}$ bulk gauge field couples to a $U(1)$ zero mode on a string and consequently a persistent superconducting current flows along the string. In our case, non-Abelian vortices are not superconducting because of the difference between the zero modes. Instead, an interesting property is found. When an electromagnetic wave enters a vortex lattice, the magnitude of the electric field parallel to the lattice is reduced; consequently, the vortex lattice acts as a polarizer [171]. This may give an observational signal if a rotating CFL matter exists.

Apart from the CFL phase or other color superconductors, it is likely that the *npe* phase is present in the interiors of neutron stars. The *npe* phase is composed of a neutron superfluid and a proton superconductor [42], where the neutron pairing is likely a spin triplet at high density. There, superfluid

neutron vortices and superconducting proton vortices should exist under a rapid rotation and a strong magnetic field of a neutron star, respectively. Such vortices are expected to explain the pulsar glitch phenomenon [19]. If the CFL phase is realized in a neutron star core, it may be surrounded by the *npe* phase. Then, one can ask how these vortices in the *npe* phase are connected to the CFL phase. The endpoints of vortices at the interfaces of various superfluids are known as boojums. There appear colorful boojums at the interface between the CFL phase and the *npe* phase, between which there may be other phases such as the CFL+K, 2SC phases and so on. Three neutron vortices and three proton vortices meet at the colorful boojum at which three non-Abelian vortices in the CFL phase join with the total color magnetic flux canceled out. This boojum is accompanied by colored monopoles appearing on non-Abelian vortices due to the presence of strange quark mass, a Dirac monopole of the massless gauge field, and the surface current of the massive gauge field.

This paper is intended to be a catalog of topological solitons in dense QCD. We discuss various properties of topological solitons and their phenomenological implications. Particular emphasis is placed on the CFL phase, which accommodates a wide variety of topological solitons like vortices, domain walls, kinks, monopoles and so on. The paper is organized as follows.

In Sect. 2, we review the effective theories for high density QCD, in terms of the Ginzburg–Landau theory (for around the critical temperature) and the chiral Lagrangian (for zero temperature). In Sect. 2.1, the CFL ground state, the pattern of symmetry breaking, the order parameter manifold of the CFL phase, and the mass spectrum are discussed. The effect of finite strange quark mass, the electromagnetic interaction, and the mixing of gluons and photons in the CFL ground state are also discussed in the GL theory. We then give the time-dependent Ginzburg–Landau (TDGL) Lagrangian. In Sect. 2.2, chiral symmetry breaking, $U(1)_{\rm B}$ phonons, and CFL mesons are studied in the framework of the chiral Lagrangian valid at zero temperature.

In Sect. 3, we turn to vortices in the CFL phase. In Sect. 3.1, we first study Abelian vortices, i.e., $U(1)_{\rm B}$ superfluid vortices and $U(1)_{\rm A}$ axial vortices. In Sect. 3.2, we introduce non-topological color magnetic flux tubes. In Sect. 3.3, we describe non-Abelian vortices. The numerical solutions, asymptotic behaviors of the profile functions at large distances, and the tension of the minimal stable non-Abelian vortices are obtained [112]. We also discuss non-minimal (unstable) non-Abelian vortices. In Sect. 3.3.3, we discuss orientational zero modes (collective coordinates) of a non-Abelian vortex. These modes are gapless modes propagating along the non-Abelian vortex and play important roles in the dynamics of non-Abelian vortices.

In Sect. 4, we study the dynamics of non-Abelian vortices. In Sect. 4.1, we construct the effective field theory of translational zero modes, known as Kelvin modes, and study the dynamics of a single vortex string in terms of the low-energy effective theory [207]. We also discuss Magnus and inertial forces exerted on vortices. In Sect. 4.2, the interaction between two non-Abelian vortices at large distances is shown to be repulsive, independent of orientational modes, and 1/3 of that between two Abelian superfluid vortices [242,243]. We also review the dynamics of two vortices and a vortex ring. In Sect. 4.3, we discuss decays of a $U(1)_{\rm B}$ vortex and an M_2 vortex into three and two non-Abelian vortices, respectively. In Sect. 4.4, colorful vortex lattices under rotation are discussed. In Sect. 4.5, we discuss a relation between relativistic strings in relativistic scalar theories and superfluid vortices by following Refs. [85,128,223], in which the dynamics of superfluid vortices is reproduced in relativistic theory with a constant three-form field.

In Sect. 5, we discuss the dynamics of the orientational zero modes of non-Abelian vortices, which is one of the main parts of this review paper. In Sect. 5.1, we first construct the low-energy effective theory of the orientational zero modes of a non-Abelian vortex in the limit of zero quark masses

and neglecting electromagnetic interactions, which is the $\mathbb{C}P^2$ model [110]. This model describes gapless propagations of the $\mathbb{C}P^2$ orientational zero modes along the vortex string. In Sect. 5.2, we take into account the strange quark mass, which induces an effective potential in the $\mathbb{C}P^2$ vortex effective theory [115]. It turns out that all vortices decay into one kind immediately by this potential term. In Sect. 5.3, we take into account the electromagnetic interactions [356]. First, the tension of the non-Abelian vortex has a finite correction, which appears as the effective potential in the $\mathbb{C}P^2$ vortex effective theory. Second, the low-energy effective vortex theory becomes a $U(1)$ gauged $\mathbb{C}P^2$ model. As stationary solutions of the effective potential, there exist the Balachandran–Digal–Matsuura (BDM) vortex, which is the ground state in the absence of quark masses, metastable $\mathbb{C}P^1$ vortices, and the unstable pure color vortex. We present the decay probability of metastable $\mathbb{C}P^1$ vortices into the BDM vortex through quantum tunneling. In Sect. 5.4, we take into account the quantum corrections in the low-energy effective theory in the vortex world-sheet in the high density limit, in which strange quark mass can be neglected. There appears a quantum mechanically induced potential in the low-energy $\mathbb{C}P^2$ vortex effective theory through non-perturbative effects, which is consistent with the Coleman–Mermin–Wagner theorem [78,239]. One of the important consequences is the appearance of quantum monopoles that are confined by non-Abelian vortices [116,150]. They provide proof of some aspects of the quark–hadron duality [116], i.e., in the confining phase, quarks are confined and monopoles are condensed while in the CFL phase, monopoles are confined and quarks are condensed. In Sect. 5.5, Yang–Mills instantons trapped inside a non-Abelian vortex are discussed. They become lumps or sigma model instantons in the $d = 1 + 1$ dimensional $\mathbb{C}P^2$ model in the vortex world-sheet.

In Sect. 6, we study interactions of non-Abelian vortices with quasiparticles. In Sect. 6.1, the interactions between a non-Abelian vortex and phonons and gluons are discussed. The interaction with phonons is obtained by a dual transformation in which the phonon field is dualized to a Abelian two-form field, while the interaction with gluons is achieved [170] by non-Abelian dual transformation in which the gluon field is dualized to a non-Abelian massive two-form field [314]. The latter provides interaction between two non-Abelian vortices at short distances intermediated by gluons. We also give the orientation moduli dependence of the intervortex force mediated by exchange of massive gluons, which is a new result in this paper. In Sect. 6.2, we also provide the chiral Lagrangian of the mesons in the presence of a non-Abelian vortex, which is also a new result in this paper. In Sect. 6.3, we study the interaction between a non-Abelian vortex and photons, which is described by a $U(1)$ gauged $\mathbb{C}P^2$ model. As an interesting consequence, we show that a lattice of non-Abelian vortices behaves as a polarizer [171].

In Sect. 7, we study the interface of the CFL phase and the confining phase and find colorful boojums [76]. Boojums appear at the interface of various superfluids as the endpoints of vortices. In the interface between the CFL phase and the confining phase, there appears a colorful boojum, at which three non-Abelian vortices join with canceling the total magnetic flux in the CFL phase; three neutron vortices and three proton vortices join in the *npe* phase. In the CFL phase side, non-Abelian vortices decay into one kind by the strange quark mass producing color magnetic monopoles, and $U(1)_{\rm EM}$ magnetic fluxes of proton vortices are decomposed into massless and massive fluxes. The former forms a Dirac monopole and the latter forms the surface current. The shape of a colorful boojum is calculated in a simplified model.

In Sect. 8, we study microscopic theory, i.e., the Bogoliubov–de Gennes (BdG) theory, which is valid at any temperature, while the GL theory is valid only just below the critical temperature and at the large distance scale. In Sect. 8.1, the BdG equations are discussed in the background of a

non-Abelian vortex, in order to study structures of vortices far from the critical temperature and/or core structures of the vortices. Fermions trapped inside the core of the vortex are found. Inside the vortex core, the $SU(2)_{\rm C+F}$ symmetry remains, so that localized fermions are classified by the representations of $SU(2)_{\rm C+F}$. Triplet Majorana fermion zero modes, which are localized and normalizable, and a singlet Majorana fermion zero mode, which is localized but non-normalizable, are found [378]. In Sect. 8.3, we construct the low-energy effective theory of the localized gapless fermions propagating along the vortex string [378]. The chemical potential dependence of the velocity of gapless modes is obtained. In Sect. 8.4, we show the absence of supercurrent by Majorana fermion zero modes as a new result of this paper, unlike the case of Witten's superconducting fermionic strings. In Sect. 8.5, we study the index theorem for the fermion zero modes in the background of a non-Abelian vortex [134]. We calculate the topological and analytical indices and find the agreement between them. In Sect. 8.6, the characterization of color superconductors as a topological superconductor is discussed [253]. Topological superconductors are a the topics of considerable interest in condensed matter physics these days.

In Sect. 9, as a novel application of Majorana fermion zero modes of a non-Abelian vortex, we study the exchange statistics of non-Abelian vortices in $d = 2 + 1$ dimensions. Zero-mode Majorana fermions inside vortices lead to a new kind of non-Abelian anyons [172,379].

In Sect. 10, topological objects associated with chiral symmetry breaking, axial domain walls, non-Abelian and Abelian axial vortices (strings) and Skyrmions, are discussed. In Sect. 10.1, axial domain walls are discussed. In the chiral limit with massless quarks, the instanton-induced potential term allows a fractional axial domain wall with 1/3 $U(1)_{\rm A}$ winding. In the presence of quark masses, this domain wall cannot exist alone, and only an integer axial domain wall, made of a set of three axial domain walls with the unit $U(1)_{\rm A}$ winding, is allowed as a composite wall. In Sect. 10.3, Abelian and non-Abelian axial vortices are discussed in the absence of quark masses and instanton effects [33,34,111,244,261]. These vortices are also accompanied by $\mathbb{C}P^2$ orientational zero modes, but these modes are non-normalizable, unlike those of non-Abelian semi-superfluid vortices. In the presence of the instanton-induced potential in the chiral limit, each non-Abelian axial vortex is attached by one axial domain wall, while each Abelian axial vortex is attached by three axial domain walls [33] and decays into three non-Abelian axial vortices each of which is attached by an axial domain wall. In the presence of quark masses, an Abelian axial vortex is attached by a composite domain wall consisting of three axial domain walls. In Sect. 10.5, we discuss decays of axial domain walls through quantum tunneling. In Sect. 10.6, we discuss the effects of axial anomaly on axial vortices and axial domain walls. The axial current flows along $U(1)_{\rm B}$ vortices, and the electric magnetic current flows along axial vortices, producing large magnetic fields perpendicular to axial domain walls in the presence of the external magnetic field. In Sect. 10.7, Skyrmions as qualitons are discussed [175].

In Sect. 11, we review the topological solitons in phases other than the CFL phase. The CFL phase is the ground state at high densities where all three flavors can be treated as massless. If one lowers the density gradually, the strange quark mass should be taken into account. Then it is expected that kaons form a condensation in addition to the CFL condensates. This is called the CFL+K phase [47]. If the density is further decreased, only the light flavors (u and d) contribute to the condensate, which is called the 2SC phase [32]. In Sect. 11.1, we discuss the domain walls and color magnetic fluxes in the 2SC phase. In Sect. 11.2, we review the superconducting strings, vortons, domain walls, and drum vortons in the CFL+K phase.

Section 12 is devoted to a summary and discussions. A lot of future problems including possible applications to neutron star physics are addressed.

In Appendix A, we summarize the properties of non-Abelian vortices in supersymmetric QCD as a comparison. In Appendix B, we give a brief review of the toric diagram, which is useful to understand the $\mathbb{C}P^2$ zero modes of non-Abelian vortices. In Appendix C, we give a detailed derivation of the low-energy effective action of the $\mathbb{C}P^2$ zero modes, which was not explained in detail in the original papers. In Appendix D, we give the derivation of the dual Lagrangian for phonons and gluons, which describes the interaction of vortices with those particles. In Appendix E, we give a detailed derivation of the fermion zero modes, which were not explained in the original paper.

This review paper is based on our papers on non-Abelian semi-superfluid vortices [76,110,112,115, 116,134,170–172,242,243,356,377–379], non-Abelian axial vortices and axial domain walls [102, 111,244,261], superfluid vortices [207], and other developments, but this paper also contains several new results in Sects. 4.3, 4.4, 6.1.2, 6.2, 8.4, 10.1.2 and detailed calculations, which were not given in the original papers, in Appendices C and E.

2. Low-energy effective theories for high density QCD

In this section, we give a brief review of effective descriptions of the color–flavor-locking (CFL) phase in high density QCD, i.e., the Ginzburg–Landau (GL) theory, which is valid around the critical temperature $T \sim T_c$, and the effective theories of massless Nambu–Goldstone bosons, which are valid at zero temperature $T = 0$. In Sect. 2.1, we first explain the Ginzburg–Landau (GL) theory, and take into account the finite strange quark mass and the electromagnetic interaction. We then extend the GL theory to incorporate the time dependence of the fields. In Sect. 2.2, we first briefly review the effective field theories for $U(1)_B$ phonons at zero temperature, and we introduce the effective theory for chiral symmetry breaking, i.e., the chiral Lagrangian describing the (pseudo) Nambu–Goldstone bosons, the CFL pions, and the η' meson.

2.1. *Ginzburg–Landau theories*

2.1.1. The CFL phase. Let us start with giving a brief review of the GL free energy [143,181,182], which is a low-energy effective theory for the CFL phase in the color superconductivity of massless three-flavor QCD at sufficiently high baryonic densities. We first ignore the masses of the quarks, which are taken into account in the subsequent sections.

The order parameters are the diquark condensates $\Phi_{L,R}$ defined by

$$(\Phi_L)^A_a \sim \epsilon_{abc}\epsilon_{ABC}\langle (q_L)^B_b C (q_L)^C_c \rangle, \tag{2.1}$$

$$(\Phi_R)^i_a \sim \epsilon_{abc}\epsilon_{ABC}\langle (q_R)^B_b C (q_R)^C_c \rangle, \tag{2.2}$$

where $q_{L,R}$ stand for the left- (right)-handed quarks with the indices $a, b, c = 1, 2, 3 = r, g, b$ being those of colors while $A, B, C = 1, 2, 3 = u, d, s$ are those of flavors, and C is the charge conjugation operator. The diquark Cooper pairs are induced by an attractive interaction via one-gluon exchange in the s-wave color antisymmetric channel. The flavor indices must also be antisymmetric because of Pauli's principle. The most generic form of the GL free energy for uniform matter is

$$\begin{aligned}\Omega_0 = {} & a_{0L}\mathrm{Tr}[\Phi_L^\dagger \Phi_L] + a_{0R}\mathrm{Tr}[\Phi_R^\dagger \Phi_R] \\ & + b_{1L}\left(\mathrm{Tr}[\Phi_L^\dagger \Phi_L]\right)^2 + b_{1R}\left(\mathrm{Tr}[\Phi_R^\dagger \Phi_R]\right)^2 + b_{2L}\mathrm{Tr}[(\Phi_L^\dagger \Phi_L)^2] \\ & + b_{2R}\mathrm{Tr}[(\Phi_R^\dagger \Phi_R)^2] + b_3\mathrm{Tr}[\Phi_L^\dagger \Phi_L \Phi_R^\dagger \Phi_R] + b_4\mathrm{Tr}[\Phi_L^\dagger \Phi_L]\mathrm{Tr}[\Phi_R^\dagger \Phi_R].\end{aligned} \tag{2.3}$$

The color symmetry $SU(3)_{\rm C}$, the flavor symmetry $SU(3)_{\rm L} \times SU(3)_{\rm R}$, the $U(1)_{\rm B}$ symmetry, and the $U(1)_{\rm A}$ symmetry act on $\Phi_{\rm L}$ and $\Phi_{\rm R}$ as

$$\begin{aligned} \Phi_{\rm L} &\to e^{i\theta_{\rm B}+i\theta_{\rm A}} U_{\rm C} \Phi_{\rm L} U_{\rm L}, \\ \Phi_{\rm R} &\to e^{i\theta_{\rm B}-i\theta_{\rm A}} U_{\rm C} \Phi_{\rm R} U_{\rm R}, \end{aligned} \tag{2.4}$$

with $e^{i\theta_{\rm B}} \in U(1)_{\rm B}$, $e^{i\theta_{\rm A}} \in U(1)_{\rm A}$, $U_{\rm C} \in SU(3)_{\rm C}$, and $U_{\rm L,R} \in SU(3)_{\rm L,R}$. Hereafter, we omit the last two terms since they can be neglected in the high baryon density region[1]. Although the interactions induced by the perturbative gluon exchanges do not distinguish the positive diquark condensates from the negative one, the non-perturbative instanton effects do. It was found that the state with positive parity is favored compared to the one with negative parity as a ground state [12,280]. We then choose the positive-parity state in what follows,

$$\Phi_{\rm L} = -\Phi_{\rm R} \equiv \Phi. \tag{2.5}$$

For later convenience, let us explicitly show the structure of indices of the 3×3 matrix field $(\Phi)_a{}^A$

$$\Phi = \begin{pmatrix} \Phi_{gb}{}^{ds} & \Phi_{gb}{}^{su} & \Phi_{gb}{}^{ud} \\ \Phi_{br}{}^{ds} & \Phi_{br}{}^{su} & \Phi_{br}{}^{ud} \\ \Phi_{rg}{}^{ds} & \Phi_{rg}{}^{su} & \Phi_{rg}{}^{ud} \end{pmatrix}, \tag{2.6}$$

with the color indices $a, b, c = 1, 2, 3 = gb, br, rg$ and the flavor indices $A, B, C = ds, su, ud$. Let us next give a GL free energy for the inhomogeneous condensate Φ, which includes gradient energies and gluon fields to Ω_0 given in Eq. (2.3),

$$\begin{aligned} \Omega &= {\rm Tr}\left[\frac{1}{4\lambda_3} F_{ij}^2 + \frac{\varepsilon_3}{2} F_{0i}^2 + K_3 \mathcal{D}_i \Phi^\dagger \mathcal{D}_i \Phi\right] + V, \\ V &= \alpha {\rm Tr}\left(\Phi^\dagger \Phi\right) + \beta_1 \left[{\rm Tr}(\Phi^\dagger \Phi)\right]^2 + \beta_2 {\rm Tr}\left[(\Phi^\dagger \Phi)^2\right] + \frac{3\alpha^2}{4(\beta_1 + 3\beta_2)}, \end{aligned} \tag{2.7}$$

where λ_3 is a magnetic permeability, and ε_3 is a dielectric constant for gluons, $i, j = 1, 2, 3$ are indices for space coordinates, and the covariant derivative and the field strength of gluons are defined by

$$\mathcal{D}_\mu \Phi = \partial_\mu \Phi - i g_{\rm s} A_\mu^a T^a \Phi, \tag{2.8}$$

$$F_{\mu\nu} = \partial_\mu A_\nu - \partial_\nu A_\mu - i g_{\rm s} [A_\mu, A_\nu]. \tag{2.9}$$

Here, μ, ν are indices for spacetime coordinates and $g_{\rm s}$ stands for the $SU(3)_{\rm C}$ coupling constant. The coupling constants α, $\beta_{1,2}$, $K_{0,3}$ are obtained from the weak-coupling calculations, which are valid at a sufficiently high density as [143,181]

$$\alpha = 4N(\mu) \log \frac{T}{T_{\rm c}}, \tag{2.10}$$

$$\beta_1 = \beta_2 = \frac{7\zeta(3)}{8(\pi T_{\rm c})^2} N(\mu) \equiv \beta, \tag{2.11}$$

$$K_3 = \frac{7\zeta(3)}{12(\pi T_{\rm c})^2} N(\mu), \tag{2.12}$$

$$\lambda_0 = \epsilon_0 = 1, \quad \lambda_3 = \epsilon_3 = 1, \tag{2.13}$$

[1] The coefficients b_3 and b_4 in (2.3) come from two loop diagrams in which bubble graphs are connected by the gluon propagator; see Ref. [236] for details.

where μ stands for the quark chemical potential. We have introduced the density of state $N(\mu)$ at the Fermi surface

$$N(\mu) = \frac{\mu^2}{2\pi^2}. \tag{2.14}$$

The Lagrangian (2.7) has the same symmetry as QCD except for the chiral symmetry, which is spontaneously broken to the diagonal one, reflecting the fact that the positive parity state is favored in the ground state as Eq. (2.5). When only $\Phi_{\rm L}$ ($\Phi_{\rm R}$) condenses, the color $SU(3)_{\rm C}$ and the flavor $SU(3)_{\rm L}$ ($SU(3)_{\rm R}$) are spontaneously broken down to their diagonal subgroup $SU(3)_{\rm C+L}$ ($SU(3)_{\rm C+R}$). The ground state can be found by minimizing the potential energy in Eq. (2.7),

$$\Phi = {\rm diag}(\Delta_{\rm CFL}, \Delta_{\rm CFL}, \Delta_{\rm CFL}), \quad \Delta_{\rm CFL} \equiv \sqrt{-\frac{\alpha}{8\beta}}, \tag{2.15}$$

up to a color and flavor rotation. This is the so-called color–flavor-locking (CFL) phase of the QCD. The chiral symmetry is spontaneously broken as $SU(3)_{\rm L} \times SU(3)_{\rm R} \to SU(3)_{\rm L+R}$ as explained above. Since the condensate matrix Φ is proportional to the identity matrix, the diagonal symmetry of the color $SU(3)_{\rm C}$ and the flavor $SU(3)_{\rm L+R}$ remains as the genuine symmetry in the CFL phase.

Let us see the detailed structure of the spontaneous symmetry breaking in CFL. Firstly, recall the actions of the symmetries on the order parameter Φ,

$$\Phi \to e^{i\theta_{\rm B}} U_{\rm C} \Phi U_{\rm F}, \tag{2.16}$$

with $e^{i\theta_{\rm B}} \in U(1)_{\rm B}$, $U_{\rm C} \in SU(3)_{\rm C}$, and $U_{\rm F} \in SU(3)_{\rm L+R}$. There is a redundancy in the action of the symmetries, and the actual symmetry group is given by

$$G = \frac{SU(3)_{\rm C} \times SU(3)_{\rm F} \times U(1)_{\rm B}}{(\mathbb{Z}_3)_{\rm C+B} \times (\mathbb{Z}_3)_{\rm F+B}}, \tag{2.17}$$

where the discrete groups are defined by

$$(\mathbb{Z}_3)_{\rm C+B} : \left(\omega^k \mathbf{1}_3, \mathbf{1}_3, \omega^{-k}\right) \in SU(3)_{\rm C} \times SU(3)_{\rm F} \times U(1)_{\rm B}, \tag{2.18}$$

$$(\mathbb{Z}_3)_{\rm F+B} : \left(\mathbf{1}_3, \omega^k \mathbf{1}_3, \omega^{-k}\right) \in SU(3)_{\rm C} \times SU(3)_{\rm F} \times U(1)_{\rm B}, \tag{2.19}$$

with $k = 0, 1, 2$ and ω being

$$\omega \equiv e^{2\pi i/3}. \tag{2.20}$$

Note that the discrete groups can be rearranged as

$$(\mathbb{Z}_3)_{\rm C+B} \times (\mathbb{Z}_3)_{\rm F+B} \simeq (\mathbb{Z}_3)_{\rm C+F} \times (\mathbb{Z}_3)_{\rm C-F+B} \tag{2.21}$$

with

$$(\mathbb{Z}_3)_{\rm C+F} : \left(\omega^k \mathbf{1}_3, \omega^{-k} \mathbf{1}_3, 1\right) \in SU(3)_{\rm C} \times SU(3)_{\rm F} \times U(1)_{\rm B}, \tag{2.22}$$

$$(\mathbb{Z}_3)_{\rm C-F+B} : \left(\omega^k \mathbf{1}_3, \omega^k \mathbf{1}_3, \omega^{-2k}\right) \in SU(3)_{\rm C} \times SU(3)_{\rm F} \times U(1)_{\rm B}. \tag{2.23}$$

In the ground state, the full symmetry group G is spontaneously broken down to

$$H = \frac{SU(3)_{\rm C+F} \times (\mathbb{Z}_3)_{\rm C-F+B}}{(\mathbb{Z}_3)_{\rm C+B} \times (\mathbb{Z}_3)_{\rm F+B}} \simeq \frac{SU(3)_{\rm C+F}}{(\mathbb{Z}_3)_{\rm C+F}}. \tag{2.24}$$

Thus, we find the order parameter space of the ground state as

$$\frac{G}{H} \simeq \frac{SU(3)_{\rm C-F} \times U(1)_{\rm B}}{(\mathbb{Z}_3)_{\rm C-F+B}} \simeq U(3)_{\rm C-F+B}. \tag{2.25}$$

This $U(3)$ manifold is parametrized by 9 would-be NG modes, among which 8 are eaten by the gluons via the Higgs mechanism and only one massless scalar field (referred to as the H boson) associated with the $U(1)_{\rm B}$ symmetry breaking remains in the physical spectrum[2].

Including the broken $U(1)_{\rm A}$ symmetry and the chiral symmetry, the full order parameter space (OPS) in the CFL phase is given by

$$\mathcal{M}_{\rm CFL} = U(3)_{\rm C-F+B} \times U(3)_{\rm L-R+A}. \tag{2.26}$$

The GL Lagrangian (2.7) describes only the first part, while the second part describing the NG modes associated with the broken $U(1)_{\rm A}$ and the chiral symmetry is discussed in Sect. 2.2.2.

The spectrum of the GL theory (2.7) can be found by expanding the order parameter Φ around the ground state given in Eq. (2.15) as

$$\Phi(x) = \Delta_{\rm CFL}\mathbf{1}_3 + \frac{\phi_1(x) + i\varphi(x)}{\sqrt{2}}\mathbf{1}_3 + \frac{\phi_8^a(x) + i\zeta^a(x)}{\sqrt{2}}T^a. \tag{2.27}$$

The fields proportional to $\mathbf{1}_3$ and T^a belong to the singlet (**1**) and adjoint (**8**) representations of the CFL symmetry given in Eq. (2.24). The small fluctuations $\zeta^a(x)$ are absorbed by the gluons and $\varphi(x)$ remains the massless $U(1)_{\rm B}$ NG mode (phonon). The masses of the gluons, ϕ_1, and ϕ_8^a are given respectively as follows:

$$m_{\rm g}^2 = 2\lambda_3 g_{\rm s}^2 \Delta_{\rm CFL}^2 K_3, \quad m_1^2 = -\frac{2\alpha}{K_3}, \quad m_8^2 = \frac{4\beta\Delta_{\rm CFL}^2}{K_3}. \tag{2.28}$$

From this, together with Eq. (2.13), we find the following relation

$$m_{\rm g} \sim \sqrt{\lambda_3} g_{\rm s}\mu, \quad m_1 = 2m_8 \sim 2\Delta_{\rm CFL}. \tag{2.29}$$

Note that $g_{\rm s}\mu \gg \Delta_{\rm CFL}$ at the high density limit, so that we have

$$\kappa_{1,8} \equiv \frac{m_{1,8}}{m_{\rm g}} \ll 1. \tag{2.30}$$

This implies that the CFL phase is in the type I superconductor [144].[3]

Note that the lightest mode in the GL Lagrangian (2.7) is the NG mode. As explained above, this exists because of the $U(1)_{\rm B}$ symmetry spontaneously broken by the condensations, implying that the CFL phase is the $U(1)_{\rm B}$ superfluid. Namely, the CFL phase of the color superconductivity of high density QCD has the peculiarity of the coexistence of superfluidity and superconductivity.

2.1.2. Including strange quark mass. So far, we have considered the CFL phase at the asymptotically high density where all the quark masses $m_{\rm u,d,s}$ are negligible compared to the baryon chemical potential μ. In this subsection, let us consider the effect of the finite non-zero strange quark mass while the masses of the u and d quarks are kept at zero,

$$0 \simeq m_{\rm u,d} < m_{\rm s} \ll \mu. \tag{2.31}$$

The effects of non-zero quark masses become important at smaller baryon chemical potentials. It was found [179] that the non-zero quark mass together with the β-equilibrium and the electric charge

[2] To be precise, the $U(1)_{\rm B}$ is broken to $\mathbb{Z}_2$, which flips the signs of L and R quarks ($q_L \to -q_L$ and $q_R \to -q_R$). This $\mathbb{Z}_2$ cannot be described in the GL theory.

[3] This does not mean that a state with vortices is unstable in the CFL phase. NG bosons for the $U(1)_{\rm B}$ symmetry breaking induce a repulsive force between vortices, which stabilizes the multi-vortex state.

neutrality changes the CFL phase to the modified CFL (mCFL) phase where the color–flavor-locking symmetry is further broken as

$$SU(3)_{\mathrm{C+L+R}} \to U(1)^2. \tag{2.32}$$

The important difference between the CFL and mCFL phases is that the quark chemical potentials $\mu_{\mathrm{u}}, \mu_{\mathrm{d}}, \mu_{\mathrm{s}}$ take different values. Hence, there appear difference between the Fermi momenta and the gaps of the diquark condensation take different values as [179]

$$\Delta_{\mathrm{ud}} > \Delta_{\mathrm{ds}} > \Delta_{\mathrm{us}}. \tag{2.33}$$

This is responsible for the symmetry breaking in Eq. (2.32). The correction to quadratic order to the GL potential in Eq. (2.7) was obtained as [178,179]

$$\delta V = \frac{2}{3}\varepsilon \,\mathrm{Tr}\left[\Phi^\dagger \Phi\right] + \varepsilon \,\mathrm{Tr}\left[\Phi^\dagger X_3 \Phi\right], \tag{2.34}$$

$$\varepsilon = N(\mu)\frac{m_{\mathrm{s}}^2}{\mu^2}\log\frac{\mu}{T_{\mathrm{c}}}, \tag{2.35}$$

$$X_3 = \mathrm{diag}\left(0, \frac{1}{2}, -\frac{1}{2}\right). \tag{2.36}$$

The first term in Eq. (2.34) can be absorbed into the definition of α as

$$\alpha' \equiv \alpha + \frac{2}{3}\varepsilon. \tag{2.37}$$

If we ignore the second term in Eq. (2.34), all the results in the previous sections are still valid under the understanding of the replacement α with α' in all equations. For instance, Δ_{CFL} is replaced with

$$\Delta_\varepsilon \equiv \sqrt{-\frac{\alpha'}{8\beta}}. \tag{2.38}$$

Therefore, an essential difference from the massless case is given rise to by the second term in Eq. (2.34). Since the term is sufficiently small if $m_{\mathrm{s}} \ll \mu$, we will treat it as a perturbation in Sect. 5.2.

2.1.3. Including electromagnetic interactions. Let us next include the electromagnetic interaction that is realized as a $U(1)$ action from the right-hand side on Φ as

$$\Phi \to \Phi e^{ieT^{\mathrm{EM}}}, \quad T^{\mathrm{EM}} = \sqrt{\frac{2}{3}}\,T^8 = \mathrm{diag}\left(-\frac{2}{3}, \frac{1}{3}, \frac{1}{3}\right). \tag{2.39}$$

The covariant derivative of Φ is changed from Eq. (2.8) to

$$\mathcal{D}_\mu \Phi = \partial_\mu \Phi - i g_{\mathrm{s}} A_\mu^a T^a \Phi - ieA_\mu^{\mathrm{EM}} \Phi T^{\mathrm{EM}}, \tag{2.40}$$

and the field strength is

$$F_{\mu\nu}^{\mathrm{EM}} = \partial_\mu A_\nu^{\mathrm{EM}} - \partial_\nu A_\mu^{\mathrm{EM}}. \tag{2.41}$$

The GL thermodynamic potential is modified as

$$\begin{aligned}\Omega = \mathrm{Tr}\left[\frac{1}{4\lambda_3}F_{ij}^2 + \frac{\varepsilon_3}{2}F_{0i}^2 + K_3 \mathcal{D}_i \Phi^\dagger \mathcal{D}_i \Phi\right] \\ + \frac{1}{4\lambda_0}(F_{ij}^{\mathrm{EM}})^2 + \frac{\varepsilon_0}{2}(F_{0i}^{\mathrm{EM}})^2 + V,\end{aligned} \tag{2.42}$$

where V is the same as the one in Eq. (2.7) and λ_0 and ε_0 are the magnetic permeability and the dielectric constant for the electromagnetic field.

There is mixing between $A_i^{\rm EM}$ and A_i^8 in the CFL phase, since the electric charge is proportional to T_8 as shown in Eq. (2.39) [12]. Let us first rescale the gauge fields by

$$\mathcal{A}_i^a = \frac{1}{\sqrt{\lambda_3}} A_i^a, \quad \mathcal{A}_i^{\rm EM} = \frac{1}{\sqrt{\lambda_0}} A_i^{\rm EM}. \tag{2.43}$$

This redefinition changes the kinetic terms of the electromagnetic fields and the gluons into the canonical forms as $-\frac{1}{4}{\rm Tr}[(\mathcal{F}_{ij})^2] - \frac{1}{4}(\mathcal{F}_{ij}^{\rm EM})^2$. Then, the covariant derivatives are rewritten as

$$\mathcal{D}_i \Phi = \partial_i \Phi - i\sqrt{\lambda_3} g_{\rm s} \mathcal{A}_i^a T^a \Phi - i\sqrt{\lambda_0} e \Phi \mathcal{A}_i^{\rm EM} T^{\rm EM}. \tag{2.44}$$

When the order parameter Φ is diagonal (in particular in the ground state), the covariant derivative acting on the Φ can be rewritten as

$$\mathcal{D}_i \Phi = \partial_i \Phi - i\sqrt{\lambda_3} g_{\rm s} \mathcal{A}_i^{\tilde{a}} T^{\tilde{a}} \Phi - i\sqrt{\lambda_0} g_{\rm M} \mathcal{A}_i^{\rm M} T^{\rm EM} \Phi, \tag{2.45}$$

$$g_{\rm M} \equiv \sqrt{e^2 + \frac{3}{2}\frac{\lambda_3}{\lambda_0} g_{\rm s}^2}, \tag{2.46}$$

$$T^{\rm M} \equiv T^{\rm EM} \tag{2.47}$$

with $\tilde{a} = 1, 2, \ldots, 7$, in terms of rotated gauge fields defined by

$$\mathcal{A}_i^{\rm M} \equiv \cos\chi \mathcal{A}_i^{\rm EM} + \sin\chi \mathcal{A}_i^8, \tag{2.48}$$

$$\mathcal{A}_i^0 \equiv -\sin\chi \mathcal{A}_i^{\rm EM} + \cos\chi \mathcal{A}_i^8, \tag{2.49}$$

with the mixing angle defined by

$$\tan\chi = \frac{\sqrt{\frac{3}{2}\frac{\lambda_3}{\lambda_0}} g_{\rm s}}{e}. \tag{2.50}$$

We have rewritten $T^{\rm EM}$ by $T^{\rm M}$ in order to remember that it acts on Φ from its left while $T^{\rm EM}$ acts on its right. One can see from Eq. (2.45) that $\mathcal{A}_i^{\rm M}$ couples to Φ and so is massive in the ground state [see Eq. (2.52), below], while $\mathcal{A}_i^0$ decouples from Φ and so is massless. However, one should note that this rotation is valid only when Φ is diagonal, and it is meaningless for general Φ.

The ground state of the theory is unchanged with respect to the case without the electromagnetic interaction:

$$\langle \Phi_a{}^A \rangle = \Delta_{\rm CFL} \delta_a{}^A. \tag{2.51}$$

Because of the nontrivial mixing, the masses of gluons are modified in the CFL phase as

$$m_{{\rm g},\tilde{a}}^2 = 2\lambda_3 g_{\rm s}^2 \Delta_{\rm CFL}^2 K_3, \quad m_{\rm g,M}^2 = \frac{4}{3}\lambda_0 g_{\rm M}^2 \Delta_{\rm CFL}^2 K_3, \tag{2.52}$$

where $\tilde{a}$ runs from 1 to 7 and $m_{\rm g,M}$ is the mass of the gluon corresponding to the generator T^8.

One of the important effects of introducing electromagnetic interactions is the explicit breaking of the $SU(3)_{\rm F}$ flavor symmetry, even if we still consider all quarks to be massless. Introducing electromagnetic interactions is equivalent to gauging the $U(1)$ subgroup generated by $T^{\rm EM}$ inside the $SU(3)_{\rm F}$ flavor symmetry. Therefore, the flavor $SU(3)$ is explicitly broken as

$$SU(3)_{\rm F} \xrightarrow{T^{\rm EM}} SU(2)_{\rm F} \times U(1)_{\rm EM}, \tag{2.53}$$

where $SU(2)_{\rm F}$ is a subgroup of $SU(3)_{\rm F}$ commuting with $T_{\rm EM}$. The full set of symmetries of the CFL phase of QCD with electromagnetic interactions is thus given by the following (apart from the chiral

symmetry):

$$G = U(1)_{\rm B} \times U(1)_{\rm EM} \times SU(3)_{\rm C} \times SU(2)_{\rm F}. \tag{2.54}$$

Apart from the unbroken gauge $U(1)$ symmetry, the CFL ground state Eq. (2.51) has the following diagonal color–flavor symmetry:

$$H_{\rm EM} = SU(2)_{\rm C+F}. \tag{2.55}$$

This reduced symmetry is crucial to understanding the property of non-Abelian vortices with electromagnetic coupling.

2.1.4. Time-dependent Ginzburg–Landau theory. In this section, let us discuss the time-dependent Ginzburg–Landau Lagrangian (TDGL) for the CFL phase [4]. The time-independent part of the TDGL is the same as Eq. (2.7). Then, the TDGL is given by

$$\begin{aligned}\mathcal{L} = {\rm Tr}\left[-\frac{\varepsilon_3}{2}F_{0i}F^{0i} - \frac{1}{4\lambda_3}F_{ij}F^{ij}\right] - \frac{\varepsilon_0}{2}(F^{\rm EM})_{0i}(F^{\rm EM})^{0i} - \frac{1}{4\lambda_0}(F^{\rm EM})_{ij}(F^{\rm EM})^{ij} \\ + {\rm Tr}\left[2i\gamma K_0(\mathcal{D}_0\Phi^\dagger\Phi - \Phi^\dagger\mathcal{D}_0\Phi) + K_0\mathcal{D}_0\Phi^\dagger\mathcal{D}^0\Phi + K_3\mathcal{D}_i\Phi^\dagger\mathcal{D}^i\Phi\right] - V,\end{aligned} \tag{2.56}$$

with

$$K_0 = 3K_3. \tag{2.57}$$

K_0 has not been calculated in the literature, but can be derived following the same procedure as in Refs. [2,287].

At zero temperature, there is no dissipation. However, the dissipation is present at finite temperature, which cannot be incorporated in the Lagrangian. Instead, the Euler–Lagrange equation can be modified as

$$K_{\rm D}\frac{\partial\Phi}{\partial t} = \frac{\delta\mathcal{L}}{\delta\Phi^*} \tag{2.58}$$

with a real GL parameter $K_{\rm D} = K_{\rm D}(T,\mu)$, which has not been calculated from microscopic theory. Formally, this term can be obtained by replacing $2iK_0\gamma\partial/\partial t$ by $(2iK_0\gamma - K_{\rm D})\partial/\partial t$ in the Euler–Lagrange equation of the Lagrangian in Eq. (2.56).

Let us construct the $U(1)_{\rm B}$ Noether current:

$$\begin{aligned}j_0^{\rm B} &= \gamma K_0{\rm Tr}(\Phi^\dagger\Phi) + 2iK_0{\rm Tr}\left[\mathcal{D}_0\Phi^\dagger\Phi - \Phi^\dagger\mathcal{D}_0\Phi\right], \\ j_i^{\rm B} &= 2iK_3{\rm Tr}(\mathcal{D}_i\Phi^\dagger\Phi - \Phi^\dagger\mathcal{D}_i\Phi).\end{aligned} \tag{2.59}$$

The Noether current satisfies the continuity equation:

$$\partial_0 j_0^{\rm B} - \partial_i j_i^{\rm B} = 0. \tag{2.60}$$

The Noether charge defined by

$$Q^{\rm B} = \int d^3x\, j_0^{\rm B} \tag{2.61}$$

is a conserved quantity.

When we ignore the second derivative with respect to the time coordinate, the charge density is reduced as

$$j_0^{\mathrm{B}} \sim \gamma K_0 \,\mathrm{Tr}\,\Phi^\dagger \Phi \equiv \rho, \tag{2.62}$$

where ρ is called the superfluid density. Then, the superfluid velocity is defined by dividing the spatial components of the Noether current by the superfluid density:

$$J_i^{\mathrm{B}} = \frac{2iK_3}{\gamma K_0} \frac{\mathrm{Tr}(\mathcal{D}_i\Phi^\dagger\Phi - \Phi^\dagger\mathcal{D}_i\Phi)}{\mathrm{Tr}(\Phi^\dagger\Phi)}. \tag{2.63}$$

The vorticity is defined by the rotation of the superfluid velocity

$$\omega_i = \frac{1}{2}\epsilon_{ijk}\partial_j J_k^{\mathrm{B}}. \tag{2.64}$$

The conjugate momentum of Φ is

$$\Pi_\Phi = K_0\left(\mathcal{D}_0\Phi^\dagger - 2i\gamma\Phi^\dagger\right), \tag{2.65}$$

and the Hamiltonian is given by

$$\begin{aligned}\mathcal{H} = \mathrm{Tr}\left[\frac{\varepsilon_3}{2}(F_{0i})^2 + \frac{1}{4\lambda_3}(F_{ij})^2 + K_0\,|\mathcal{D}_0\Phi|^2 + K_3\,|\mathcal{D}_i\Phi|^2\right] \\ + \frac{\varepsilon_0}{2}(F_{0i}^{\mathrm{EM}})^2 + \frac{1}{4\lambda_0}(F_{ij}^{\mathrm{EM}})^2 + V.\end{aligned} \tag{2.66}$$

2.2. Effective theories for light fields at zero temperature

Thus far, we have explained the GL theory, which is valid around the transition temperature $T \sim T_{\mathrm{c}}$. In this section, we introduce the effective Lagrangians for Nambu–Goldstone modes associated with spontaneous symmetry breaking, which are valid around the zero temperature $T \sim 0$. We study the low-energy effective theory for $U(1)_{\mathrm{B}}$ phonons in Sect. 2.2.1 and the chiral Lagrangian describing the CFL mesons and the η' meson in Sect. 2.2.2. In general, the effective theory for Nambu–Goldstone modes can be constructed by nonlinear realizations up to decay constants [66,79]. At low baryon densities, the decay constant of the chiral Lagrangian is determined experimentally. On the other hand, at high baryon densities, the decay constant can be microscopically calculated from QCD, as explained below.

2.2.1. Effective theory for $U(1)_{\mathrm{B}}$ phonons at zero temperature. In the CFL phase the baryonic $U(1)_{\mathrm{B}}$ symmetry is spontaneously broken, so that a corresponding massless Nambu–Goldstone boson φ_{B} appears. It will play important roles since it is deeply related to superfluidity. In this section we give an brief review of low energy effective theories at high density and zero temperature [71,331,333,334] of the $U(1)_{\mathrm{B}}$ Nambu–Goldstone mode.

Let us first take the phase of the diquark condensate qq as the Nambu–Goldstone field. An effective action takes the form

$$\mathcal{L}_{\mathrm{B}} = 12 f_{\mathrm{B}}^2\left[(\partial_0\varphi_{\mathrm{B}} + 2\mu)^2 - v_{\mathrm{B}}^2(\partial_i\varphi_{\mathrm{B}})^2\right], \tag{2.67}$$

where the coefficients were calculated [333,334] as

$$f_{\mathrm{B}}^2 = \frac{3\mu^2}{8\pi^2}, \quad v_{\mathrm{B}}^2 = \frac{1}{3}, \tag{2.68}$$

and μ is the quark chemical potential. Note that the time derivative is not ∂_0 but $\partial_0 + 2\mu$. This is needed for the effective theory to have the same symmetry as QCD. This can be understood as

follows. The Lagrangian of QCD in the medium is given by

$$\mathcal{L}_{\rm QCD} = \bar{q}(i\gamma_\nu \partial^\nu)q + \mu q^\dagger q = \bar{q}(i\gamma^\nu D_\nu)q, \tag{2.69}$$

where we introduced a covariant derivative $D_\nu = \partial_\nu + iB_\nu$ with a fictitious (spurion) gauge field B_μ, which corresponds to the baryon current [128]. B_μ will be set to $B_\mu = (\mu, 0, 0, 0)$ in the end. The QCD Lagrangian is invariant under the $U(1)_{\rm B}$ rotation

$$q \to e^{i\theta_{\rm B}} q, \quad \varphi_{\rm B} \to \varphi_{\rm B} + 2\theta_{\rm B}, \quad B_\nu \to B_\nu - \partial_\nu \theta_{\rm B}. \tag{2.70}$$

We now require the low energy effective field to have this symmetry; one then reaches the Lagrangian (2.67).

There is another derivation of the effective theory in gauge invariant fashion [331] by taking the phase of the gauge invariant operator $qqqqqq$ as the $U(1)_{\rm B}$ Nambu–Goldstone field. In Ref. [331], it was found that the effective field theory takes the form

$$\mathcal{L}'_{\rm B} = \frac{N_{\rm C} N_{\rm F}}{12\pi^2}\left[(\partial_0 \varphi_{\rm B} - 6\mu)^2 - (\partial_i \varphi_{\rm B})^2\right]^2. \tag{2.71}$$

Expanding this Lagrangian and taking terms to the quadratic order in the derivative with $N_{\rm C} = N_{\rm F} = 3$, one reproduces the same Lagrangian as Eq. (2.67).

Although we have ignored the amplitude (Higgs) modes in this section, they have been taken into account in Ref. [23] and interactions between the $U(1)_{\rm B}$ mode and the amplitude modes have been studied.

2.2.2. Chiral Lagrangian of the CFL mesons: pions and the η' meson. In this subsection, we study the chiral Lagrangian describing the Nambu–Goldstone modes for chiral symmetry breaking, i.e., the CFL mesons and the η' meson. So far, we have not considered the spontaneous symmetry breaking of the axial $U(1)_{\rm A}$ symmetry, since it is explicitly broken by quantum effects (the chiral anomaly). Instantons induce vertices that break the $U(1)_{\rm A}$ symmetry, since instantons flip the chirality of fermions. The instanton effects becomes arbitrarily small at the high density limit, so that the chiral anomaly is suppressed. Therefore, at high density, the spontaneous broken $U(1)_{\rm A}$ symmetry introduces a light meson, namely the η' meson. Accordingly, there appears an order parameter corresponding to this. Including the axial $U(1)_{\rm A}$ symmetry, the flavor symmetry $SU(3)_{\rm L} \times SU(3)_{\rm R} \times U(1)_{\rm A}$ of QCD acts on the gauge invariant

$$\Sigma \equiv \Phi_{\rm L}^\dagger \Phi_{\rm R}, \tag{2.72}$$

as

$$\Sigma \to g_{\rm L}^\dagger \Sigma g_{\rm R} e^{2i\theta_{\rm A}}, \quad (g_{\rm L}, g_{\rm R}, e^{2i\theta_{\rm A}}) \in SU(3)_{\rm L} \times SU(3)_{\rm R} \times U(1)_{\rm A}. \tag{2.73}$$

While discrete groups are not well discussed in the literature, here we discuss them in more detail. There is a redundancy of discrete groups in this action, and the actual flavor symmetry is

$$G_{\rm F} = \frac{SU(3)_{\rm L} \times SU(3)_{\rm R} \times U(1)_{\rm A}}{(\mathbb{Z}_3)_{\rm L+A} \times (\mathbb{Z}_3)_{\rm R+A}} \simeq \frac{SU(3)_{\rm L} \times SU(3)_{\rm R} \times U(1)_{\rm A}}{(\mathbb{Z}_3)_{\rm L+R} \times (\mathbb{Z}_3)_{\rm L-R+A}}, \tag{2.74}$$

where the redundant discrete groups are

$$(\mathbb{Z}_3)_{\mathrm{L+A}} \ : \ \left(\omega^k \mathbf{1}_3, \mathbf{1}_3, \omega^{-k}\right) \in SU(3)_{\mathrm{L}} \times SU(3)_{\mathrm{R}} \times U(1)_{\mathrm{A}}, \tag{2.75}$$

$$(\mathbb{Z}_3)_{\mathrm{R+A}} \ : \ \left(\mathbf{1}_3, \omega^k \mathbf{1}_3, \omega^{-k}\right) \in SU(3)_{\mathrm{L}} \times SU(3)_{\mathrm{R}} \times U(1)_{\mathrm{A}}, \tag{2.76}$$

$$(\mathbb{Z}_3)_{\mathrm{L+R}} \ : \ \left(\omega^k \mathbf{1}_3, \omega^{-k} \mathbf{1}_3, 1\right) \in SU(3)_{\mathrm{L}} \times SU(3)_{\mathrm{R}} \times U(1)_{\mathrm{A}}, \tag{2.77}$$

$$(\mathbb{Z}_3)_{\mathrm{L-R+A}} \ : \ \left(\omega^k \mathbf{1}_3, \omega^k \mathbf{1}_3, \omega^{-2k}\right) \in SU(3)_{\mathrm{L}} \times SU(3)_{\mathrm{R}} \times U(1)_{\mathrm{A}}, \tag{2.78}$$

with ω in Eq. (2.20). Here the suffix A always implies $U(1)_{\mathrm{A}}$. With the same group structures as Eqs. (2.24) and (2.25), the unbroken symmetry in the ground state $\Sigma \sim \mathbf{1}_3$ is

$$H_{\mathrm{F}} = \frac{SU(3)_{\mathrm{L+R}} \times (\mathbb{Z}_3)_{\mathrm{L-R+A}}}{(\mathbb{Z}_3)_{\mathrm{L+A}} \times (\mathbb{Z}_3)_{\mathrm{R+A}}} \simeq \frac{SU(3)_{\mathrm{L+R}}}{(\mathbb{Z}_3)_{\mathrm{L+R}}} \tag{2.79}$$

and the order parameter space is found to be

$$\frac{G_{\mathrm{F}}}{H_{\mathrm{F}}} \simeq \frac{SU(3)_{\mathrm{L-R}} \times U(1)_{\mathrm{A}}}{(\mathbb{Z}_3)_{\mathrm{L-R+A}}} \simeq U(3)_{\mathrm{L-R+A}}. \tag{2.80}$$

The low-energy effective field theory for the $U(3)_{\mathrm{L-R+A}}$ NG modes, the chiral Lagrangian at high baryon density and at zero temperature, was first obtained in Ref. [71]. Let us first restrict the generic field Σ in Eq. (2.72) by the constraints[4]

$$\Sigma = \Phi_{\mathrm{L}}^\dagger \Phi_{\mathrm{R}}, \quad \Phi_{\mathrm{L}} \Phi_{\mathrm{L}}^\dagger = \Phi_{\mathrm{R}} \Phi_{\mathrm{R}}^\dagger = \mathbf{1}_3. \tag{2.81}$$

Furthermore, we decompose Σ into $SU(3)$ and $U(1)$ parts as

$$\Sigma = \tilde{\Sigma} e^{i\varphi_{\mathrm{A}}}, \quad \tilde{\Sigma} = \Phi_{\mathrm{L}}^\dagger \Phi_{\mathrm{R}}. \tag{2.82}$$

Then, the chiral Lagrangian is given by [71]

$$\begin{aligned}\mathcal{L} = {} & \frac{f_\pi^2}{4} \mathrm{Tr}\left[\nabla_0 \tilde{\Sigma} \nabla_0 \tilde{\Sigma}^\dagger - v_\pi^2 \partial_i \tilde{\Sigma} \partial_i \tilde{\Sigma}^\dagger\right] + \frac{3f^2}{4}\left[\partial_0 V \partial_0 V^* - v_{\eta'}^2 \partial_i V \partial_i V^*\right] \\ & + \left(A \mathrm{Tr}\left[M \tilde{\Sigma}^\dagger\right] V^* + \mathrm{h.c.}\right) + \left(B_1 \mathrm{Tr}[M \tilde{\Sigma}^\dagger] \mathrm{Tr}[M \tilde{\Sigma}^\dagger] V \right. \\ & \left. + B_2 \mathrm{Tr}[M \tilde{\Sigma}^\dagger M \tilde{\Sigma}^\dagger] V + B_3 \mathrm{Tr}[M \tilde{\Sigma}^\dagger] \mathrm{Tr}[M^\dagger \tilde{\Sigma}] + \mathrm{h.c.}\right) + \cdots,\end{aligned} \tag{2.83}$$

where we have omitted the electromagnetic interaction. Here $M = \mathrm{diag}(m_{\mathrm{u}}, m_{\mathrm{d}}, m_{\mathrm{s}})$ is a mass matrix, $\tilde{\Sigma}$ stands for the octet chiral field, and V is the axial $U(1)_{\mathrm{A}}$ field

$$\tilde{\Sigma} = \exp\left(i \frac{\pi^a T^a}{f_\pi}\right), \quad V = e^{i\varphi_{\mathrm{A}}} = \exp\left(i \frac{2\eta'}{\sqrt{6} f}\right), \tag{2.84}$$

with f_π and f being the octet and singlet decay constants. The covariant derivative of the time derivative for $\tilde{\Sigma}$ is defined by [47]

$$\nabla_0 \tilde{\Sigma} = \partial_0 \tilde{\Sigma} + i\left(\frac{M M^\dagger}{2\mu}\right) \tilde{\Sigma} - i \tilde{\Sigma}\left(\frac{M^\dagger M}{2\mu}\right). \tag{2.85}$$

[4] Note that the GL theory can correctly describe physics at slightly lower temperatures than the transition temperature. Only there does expansion in terms of the gap Δ_{CFL} work well because Δ_{CFL} is sufficiently small and can be treated as an expansion parameter. On the other hand, the chiral Lagrangian is an effective theory including only the derivative of massless zero modes; it can describe physics at zero temperature even if it is not close to a transition temperature.

The decay constants and speed of mesons are obtained as [333,334]

$$f_\pi^2 = \frac{21 - 8\log 2}{18}\frac{\mu^2}{2\pi^2}, \quad f^2 = \frac{3}{4}\frac{\mu^2}{2\pi^2}, \quad v_\pi^2 = v_{\eta'}^2 = \frac{1}{3}. \tag{2.86}$$

The mechanism of chiral symmetry breaking in the high baryon density is very different from that at low densities. Indeed, the dominant contribution is not the usual $\langle\bar{\psi}\psi\rangle$ but a four fermion operator $\langle(\bar{\psi}\psi)^2\rangle \sim \langle\psi\psi\rangle^2$. Thus, dominant contributions from the quark mass terms appear as quadratic terms of M in the chiral Lagrangian, namely the terms proportional to B_i. These coefficients are obtained as [303,333,334]

$$B_1 = -B_2 = \frac{3\Delta_{\rm CFL}^2}{4\pi^2}, \quad B_3 = 0, \tag{2.87}$$

with $\Delta_{\rm CFL}$ being the gap in the quasiparticle spectrum. The terms linear in M appear when $\langle\bar{\psi}\psi\rangle$ is not zero. Although they vanish at the asymptotically high density limit, they appear through non-perturbative effects, instantons [233,301,302,335,336]. The coefficient A is calculated by Ref. [302] to the one-instanton level as

$$A = C_N \frac{8\pi^4}{3}\frac{\Gamma(6)}{3^6}\left[\frac{3\sqrt{2}\pi}{g_{\rm s}}\Delta_{\rm CFL}\left(\frac{\mu^2}{2\pi^2}\right)\right]^2\left(\frac{8\pi^2}{g_{\rm s}^2}\right)^6\left(\frac{\Lambda}{\mu}\right)^{12}\Lambda^{-3}, \tag{2.88}$$

with $C_N = 0.466\exp(-1.679N_{\rm C})1.34^{N_{\rm F}}/(N_{\rm C}-1)!(N_{\rm C}-2)!$. Note that A is related to the chiral condensate by $A = -\langle\bar{\psi}\psi\rangle/2$ [302].

From the chiral Lagrangian (2.84), one can read the masses of meson spectra. For instance, when all the quark masses are equal, $M = m\mathbf{1}_3$, setting $\Sigma = \mathbf{1}_3$, we have

$$\mathcal{L}_{\eta'} = \frac{1}{2}(\partial_0\eta')^2 - \frac{v_{\eta'}^2}{2}(\partial_i\eta')^2 - V_{1-\rm inst}(\eta'), \tag{2.89}$$

$$V_{1-\rm inst}(\eta') = \left(\frac{2Am}{f^2} + \frac{4m^2B}{f^2}\right)(\eta')^2 + \cdots. \tag{2.90}$$

Thus the mass of η' is

$$m_{\eta'}^2\big|_{1-\rm inst} = \frac{4A}{f^2}m + \frac{8B}{f^2}m^2. \tag{2.91}$$

Therefore, in the chiral limit, η' is massless at the one-instanton level [302]. The η'-mass in the chiral limit is generated by the two-instanton contribution. Although it is hard to evaluate it, the potential for η' can be easily read as [302]

$$V_{\rm sym.}(\varphi_{\rm A}) = -6mA\cos\varphi_{\rm A} - 12m^2B\cos\varphi_{\rm A} - 2C\cos 3\varphi_{\rm A}, \tag{2.92}$$

where we have set the θ angle of QCD to zero and $B_1 = -B_2 = B$. The first term is the one-instanton contribution and the last term is the two-instanton contribution. We leave C as a free parameter in this work. "sym." in the subscript indicates the flavor symmetric limit $m_{\rm u} = m_{\rm d} = m_{\rm s} = m$.

Before closing this section, let us show the original derivation of the above chiral Lagrangian by Ref. [71]. Let $\Phi_{\rm L}$ and $\Phi_{\rm R}$ be coset fields for $SU(3)_{\rm C} \times SU(3)_{\rm L}$ and $SU(3)_{\rm C} \times SU(3)_{\rm R}$, respectively:

$$\Phi_{\rm L}\Phi_{\rm L}^\dagger = \Phi_{\rm R}\Phi_{\rm R}^\dagger = \mathbf{1}_3, \quad \det\Phi_{\rm L} = \det\Phi_{\rm R} = 1. \tag{2.93}$$

Since an effective theory of QCD should have the same symmetry as QCD, the effective Lagrangian derived in Ref. [71] is of the form

$$\begin{aligned}\mathcal{L} = &-\frac{f_\pi^2}{4}{\rm Tr}\left[\left(\Phi_{\rm R}\partial_0\Phi_{\rm R}^\dagger - \Phi_{\rm L}\partial_0\Phi_{\rm L}^\dagger\right)^2 - v_\pi^2\left(\Phi_{\rm R}\partial_i\Phi_{\rm R}^\dagger - \Phi_{\rm L}\partial_i\Phi_{\rm L}^\dagger\right)^2\right] \\ &- C_\alpha\frac{f_\pi^2}{4}{\rm Tr}\left[\left(\Phi_{\rm R}\partial_i\Phi_{\rm R}^\dagger + \Phi_{\rm L}\partial_i\Phi_{\rm L}^\dagger + 2ig_{\rm s}A_0\right)^2 - v_\pi^2\left(\Phi_{\rm R}\partial_i\Phi_{\rm R}^\dagger + \Phi_{\rm L}\partial_i\Phi_{\rm L}^\dagger + 2ig_{\rm s}A_i\right)^2\right] \\ &- \frac{3f^2}{4}\left(|\partial_0 V|^2 - v_{\eta'}^2|\partial_i V|^2\right) - \frac{1}{4}{\rm Tr}\left[F_{\mu\nu}F^{\mu\nu}\right].\end{aligned} \tag{2.94}$$

Since we are interested in the low-energy dynamics, we integrate out the gluons A_μ, which are heavy. This can be done by neglecting the kinetic term of the gluons. Then, in this Lagrangian, the gluon is just an auxiliary field and can be eliminated by its equation of motion. After eliminating the gluon, we are left with the chiral Lagrangian

$$\begin{aligned}\mathcal{L} &= -\frac{f_\pi^2}{4}{\rm Tr}\left[\left(\Phi_{\rm R}\partial_0\Phi_{\rm R}^\dagger - \Phi_{\rm L}\partial_0\Phi_{\rm L}^\dagger\right)^2 - v_\pi^2\left(\Phi_{\rm R}\partial_i\Phi_{\rm R}^\dagger - \Phi_{\rm L}\partial_i\Phi_{\rm L}^\dagger\right)^2\right] \\ &\quad - \frac{3f^2}{4}\left(|\partial_0 V|^2 - v_{\eta'}^2|\partial_i V|^2\right) \\ &= \frac{f_\pi^2}{4}{\rm Tr}\left[\partial_0\Sigma\partial_0\Sigma^\dagger - v_\pi^2\partial_i\Sigma\partial_i\Sigma^\dagger\right] - \frac{3f^2}{4}\left(|\partial_0 V|^2 - v_{\eta'}^2|\partial_i V|^2\right).\end{aligned} \tag{2.95}$$

Based on the formulations above, we discuss the topological solitons associated with the chiral symmetry breaking in Sect. 10.

3. Vortices

In this section we explain various kinds of vortices in the CFL phase. While we use the Ginzburg–Landau theory valid around the transition temperature $T \sim T_{\rm c}$ to study vortices, the chiral Lagrangian before integrating out gluon fields, Eq. (2.94), valid at zero temperature $T \sim 0$ can alternatively be used if we study vortices with singular cores at large distances. In Sect. 3.1, we discuss Abelian vortices, i.e., $U(1)_{\rm B}$ superfluid vortices, and $U(1)_{\rm A}$ vortices or axion strings. We also discuss non-topological color-magnetic flux tubes in Sect. 3.2. In Sect. 3.3, we introduce non-Abelian vortices, sometimes called semi-superfluid vortices. A peculiar feature of non-Abelian vortices, the existence of internal orientational zero modes (collective coordinates), is explained in detail.

3.1. Abelian vortices

In this subsection, we give two concrete examples of Abelian vortices in the CFL phase. The first one is Abelian $U(1)_{\rm B}$ global vortices [128,183], which are topologically stable, while the second one is $U(1)_{\rm A}$ vortices or axion strings [128]. Since the authors in Ref. [128] used the effective theory at $T \sim 0$ describing only massless particles, reviewed in Sect. 2.2.1, the core structures of vortices cannot be described in the absence of massive particles. Here, we use the GL theory that can deal with the core structures of vortices. We also study color magnetic fluxes [180], which are non-topological and decay immediately.

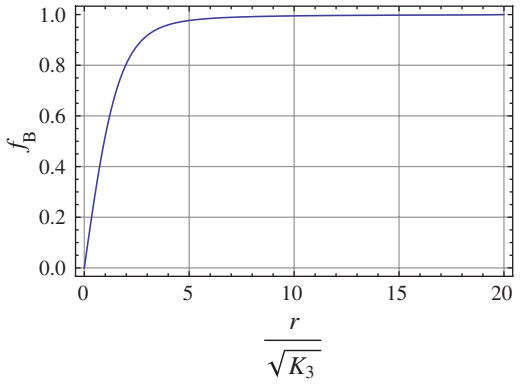

Fig. 2. A profile function $f_{\rm B}(r)$ of a minimally winding ($k = 1$) $U(1)_{\rm B}$ vortex. The parameters are $\alpha = -1$ and $\beta = 2$ for simplicity.

3.1.1. $U(1)_{\rm B}$ superfluid vortices. Let us discuss $U(1)_{\rm B}$ superfluid vortices. The phases of diquark condensates can be parametrized as

$$\Phi_{\rm L} = e^{i\theta_{\rm A}+i\theta_{\rm B}}\Delta_{\rm CFL}\mathbf{1}_3, \quad \Phi_{\rm R} = e^{-i\theta_{\rm A}+i\theta_{\rm B}}\Delta_{\rm CFL}\mathbf{1}_3. \tag{3.1}$$

The phases $\varphi_{\rm A}$ and $\varphi_{\rm B}$ are the phases of the $U(1)_{\rm A}$ and $U(1)_{\rm B}$ symmetries, respectively. Both phase symmetries $U(1)_{\rm B}$ and $U(1)_{\rm A}$ are spontaneously broken when the diquarks are condensed, while the $U(1)_{\rm A}$ is also broken explicitly by the chiral anomaly, namely the instanton effects. The spontaneous breaking of $U(1)_{\rm B}$ and $U(1)_{\rm A}$ gives rise to $U(1)_{\rm B}$ and $U(1)_{\rm A}$ global vortices, respectively.

The $U(1)_{\rm B}$ global vortices can be easily found in Eq. (2.7) by requiring the condensate matrix to be proportional to the unit matrix $\Phi(x) = \phi(x)\mathbf{1}_3/\sqrt{3}$. Then, the Lagrangian is reduced to the following linear sigma model for the complex scalar field $\phi(x)$:

$$\mathcal{L}_{U(1)_{\rm B}} = K_0\left(|\partial_0\phi|^2 - v_{\rm B}^2|\partial_i\phi|^2\right) - \left[\alpha|\phi|^2 + \frac{4\beta}{3}|\phi|^4\right] + \frac{3\alpha^2}{16\beta},$$
$$v_{\rm B} \equiv \sqrt{\frac{K_3}{K_0}} = \frac{1}{\sqrt{3}}. \tag{3.2}$$

The effective field ϕ develops the VEV $\langle\phi\rangle = \sqrt{3}\Delta_{\rm CFL}$ in the ground state, so that the $U(1)_{\rm B}$ is spontaneously broken. Since the first homotopy group is nontrivial,

$$\pi_1[U(1)_{\rm B}] \simeq \mathbb{Z}, \tag{3.3}$$

there exist topologically stable k vortices in general with $k \in \mathbb{Z}$.

We make a standard ansatz for the axially symmetric k vortex strings, which are infinitely long straight lines, say, along the x_3 axis:

$$\phi(r,\theta) = \sqrt{3}\Delta_{\rm CFL}f_{\rm B}(r)e^{ik\theta}, \tag{3.4}$$

with the cylindrical coordinates (r,θ,z), i.e., $x^1 + ix^2 \equiv re^{i\theta}$. A numerically obtained profile function $f_{\rm B}$ is shown in Fig. 2.

The circulation of the superfluid velocity in Eq. (2.63) obeys the famous Onsager–Feynman quantization

$$c_B = \oint dx^i J_i^{\rm B} = 2\pi\frac{4K_3}{\gamma K_0}k \tag{3.5}$$

with the vortex number $k \in \pi_1[U(1)_{\rm B}]$.

The Hamiltonian density with respect to the amplitude function $f_{\rm B}(r)$ is given by

$$\mathcal{H}_{U(1)_{\rm B}} = 3\Delta_{\rm CFL}^3 \left(K_3 f_{\rm B}'^2 + \left(\frac{K_3 k^2}{r^2} + \alpha \right) f_{\rm B}^2 + 4\beta \Delta_{\rm CFL}^2 f_{\rm B}^4 \right). \tag{3.6}$$

The k static global string solution is obtained by solving the following equation of motion:

$$K_3 \left(f_{\rm B}'' + \frac{f_{\rm B}'}{r} \right) - \frac{k^2 K_3}{r^2} f_{\rm B} - \left(\alpha + 8\beta \Delta_{\rm CFL}^2 f_{\rm B}^2 \right) f_{\rm B} = 0, \tag{3.7}$$

with the boundary conditions $f_{\rm B}(0) = 0$ and $f_{\rm B}(\infty) \to 1$. The tension of the string logarithmically diverges as

$$T_{U(1)_{\rm B}} = 6\pi \Delta_{\rm CFL}^2 K_3 k^2 \log \frac{L}{\xi} + \cdots, \tag{3.8}$$

where $\cdots$ stands for a finite contribution to the tension, L is an IR cutoff scale representing the system size and $\xi \sim m_1^{-1}$ is a UV cutoff representing the size of the vortex core.

Asymptotic solutions of a minimally winding vortex are given by

$$f_{\rm B} = c_1 (r/\sqrt{K_3}) + \cdots, \qquad r \to 0, \tag{3.9}$$

$$f_{\rm B} = 1 - \frac{2}{-\alpha (r/\sqrt{K_3})^2} + \cdots, \qquad r \to \infty. \tag{3.10}$$

Here the constant c_1 is known to be $c_1 = 0.58\cdots$ [355].

Note that if one takes quantum anomalies into account, an axial $U(1)_{\rm A}$ current runs inside the $U(1)_{\rm B}$ vortex [337]. This phenomenon is explained in Sect. 10.6.

3.1.2. $U(1)_{\rm A}$ axial vortices. There exists another vortex string in the CFL phase that is associated with the broken $U(1)_{\rm A}$ symmetry at the high density limit. It is topologically stable because of nontrivial homotopy [128,183]

$$\pi_1[U(1)_{\rm A}] \simeq \mathbb{Z}. \tag{3.11}$$

Note that the instanton-induced potential given in Eq. (2.92) explicitly breaks $U(1)_{\rm A}$, so that a $U(1)_{\rm A}$ vortex cannot exist alone but is always accompanied by sine-Gordon domain walls at an intermediate density. This is explained in Sect. 10.

3.2. Non-topological color-magnetic fluxes

Here, we discuss color-magnetic flux tubes [180] that are non-topological because of a trivial homotopy group[5]

$$\pi_1[SU(3)_{\rm C}] = 0 \tag{3.12}$$

and consequently are unstable. A color magnetic flux is generated by one generator of the $SU(3)_{\rm C}$ color group. Among all possible generators, T_8 gives the lightest fluxes, because it can be mixed with the electromagnetic $U(1)_{\rm EM}$ acting on Φ from its right. The corresponding massive gauge field is given in Eq. (2.48).

[5] More precisely, gauge symmetry is spontaneously broken as $SU(3)_{\rm C} \times U(1)_{\rm EM} \to U(1)_0$, and the order parameter for gauge symmetry is $[SU(3)_{\rm C} \times U(1)_{\rm EM}]/U(1)_0 \simeq SU(3)$. The first homotopy group is trivial for this $SU(3)$.

To construct the vortex, we make the ansatz that all the off-diagonal elements of Φ are zero and denote

$$\Phi(x) = \mathrm{diag}\left(\phi_1(x), \frac{\phi_2(x)}{\sqrt{2}}, \frac{\phi_2(x)}{\sqrt{2}}\right). \tag{3.13}$$

Then, the Hamiltonian density is reduced as

$$\tilde{\mathcal{H}} = \frac{1}{4}(\mathcal{F}_{ij}^{\mathrm{M}})^2 + |\mathcal{D}_i\phi_1|^2 + |\mathcal{D}_i\phi_2|^2 + \tilde{V}, \tag{3.14}$$

$$\tilde{V} = \alpha\left(|\phi_1|^2 + |\phi_2|^2\right) + \beta\left(|\phi_1|^2 + |\phi_2|^2\right)^2 + \beta\left(|\phi_1|^4 + \frac{|\phi_2|^4}{2}\right), \tag{3.15}$$

with

$$\mathcal{D}_i\phi_1 = \partial_i\phi_1 + i\frac{2g_{\mathrm{M}}}{3}\mathcal{A}_i^{\mathrm{M}}\phi_1, \tag{3.16}$$

$$\mathcal{D}_i\phi_2 = \partial_i\phi_2 - i\frac{g_{\mathrm{M}}}{3}\mathcal{A}_i^{\mathrm{M}}\phi_2, \tag{3.17}$$

$$\mathcal{F}_{ij}^{\mathrm{M}} = \partial_i\mathcal{A}_j^{\mathrm{M}} - \partial_j\mathcal{A}_i^{\mathrm{M}}, \tag{3.18}$$

and $g_{\mathrm{M}} = \sqrt{e^2 + 3\lambda_3 g_{\mathrm{s}}^2/2\lambda_0}$ as defined in Eq. (2.46). In the ground state, the fields develop the VEV as $\langle\phi_1\rangle = \Delta_{\mathrm{CFL}}$ and $\langle\phi_2\rangle = \sqrt{2}\Delta_{\mathrm{CFL}}$, so that the A_μ^{M} in Eq. (2.48) is massive and A_μ^0 in Eq. (2.49) remains massless, as discussed before.

Now, we are ready to construct the magnetic flux tube by making the axially symmetric ansatz by

$$\phi_1(r,\theta) = f_1(r)e^{-2i\theta}, \quad \phi_2(r,\theta) = f_2(r)e^{i\theta},$$
$$A_i^{\mathrm{M}}(r,\theta) = -\frac{3\epsilon_{ij}}{\tilde{g}}\frac{x^j}{r^2}\chi(r), \tag{3.19}$$

with the boundary condition

$$f_1(0) = f_2(0) = \chi(0) = 0, \quad f_1(\infty) = f_2(\infty) = \chi(\infty) = 1. \tag{3.20}$$

The magnetic flux that this vortex carries can be calculated as

$$\int d^2x\ \mathcal{F}_{12}^{\mathrm{M}} = \frac{3}{g_{\mathrm{M}}}\int d^2x\ \frac{\chi'}{r} = \frac{6\pi}{g_{\mathrm{M}}}. \tag{3.21}$$

This solution was studied in Ref. [180]. The flux in Eq. (3.21) is quantized but the solution is unstable and decays by turning on the other components of gauge fields.

For later convenience, let us set $\lambda_0 = \lambda_3 = 1$ and decompose the flux in Eq. (3.21) into gluon $SU(3)_{\mathrm{C}}$ and electromagnetic $U(1)_{\mathrm{EM}}$ parts as

$$F_{12}^8 = F_{12}^{\mathrm{M}}\sin\zeta, \quad F_{12}^{\mathrm{EM}} = F_{12}^{\mathrm{M}}\cos\zeta, \tag{3.22}$$

and take the limit $\zeta = \pi/2$, namely the limit where the electromagnetic interaction is ignored. Then we find that this flux tube has the pure color-magnetic flux

$$\Phi_{\mathrm{A}}^8 = \int d^2x\ F_{12}^8 = \frac{4\sqrt{3}\pi}{g_{\mathrm{s}}}. \tag{3.23}$$

Note that F_{12}^8 is not a gauge invariant quantity but $\mathrm{Tr}\,[(F_{12})^2] = (F_{12}^8)^2$ is gauge invariant.

We should mention the stability of this flux tube. Since we chose one $U(1)$ gauge orbit inside the $SU(3)$ group by hand, this flux tube is a kind of a trivial embedding of the $U(1)$ local vortex in a

non-Abelian gauge theory. Of course, there are no reasons for such vortices to be stable, because they are not protected by topology. In order to clarify the stability, one should work out the small fluctuation analysis expanded around this solution.

Unstable color-flux tubes were also studied in the 2SC phase [14,308]. Color-magnetic flux tubes in quark–gluon plasma were studied in Ref. [219], where they are claimed to be metastable.

3.3. Non-Abelian vortices: stable color-magnetic flux tubes

In this section, we study non-Abelian vortices in the CFL phase in the GL theory. While the use of the GL theory is limited near the transition temperature where the gap $\Delta_{\rm CFL}$ is sufficiently small, the existence of non-Abelian vortices is not restricted to that region. One can also construct these vortices by using the chiral Lagrangian (2.94) before integrating out the gluons, although the chiral Lagrangian cannot describe the short distance structure at the center of the vortex, and the vortex configurations are singular at their core since we restricted $|\det\Phi_{\rm L}| = |\det\Phi_{\rm R}| = 1$. We also study vortices in the BdG equation in Sect. 8, which is not restricted to any region.

3.3.1. Minimal (M_1) non-Abelian vortices. In this subsection, we explain the so-called non-Abelian vortices, which are the most stable vortices in the CFL phase [35]. For simplicity, here we omit the mixing of the color and electric charges by simply setting $e = 0$, which we take into account in Sect. 5.3. We consider only static configurations. Therefore, we study solutions to the Euler–Lagrange equations associated with the Lagrangian

$$\begin{aligned}\mathcal{L} = {\rm Tr}\left[-K_3\mathcal{D}_i\Phi^\dagger\mathcal{D}_i\Phi - \frac{F_{ij}^2}{4\lambda_3}\right] - \alpha\,{\rm Tr}\left(\Phi^\dagger\Phi\right)\\ - \beta\left(\left[{\rm Tr}(\Phi^\dagger\Phi)\right]^2 - {\rm Tr}\left[(\Phi^\dagger\Phi)^2\right]\right) + \frac{3\alpha^2}{16\beta},\end{aligned} \tag{3.24}$$

where we discarded the terms irrelevant for the discussions below. In the rest of this section, we will set $\lambda_3 = 1$. In order to get a static straight vortex string along the x_3-axis, we make the following ansatz:

$$\Phi(r,\theta) = \Delta_{\rm CFL}\begin{pmatrix} e^{i\theta}f(r) & 0 & 0\\ 0 & g(r) & 0\\ 0 & 0 & g(r)\end{pmatrix}, \tag{3.25}$$

$$A_i(r,\theta) = \frac{\epsilon_{ij}x^j}{g_s r^2}(1-h(r))\begin{pmatrix} -\frac{2}{3} & 0 & 0\\ 0 & \frac{1}{3} & 0\\ 0 & 0 & \frac{1}{3}\end{pmatrix}. \tag{3.26}$$

Similarly, we can take

$$\Phi(r,\theta) = \Delta_{\rm CFL}\begin{pmatrix} g(r) & 0 & 0\\ 0 & e^{i\theta}f(r) & 0\\ 0 & 0 & g(r)\end{pmatrix}, \tag{3.27}$$

$$A_i(r,\theta) = \frac{\epsilon_{ij}x^j}{g_s r^2}(1-h(r))\begin{pmatrix} \frac{1}{3} & 0 & 0\\ 0 & -\frac{2}{3} & 0\\ 0 & 0 & \frac{1}{3}\end{pmatrix}, \tag{3.28}$$

or

$$\Phi(r,\theta) = \Delta_{\rm CFL} \begin{pmatrix} g(r) & 0 & 0 \\ 0 & g(r) & 0 \\ 0 & 0 & e^{i\theta} f(r) \end{pmatrix}, \tag{3.29}$$

$$A_i(r,\theta) = \frac{\epsilon_{ij} x^j}{g_{\rm s} r^2} (1 - h(r)) \begin{pmatrix} \frac{1}{3} & 0 & 0 \\ 0 & \frac{1}{3} & 0 \\ 0 & 0 & -\frac{2}{3} \end{pmatrix}. \tag{3.30}$$

These vortices were first found by Balachandran, Digal, and Matsuuta in Ref. [35]. They call them semi-superfluid non-Abelian vortices. For either case, the boundary conditions for the profile functions f, g, h at spatial infinity should be determined in such a way that the configurations reach the ground state. Therefore, we impose the boundary condition

$$f(\infty) = 1, \quad g(\infty) = 1, \quad h(\infty) = 0, \tag{3.31}$$

where the last condition implies that we are in the pure gauge at infinity. We also need to fix the values of the fields at the origin, which ensures that the solutions are regular there:

$$f(0) = 0, \quad g'(0) = 0, \quad h(0) = 1. \tag{3.32}$$

The decomposition of the $U(3)$ action in Eq. (3.25) to the $U(1)_{\rm B}$ and $SU(3)_{\rm C}$ actions can be found as

$$\Phi = \Delta_{\rm CFL} \begin{pmatrix} e^{i\theta} f(r) & & \\ & g(r) & \\ & & g(r) \end{pmatrix} = \Delta_{\rm CFL} e^{\frac{i\theta}{3}} \begin{pmatrix} e^{\frac{2i\theta}{3}} f(r) & & \\ & e^{-\frac{i\theta}{3}} g(r) & \\ & & e^{-\frac{i\theta}{3}} g(r) \end{pmatrix}. \tag{3.33}$$

At the end $\theta = 2\pi$ of the closed loop in the order parameter space, the $U(1)_{\rm B}$ contribution becomes $\omega = \exp(2\pi i/3)$. This factor is canceled by the $SU(3)_{\rm C}$ part $\mathrm{diag}(\omega^2, \omega^{-1}, \omega^{-1}) = \omega^{-1}\mathbf{1}_3$. Only the $U(1)_{\rm B}$ part with fractional winding cannot make a closed loop, while a contribution from the $SU(3)_{\rm C}$ part makes it possible to have a closed loop. One observes that the presence of the center group $\mathbb{Z}_3$ of the $SU(3)_{\rm C}$ group is essential. This is the same for the other two configurations.

Let us discuss the shape of the profile functions f, g, h. The corresponding Euler–Lagrange equations are given by

$$\left[\triangle - \frac{(2h+1)^2}{9r^2} - \frac{m_1^2}{6} \left(f^2 + 2g^2 - 3 \right) - \frac{m_8^2}{3} (f^2 - g^2) \right] f = 0, \tag{3.34}$$

$$\left[\triangle - \frac{(h-1)^2}{9r^2} - \frac{m_1^2}{6} \left(f^2 + 2g^2 - 3 \right) - \frac{m_8^2}{6} (f^2 - g^2) \right] g = 0, \tag{3.35}$$

$$h'' - \frac{h'}{r} - \frac{m_{\rm g}^2}{3} \left(g^2 (h-1) + f^2 (2h+1) \right) = 0. \tag{3.36}$$

Here the masses m_1, m_8, and $m_{\rm g}$ are given in Eq. (2.28).

To get the vortex configurations, we should solve the above coupled three ordinary differential equations. Although it is impossible to solve them analytically, we can solve them numerically.

Before demonstrating the numerical solutions, let us examine the asymptotic behavior of the profile functions that can be analytically solvable. From these asymptotics, we find several peculiar properties of the non-Abelian vortices in the CFL phase. To this end, we consider small fluctuations around

the asymptotic values $(f, g, h) = (1, 1, 0)$ and define

$$\delta F(r) = (f(r) + 2g(r)) - 3, \quad \delta G(r) = f(r) - g(r) - 0, \quad \delta h(r) = h(r) - 0. \tag{3.37}$$

$\delta F(r)$ is the fluctuation of the trace part of Φ and $\delta G(r)$ is that for the traceless part proportional to T_8 as

$$\Phi = \Delta_{\rm CFL}\mathbf{1}_3 + \Delta_{\rm CFL}\begin{pmatrix} \frac{1}{3} & & \\ & \frac{1}{3} & \\ & & \frac{1}{3} \end{pmatrix}\delta F(x) + \Delta_{\rm CFL}\begin{pmatrix} \frac{2}{3} & & \\ & -\frac{1}{3} & \\ & & -\frac{1}{3} \end{pmatrix}\delta G(r) + \cdots . \tag{3.38}$$

The linearized field equations for the fluctuations are given by

$$\left(\triangle - m_1^2 - \frac{1}{9r^2}\right)\delta F = \frac{1}{3r^2}, \tag{3.39}$$

$$\left(\triangle - m_8^2 - \frac{1}{9r^2}\right)\delta G = \frac{2}{3r^2}\delta h, \tag{3.40}$$

$$\delta h'' - \frac{\delta h'}{r} - m_{\rm g}^2\delta h = \frac{2}{3}m_{\rm g}^2\delta G. \tag{3.41}$$

An approximate solution of the first equation is [112]

$$\delta F = q_1\sqrt{\frac{\pi}{2m_1 r}}\,e^{-m_1 r} - \frac{1}{3m_1^2 r^2} + O\left((m_1 r)^{-4}\right). \tag{3.42}$$

The first term is much smaller than the others, and is usually neglected, as in the case of the $U(1)$ global vortex. The dominant terms decrease polynomially, which is a common feature of global vortices. At high baryon density where $m_{\rm g} \gg m_{1,8}$, the solutions of Eqs. (3.40) and (3.41) are given by

$$\delta G = q_8\sqrt{\frac{\pi}{2m_8 r}}\,e^{-m_8 r}, \quad \delta h = -\frac{2}{3}\frac{m_{\rm g}^2}{m_{\rm g}^2 - m_8^2}\delta G. \tag{3.43}$$

Here $q_{1,8}$ are some constants that should be determined numerically. This behavior of δh is counter-intuitive because the gluon has the magnetic mass $m_{\rm g}$ by the Higgs mechanism in the CFL phase, so naively one expects $\delta h \sim e^{-m_{\rm g} r}$. Since the asymptotic behaviors of the vortex string are deeply related to the intervortex forces, we expect that the intervortex forces of the non-Abelian vortices in CFL are quite different from those in conventional metallic superconductors.[6] In the opposite case $m_{\rm g} \ll m_8$, the asymptotic behaviors are changed from Eq. (3.43) as

$$\delta G = -\frac{2q_{\rm g}}{3}\frac{1}{(m_8^2 - m_{\rm g}^2)r^2}\sqrt{\frac{\pi}{2m_8 r}}\,e^{-m_8 r}, \quad \delta h = q_{\rm g}\sqrt{\frac{\pi m_{\rm g} r}{2}}\,e^{-m_{\rm g} r}. \tag{3.44}$$

In this case the asymptotic behaviors are governed by $m_{\rm g}$, which is smaller than m_8. The coefficients q_8 and $q_{\rm g}$ depend on the masses m_1, m_8, and $m_{\rm g}$ and can be determined numerically [112].

The full numerical solutions for Eqs. (3.34), (3.35), and (3.36) were obtained in Ref. [112]. It was found there that the shapes of the profile functions depend on the mass parameters $m_{1,8,g}$. In particular, the value of $g(0)$ at the origin is quite sensitive to the ratio m_1/m_8. Roughly speaking, $g(0)$

[6] The exponential tails of the famous Abrikosov–Nielsen–Olesen vortices [3,251] in a conventional Abelian–Higgs model are like $\exp(-m_H r)$ for the massive Higgs field H with mass m_H and $\exp(-m_e r)$ for the massive Abelian gauge boson with mass m_e. The layer structures are exchanged for $m_e > m_H$ (type II) and $m_e < m_H$ (type I). However, for the strong type II region ($m_e > 2m_H$), the tail of the gauge boson becomes $\exp(-2m_H r)$ [95,271,275]. The width of the gauge field cannot become smaller than half of that $1/m_H$ of the scalar field.

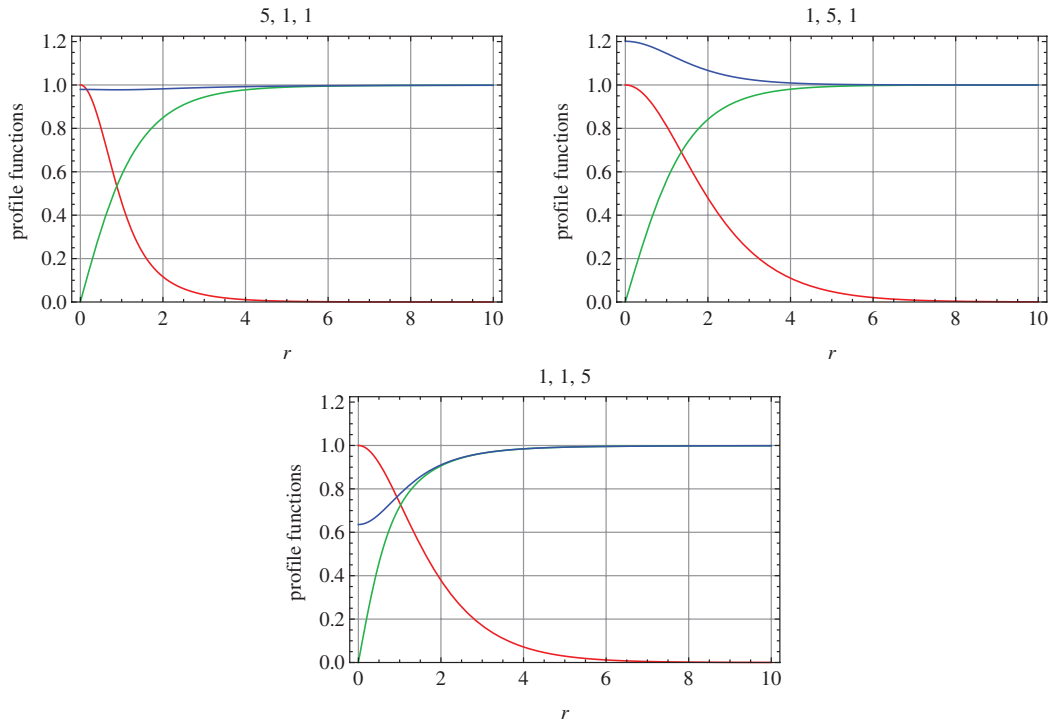

Fig. 3. The non-Abelian vortex profile functions $\{f(r), g(r), h(r)\} = \{\text{green, blue, red}\}$. The mass parameters are set to be $\{m_{\rm g}, m_1, m_8\} = \{5, 1, 1\}, \{1, 5, 1\}, \{1, 1, 5\}$. $g(r)$ is almost flat when $m_1 \simeq m_8$.

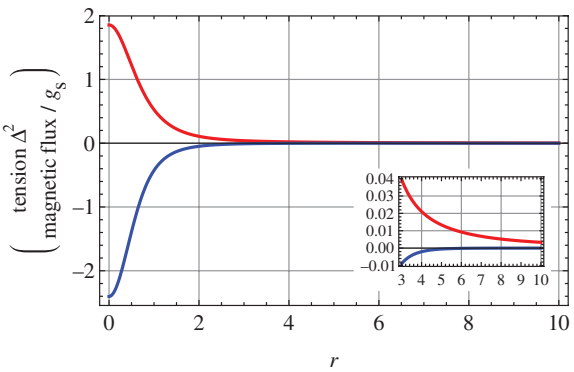

Fig. 4. Distributions of the energy density (red) and the non-Abelian magnetic flux (blue) for the minimally winding non-Abelian vortex. The parameters are chosen to be $(m_{\rm g}, m_1, m_8) = (10, 2, 1)$. While the energy density has a long tail, the magnetic flux whose transverse size is of order m_8^{-1} exponentially converges to 0.

becomes larger than 1 for $m_1 > m_8$, and is smaller than 1 for $m_1 < m_8$; see Fig. 3. Since $f(r) - g(r)$ plays the role of an order parameter for the breaking of $SU(3)_{\rm C+F}$, information on the profile functions $f(r)$ and $g(r)$ is important. For the high baryon density region, we have $m_1 = 2m_8 \ll m_{\rm g}$. Therefore, the non-Abelian vortex in the CFL phase has $g(0)$ greater than 1, as shown in the right panel of Fig. 3. The profile functions $f(r)$, $g(r)$, $h(r)$, the energy, and the color-magnetic flux densities for a particular choice of parameters $(m_1, m_8, m_{\rm g}) = (2, 1, 10)$ are shown in Fig. 4. Note that $m_{\rm g}$ is much greater than $m_{1,8}$; nevertheless, the color-magnetic flux has almost the same width as the scalar density distribution. One way to explain this counterintuitive behavior is the asymptotic behavior of the profile functions that we explained above. The asymptotic tail of the gluon is $\sim e^{-m_8 r}$,

which depends only on m_8 when $m_8 < m_g$. Therefore, the width of the flux density is not of order $m_g^{-1} \sim 10$ but is of order $m_8^{-1} \sim 1$.

Let us compare the non-Abelian vortex explained in this section with the Abelian vortices in Sect. 3.1. The $U(1)_B$ vortex is characterized by the first homotopy group $\pi_1[U(1)_B]$. As can be seen from Eq. (3.4), the $U(1)_B$ vortex has an integer winding number. Therefore, this vortex is called an integer vortex. The non-Abelian vortex is also characterized by $\pi_1[U(1)_B]$, but its winding number takes the value of a fractional number. The minimal winding number is quantized by 1/3. The vortices with fractional winding numbers are the so-called fractional vortices. To understand this, let us write the asymptotic behavior of Φ given in Eq. (3.33) at $r \to \infty$ as

$$\Phi \sim \Delta_{\rm CFL} e^{\frac{i\theta}{3}} \mathbf{1}_3. \tag{3.45}$$

Here "$\sim$" stands for the equivalence under the $SU(3)_C$ gauge transformation. This explicitly shows that the minimally winding non-Abelian vortex has only 1/3 winding number in the $U(1)_B$ space. Consequently, the circulation of the superfluid velocity in Eq. (2.63) obeys a fractional Onsager–Feynman quantization

$$c_B = \oint dx^i J_i^B = \frac{2\pi}{3} \frac{4K_3}{\gamma K_0} k \tag{3.46}$$

with the vortex number $k \in \pi_1[U(3)_{C-F+B}]$. This is 1/3 of the circulation (3.5) of a $U(1)_B$ vortex.[7]

Finding the minimally winding solution is very important to find which configuration is the most stable in the CFL phase. Since the non-Abelian vortex is a global vortex, its tension consists of two parts: a logarithmically divergent part and a finite part.

$$\mathcal{T}_{M_1} = \mathcal{T}_{{\rm div};M_1} + \mathcal{T}_{{\rm fin};M_1}. \tag{3.47}$$

A dominant contribution to the tension (logarithmically divergent) comes from the kinetic term as

$$\mathcal{T}_{{\rm div};M_1} \simeq K_3 \int d^2x \, {\rm Tr}\, \mathcal{D}_i \Phi (\mathcal{D}_i \Phi)^\dagger = \frac{1}{9} \times 6\pi \Delta_{\rm CFL}^2 K_3 \log \frac{L}{\xi}. \tag{3.48}$$

This should be compared with the tension of the $U(1)_B$ integer vortex given in Eq. (3.8). Since the minimal winding number of the non-Abelian vortex is 1/3, the tension of the non-Abelian vortex is $1/3^2 = 1/9$ times as large as that of the $U(1)_B$ integer vortex. Thus, we conclude that the non-Abelian vortex is the most stable string configuration in the CFL phase. In Sect. 4.3, we discuss how a $U(1)_B$ integer vortex decays into non-Abelian vortices.

Let us next consider the finite contribution to the vortex tension. We discuss the dependence of the energy on the coupling constant g_s. As shown in Eq. (3.48), the logarithmically divergent contribution to the tension does not depend on the gauge coupling. However, finite corrections to the energy do depend in general on the gauge coupling and on the various coefficients in the potential energy. These finite contributions have been numerically calculated as the behavior during a change in g_s in Ref. [356]. Figure 5 shows that the tension decreases monotonically with increasing gauge coupling. This behavior is generic and independent of the values of scalar masses. It can be intuitively understood by noticing the $1/g_s^2$ dependence in the kinetic terms for the gauge potentials.

[7] The rational Onsager–Feynman quantizations are known for superfluid ^{3}He [290,291,361], chiral p-wave superconductors [185,192,290,291,361], and spinor BECs [173,206,264,312], while irrational Onsager–Feynman quantizations are known for multi-gap or multi-component superconductors [27–29,152,258,329, 343,344] and multi-component (non-spinor) BECs [74,75,108,113,114,200,241,257].

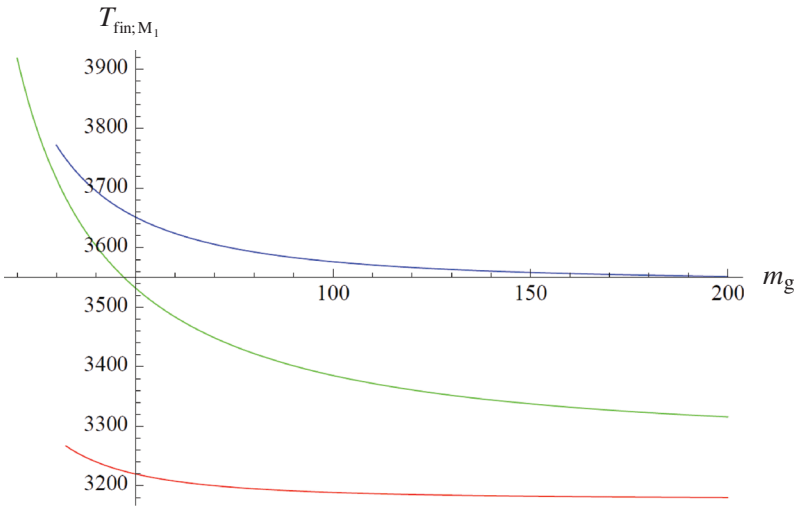

Fig. 5. The monotonic decreasing of the finite contribution to the tension of the vortex as a function of the gauge coupling g_{s}. The plot is against the mass of the gauge bosons m_{g}. The blue line corresponds to the "realistic" parameters: $\mu \sim 500\,\mathrm{MeV}$, $\Lambda \sim 200\,\mathrm{MeV}$, $T_{\mathrm{c}} \sim 10\,\mathrm{MeV}$, $T \sim 0.9T_{\mathrm{c}}$, which correspond to $\Delta_{\mathrm{CFL}} = 7\,\mathrm{MeV}$, $K_1 = 9$, $m_1 = 34\,\mathrm{MeV}$, $m_8 = 17\,\mathrm{MeV}$. The red and green lines correspond respectively to $(m_1, m_8) = (50\,\mathrm{MeV}, 10\,\mathrm{MeV})$ and $(m_1, m_8) = (10\,\mathrm{MeV}, 50\,\mathrm{MeV})$. The logarithmically divergent tension has been cut off at a distance $L = 0.4\,\mathrm{MeV}^{-1}$. Notice that the choice of L is arbitrary. A different value would correspond to a logarithmic shift in the total tension, but the monotonic decrease of the tension would be the same, since it is only given by the dependence on g_{s} of the finite term $\mathcal{T}_{\mathrm{fin;M_1}}$.

Let us next compare the color-magnetic fluxes of the non-Abelian vortices and non-topological color fluxes discussed in Sect. 3.2. As shown in Eq. (3.23), the flux of the 8th direction in the $SU(3)_c$ space of the Abelian vortex (in the limit of $\zeta = \pi/2$) is $4\sqrt{3}\pi/g_{\mathrm{s}}$. With the ansatz (3.26), the amount of flux of the non-Abelian vortex can be easily obtained as

$$A_i = -\sqrt{\frac{2}{3}}\frac{\epsilon_{ij}x^j}{g_{\mathrm{s}}r^2}(1-h)T_8 \quad \to \quad \Phi^8_{\mathrm{NA}} = \int d^2x\ F^8_{12} = \frac{1}{3} \times \Phi^8_{\mathrm{A}}. \tag{3.49}$$

Thus, with respect to the color-magnetic flux, the non-Abelian vortex is the minimal configuration in the CFL phase.

3.3.2. Non-minimal (M_2) non-Abelian vortices. A similar but slightly different vortex configuration from the minimal (M_1) vortices, called M_2 vortices, was also found in Ref. [35]. The ansatz for the M_2 vortex is quite similar to that in Eqs. (3.25) and (3.26) as

$$\Phi(r,\theta) = \Delta_{\mathrm{CFL}} \begin{pmatrix} q(r) & 0 & 0 \\ 0 & e^{i\theta}p(r) & 0 \\ 0 & 0 & e^{i\theta}p(r) \end{pmatrix}, \tag{3.50}$$

$$A_i(r,\theta) = -\frac{\epsilon_{ij}x^j}{g_{\mathrm{s}}r^2}\,(1-h(r)) \begin{pmatrix} -\frac{2}{3} & 0 & 0 \\ 0 & \frac{1}{3} & 0 \\ 0 & 0 & \frac{1}{3} \end{pmatrix}. \tag{3.51}$$

The ansatz for Φ can be rewritten as

$$\Phi(r,\theta) = \Delta_{\mathrm{CFL}} e^{i\frac{2\theta}{3}} \begin{pmatrix} e^{-i\frac{2\theta}{3}} & 0 & 0 \\ 0 & e^{i\frac{\theta}{3}} & 0 \\ 0 & 0 & e^{i\frac{\theta}{3}} \end{pmatrix} \begin{pmatrix} q(r) & 0 & 0 \\ 0 & p(r) & 0 \\ 0 & 0 & p(r) \end{pmatrix}. \tag{3.52}$$

This shows that an M_2 vortex has 2/3 winding in the $U(1)_B$ space, which is twice as large as that of an M_1 vortex. For the rest, the ansatz goes into the $SU(3)_C$ orbit; more explicitly, $S^1 \subset SU(3)_C$, which is generated by T_8. In comparison with the M_1 vortex given in Eqs. (3.25) and (3.26), one finds that the circulation of the M_2 vortex goes in the opposite direction in the $SU(3)_C$ orbit. Namely, the color of the M_1 vortex in Eq. (3.25) is $\bar{r} = gb$, while that of the M_2 vortex in Eq. (3.52) is $r = \overline{gb}$. Like the M_1 vortex, the tension of the M_2 vortex consists of a divergent part and a finite part. The divergent part is given by

$$\mathcal{T}_{\mathrm{div};M_2} = \frac{4}{9} \times 6\pi^2 \Delta_{\mathrm{CFL}}^2 K_3 \log \frac{L}{\xi}. \tag{3.53}$$

This is four times as large as the divergent part of the tension of the M_1 vortex. This implies that an M_2 vortex with a red flux decays into two M_1 vortices with green and blue colors with opposite directions, as illustrated in Fig. 11(b).

On the other hand, the color-magnetic flux contributions to the tension are almost the same as those of the M_1 vortex. This is because the differences are just $\bar{r}$ or r.

Notice that an M_1 vortex with winding number 2 has the same divergent tension as $\mathcal{T}_{\mathrm{div};M_2}$ because of

$$\Phi(r,\theta) = \Delta_{\mathrm{CFL}} e^{i\frac{2\theta}{3}} \begin{pmatrix} e^{i\frac{4\theta}{3}} & 0 & 0 \\ 0 & e^{-i\frac{2\theta}{3}} & 0 \\ 0 & 0 & e^{-i\frac{2\theta}{3}} \end{pmatrix} \begin{pmatrix} f_2(r) & 0 & 0 \\ 0 & g_2(r) & 0 \\ 0 & 0 & g_2(r) \end{pmatrix}. \tag{3.54}$$

For the finite contribution of the color-magnetic flux to the energy, the M_2 vortex has lower cost since the M_1 vortex with winding number 2 has a color-magnetic flux twice as great as that of an M_2 vortex.

3.3.3. Orientational zero modes of non-Abelian vortices. Minimal (M_1) non-Abelian vortices

The vortices in the CFL phase are called non-Abelian vortices because they carry color magnetic fluxes, or equivalently the color gauge $SU(3)_C$ transformation participate in the loop in the order parameter space. The three configurations in Eqs. (3.25)–(3.28) carry corresponding color magnetic fluxes. Since these configurations cannot be transformed into each other by the gauge transformation, these are all physically different vortices. However, note that the above three vortices do not exhaust all possible configurations. Indeed, there exists a continuous family of an infinite number of vortex configurations. To see it, let us decompose the ansatz Eqs. (3.25) and (3.26) as

$$\Phi = \Delta_{\mathrm{CFL}} \mathrm{diag}(f e^{i\theta}, g, g) \sim \Delta_{\mathrm{CFL}} e^{\frac{i\theta}{3}} \left(\frac{F}{3} \mathbf{1}_3 + \sqrt{\frac{2}{3}} G T_8 \right), \tag{3.55}$$

where we have introduced

$$F \equiv f + 2g, \quad G \equiv f - g \tag{3.56}$$

and have transformed the configuration by a certain $SU(3)_C$ gauge symmetry. Continuously degenerate configurations can be obtained by the color–flavor rotation as

$$\Phi \to \Delta_{\mathrm{CFL}} e^{\frac{i\theta}{3}} \left(\frac{F}{3} \mathbf{1}_3 + \sqrt{\frac{2}{3}} G U T_8 U^\dagger \right), \quad U \in SU(3)_{\mathrm{C+L+R}}. \tag{3.57}$$

The three configurations in Eqs. (3.25)–(3.28) are particular diagonal configurations. It is now obvious that the color–flavor $SU(3)_{\mathrm{C+L+R}}$ symmetry of the ground state in the CFL phase is *spontaneously* broken in the presence of a non-Abelian vortex because of the term proportional to T_8 in

Eq. (3.55). In the vortex core, there remains the unbroken symmetry

$$K = U(1)_{\rm C+L+R} \times SU(2)_{\rm C+L+R} \tag{3.58}$$

where $U(1)_{\rm C+L+R}$ is the Abelian subgroup generated by T_8 and $SU(2)_{\rm C+L+R}$ is a $SU(2)$ subgroup that commutes with $U(1)_{\rm C+L+R}$. Therefore, there appear, in the *vicinity* of the vortex, Nambu–Goldstone (NG) modes associated with this spontaneous symmetry breaking:

$$\frac{H_{\rm CFL}}{K} = \frac{SU(3)_{\rm C+L+R}}{U(1)_{\rm C+L+R} \times SU(2)_{\rm C+L+R}} \simeq \mathbb{C}P^2. \tag{3.59}$$

This space is known as the 2D complex projective space. These modes are called the orientational moduli (collective coordinates) of the non-Abelian vortex. The existence of these modes was first pointed out in Ref. [242] in the context of dense QCD, but it was known before in the context of supersymmetric QCD, as summarized in Appendix A. Points on the $\mathbb{C}P^2$ manifold correspond to the different fluxes. One can move from point to point by $SU(3)_{\rm C+L+R}$.

The order parameter of the breaking of $SU(3)_{\rm C+L+R}$ is $|G| = |f - g|$. Since both f and g asymptotically reach 1 at the boundary, the color–flavor-locked symmetry is not broken far from the non-Abelian vortex. On the other hand, as can be seen in Fig. 4, $|G|$ takes a maximum value at the center of the non-Abelian vortex. Hence, we expect that the orientational NG modes are localized on the non-Abelian vortex. In Sect. 5, we prove that the orientational modes are in fact normalized and propagate along the non-Abelian vortex as gapless excitations. We construct the low-energy effective theory of these modes on the vortex world-volume.

Non-minimal ($\rm M_2$) non-Abelian vortices

Let us next consider the orientation of the $\rm M_2$ vortex. Going away from the $\rm M_2$ vortex, one asymptotically reaches the ground state where the $SU(3)_{\rm C+L+R}$ color–flavor symmetry holds. On the other hand, since the condensation field Φ at the center of the $\rm M_2$ vortex is

$$\Phi \propto {\rm diag}(1, 0, 0), \tag{3.60}$$

the color–flavor symmetry that does not change this is the same as that for the M1 vortex. Namely, $U(1)_{\rm C+L+R} \times SU(2)_{\rm C+L+R}$. There the $\rm M_2$ vortex also has the orientational zero modes

$$\frac{H_{\rm CFL}}{K} = \frac{SU(3)_{\rm C+L+R}}{U(1)_{\rm C+L+R} \times SU(2)_{\rm C+L+R}} \simeq \mathbb{C}P^2. \tag{3.61}$$

However, the symmetry restored at the center of an $\rm M_2$ vortex is not $U(1)_{\rm C+L+R} \times SU(2)_{\rm C+L+R}$ but is enlarged to $U(1)_{\rm C+L+R} \times SU(2)_{\rm L+R} \times SU(2)_{\rm C}$. The restoration of the gauge symmetry $SU(2)_{\rm C}$ is in sharp contrast to the $\rm M_1$ vortex, for which no gauge symmetries are recovered.

4. Dynamics of vortices

The dynamics of non-Abelian semi-superfluid vortices are generally similar to those of vortices in superfluids and atomic BEC, which have been studied extensively [125,126,199]. (From a field theoretical point of view, see Refs. [231,265].) In Sect. 4.1, we construct the effective field theory of translational zero modes, known as Kelvin modes, and study the dynamics of a single vortex string in terms of the low-energy effective theory. In Sect. 4.2, the intervortex force between two non-Abelian vortices is derived and the dynamics of two vortices and a vortex ring is summarized. In Sect. 4.3, we discuss the decaying process of a $U(1)_{\rm B}$ Abelian superfluid vortex ($\rm M_2$ vortex) into a set of three (two) non-Abelian vortices. The creation of vortices and formation of a colorful lattice of non-Abelian vortices under rotation are discussed in Sect. 4.4. In Sect. 4.5, we discuss the relation between relativistic strings in relativistic scalar field theories and superfluid vortices.

4.1. The translational zero modes (Kelvin modes)

4.1.1. The effective theory of translational zero modes. In this subsection, we study the dynamics of vortices in terms of the effective field theory. Here, we concentrate on translational zero modes, which are common for $U(1)$ Abelian vortices and non-Abelian vortices, so that we calculate in $U(1)$ Abelian vortices. The dynamics of orientational zero modes is studied in the next section.

The existence of a vortex spontaneously breaks the translational symmetry. When a vortex is placed along the z-axis, it breaks two translational symmetries in the x–y plane. When the vortex string fluctuates, the configuration can be written as

$$\Phi = f(\bar{r})e^{i(\bar{\theta}+\alpha)}, \quad \bar{r} = \sqrt{(x-X)^2+(y-Y)^2}, \\ \bar{\theta} = \tan^{-1}\left(\frac{y-Y}{x-X}\right), \tag{4.1}$$

where $X = X(t,z)$ and $Y = Y(t,z)$ denote the position of the vortex in the x–y plane, which is a field in the vortex world-sheet, and $(\bar{r},\bar{\theta})$ are the polar coordinates from the vortex center. Inserting Eq. (4.1) into Eq. (2.56), and integrating the Lagrangian density over the x–y plane, we obtain the effective theory [207]

$$\mathcal{L}_{\rm eff} = -\mathcal{T} + 4\pi\gamma K_0(Y\partial_t X - X\partial_t Y) - \frac{\mathcal{T}}{2}[(\partial_z X)^2 + (\partial_z Y)^2], \tag{4.2}$$

up to the quadratic order of X and Y and the leading order in derivatives. Here, $\mathcal{T}$ is the tension of the vortex, given in Eq. (3.8) for a $U(1)_{\rm B}$ vortex and Eq. (3.48) for a non-Abelian vortex. For a vortex in $d = 2+1$, the second term can be found in Refs. [231,265]. The first and third terms in Eq. (4.2) are consistent with the spatial part of the Nambu–Goto action [153,245] at this order:

$$\mathcal{L}_{\rm NG} = -\mathcal{T}\sqrt{1-(\partial_z X)^2-(\partial_z Y)^2}. \tag{4.3}$$

Let us remark on the effective Lagrangian in Eq. (4.2). Because the time derivative is at the first order in the Lagrangian, X and Y are not independent fields; rather, they are momentum conjugate to each other:

$$P_X = \frac{\partial\mathcal{L}}{\partial(\partial_t X)} \sim Y, \quad P_Y = \frac{\partial\mathcal{L}}{\partial(\partial_t Y)} \sim X. \tag{4.4}$$

Therefore, although two translational symmetries are broken, there appears only one independent gapless Nambu–Goldstone mode, known a Kelvin mode or Kelvon if quantized. There are two typical solutions of the effective Lagrangian (4.2):

$$X_1 = A\cos(k_z z - \omega t + \delta_1), \quad Y_1 = A\sin(k_z z - \omega t + \delta_1), \tag{4.5}$$

$$X_2 = A\sin(k_z z + \omega t + \delta_2), \quad Y_2 = A\cos(k_z z + \omega t + \delta_2), \tag{4.6}$$

where δ_1 and δ_2 are arbitrary constants. The first and second solutions show the clockwise and counterclockwise spiral Kelvin waves propagating along the vortex string in opposite directions, as illustrated in Fig. 6. The Kelvin waves have "chirality": the (counter)clockwise waves can propagate only in one (the other) direction, which is well known in superfluids.

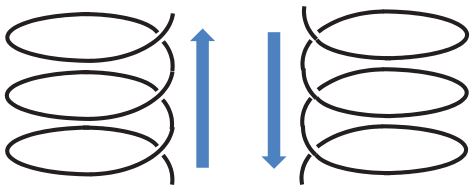

Fig. 6. Kelvin waves. The Kelvin waves in Eqs. (4.5) and (4.6) propagate in definite directions indicated by the arrows.

Since X and Y are not independent but are momentum conjugate to each other, there is only one dispersion relation

$$\omega = \frac{\mathcal{T}}{4\pi\gamma K_0} k_z^2, \tag{4.7}$$

which is quadratic. The Kelvon is an example of type-II Nambu–Goldstone modes.[8]

Defining $\psi \equiv X + iY$, the effective Lagrangian in Eq. (4.2) can be rewritten as

$$\mathcal{L}_{\text{eff}} = -\mathcal{T} + 2\pi i\gamma K_0(\psi^*\partial_t\psi - \psi\partial_t\psi^*) - \frac{\mathcal{T}}{2}|\partial_z\psi|^2. \tag{4.8}$$

The two comments are addressed here. The translational modes are exact Nambu–Goldstone modes only for an infinite system size. For a finite system, a gap as a correction is present in the effective theory [207]:

$$\mathcal{L}_{\text{gap}} = \frac{\pi}{R^2}(X^2 + Y^2), \tag{4.9}$$

which is "tachyonic." However, this does not imply instability in non-relativistic cases. Instead, the chirality is broken because of this term: Kelvin waves with wavelengths longer than some critical length propagate in a direction opposite to that of modes with shorter lengths, which is contrary to conventional understanding.

When one includes higher order terms as the next-leading order, one obtains the nonlinear term $V \sim |\psi|^4$ as the potential in the effective Lagrangian. The Euler–Lagrange equation of the total Lagrangian is a nonlinear Schrödinger equation, which is integrable and and admits soliton solutions. These solitons describe nonlinear waves propagating along the vortex string, known as Hasimoto solitons [162].

[8] When a continuous symmetry is spontaneously broken in *relativistic* field theories, there appear as many Nambu–Goldstone modes as the number of broken generators (for internal symmetries), but this is not the case for *non-relativistic* field theories. The type-I and II Nambu–Goldstone modes are defined as gapless modes with linear and quadratic dispersion relations, respectively. For spontaneously broken *internal* symmetries, it has been proved in Refs. [168,363] that one type-I Nambu–Goldstone mode corresponds to one broken generator and one type-II Nambu–Goldstone mode corresponds to two broken generators, showing the saturation of the equality of the Nielsen–Chadha inequality [250], $N_{\text{I}} + 2N_{\text{II}} \geq N_{\text{BG}}$, where N_{I}, N_{II}, and N_{BG} are the numbers of type-I and type-II Nambu–Goldstone modes and spontaneously broken generators, respectively. However, there is no general statement for space-time symmetries for either relativistic or non-relativistic theories. The presence of a vortex breaks the rotational and translational symmetries but the former do not give independent Nambu–Goldstone modes [186] (see also Ref. [77]), since a rotation can be reproduced by infinitesimal local translations [222]. Then, the equality of the Nielsen–Chadha inequality is saturated for both the relativistic and non-relativistic cases if one counts only translational modes [207]. See also Ref. [260] for a discussion of Nambu–Goldstone modes for space-time symmetry in the presence of a vortex.

4.1.2. Magnus and inertial forces. Here, we restrict ourselves to $2+1$ dimensions. The translational zero modes X and Y are free fields in the leading order. Let us consider multiple vortices with the position (X_i, Y_i) of the ith vortex. The effective Lagrangian of interacting vortices can be written as

$$\mathcal{L}_{\rm eff} = \sum_i [-\mathcal{T} + 4\pi\gamma K_0 (Y_i \partial_t X_i - X_i \partial_t Y_i)] - E_{\rm int}(X_i, Y_i) \tag{4.10}$$

where $E_{\rm int}$ is the interaction energy among vortices, which is calculated in the next subsection. The interaction of vortices with an external superfluid velocity can be introduced by the Galilei transformation

$$(X', Y') = (X, Y) - (J_x^{\rm B,ext}, J_y^{\rm B,ext})t \tag{4.11}$$

with an external superfluid velocity $J_{x,y}^{\rm B,ext}$:

$$\begin{aligned}\mathcal{L}_{\rm eff} = &\sum_i [-\mathcal{T} + 4\pi\gamma K_0 (Y_i \partial_t X_i - X_i \partial_t Y_i)] \\ &- E_{\rm int}(X_i, Y_i) - 4\pi\gamma K_0 \sum_i (Y_i J_x^{\rm B,ext} - X_i J_y^{\rm B,ext}).\end{aligned} \tag{4.12}$$

The equations of motion in the presence of contributions from other vortices and an external flow can be written as

$$\begin{aligned}4\pi\gamma K_0 \frac{\partial X^i}{\partial t} &= +\frac{\partial E_{\rm int}}{\partial Y^i} + 4\pi\gamma K_0 J_x^{\rm B,ext} \\ 4\pi\gamma K_0 \frac{\partial Y^i}{\partial t} &= -\frac{\partial E_{\rm int}}{\partial X^i} + 4\pi\gamma K_0 J_y^{\rm B,ext}.\end{aligned} \tag{4.13}$$

The first terms on the right-hand sides are called the inertial force.

The dissipation is present at finite temperature as the term proportional to $K_{\rm D}$ in Eq. (2.58). It is known that the contributions from the dissipation can be taken into account in the equations of motion in Eq. (4.13) as [125,126,199]

$$\begin{aligned}4\pi\gamma K_0 \frac{\partial X^i}{\partial t} &= +\frac{\partial E_{\rm int}}{\partial Y^i} + 4\pi\gamma K_0 J_x^{\rm B,ext} - K_{\rm D}\frac{\partial E_{\rm int}}{\partial X^i} - K_{\rm D} J_y^{\rm B,ext}, \\ 4\pi\gamma K_0 \frac{\partial Y^i}{\partial t} &= -\frac{\partial E_{\rm int}}{\partial X^i} + 4\pi\gamma K_0 J_y^{\rm B,ext} - K_{\rm D}\frac{\partial E_{\rm int}}{\partial Y^i} + K_{\rm D} J_x^{\rm B,ext}.\end{aligned} \tag{4.14}$$

The third and fourth terms on the right-hand sides are called the Magnus forces, both proportional to the coefficient $K_{\rm D}$ of the dissipation term in Eq. (2.58). In particular, the third term is a contribution from the other vortices and the fourth term is a contribution from the external flow. Note that the Magnus forces exist only when the dissipation $K_{\rm D}$ is present at finite temperature. When a vortex moves with velocity v, there is an external flow in the rest frame of the vortex. Therefore, the vortex feels the Magnus force from the external flow as illustrated in Fig. 7. The trajectories of the vortex and anti-vortex are bent into the directions of $f_{\rm Magnus}$, as a curve ball in fluid dynamics.

4.2. Interaction between non-Abelian vortices

In this subsection, we study the interaction between two vortices with general orientation in the internal space at large distance [242,243].

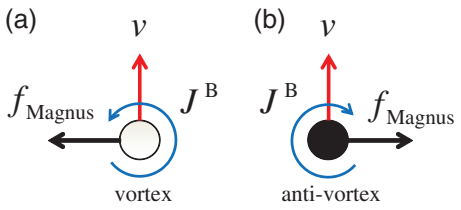

Fig. 7. Magnus force. v is the velocity of a moving vortex or anti-vortex. f_{Magnus} is the Magnus force. The trajectories of the vortex and anti-vortex are bent into the direction of f_{Magnus}, as a curve ball.

4.2.1. Intervortex force. We first take one vortex as a reference Φ_0,

$$\Phi_0 = \text{diag}(e^{i\theta} f, g, g). \tag{4.15}$$

Then, the other vortex Φ with general orientation in $\mathbb{C}P^2$ relative to the reference vortex should be obtained by $SU(3)_{\text{C+F}}$ transformation to Φ_0. When we consider two vortices only, only an $SU(2)_{\text{C+F}}$ ($\subset SU(3)_{\text{C+F}}$) rotation is enough to be considered for relative orientation to Φ_0 without loss of generality:

$$\Phi = \Phi_0 U_{\text{F}} = \begin{pmatrix} \begin{pmatrix} e^{i\theta} f & 0 \\ 0 & g \end{pmatrix} u_{\text{F}}^{-1} & \begin{matrix} 0 \\ 0 \end{matrix} \\ \begin{matrix} 0 & 0 \end{matrix} & g \end{pmatrix} = \begin{pmatrix} \begin{pmatrix} e^{i\theta} af & e^{i\theta} bf \\ -b^* g & a^* g \end{pmatrix} & \begin{matrix} 0 \\ 0 \end{matrix} \\ \begin{matrix} 0 & 0 \end{matrix} & g \end{pmatrix}, \tag{4.16}$$

where $u_{\text{F}} \equiv \begin{pmatrix} a^* & -b \\ b^* & a \end{pmatrix}$ (with $|a|^2 + |b|^2 = 1$) is an element of $SU(2)_{\text{F}}$. This corresponds to a $\mathbb{C}P^1$ submanifold in the whole $\mathbb{C}P^2$. Any color gauge transformation keeps the physical situation unchanged if they are regular. Here we implement a *twisted* color transformation of $SU(2)_{\text{C}}$, given by

$$u_{\text{C}}(\theta, r) = \begin{pmatrix} a^* & -be^{i\theta F(r)} \\ b^* e^{-i\theta F(r)} & a \end{pmatrix} \tag{4.17}$$

with $F(r)$ being an arbitrary regular function with boundary conditions $F(0) = 0$ and $F(\infty) = 1$. The former condition has been imposed to make the transformation regular at the center of the string. This is possible because $\pi_1[SU(2)_{\text{C}}] = 0$. The upper left 2×2 minor matrix of Φ in Eq. (4.16) is transformed to

$$\begin{aligned} u_{\text{C}}(r, \theta) \begin{pmatrix} e^{i\theta} af & e^{i\theta} bf \\ -b^* g & a^* g \end{pmatrix} &= \begin{pmatrix} |a|^2 f e^{i\theta} + |b|^2 g e^{i\theta F} & a^* b \left[-e^{i\theta F} + f e^{i\theta} \right] \\ ab^* \left[-1 + f e^{i(1-F)\theta} \right] & |a|^2 g + |b|^2 f e^{i(1-F)\theta} \end{pmatrix} \\ &\simeq \begin{pmatrix} e^{i\theta} & 0 \\ 0 & 1 \end{pmatrix} \quad \text{for} \quad r \gg m_1^{-1}, m_8^{-1}, m_{\text{g}}^{-1}. \end{aligned} \tag{4.18}$$

This result means that $\Phi \simeq \Phi_0$ for the large distance $r \gg m_1^{-1}, m_8^{-1}, m_{\text{g}}^{-1}$. Also, the fully opposite orientation can be obtained by another color gauge transformation,

$$\begin{aligned} &\begin{pmatrix} e^{-i\theta F(r)} & 0 \\ 0 & e^{i\theta F(r)} \end{pmatrix} u_{\text{C}} \begin{pmatrix} f e^{i\theta} & 0 \\ 0 & g \end{pmatrix} u_{\text{F}}^{-1} \\ &\simeq \begin{pmatrix} 1 & 0 \\ 0 & e^{i\theta} \end{pmatrix} \quad \text{for} \quad r \gg m_1^{-1}, m_8^{-1}, m_{\text{g}}^{-1}. \end{aligned} \tag{4.19}$$

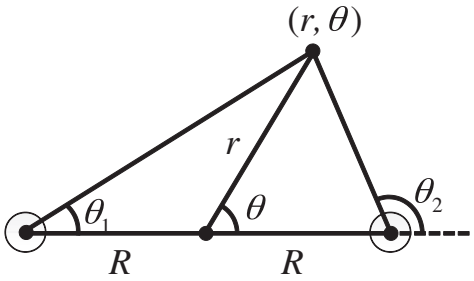

Fig. 8. A configuration of two semi-superfluid non-Abelian vortices with interval $2R$ in the polar coordinates (r, θ). $r_{1,2}$ is the distance from the vortices $\Phi_{1,2}$, and $\theta_{1,2}$ is the angle around them.

Note that one cannot change the topological number by use of this kind of regular gauge transformation. We have thus seen that spatial infinity of the string configurations is the same and does not depend on the orientational zero modes. This is just a consequence of the fact that the orientational zero modes are normalizable.

All semi-superfluid vortices with general orientation are equivalent to each other away from the core. In other words, vortices rotated by the flavor $SU(2)_{\rm F}$ revert to the reference vortex given by Eq. (4.15) via the color gauge transformation at much longer distances than the coherence length. This fact simplifies the problem of the static long range force between two strings significantly.

Here, we consider the interaction between arbitrary two vortices Φ_1 and Φ_2 placed at $(r, \theta) = (R, \pi)$ and $(R, 0)$ in parallel along the z-axis; see Fig. 8. We eventually decide on the expression of a long range static force between two strings, which is valid if the strings are sufficiently separated. The interval between strings is much larger than both the coherence length and the penetration depth: $R \gg m_1^{-1}, m_8^{-1}, m_{\rm g}^{-1}$. The first vortex Φ_1 is approximated everywhere by the asymptotic profile (4.15): $\Phi_1 = {\rm diag}\left(e^{i\theta_1}, 1, 1\right)$. The second string Φ_2 has the profile (4.16) with general orientation relative to Φ_1. At the large distance of interest, however, it is equivalent to the reference string configuration (4.15): $\Phi_2 \simeq {\rm diag}\left(e^{i\theta_2}, 1, 1\right)$. $\Phi_{1,2}$ becomes an anti-string by changing the signs of $\theta_{1,2}$.

The total profile of the two string system is given by the Abrikosov ansatz:

$$\Phi_{\rm tot} = \Phi_1 \Phi_2, \quad A^\theta_{\rm tot} = A^\theta_1 + A^\theta_2. \tag{4.20}$$

The first ansatz does not depend on the ordering of the matrices because the second vortex transforms to diagonal at large distances, as shown in Sect. 3. $A^\theta_{1,2}$ is the gauge field configuration accompanied with the single string system of $\Phi_{1,2}$. For an anti-vortex, $A^\theta_{1,2}$ changes the signs.

In order to obtain the static force between them, we first calculate the interaction energy density of the two string system, which is obtained by subtracting two individual string energy densities from the total configuration energy density;

$$\begin{aligned} \mathcal{E}_{\rm int}(r, \theta, R) &\simeq {\rm Tr}\left(|D\Phi_{\rm tot}|^2 - |D\Phi_1|^2 - |D\Phi_2|^2\right) \\ &= \pm\frac{2}{3}\left[\frac{-R^2 + r^2}{R^4 + r^4 - 2R^2 r^2 \cos(2\theta)}\right], \end{aligned} \tag{4.21}$$

where we have neglected the potentials $V(\Phi_{\rm tot}) = V(\Phi_1) = V(\Phi_2) = 0$ and the field strength $F^a_{ij} F^{aij} = 0$ at large distance [270]. Here and below, the upper (lower) sign indicates the quantity for the vortex–vortex (vortex–anti-vortex) configuration.

The tension, the energy of the string per unit length, is obtained for $R \ll L$ by integrating the energy density over the x–y plane as

$$E_{\rm int}(R, L) = \pm \int_0^L dr \int_0^{2\pi} d\theta r \mathcal{E}_{\rm int}(r, \theta, R) = \pm \frac{2\pi}{3} \left[-\log 4 - 2\log R + \log\left(R^2 + L^2\right) \right], \tag{4.22}$$

where the system size L has been introduced as the IR cutoff. The force between the two vortices is obtained by differentiating E by the interval:

$$f(a, L) = \mp \frac{\partial E_{\rm int}}{2\partial R} = \pm \frac{2\pi}{3} \left(\frac{1}{R} - \frac{R}{R^2 + L^2} \right) \simeq \pm \frac{2\pi}{3R}, \tag{4.23}$$

where the last expression is for $L \to \infty$. We can see that the force is repulsive (attractive) for the vortex–vortex (vortex–anti-vortex) configuration. The overall factors $1/3$ in Eqs. (4.21)–(4.23) are attributed to the fact that the tension of the fundamental non-Abelian vortex is reduced by $1/3$ compared to the usual Abelian vortex, then leading to $1/3$ erosion in the magnitude of the force.

Note that the result does not depend on whether the superconductivity is of type I or II. This has an important meaning in the case of color superconductivity since, although the perturbation theory indicates the color superconductivity is of type I for the whole density regime [144], the most fundamental strings, semi-superfluid strings, can be stable at any density regime where the CFL phase is realized. This result also implies that the global $U(1)_{\rm B}$ superfluid vortices [128,183] $\Phi \simeq {\rm diag}(e^{i\theta}, e^{i\theta}, e^{i\theta})$, studied in Sect. 3.1.1, as well as the M_2 vortices [35] $\Phi \simeq {\rm diag}(1, e^{-i\theta}, e^{-i\theta}) \simeq (e^{2i\theta}, 1, 1)$, studied in Sect. 3.3.2, are both unstable to decay into 3 or 2 semi-superfluid vortices, respectively, as discussed in Sect. 4.3.

This contrasts with the case of global non-Abelian vortices [244], discussed in Sect. 10, where the $U(1)$ Abelian string is marginally unstable, i.e., no force exists between two strings with opposite orientations.

The force between two vortices at a short distance remains an important problem. In this regard, the intervortex force at arbitrary distance was calculated in a related model in which $U(1)_{\rm B}$ is gauged [26].

4.2.2. Dynamics of two vortices and a vortex ring. We denote the positions of two vortices by (X_1, Y_1) and (X_2, Y_2). In the absence of the dissipation ($K_{\rm D} = 0$) at zero temperature, the equations of motion contain only the inertial force terms on the right-hand sides of Eq. (4.14). Then, the two vortices separated by the interval $2R$ rotate around each other, as in Fig. 9(a):

$$X_1 + iY_1 = -X_2 - iY_2 = R\exp(it/R^2), \tag{4.24}$$

where we set the coefficients at one. On the other hand, a vortex and an anti-vortex move parallel to each other due to the inertial force, as in Fig. 9(b):

$$X_1 + iY_1 = -X_2 + iY_2 = R + i(1/R)t, \tag{4.25}$$

where we set the coefficients at one. The velocity of the pair is faster when the distance between them is smaller.

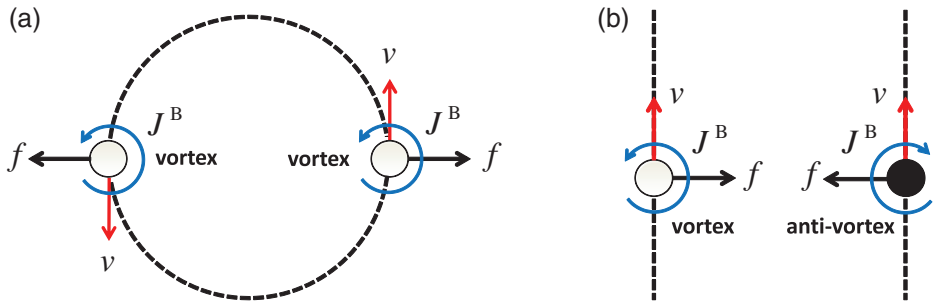

Fig. 9. Dynamics of two vortices. (a) Two vortices repelling each other rotate around each other by the inertial force represented by f in Eq. (4.23). The velocity is faster as the radius of the circular orbit is smaller. (b) A vortex and an anti-vortex attracting each other move parallel by the inertial force. The velocity is faster as the distance between them is shorter.

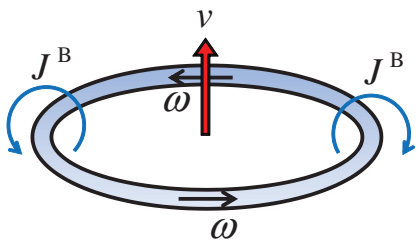

Fig. 10. A vortex ring. It moves in the direction perpendicular to the ring. The velocity is faster as the size of the ring is smaller. The red, black, and white arrows denote the velocity, vorticity, and flow, respectively.

Let us mention what happens when the dissipation term is present ($K_{\rm D} \neq 0$) at finite temperature. For a pair of vortices, the radius of the circle orbit gradually increases because of the Magnus force from each other, the second terms of Eq. (4.14). For a vortex and an anti-vortex, the distance between them gradually decreases due to the Magnus force from each other, and eventually they collide and annihilate each other.

The situation of a vortex and anti-vortex pair in $d = 2 + 1$ dimensions can be extended to a vortex ring in $3 + 1$ dimensions, as illustrated in Fig. 10. The vortex ring moves by the inertial force and is stable in the absence of the dissipation at zero temperature. In the presence of the dissipation at finite temperature, the radius of the ring decreases in time due to the Magnus force and eventually it decays. As the radius becomes smaller, the velocity becomes faster according to Eq. (4.25).

4.3. Decays of $U(1)_{\rm B}$ vortices and non-minimal M_2 non-Abelian vortices

The logarithmically divergent part of the tension of non-Abelian vortices is given in Eq. (3.48), while the tension of a $U(1)_{\rm B}$ integer vortex is given in Eq. (3.8). Therefore, the tension of a non-Abelian vortex is $1/3^2 = 1/9$ times as large as the tension of a $U(1)_{\rm B}$ vortex. Since the total energy of the constituent three non-Abelian vortices is $3 \times 1/9 = 1/3$ of that of the $U(1)_{\rm B}$ vortex when they are infinitely separated, we conclude that the $U(1)_{\rm B}$ vortex breaks up into three non-Abelian vortices with three different color fluxes, say red, blue, and green color fluxes, with total fluxes canceled out, as illustrated in Fig. 11(a):

$$\begin{aligned}\Phi &= \Delta_{\rm CFL}{\rm diag}\,(e^{i\theta}, e^{i\theta}, e^{i\theta}) \\ &\to \Delta_{\rm CFL}{\rm diag}\,(e^{i\theta_1}, 1, 1) \times {\rm diag}\,(1, e^{i\theta_2}, 1) \times {\rm diag}\,(1, 1, e^{i\theta_3}),\end{aligned} \tag{4.26}$$

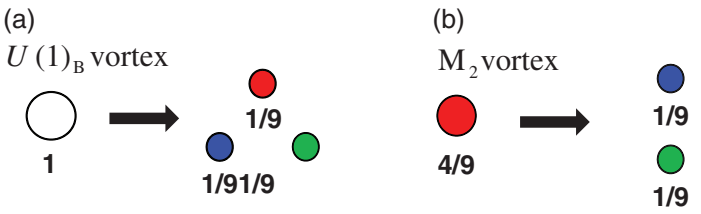

Fig. 11. Decays of a $U(1)_B$ superfluid vortex and an M_2 vortex. (a) A global $U(1)_B$ superfluid vortex decays into a set of three non-Abelian vortices with the total magnetic flux canceled out. (b) An M_2 vortex with a red magnetic flux decays into two M_1 vortices with green and blue magnetic fluxes directed in the opposite direction. The numbers represent the energy ratio when all of them are infinitely separated.

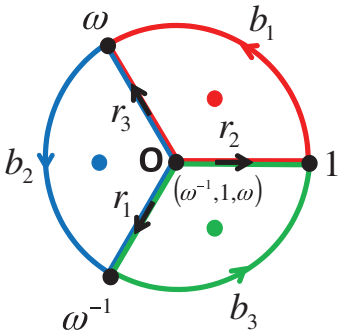

Fig. 12. Detailed configurations of decays of a $U(1)_B$ superfluid vortex. The $U(1)_B$ vortex initially located at the origin O decays into three non-Abelian vortices, denoted by the red, green, and blue dots. b_1, b_2, and b_3 are paths with angles $2\pi/3$ at the boundary at spatial infinity, and r_1, r_2, r_3 denote the paths from the origin O to spatial infinities. For b_1, b_2, and b_3, the $U(1)_A$ phase is rotated by $\exp[i\theta\,\mathrm{diag}(1,1,1)]$ with the angle θ of the polar coordinates.

where $\theta_{1,2,3}$ is the angle of polar coordinates at each vortex. In fact, in Sect. 4.2, we have seen that the interaction between two non-Abelian vortices is repulsive at large separation. There remains the possibility of metastability of the $U(1)_B$ vortices, since each vortex in Eq. (4.26) must carry a color magnetic flux that contributes finite energy corrections to the tension. However, they decay with perturbations. After the decay, these three vortices rotate as in Fig. 9, because of the inertial force. Without dissipation at zero temperature, they rotate forever, while the radius increases in the presence of the dissipation at a finite temperature.

In the same way, a non-minimal M_2 vortex also decays into two non-Abelian vortices, as in Fig. 11(b). Let us suppose that an M_2 vortex carries a red magnetic flux; it then decays into two M_1 vortices with green and blue magnetic fluxes directed in the opposite direction.

Next, let us show a detailed configuration of the decay process of a $U(1)_B$ Abelian vortex in Fig. 12. The Abelian vortex initially located at the origin O decays into three non-Abelian vortices, denoted by the red, green, and blue dots, carrying corresponding color fluxes. The red, blue, and green non-Abelian vortices are encircled by the paths

$$b_1 - r_3 + r_2, \quad b_2 - r_1 + r_3, \quad b_3 - r_2 + r_1 \tag{4.27}$$

respectively. At the boundary of spatial infinity, the $U(1)_B$ phase is rotated by $\exp[i\theta\,\mathrm{diag}(1,1,1)]$ with the angle θ of the polar coordinates from the origin O. Therefore, the $U(1)_B$ phase is rotated by $2\pi/3$ along each of the paths b_1, b_2, and b_3. Let us suppose that the three paths in Eq. (4.27) enclose the three configurations in Eqs. (3.25), (3.27), and (3.29), respectively. Then, we find that the *color*

gauge transformations $g(r) \in SU(3)_{\rm C}$ occur along the paths r_1, r_2, and r_3 as

$$\begin{aligned} r_1: \quad & g(r) = \exp[iu(r)\mathrm{diag}(0,-1,1)] = \begin{cases} \mathrm{diag}(1,1,1), & r=0 \\ \mathrm{diag}(1,\omega^{-1},\omega), & r=\infty \end{cases}, \\ r_2: \quad & g(r) = \exp[iu(r)\mathrm{diag}(1,0,-1)] = \begin{cases} \mathrm{diag}(1,1,1), & r=0 \\ \mathrm{diag}(\omega,1,\omega^{-1}), & r=\infty \end{cases}, \\ r_3: \quad & g(r) = \exp[iu(r)\mathrm{diag}(-1,1,0)] = \begin{cases} \mathrm{diag}(1,1,1), & r=0 \\ \mathrm{diag}(\omega^{-1},\omega,1), & r=\infty \end{cases}, \end{aligned} \tag{4.28}$$

respectively, with a monotonically increasing function $u(r)$ with the boundary conditions $u(r=0) = 0$ and $u(r=\infty) = 2\pi/3$.[9] We find that the origin O is consistently given by

$$\Phi = \Delta_{\rm CFL}\mathrm{diag}(\omega^{-1},1,\omega). \tag{4.29}$$

From a symmetry, permutations of each component are equally possible. The configuration of Fig. 12) is a $U(1)_{\rm B}$ vortex encircled by the path $b_1 + b_2 + b_3$ corresponding to unit circulation at large distance. However, at short distance, it is separated into a set of three non-Abelian vortices, each of which is encircled by the paths in Eq. (4.27). The paths r_i contribute to color magnetic fluxes and each b_i corresponds to 1/3 quantized circulation.

4.4. Colorful vortex lattices under rotation

4.4.1. Vortex formation and vortex lattices as a response to rotation in conventional superfluids.

Here we consider the response of the CFL matter to rotation. Let us first recall what happens if one rotates an ordinary superfluid. Suppose that one has a superfluid in a vessel; let us rotate the vessel with angular velocity Ω. The ground state of the system can be determined by minimizing the free energy. In a rotating system, the free energy is modified as $F' = F - \boldsymbol{\Omega}\cdot\boldsymbol{L}$, where $\boldsymbol{L}$ is the angular momentum vector. At low temperatures, the entropy term can be neglected and we just have to minimize $H' = H - \boldsymbol{\Omega}\cdot\boldsymbol{L}$, where H and H' are the Hamiltonian in the rest and rotating frames.

The time evolution of a rotating system is generated by H'. Let us first recall the reason for this using a simple example, a non-relativistic point particle in a rotating frame. The Lagrangian of a point particle with mass m is written as $L = m\boldsymbol{v}^2/2$, where $\boldsymbol{v}$ is the velocity in the rest frame. The conjugate momentum and the Hamiltonian are given by

$$\boldsymbol{p} = \frac{\partial L}{\partial \boldsymbol{v}} = m\boldsymbol{v}, \quad H = \boldsymbol{p}\cdot\boldsymbol{v} - L = \frac{m\boldsymbol{v}^2}{2}. \tag{4.30}$$

Now let us move to the description in the rotating frame at an angular velocity $\boldsymbol{\Omega}$. Let $\boldsymbol{v}'$ be the velocity of the particle in the rotating system. The two velocities are related by

$$\boldsymbol{v} = \boldsymbol{v}' + \boldsymbol{\Omega}\times\boldsymbol{r}. \tag{4.31}$$

Since the Lagrangian mechanics is covariant under general coordinate transformation, we can switch to the rotating frame just by substituting $\boldsymbol{v}'$ into $\boldsymbol{v}$,

$$L = \frac{m}{2}\left(\boldsymbol{v}' + \boldsymbol{\Omega}\times\boldsymbol{r}\right)^2. \tag{4.32}$$

[9] This route for the decomposition of an integer vortex into three fractional vortices is exactly the same as that of three-gap superconductors [258] and three-component Bose–Einstein condensates [75,113,257].

The conjugate momentum and Hamiltonian in the rotating system are given by

$$\boldsymbol{p}' = \frac{\partial L}{\partial \boldsymbol{v}'} = m(\boldsymbol{v}' + \boldsymbol{\Omega} \times \boldsymbol{r}) \, (= \boldsymbol{p}) \, , \quad H' = \boldsymbol{p}' \cdot \boldsymbol{v}' - L = \frac{\boldsymbol{p}'^2}{2m} - \boldsymbol{\Omega} \cdot \left(\boldsymbol{r} \times \boldsymbol{p}' \right) , \tag{4.33}$$

where we have used the cyclic property of the cross product, $\boldsymbol{p}' \cdot (\boldsymbol{\Omega} \times \boldsymbol{r}) = \boldsymbol{\Omega} \cdot (\boldsymbol{r} \times \boldsymbol{p}')$. Noting that $\boldsymbol{p}' = \boldsymbol{p}$, we can rewrite the Hamiltonian in the rotating frame as

$$\begin{aligned} H' &= \frac{\boldsymbol{p}'^2}{2m} - \boldsymbol{\Omega} \cdot \left(\boldsymbol{r} \times \boldsymbol{p}' \right) \\ &= \frac{\boldsymbol{p}^2}{2m} - \boldsymbol{\Omega} \cdot (\boldsymbol{r} \times \boldsymbol{p}) \\ &= H - \boldsymbol{\Omega} \cdot \boldsymbol{L}, \end{aligned} \tag{4.34}$$

which connects the Hamiltonians in the rest and rotating frames. The discussion above can be straightforwardly extended to many-body systems, as long as the interaction potential is invariant under rotation.

Now let us discuss the response of a superfluid to rotation. We consider the situation where a cylinder with radius R is filled with a superfluid and there is one vortex in the center of the vessel. Then the superfluid velocity is given by $\boldsymbol{v} = \frac{n}{2\pi r} \boldsymbol{e}_\theta$ with n the winding number. The energy of a vortex per unit length is

$$E = \int d^2x \frac{1}{2} \rho \, \boldsymbol{v}^2 = \frac{\rho n^2}{4\pi} \log \left(\frac{R}{a} \right) , \tag{4.35}$$

where ρ is the superfluid density and a is the core radius ($R \gg a$). The angular velocity per unit length is written as

$$L = \int d^2x \, (\boldsymbol{r} \times (\rho \boldsymbol{v}))_z = \int_a^R 2\pi r \cdot r\rho |\boldsymbol{v}| \simeq \frac{1}{2} n \rho R^2, \tag{4.36}$$

where the term proportional to a^2 is neglected. Thus, the energy in the rotating system is given by

$$E' = \frac{\rho n^2}{4\pi} \log \left(\frac{R}{a} \right) - \frac{1}{2} \Omega n \rho R^2. \tag{4.37}$$

If this energy is less than 0, one vortex state is favored compared to the state without a vortex. We can define the critical angular velocity $\Omega_{\rm c}$,

$$\Omega_{\rm c} \equiv \frac{n}{2\pi R} \log \left(\frac{R}{a} \right) . \tag{4.38}$$

Thus, if $\Omega > \Omega_{\rm c}$, the state with the vortex is more favorable than the trivial state.

If one further increases the rotational speed, multiple vortices are generated along the rotational axis. They all have the same winding number, so the intervortex force is repulsive. All the vortices repel each other, resulting in the formation of a vortex lattice. In the end, the vortex lattice co-rotates with the vessel, which means that the superfluid velocity at the edge coincides with the speed of the wall. Then the circulation Γ can be calculated as $2\pi R \cdot R\Omega$. This should be equal to the sum of the circulations of all the vortices inside the vessel, $\Gamma = nN$, where N is the total number of vortices. Therefore, the total number of vortices

$$N = \frac{2S\Omega}{n}, \tag{4.39}$$

where S is the cross section of the vessel. In the case of an ordinary superfluid, the circulation of each vortex is equal to one, $n = 1$.

Let us see the creation of vortices from another point of view. We here consider a BEC and denote the condensate by a complex scalar field $\Phi(x)$. In a rotating frame, the gradient term of the energy functional can be written as (see Eq. (4.34))

$$E_{\rm grad} = \Phi^* \left(\frac{\hat{\mathbf{p}}^2}{2m} - \mathbf{\Omega} \cdot \hat{\mathbf{L}} \right) \Phi = \frac{1}{2m} |[\partial_i - im(\mathbf{r} \times \mathbf{\Omega})_i]\Phi|^2 - \frac{1}{2} m r^2 \Omega^2 |\Phi|^2 \tag{4.40}$$

where $\hat{L}_i = i\epsilon_{ijk} r_j \partial_k$ and $\hat{p}_i = \partial_i$, and the equality is meant up to a total derivative. The combination $D_i = \partial_i - im(\mathbf{r} \times \mathbf{\Omega})_i$ can be seen as a covariant derivative on the field Φ. Then $A_i \equiv m\mathbf{r} \times \mathbf{\Omega}$ can be seen as a gauge field and this system looks like a charged field under a constant magnetic field $2\mathbf{\Omega}$. Therefore, just like a type II superconductor under an external magnetic field, vortices come into a rotating superfluid. Let us make a comment on the trapping potential. One should add an external potential to trap the condensate, such as $V_{\rm trap} = \frac{1}{2}\omega^2 r^2$ for BECs. This term and the last term in Eq. (4.40) can be combined as $-\frac{1}{2} r^2 \Omega^2 |\Phi|^2 + V_{\rm trap} = \frac{1}{2}(\omega^2 - \Omega^2) r^2 |\Phi|^2$. When the rotation speed Ω is less than ω, the condensates can be trapped.

4.4.2. Colorful vortex lattices. Then, what happens if one rotates CFL matter? We can repeat the energetical argument. When the vessel is large enough, the energy of a vortex is dominated by the superfluid velocity part and the contribution from the color flux is negligible, Thus, what is modified in the argument above is that n should be equal to one third, $n = 1/3$. For realistic neutron stars, the number of vortices can be estimated as

$$N_v \simeq 1.9 \times 10^{19} \left(\frac{1\,{\rm ms}}{P_{\rm rot}} \right) \left(\frac{\mu/3}{300\,{\rm MeV}} \right) \left(\frac{R}{10\,{\rm km}} \right)^2 , \tag{4.41}$$

where $P_{\rm rot}$ is the rotational period, μ is the baryon chemical potential, and the parameters are normalized by typical values. The corresponding intervortex spacing is given by

$$\ell \equiv \left(\frac{\pi R^2}{N_v} \right)^{1/2} \simeq 4.0 \times 10^{-6} {\rm m} \left(\frac{P_{\rm rot}}{1\,{\rm ms}} \right)^{1/2} \left(\frac{300\,{\rm MeV}}{\mu/3} \right)^{1/2} . \tag{4.42}$$

Since the intervortex spacing is far larger than the size of a vortex core, which is given by inverse gluon/meson masses, gluons and mesons would not affect the force between two vortices. The intervortex force is dominated by the exchange of $U(1)_{\rm B}$ phonons. This justifies the treatment above, in which we have only considered the contribution of $U(1)_{\rm B}$ circulations.

In the discussion using the free energy, we can only determine the ground state of the system. The dynamical process of vortex generation can be nontrivial, especially for non-Abelian vortices. Basically, as one gradually increases the speed of rotation, vortices enter one by one from the edge of the superfluid. However, in the case of the non-Abelian vortices, it has a color flux and one vortex cannot be created because of the color conservation. A vortex with unit $U(1)_{\rm B}$ winding number does not have a color flux, but it is energetically unstable. So, one plausible idea is that a $U(1)_{\rm B}$ vortex is created first; it then decays into three non-Abelian vortices, as discussed in Sect. 4.3. Such two-fold vortex generation is seen in the simulation of a rotating three-component BEC [75], in which integer-quantized vortices are created first and then decay into fractional vortices.

Another feature of rotating CFL matter is that the lattice is "colorful" in the sense that each vortex carries a color flux. There can be various patterns of the configurations of the colored vortices, with vanishing total color fluxes. In Fig. 13(a), we show a possibility for an "ordered" colorful vortex lattice. In this case, the color magnetic fluxes of each color constitute an Abrikosov lattice, and the total configuration itself neglecting colors is also in the form of an Abrikosov lattice. In general, even

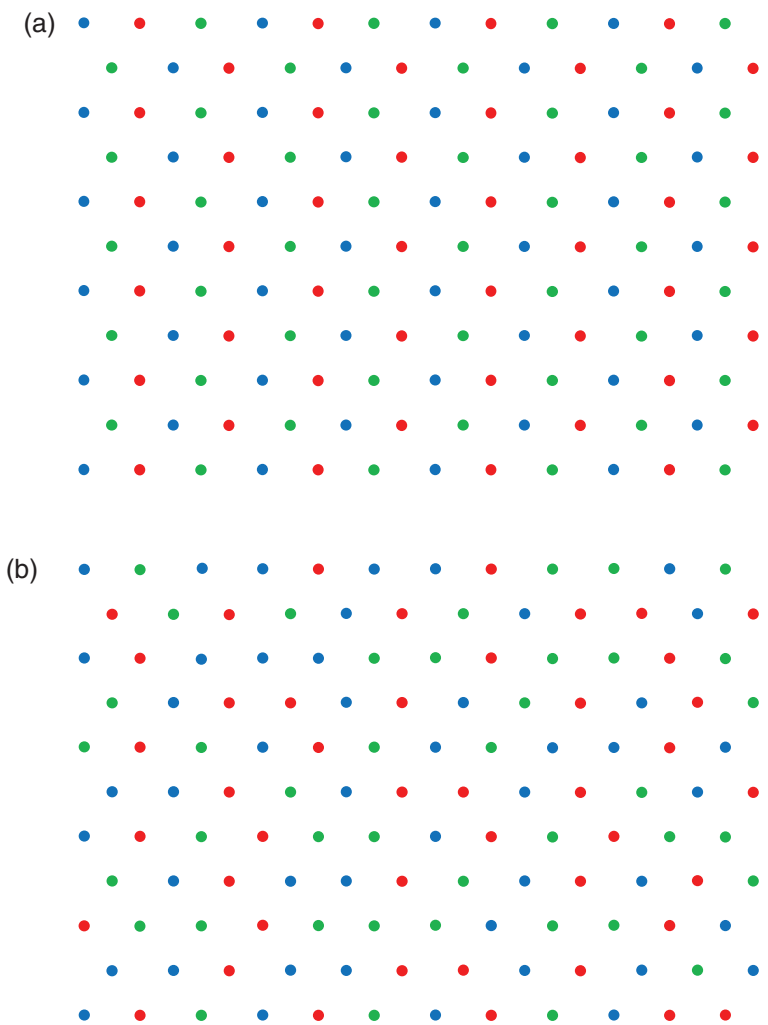

Fig. 13. Colorful vortex lattices in a rotating frame. Colors are (a) ordered and (b) disordered. In both cases, vortices ignoring color constitute an Abrikosov lattice, and total color fluxes are canceled out. (a) The color magnetic fluxes of each color constitute an Abrikosov lattice. (b) The color magnetic fluxes of each color *do not* constitute an Abrikosov lattice.

when the total configuration neglecting colors is in the form of an Abrikosov lattice, there may exist a vortex lattice that is "disordered" as in Fig. 13(b), in the sense that each color is placed at random with total colors canceled out. Even ordered, there can be a defect of color orderings.

In the simulation of a three-component BEC, ordered lattices have always been obtained, as mentioned above [75]. However, in this simulation, one has introduced a very small perturbation to split one integer vortex into three fractional vortices after the integer vortex lattice is formed. In this sense, there could be a defect of color ordering in general if several perturbations were introduced.

Gravitational waves from vortex lattices in the CFL phase (and the 2SC phase) were studied in Ref. [145] and compared with neutron star observations. However, vortex lattices of unstable color magnetic fluxes were assumed, so the calculation should be revised by considering colorful vortex lattices.

4.4.3. Tkachenko modes. A Tkachenko mode is a gapless excitation with a quadratic dispersion in the presence of a vortex lattice in a rotating system. This mode corresponds to deformation of the

lattice and the phonon does not appear independently; see Ref. [338] for a review of the Tkachenko modes. If one ignores the centrifugal force, there are approximate translational symmetries in the system, which are spontaneously broken by the lattice, resulting in an approximate type-II Nambu–Goldstone mode identified with the Tkachenko mode [364].

The Tkachenko mode should also exist in a vortex lattice of non-Abelian vortices, if the CFL phase is realized inside neutron stars. The characteristic timescale of this oscillation is consistent with the quasiperiodic oscillation, which is of the order of 100–1000 days, observed in the pulsars PSR B0531 + 21 and PSR B1828-11 [263,315]. It is an open question whether there is a color effect for the Tkachenko mode of a colorful vortex lattice.

4.5. Superfluid vortices from relativistic strings

A direct relation between a relativistic global vortex in a medium and a non-relativistic superfluid vortex was discussed in Refs. [85,223] and later also in the CFL phase [128]. When a relativistic global vortex is put into an uniform medium that violates the Lorentz invariance, it acquires a non-zero angular momentum and behaves as if it is a non-relativistic superfluid vortex [85]. To see this, let us consider the low energy effective theory for the $U(1)_{\rm B}$ Nambu–Goldstone mode at high density and zero temperature in Sect. 2.2.1,

$$\mathcal{L} = f_{\rm B}^2 \left[(\partial_0 \varphi_{\rm B} + 2\mu)^2 - v_{\rm B}^2 (\partial_i \varphi_{\rm B})^2 \right]. \tag{4.43}$$

Note that the time derivative $\partial_0 \varphi_{\rm B}$ is replaced by $\partial_0 \varphi_{\rm B} + 2\mu$ in order for the effective theory to have the same symmetry as the microscopic theory, QCD. Because of this peculiar dependence of μ, the order parameter gets the following time rotation:

$$e^{i\varphi_{\rm B}} \sim e^{-2i\mu t}. \tag{4.44}$$

As a result, a global $U(1)_{\rm B}$ vortex acquires a non-zero angular momentum [128]. From the time dependence in Eq. (4.44), one can easily see that a relativistic global string in a medium has non-zero angular momentum [128]:

$$M_{12} = K_0 \int d^2x \left(x_1 \partial_2 \phi^* \partial_0 \phi - x_2 \partial_1 \phi^* \partial_0 \phi \right) + \text{c.c.} \sim k\mu K_0. \tag{4.45}$$

Furthermore, by interpreting a dual of the Kalb–Ramond field strength $H^{\nu\lambda\rho}$ (completely antisymmetric tensor) as the superfluid velocity $\partial_\mu \varphi_{\rm B}$ [85,223],

$$2\mu\, \delta_{0\kappa} = \partial_\kappa \theta_{\rm B} \sim \epsilon_{\kappa\nu\rho\lambda} H^{\nu\lambda\rho}, \tag{4.46}$$

one can reproduce interaction similar to the inertial force of superfluid vortices, which is one of the peculiar properties of superfluid vortices; see Sect. 4.2.2. For instance, the stability of a moving vortex ring was shown in Refs. [83,85].

5. Dynamics of orientational zero modes

In this section, we review the dynamics of the orientational zero modes of non-Abelian vortices. In Sect. 5.1 we explain the low-energy effective theory for the orientational zero modes on a non-Abelian vortex world-sheet, which is a basis throughout this section. We include the effects of the strange quark mass in Sect. 5.2 and discuss the instability of non-Abelian vortices. The effects of electromagnetic interaction are taken into account in Sect. 5.3. In Sect. 5.4, we discuss quantum monopoles on a non-Abelian vortex. The monopoles form a bound state, which can be thought of as

bounded kinks that appear on the vortex world-sheet $\mathbb{C}P^2$ theory when we take quantum effects into account. Application to the quark–hadron duality is also discussed. Yang–Mills instantons trapped inside a non-Abelian vortex are discussed in Sect. 5.5.

5.1. Low-energy effective theory of orientational zero modes

As is shown in Sect. 3.3.3, the non-Abelian vortex has the internal orientational moduli $\mathbb{C}P^2$ associated with the spontaneous symmetry breaking of the color–flavor-locking symmetry. The orientational moduli are massless modes that propagate along the host non-Abelian vortex. In this subsection, we study the propagation of the massless orientational modes on a straight non-Abelian vortex. We assume that the vortex is on the z-axis.

In the rest of this subsection, we omit all the massive modes and concentrate on the orientational zero modes of $\mathbb{C}P^2$. Let us first identify the orientational zero modes in the background fields Φ and A_μ. We start with a particular non-Abelian vortex solution,

$$\Phi^\star(x,y) = \Delta_{\rm CFL} e^{\frac{i\theta}{3}} \left(\frac{F(r)}{3} \mathbf{1}_3 + G(r)\sqrt{\frac{2}{3}}\, T_8 \right),$$
$$A_i^\star(x,y) = -\frac{1}{g_{\rm s}} \frac{\epsilon_{ij}x^j}{r^2} h(r) \sqrt{\frac{2}{3}}\, T_8. \tag{5.1}$$

Then the general solution can be obtained by acting the color–flavor-locked symmetry on them as

$$\Phi(x,y) = U\Phi^\star U^\dagger = \Delta_{\rm CFL} e^{\frac{i\theta}{3}} \left(\frac{F(r)}{3} \mathbf{1}_3 - G(r) \langle \phi\phi^\dagger \rangle \right), \tag{5.2}$$

$$A_i(x,y) = UA_i^\star U^\dagger = \frac{1}{g_{\rm s}} \frac{\epsilon_{ij}x^j}{r^2} h(r) \langle \phi\phi^\dagger \rangle. \tag{5.3}$$

Here $\langle \mathcal{O} \rangle$ is the traceless part of a square matrix $\mathcal{O}$ and we introduced a complex 3-component vector ϕ that satisfies the following relation:

$$-\sqrt{\frac{2}{3}}\, UT_8U^\dagger = \phi\phi^\dagger - \frac{1}{3}\mathbf{1}_3 \equiv \langle \phi\phi^\dagger \rangle. \tag{5.4}$$

Taking the trace of this definition gives a constraint

$$\phi^\dagger\phi = 1. \tag{5.5}$$

Furthermore, the phase of ϕ is redundant by definition. Thus, we find that ϕ represents the homogeneous coordinates of $\mathbb{C}P^2$.

Now we promote the moduli parameters ϕ to the fields depending on the coordinates t, z of the vortex world-sheet by using the so-called moduli space approximation (first introduced by Manton for BPS monopoles [231,232]). Since we are interested in the low-energy dynamics of the orientational moduli fields, we restrict ourself to the study of the dynamics with a typical energy scale that is much lower than the mass scales of the original theory, namely m_1, m_8, and $m_{\rm g}$. Namely, we consider the situation where

$$|\partial_\alpha \phi(z,t)| \ll \min\left\{ m_1, m_8, m_{\rm g} \right\}, \quad (\alpha = z,t). \tag{5.6}$$

Omitting the higher derivative terms (massive modes) with respect to z and t, the low-energy effective theory for the orientational moduli field can be obtained by plugging $\Phi(x,y;\phi(z,t))$ and $A_i(x,y;\phi(z,t))$ into the full Lagrangian (2.7). Note that $\Phi(x,y;\phi(z,t))$ and $A_i(x,y;\phi(z,t))$

depend on the full spacetime coordinates, which are obtained by replacing the moduli parameter ϕ with the moduli field $\phi(z,t)$ in Eq. (5.3). In order to construct the Lagrangian of the effective theory, we also have to determine the x^α dependence of the gauge fields A_α, which are exactly zeros in the background solution. For this purpose, following Ref. [318], we make an ansatz

$$A_\alpha = \frac{i\rho_\alpha(r)}{g_{\rm s}}\left[\langle\phi\phi^\dagger\rangle, \partial_\alpha\langle\phi\phi^\dagger\rangle\right], \tag{5.7}$$

where $\rho_\alpha(r)$ ($\alpha = z,t$) are unknown functions of the radial coordinate r at this stage.

Substituting all the fields Φ and A_μ into Eq. (2.7), we are led to the effective Lagrangian that consists of two parts,

$$\mathcal{L}_{\rm eff} = \mathcal{L}^{(0)}_{\rm eff} + \mathcal{L}^{(3)}_{\rm eff}, \tag{5.8}$$

with

$$\mathcal{L}^{(0)}_{\rm eff} = \int dxdy\ {\rm Tr}\left[-\frac{\varepsilon_3}{2}F_{0i}F^{0i} + K_0\mathcal{D}_0\Phi^\dagger\mathcal{D}^0\Phi\right], \tag{5.9}$$

$$\mathcal{L}^{(3)}_{\rm eff} = \int dxdy\ {\rm Tr}\left[-\frac{1}{2\lambda_3}F_{3i}F^{3i} + K_3\mathcal{D}_3\Phi^\dagger\mathcal{D}^3\Phi\right]. \tag{5.10}$$

The Lagrangian of the $\mathbb{C}P^2$ model can be uniquely written up to the overall factors of the decay constants as

$$\mathcal{L}^{(\alpha)}_{\rm eff} = C^\alpha\mathcal{L}^{(\alpha)}_{\mathbb{C}P^2}, \tag{5.11}$$

$$\mathcal{L}^{(\alpha)}_{\mathbb{C}P^2} = \partial^\alpha\phi^\dagger\partial_\alpha\phi + \left(\phi^\dagger\partial^\alpha\phi\right)\left(\phi^\dagger\partial_\alpha\phi\right), \tag{5.12}$$

where no summation is taken for α. What we have to determine is the coefficient C^α in Eq. (5.11). After manipulating straightforward but complicated calculations given in Appendix C, we find that the coefficients are expressed as

$$C^0 = \frac{4\pi\alpha_3}{\lambda_3 g_{\rm s}^2}\int dr\frac{r}{2}\left[\rho_0'^2 + \frac{h^2}{r^2}(1-\rho_0)^2 + \frac{\beta_3 m_{\rm g}^2}{\alpha_3}\left((1-\rho_0)(f-g)^2 + \frac{f^2+g^2}{2}\rho_0^2\right)\right], \tag{5.13}$$

$$C^3 = \frac{4\pi}{\lambda_3 g_{\rm s}^2}\int dr\frac{r}{2}\left[\rho_3'^2 + \frac{h^2}{r^2}(1-\rho_3)^2 + m_{\rm g}^2\left((1-\rho_0)(f-g)^2 + \frac{f^2+g^2}{2}\rho_3^2\right)\right], \tag{5.14}$$

with $\alpha_3 \equiv \varepsilon_3\lambda_3$ and $\beta_3 \equiv K_0/K_3$. The coefficients $C^{0,3}$ should be determined in such a way that the energy is minimized. To this end, we regard the coefficients as "Lagrangian" for the undetermined scalar fields ρ_α. Namely, we should solve the Euler–Lagrange equations

$$\rho_0'' + \frac{\rho_0'}{r} + (1-\rho_0)\frac{h^2}{r^2} - \frac{\beta_3 m_{\rm g}^2}{2\alpha_3}\left[(f^2+g^2)\rho_0 - (f-g)^2\right] = 0, \tag{5.15}$$

$$\rho_3'' + \frac{\rho_3'}{r} + (1-\rho_3)\frac{h^2}{r^2} - \frac{m_{\rm g}^2}{2}\left[(f^2+g^2)\rho_3 - (f-g)^2\right] = 0, \tag{5.16}$$

with the boundary conditions

$$\rho_{0,3}(0) = 1, \qquad \rho_{0,3}(\infty) = 0. \tag{5.17}$$

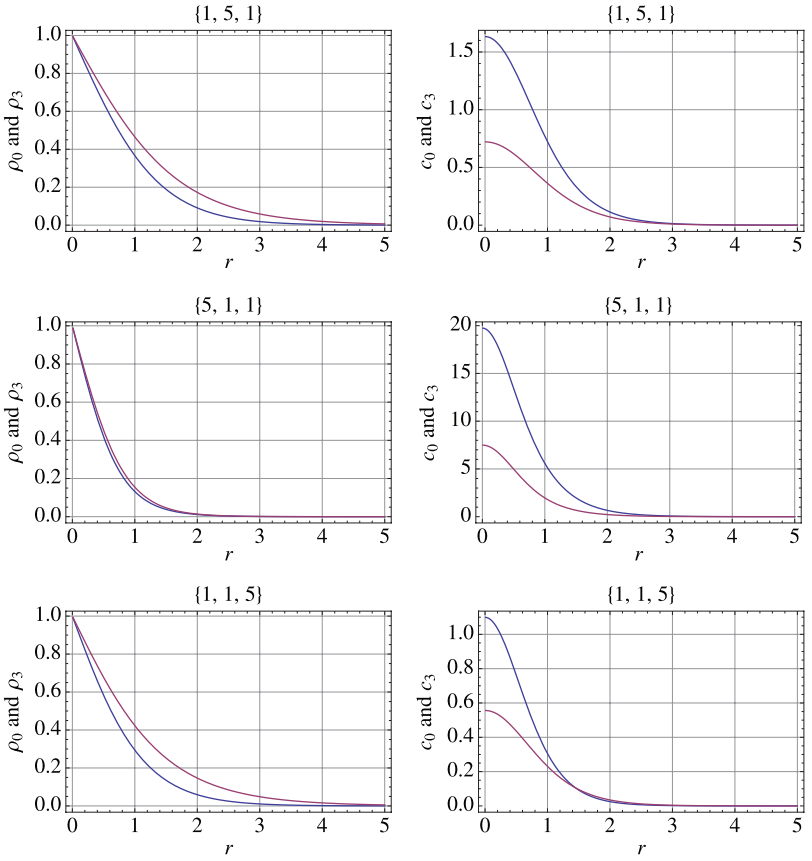

Fig. 14. The numerical solutions of $\rho_0(r)$ (blue) and $\rho_3(r)$ (purple) for $\{m_g, m_1, m_8\} = \{1, 5, 1\}$, $\{5, 1, 1\}$, $\{1, 1, 5\}$. The Kähler class densities $c_0(r)$ (blue) and $c_3(r)$ (purple) are also shown in the 2nd line.

Numerical solutions of $\rho_0(r)$, $\rho_3(r)$, and the Kähler class densities $c_0(r)$ and $c_3(r)$ ($C_i = (4\pi/g_s^2)\int dr\, r c_i(r)$) with $\lambda_i = \varepsilon_i = 1$ ($i = 0, 3$) for the mass choices $\{m_1, m_8, m_g\} = \{1, 5, 1\}$, $\{5, 1, 1\}$, $\{1, 1, 5\}$ are shown in Fig. 14. The corresponding background solutions are shown in Fig. 3.

Let us roughly estimate $C^{0,3}$. To this end, we first recall the boundary condition $f(\infty) = g(\infty) = 1$ and $h(\infty) = 0$. The profile functions $f(r)$, $g(r)$, and $h(r)$ approach the above boundary values at $r \sim \Delta_{\rm CFL}^{-1}$, which is the typical inverse mass of the background solution; see Eqs. (3.42) and (3.43). Reflecting this property, the function $\rho_{0,3}$ also approaches its boundary values $\rho_{0,3}(\infty) = 0$ around $r \sim \Delta_{\rm CFL}^{-1}$. Because of $\rho_{0,3}(0) = 1$, the values of the square brackets of the integrands of $C^{0,3}$ at the origin are $(f(0)^2 + g(0)^2)\beta_3 m_g^2/2\alpha_3 \sim \beta_3 m_g^2/2\alpha_3$ and $(f(0)^2 + g(0)^2)m_g^2/2 \sim m_g^2/2$, respectively. Therefore, one can estimate $C^{0,3}$ as

$$C^0 \sim \frac{\beta_3 m_g^2}{\lambda_3 g_s^2 \Delta_{\rm CFL}^2} \sim \frac{\beta_3 \mu^2}{\Delta_{\rm CFL}^2}, \quad C^3 \sim \frac{m_g^2}{\lambda_3 g_s^2 \Delta_{\rm CFL}^2} \sim \frac{\mu^2}{\Delta_{\rm CFL}^2}. \tag{5.18}$$

Note that λ_3 dependence disappears in the above expression. From this result, we can also estimate the velocity of the $\mathbb{C}P^2$ modes propagating along the vortex string as

$$v^2 = \frac{C^3}{C^0} \sim \beta_3^{-1} = \frac{1}{3}. \tag{5.19}$$

This should be taken with some care due to the uncertainty of the numerical solution; it is just a rough parametrical estimation. Indeed, since $C^{0,3}$ depends on the chemical potential μ, v^2 should

depend on μ as well. The precise μ dependence of the velocity of the $\mathbb{C}P^2$ mode has not yet been determined in the literature.

Let us make a comment on the types of Nambu–Goldstone modes; see footnote 8. While the Kelvin mode associated with translational symmetries is a type II Nambu–Goldstone mode with a quadratic dispersion, the $\mathbb{C}P^2$ orientational zero modes found in this section are type I Nambu–Goldstone modes with a linear dissipation. Both of them are localized Nambu–Goldstone modes in the presence of the vortex background, unlike conventional Nambu–Goldstone modes in the ground state.

5.2. *Effects of strange quark mass*

Here we consider effects of strange quark mass on the non-Abelian vortices. As addressed in Sect. 2.1.2, we can treat the effects as a perturbation in the high density region $\mu \gg m_{\rm s}$. After absorbing the small term $\varepsilon \propto m_{\rm s}^2$ given in Eq. (2.35) into α as Eq. (2.37), the background non-Abelian vortex solution, then, is given by just solving the same equations as Eqs. (3.34)–(3.36) with $\alpha \to \alpha'$. Furthermore, the leading order terms in the low-energy effective Lagrangian for the orientational moduli fields are the same as those given in Eqs. (5.8), (5.11), and (5.12) with the replacement $\alpha \to \alpha'$.

Let us now turn to find a contribution of the second term in Eq. (2.34) in the low-energy effective Lagrangian. By substituting Eq. (5.3) into the second term in Eq. (2.34), we get the following potential term in the $\mathbb{C}P^2$ nonlinear sigma model:

$$V_{\mathbb{C}P^2} = D\left(|\phi_3|^2 - |\phi_2|^2\right), \tag{5.20}$$

$$D \equiv \pi\varepsilon\Delta_\varepsilon^2 \int_0^\infty dr\, r\left(g^2 - f^2\right), \tag{5.21}$$

where (ϕ_1, ϕ_2, ϕ_3) is the homogeneous coordinate of $\mathbb{C}P^2$, which satisfies the constraint $|\phi_1|^2 + |\phi_2|^2 + |\phi_3|^2 = 1$. Note that Δ_ε, f, and g should be obtained after replacing α with α', as in Eq. (2.38). Note also that D is positive and finite because $g - f$ is positive for everything over r and gets exponentially smaller on going away from the vortex; see Eq. (3.43). In the limit $\varepsilon \to 0$, the low-energy effective theory is the massless $\mathbb{C}P^2$ nonlinear sigma model where all the points on $\mathbb{C}P^2$ are degenerate. This is because non-Abelian vortices with different orientations have the same tensions. Once non-zero ε is turned on, almost all the points of $\mathbb{C}P^2$ are lifted and only one special point $(\phi_1, \phi_2, \phi_3) = (0, 1, 0)$ remains as the global minimum of the effective potential; see Fig. 15. This means that the non-Abelian vortex with the specific orientation with color "blue–red" and flavor "s–u" is energetically favored,

$$\Phi_{su} \to \mathrm{diag}(\Delta_{ds},\ \Delta_{su}e^{i\theta},\ \Delta_{ud}), \qquad \text{as} \quad r \to \infty. \tag{5.22}$$

This matches the fact that the pairing gap Δ_{su} is smaller than Δ_{ds}, Δ_{ud} as in Eq. (2.33) so that the vortex whose string tension is proportional to Δ_{su} is more easily created than others. As shown below, the details of the dynamics suggest that all configurations except for the $(0, 1, 0)$ vortex are no longer stable, including the $(1, 0, 0)$ and $(0, 0, 1)$ vortices.

Let us estimate the lifetime of unstable vortices. For simplicity, we consider the decay from the $(1, 0, 0)$ vortex to the $(0, 1, 0)$ vortex (from the bottom-left vertex to the bottom-right vertex of the triangle in Fig. 15). Since the effective potential is lifted for $|\phi_3| \neq 0$ direction, it is reasonable to set $\phi_3 = 0$ from the beginning. Then we are left inside the $\mathbb{C}P^1$ submanifold in $\mathbb{C}P^2$. It is useful to introduce an inhomogeneous coordinate $u(t) \in \mathbb{C}$ by

$$\phi_1 = \frac{1}{\sqrt{1 + |u|^2}}, \quad \phi_2 = \frac{u}{\sqrt{1 + |u|^2}}. \tag{5.23}$$

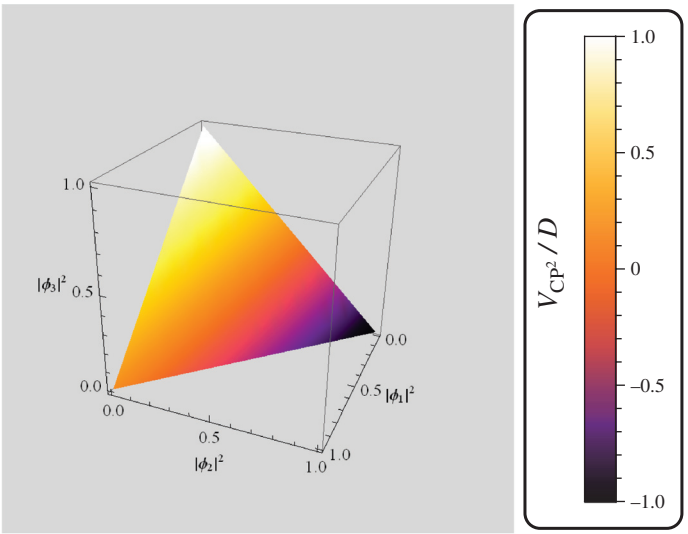

Fig. 15. Contour plot of the effective potential for the $\mathbb{C}P^2$ modes in the $|\phi_1|^2$–$|\phi_2|^2$–$|\phi_3|^2$ space. The colors represent the values of the potential.

Then the low-energy effective Lagrangian can be rewritten as

$$\mathcal{L}_{\mathbb{C}P^1} = C^0 \frac{|\dot{u}|^2}{(1+|u|^2)^2} + D\frac{|u|^2}{(1+|u|^2)}. \tag{5.24}$$

The typical timescale appearing with this Lagrangian is

$$\tau = \sqrt{\frac{C^0 K_0}{D}}. \tag{5.25}$$

In principle, we can numerically calculate τ for each μ. Instead, here, we provide a simple analytical estimation. Since the profile function $f(r)$ for the winding pairing gap (g, h, and ρ) increases (decreases) with a typical scale $r \sim \Delta_\varepsilon^{-1}$ for $m_{\rm g} \gg m_{1,8}$ as shown in Eqs. (3.42) and (3.43), we find from Eq. (5.13)

$$C^0 \sim \frac{m_{\rm g}^2}{g_{\rm s}^2 \Delta_\varepsilon^2 \lambda_3} \sim \left(\frac{\mu}{\Delta_\varepsilon}\right)^2 \frac{1}{\lambda_3}. \tag{5.26}$$

Furthermore, D is estimated from Eq. (5.21) as

$$D \sim \varepsilon \sim m_{\rm s}^2 \log \frac{\mu}{\Delta_\varepsilon}. \tag{5.27}$$

Thus, the typical timescale of the rollover from the $(1,0,0)$ vortex to the $(0,1,0)$ vortex is estimated by

$$\tau \sim \frac{1}{m_{\rm s}\sqrt{\lambda_3}} \left(\frac{\mu}{\Delta_\varepsilon}\right)^2 \left(\log \frac{\mu}{\Delta_\varepsilon}\right)^{\frac{1}{2}}. \tag{5.28}$$

In the limit $m_{\rm s} \to 0$, $\tau \to \infty$ as anticipated.

It is interesting to investigate the possible astrophysical implications of the above results. When the core of a neutron star cools down below the critical temperature of the CFL phase, a network of non-Abelian vortices will be formed by the Kibble-Zurek mechanism. Remarkably, the extrapolation of our formula (5.28) to the intermediate density regime relevant to the cores of neutron stars ($\mu \sim 500$ MeV) with $\Delta_\varepsilon \sim 10$ MeV and $m_{\rm s} \simeq 150$ MeV suggests that all the vortices decay radically with a

lifetime of order $\tau \sim 10^{-21}$ s (assuming $\lambda_3 \sim 1$). Although this result should be taken with some care due to the uncertainty of the numerical factor in Eq. (5.28), it is reasonable to expect that only one type of non-Abelian vortex, which corresponds to the point $(0, 1, 0)$ in the $\mathbb{C}P^2$ space, survives as a response to the rotation of neutron stars in reality. The other decaying non-Abelian vortices will emit NG bosons, quarks, gluons, or photons during thermal evolution of neutron stars.

Note that, since we are interested in a realistic situation like that inside the core of a neutron star, we have imposed β-equilibrium and electric charge neutrality conditions for deriving the $m_{\rm s}$-correction to the effective potential in Eq. (2.34). Let us see how the effective Lagrangian changes when we remove the conditions. The direct $m_{\rm s}$ correction was obtained in Refs. [178,179] as

$$\delta V = \frac{2}{3}\varepsilon \,\mathrm{Tr}\left[\Phi^\dagger \Phi\right] + \varepsilon \,\mathrm{Tr}\left[\Phi^\dagger X_8 \Phi\right], \tag{5.29}$$

$$X_8 = \mathrm{diag}\left(\frac{1}{3}, \frac{1}{3}, -\frac{2}{3}\right). \tag{5.30}$$

This leads to the effective potential on the $\mathbb{C}P^2$ manifold

$$V'_{\mathbb{C}P^2} = \frac{2}{3}D\left(2|\phi_3|^2 - |\phi_1|^2 - |\phi_2|^2\right) = \frac{2}{3}D\left(3|\phi_3|^2 - 1\right). \tag{5.31}$$

In this case the ground state of the potential is the $\mathbb{C}P^1$ submanifold defined by $|\phi_1|^2 + |\phi_2|^2 = 1$.

5.3. *Effects of electromagnetic fields*

5.3.1. The effects on the electromagnetic coupling on non-Abelian vortices. We have neglected the effects on the coupling of the CFL matter to the electromagnetic fields $A_\mu^{\rm EM}$ thus far. As discussed in Sect. 2.1.3, the electromagnetic symmetry is embedded into the flavor $SU(3)_{\rm F}$ symmetry, and it mixes with one of the color gauge fields in the CFL ground state. In this subsection, we discuss the electromagnetic coupling to non-Abelian vortices following Ref. [356]. There are two main consequences of the electromagnetic coupling to non-Abelian vortices. One is a gauging of $U(1)$ symmetry in the $\mathbb{C}P^2$ zero modes, i.e., the low energy theory becomes a $U(1)$ gauged $\mathbb{C}P^2$ model. The other is explicit breaking of $SU(3)_{\rm F}$ flavor symmetry, which induces the effective potential in the low energy effective theory. A physical consequence of the former is discussed later in Sect. 6.3.3. Here, we concentrate on the latter effect.

The $SU(3)_{\rm F}$ flavor symmetry is explicitly broken as in Eq. (2.53) by the electromagnetic coupling. Consequently, all non-Abelian vortices are not transformed by the $SU(3)_{\rm C+F}$ action once the electromagnetic coupling is taken into account. Only the $SU(2)_{\rm C+F} \times U(1)_{\rm EM}$ subgroup remains exact as in Eq. (2.55). In order to classify all possible configurations, we consider a closed loop in the order parameter space generated by the gauge/baryon group, which is given by the following transformation on the order parameter,

$$\langle \Phi(\infty, \theta) \rangle = e^{i\theta_{\rm B}(\theta)} e^{i\gamma^a(\theta)T^a} \langle \Phi(\infty, 0) \rangle \, e^{i\alpha(\theta)T^{\rm EM}} \tag{5.32}$$

where θ $(0 \le \theta < 2\pi)$ is the angle coordinate of the space and $\theta_{\rm B}$, γ^a, and α are monotonically increasing functions. Since Φ must be single valued, one obtains a relation at $\theta = 2\pi$:

$$e^{i\gamma^a(2\pi)T^a} = e^{-i\theta_{\rm B}(2\pi)} e^{-i\alpha(2\pi)T^{\rm EM}}. \tag{5.33}$$

This is an equation for the possible symmetry transformations giving a closed loop, or, equivalently, a possible vortex configuration. Notice that the existence and stability of vortices related to various

solutions of the above equation can in principle only be inferred by a direct study of equations of motion. It is possible to determine all the solutions of Eq. (5.33), e.g. using an explicit parametrization of the elements of $SU(3)$. In what follows we will analyze three types of solutions that cannot be related by $SU(2)$ color–flavor transformations: 1) "Balachandran–Digal–Matsuura (BDM)" case [35], 2) "$\mathbb{C}P^1$" case, and 3) "Pure color" case.

1) "BDM" case

The first possibility is a closed loop generated by T^8 in $SU(3)$ and the electromagnetic $T^{\rm EM}$ alone:

$$e^{i\gamma^8(\theta)T^8} = e^{-i\theta_{\rm B}(\theta)}e^{-i\,\alpha(\theta)T^{\rm EM}}. \tag{5.34}$$

By putting $\theta = 2\pi$, we obtain the relation

$$\frac{\gamma^8(2\pi)}{\sqrt{6}} + \frac{\alpha(2\pi)}{3} = -\frac{2\pi}{3}, \quad \theta_{\rm B}(2\pi) = \frac{2\pi}{3}. \tag{5.35}$$

The equation above determines the phases γ^8 and α only up to a linear combination. This is a consequence of the fact that the two generators T^8 and $T^{\rm EM}$ are proportional and indistinguishable from each other on diagonal configurations. The configuration above is invariant under $SU(2)$ color–flavor transformations (singlet). Balachandran, Digal, and Matsuura considered this case only [35].

2) "$\mathbb{C}P^1$" case

The second possibility is a closed loop generated by winding in the $SU(3)$ group around the T^3 direction too, in addition to T^8 and $T^{\rm EM}$:

$$e^{i(\gamma^3(\theta)T^3+\gamma^8(\theta)T^8)} = e^{-i\theta_{\rm B}(\theta)}e^{-i\,\alpha(\theta)T^{\rm EM}}. \tag{5.36}$$

By putting $\theta = 2\pi$, we obtain the relation

$$\frac{\gamma^8(2\pi)}{\sqrt{6}} + \frac{\alpha(2\pi)}{3} = \frac{\pi}{3}, \quad \gamma^3(2\pi) = \pm\sqrt{2}\pi, \quad \theta_{\rm B}(2\pi) = \frac{\pi}{3}. \tag{5.37}$$

The configuration is not preserved by color–flavor transformations, and we can generate a orientational moduli space using $SU(2)$ color–flavor transformations. In fact, we have the most general configuration of this type in the form:

$$\gamma^3(2\pi)T^3 \to \gamma^b(2\pi)T^b, \quad |\gamma^b| = \sqrt{2}\pi, \quad b = 1, 2, 3, \tag{5.38}$$

where $\to$ denotes a replacement; the T^a above are the generators of $SU(3)$ that commute with T^8 and form an $SU(2)$ subgroup. Since the continuous family generated by the $SU(2)$ group is characterized by a $\mathbb{C}P^1$ submanifold inside the whole $\mathbb{C}P^2$ space, we call them "$\mathbb{C}P^1$" vortices.

3) "Pure color" case

In terms of the vector $|\gamma^a|$ introduced above, the two previous cases correspond to $|\gamma^a| = 0$ and $|\gamma^a| = \sqrt{2}\pi$. These are the only two cases for which a nontrivial electromagnetic phase is allowed. In all the other cases, we must have:

$$e^{i\gamma^a(\theta)T^a} = e^{-i\theta_{\rm B}(\theta)}. \tag{5.39}$$

By putting $\theta = 2\pi$, we obtain the relation

$$\theta_{\rm B}(2\pi) = \frac{2\pi}{3}, \quad \alpha(2\pi) = 0. \tag{5.40}$$

We call this the "pure color" case because it does not involve electromagnetic transformations, and is thus equivalent to the case of pure color vortices studied in the previous subsections without electromagnetic coupling. Notice that this case spans a whole $\mathbb{C}P^2$, while $SU(2)$ color–flavor

transformations generate only $\mathbb{C}P^1$ orbits (apart from the case where only γ^8 is non-zero, which is invariant).

We stress again that the cases listed above are just a consequence of boundary conditions when we search for closed loops at spatial infinity. Moreover, all the cases are topologically equivalent in the absence of electromagnetic coupling.

5.3.2. BDM vortex. The "BDM case" corresponds to the vortex studied by Balachandran, Digal, and Matsuura in Ref. [35]. Since we only need T^8 to generate the correct winding for this vortex, the idea is to restrict the action (2.7) to include only the gauge fields A^8 and $A^{\rm EM}$, by keeping all the other gauge fields to zero. Formally the action reduces to that of a $U(1) \times U(1)$ gauge theory, which we can then express in terms of the massless and massive combinations in Eqs. (2.48) and (2.49):

$$SU(3)_{\rm C} \times U(1)_{\rm EM} \to U(1)_8 \times U(1)_{\rm EM} \simeq U(1)_0 \times U(1)_{\rm M}, \tag{5.41}$$

where the arrow means that we truncate the model to its Abelian subalgebra. The Lagrangian reads

$$\begin{aligned}\mathcal{L} = {\rm Tr}\left[-\frac{1}{4}\frac{3}{2}F^0_{ij}F^{0ij}\right] - {\rm Tr}\left[\frac{1}{4}\frac{3}{2}F^{\rm M}_{ij}F^{{\rm M}ij} + K_1\mathcal{D}_i\Phi^\dagger\mathcal{D}^i\Phi - \beta_2(\Phi^\dagger\Phi)^2 + m^2\Phi^\dagger\Phi\right] \\ - \beta_1({\rm Tr}[\Phi^\dagger\Phi])^2 - \frac{3m^4}{4(3\beta_1+\beta_2)},\end{aligned} \tag{5.42}$$

with

$$\mathcal{D}_i = \partial_i - ig_{\rm M}A^{\rm M}_i T^{\rm M}, \tag{5.43}$$

and $g_{\rm M}$ and $T^{\rm M}$ in Eqs. (2.46) and (2.47), respectively. This form of the Lagrangian is applicable only for diagonal configurations for the order parameter Φ. In the action above, the massless field decouples completely, as expected, while the massive field $A^{\rm M}_i$ couples to Φ in the standard way. The BDM vortex is constructed analogously to Sect. 3.3 with the only difference from the uncoupled case being the new coupling constant $g_{\rm M}$ instead of $g_{\rm s}$:

$$\begin{aligned}\Phi(r,\theta)_{\rm BDM} &= \Delta_{\rm CFL}\begin{pmatrix} e^{i\theta}f(r) & 0 & 0 \\ 0 & g(r) & 0 \\ 0 & 0 & g(r)\end{pmatrix}, \\ A^{\rm M}_i T^{\rm M} &= \frac{1}{g_{\rm M}}\frac{\epsilon_{ij}x^j}{r^2}[1-h(r)]\,T^{\rm M}, \quad A^0_i = 0.\end{aligned} \tag{5.44}$$

As shown in Fig. 5, the tension of the vortex decreases monotonically with the gauge coupling. Since we have $g_{\rm M} > g_{\rm s}$, the BDM vortex has a smaller tension as compared to the corresponding vortex in the uncoupled case.

5.3.3. $\mathbb{C}P^1$ vortex. The $\mathbb{C}P^1$ case was considered for the first time in Ref. [356]. We have identified a vortex configuration that is a solution of the equations of motion that correspond to these new boundary conditions. To see this, we notice that, similarly to the previous case, we can consistently restrict the action to include only the gauge fields corresponding to generators commuting with T^8.

This corresponds to formally reduce to the case

$$SU(3)_{\rm C} \times U(1)_{\rm EM} \to SU(2)_{\rm C} \times U(1)_8 \times U(1)_{\rm EM} \simeq SU(2)_{\rm C} \times U(1)_0 \times U(1)_{\rm M}, \tag{5.45}$$

similarly to what we have done for the BDM case. The truncated Lagrangian now is as follows:

$$\mathcal{L} = {\rm Tr}\left[-\frac{1}{4}\frac{3}{2}F^0_{ij}F^{0ij}\right] - {\rm Tr}\left[\frac{1}{4}\frac{3}{2}F^{\rm M}_{ij}F^{{\rm M}ij} - \frac{1}{4}F^b_{ij}F^{bij} + K_1\mathcal{D}_i\Phi^\dagger\mathcal{D}^i\Phi - \beta_2(\Phi^\dagger\Phi)^2 + m^2\Phi^\dagger\Phi\right] - \beta_1({\rm Tr}[\Phi^\dagger\Phi])^2 - \frac{3m^4}{4(3\beta_1+\beta_2)}, \tag{5.46}$$

where

$$\mathcal{D}_i = \partial_i - ig_{\rm M}A^{\rm M}T^{\rm M} - ig_{\rm s}A^bT^b, \quad b = 1,2,3; \quad [T^b, T^8] = 0. \tag{5.47}$$

Here, the index b is relative to the $SU(2)_{\rm C}$ factor. As before, the massless combination decouples completely, and we can set it to zero. Among $\mathbb{C}P^1$ vortices, diagonal configurations are $\mathbb{C}P^1_+$ and $\mathbb{C}P^1_-$ vortices given in the second and third configurations in Eqs. (3.27)–(3.30). One of the simplest vortex configurations of the type considered here has the following diagonal form:

$$\Phi(r,\theta)_{\mathbb{C}P^1_+} = \Delta_{\rm CFL}\begin{pmatrix} g_1(r) & 0 & 0 \\ 0 & e^{i\theta}f(r) & 0 \\ 0 & 0 & g_2(r)\end{pmatrix},$$
$$A^{\rm M}_iT^{\rm M} = -\frac{1}{2}\frac{1}{g_{\rm M}}\frac{\epsilon_{ij}x^j}{r^2}[1-h(r)]T^{\rm M},$$
$$A^3_iT^3 = \frac{1}{\sqrt{2}}\frac{1}{g_{\rm s}}\frac{\epsilon_{ij}x^j}{r^2}[1-l(r)]\,T^3. \tag{5.48}$$

As explained in Eq. (5.38), we can generate a full $\mathbb{C}P^1$ of solutions by applying $SU(2)_{\rm C+F}$ rotations to the configuration above. Once the ansatz (5.48) is inserted into the equations of motion, we obtain the equations given in the Appendix of Ref. [356]. We have numerically solved these equations, and determined the energy of the vortex configuration. The tension, as schematically shown in Fig. 16, is higher for the $\mathbb{C}P^1$ vortices than for the BDM vortex. This result can be intuitively understood if we recall the observation of the previous section, where we noticed that the tension of a color vortex decreases monotonically with the gauge coupling. The $\mathbb{C}P^1$ vortex is built with both $g_{\rm s}$ and $g_{\rm M}$ couplings; thus, the interactions depending on $g_{\rm s} < g_{\rm M}$ contribute to increase the tension with respect to a vortex built exclusively from $g_{\rm M}$.

Since the $\mathbb{C}P^1$ vortex is a solution of the equations of motion, it is a critical configuration for the energy density functional. It must be a local minimum, and thus a metastable configuration.

5.3.4. Pure color vortex. Let us now come to the third case, the "pure color" case. This situation is realized when the boundary conditions are the same as the case without electromagnetic coupling. This means that, at infinity, only the non-Abelian gauge fields give nontrivial winding, and thus non-vanishing fluxes, while the electromagnetic gauge field is zero everywhere. However, this situation is generically not compatible with the coupled equations of motion. An easy way to see this is the fact that boundary conditions in the pure color case imply a non-zero flux for the massless field A^0_i. Since A^0_i is massless and unbroken, there is no topology, compatible with the equations of motion, stabilizing and confining the flux. We thus expect that no solutions exist in general for the pure case.

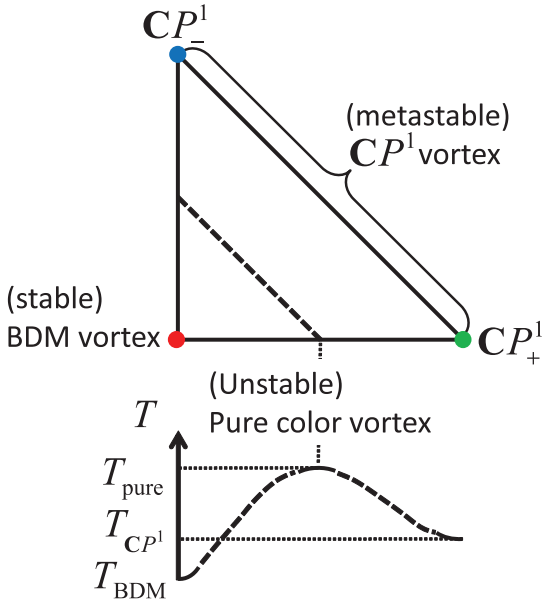

Fig. 16. The three different special vortex solutions. The BDM vortex sits in the bottom-left corner of the toric diagram and has the lowest tension. The other two diagonal vortices are located at the remaining corners and are connected by color–flavor transformations. All of the upper right edge of the diagram represents the whole family of vortex configurations related by this $SU(2)_{\rm C+F}$ transformations, namely a $\mathbb{C}P^1$ moduli space. These vortices have a slightly larger tension compared to the BDM configuration. The dashed line in the middle of the diagram corresponds to vortices not winding along the T^8 direction in the color group. These vortices have the largest tension and do not involve the electromagnetic gauge field.

However, a special configuration that we call the "pure color vortex" is an exception to this statement. This configuration is defined as that corresponding to the following boundary conditions:

$$e^{i\gamma^a(2\pi)T^a} = e^{-i\theta_{\rm B}(2\pi)}; \quad \gamma^8 \equiv 0. \tag{5.49}$$

Notice that the conditions above are perfectly consistent. We can take any configuration of γ^a phases and set γ^8 to zero using a gauge(-flavor) transformation. This means that we can consistently set:

$$A_i^8 = A_i^{\rm EM} = 0, \quad \Rightarrow \quad A_i^{\rm M} = A_i^0 = 0. \tag{5.50}$$

In fact, $A_i^{\rm EM} = 0$ means that for the pure color vortex we can consistently restrict the action by simply dropping all the terms involving $A_i^{\rm EM}$. As a consequence, the pure color vortex is exactly the same configuration as we get in the uncoupled case. Moreover, it satisfies the full equations of motion of the coupled case, because of the consistent restriction. Notice that the dependence of the electromagnetic gauge coupling also disappears completely from the restricted action. This means that the tension of the pure color vortex is also the same as the tension of the uncoupled vortices, involving only $g_{\rm s}$. As represented in Fig. 16, the tension of this vortex is larger than both the BDM and the $\mathbb{C}P^1$ vortices.

Because of this very fact we are led to conclude that the pure vortex is in fact a stationary point for the energy functional, but it corresponds to the global maximum. Both the BDM and the $\mathbb{C}P^1$ vortices are, on the other hand, local minima, with the BDM vortex being the absolute minimum. The $\mathbb{C}P^1$ vortices are, however, metastable, and if long-lived can play a crucial role in the physics of the CFL superconducting phase together with the BDM vortex. The whole situation is schematically summarized in Fig. 16. The numerical values of the tensions are compared as

$$\mathcal{T}_{\rm pure} - \mathcal{T}_{\rm BDM} = 0.0176\,{\rm MeV}^2, \quad \mathcal{T}_{\rm pure} - \mathcal{T}_{\mathbb{C}P^1} = 0.0044\,{\rm MeV}^2, \tag{5.51}$$

for the same "realistic" choice of parameters made in Fig. 5, where in addition we have chosen $m_{\rm g} = 92$ MeV and a value for the electromagnetic coupling constant of $e^2 = 1/137$. Notice that the expressions shown above do not depend on the infrared regulator L. The diverging parts of the tensions in Eq. (3.48) are equal and cancel out in the differences.

5.3.5. Magnetic fluxes. There are two main differences between color magnetic flux tubes with and without electromagnetic coupling. The first one, as we have already examined, is the lifting of the moduli space $\mathbb{C}P^2$ to leave the stable BDM vortex and the family of metastable degenerate $\mathbb{C}P^1$ vortices. The second is the fact that coupled vortices now carry a nontrivial electromagnetic flux. This is given by the fact that coupled vortices are made of the massive field $A_i^{\rm M}$, which is in turn a linear combination of color and electromagnetic gauge fields.

The BDM vortex carries a quantized $A_i^{\rm M}$ flux:

$$\Phi^{\rm M}_{\rm BDM} = \oint \vec{A}^{\rm M} \cdot d\vec{l} = \frac{2\pi}{g_{\rm M}}. \tag{5.52}$$

Because of the mixing in the ground state, this gives the following non-quantized fluxes for the color and electromagnetic fields:

$$\Phi^{8}_{\rm BDM} = \sqrt{\frac{2}{3}}\frac{1}{1+\delta^2}\frac{2\pi}{g_{\rm s}}, \quad \Phi^{\rm EM}_{\rm BDM} = \frac{\delta^2}{1+\delta^2}\frac{2\pi}{e}, \quad \delta^2 \equiv \frac{2}{3}\frac{e^2}{g_{\rm s}^2}. \tag{5.53}$$

The fluxes of the $\mathbb{C}P^1$ vortices can be similarly determined; see Fig. 17:

$$\begin{aligned} &\Phi^{\rm M}_{\mathbb{C}P^1} = -\frac{1}{2}\Phi^{\rm M}_{\rm BDM} \Rightarrow \Phi^{8}_{\mathbb{C}P^1} = -\frac{1}{2}\Phi^{8}_{\rm BDM}, \quad \Phi^{\rm EM}_{\mathbb{C}P^1} = -\frac{1}{2}\Phi^{\rm EM}_{\rm BDM}, \\ &\Phi^{3}_{\mathbb{C}P^1_+} = \oint \vec{A}^3 \cdot d\vec{l} = \frac{1}{\sqrt{2}}\frac{2\pi}{g_{\rm s}}, \quad \Phi^{3}_{\mathbb{C}P^1_-} = -\Phi^{3}_{\mathbb{C}P^1_+}. \end{aligned} \tag{5.54}$$

Moreover, the quantized circulations of the BDM and $\mathbb{C}P^1$ vortices are the same as that of the usual uncoupled vortices, and are equal to $c_B \sim 1/3$ in Eq. (3.46).

Notice that the expressions determined above imply that a color-neutral bound state of vortices necessarily also carries no electromagnetic flux, and vice versa. In particular, in the uncoupled case we need at least a bound state of three vortices, $(\bar{r}, \bar{g}, \bar{b})$ to obtain a colorless state, which is nothing but the $U(1)_{\rm B}$ vortex. In the coupled case, this "minimal" colorless bound state is obtained with the combination (BDM, $\mathbb{C}P^1_+$, $\mathbb{C}P^1_-$). The bound state carries an integer circulation $c_B \sim 1$ in Eq. (3.5).

5.3.6. Quantum mechanical decay of the $\mathbb{C}P^1$ vortices. As we have seen, the $\mathbb{C}P^1$ vortices are classically metastable because of the potential barrier provided by the presence of the pure color vortex. However, here we show that the $\mathbb{C}P^1$ vortices are quantum mechanically unstable, and they can decay to the BDM vortex by quantum tunneling. We estimate this decay probability.

As discussed in the previous subsections, we do not expect static solutions of the equations of motion apart from the BDM, the $\mathbb{C}P^1$, and the pure color vortices. However, we can try to define an effective potential interpolating between the three types of solutions. At generic orientations, the boundary conditions are the same as those for the uncoupled vortices. In fact, the uncoupled vortex evaluated on the coupled action Eq. (2.7) gives exactly the same tension as that of uncoupled vortices. This value for the tension is an upper bound for vortex configurations that have a fixed boundary condition corresponding to a generic point in $\mathbb{C}P^2$. The tension of the configuration that really minimizes the energy, for that fixed boundary condition, defines an "effective" potential on

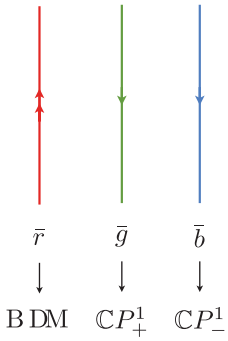

Fig. 17. The three different types of vortices we consider. The BDM vortex is labeled as the anti-red $\bar{r}$ vortex, as explained in the text, and carries twice the electromagnetic flux of the other solutions, the anti-blue $\bar{b}$ and anti-green $\bar{g}$ vortices.

the $\mathbb{C}P^2$ moduli space induced by the electromagnetic interactions. Moreover, since the tension of vortices is mainly modified by the contribution of the mixed A_i^{M}, which couples with a larger gauge coupling, we expect the qualitative behavior of the effective potential to be of the form represented in Fig. 16.

This qualitative picture is enough to address some important features of coupled color-magnetic flux tubes. The fact that the potential has more than one local minimum allows for the existence of kinks interpolating between the two vortices corresponding to the various (meta)stable configurations; these kinks are interpreted as confined monopoles. Moreover, the presence of kinks, and the higher tension of $\mathbb{C}P^1$ vortices with respect to the BDM vortex, implies a decay rate of the former vortices into the latter through quantum tunneling. This tunneling proceeds by enucleation of kink/anti-kink pairs along the vortex [277,321,358] and it is similar to the quantum decay of a false vacuum in 1+1 dimensions [358]. An analogous situation arises for pure color vortices [116,150], where the potential is generated by quantum non-perturbative effects of the $\mathbb{C}P^2$ nonlinear sigma model.

The decay rate can be roughly estimated in our case by following the arguments of Refs. [277,358]. The enucleation of a couple of kinks costs an energy of order M_{kink}. Moreover, they are created at a critical distance L_{crit} such that the energy cost for the pair production is balanced by the energy gain due to the presence of an intermediate vortex with smaller tension: $L_{\mathrm{crit}}\Delta\mathcal{T} \sim M_{\mathrm{kink}}$. The decay probability rate per unit length is thus:

$$P \sim e^{-M_{\mathrm{kink}}^2/\Delta\mathcal{T}}. \tag{5.55}$$

We now apply the formula above to our specific case. The mass of the kinks can be estimated as being of the order of the square root of the height of the potential times the "size" β of the moduli space:

$$M_{\mathrm{kink}} \sim \beta\sqrt{\mathcal{T}_{\mathrm{pure}} - \mathcal{T}_{\mathbb{C}P^1}}. \tag{5.56}$$

The quantity β has been evaluated analytically and numerically in Refs. [116,150]:

$$\beta \sim K_1^2/\beta_1 \sim \mu^2/T_{\mathrm{c}}^2, \tag{5.57}$$

and it turns out to be large for our "realistic" regime, $\beta \sim 2500$. The tension difference is given by $\Delta\mathcal{T} = \mathcal{T}_{\mathrm{pure}} - \mathcal{T}_{\mathrm{BDM}}$. We have already reported numerical estimates of the quantities above in

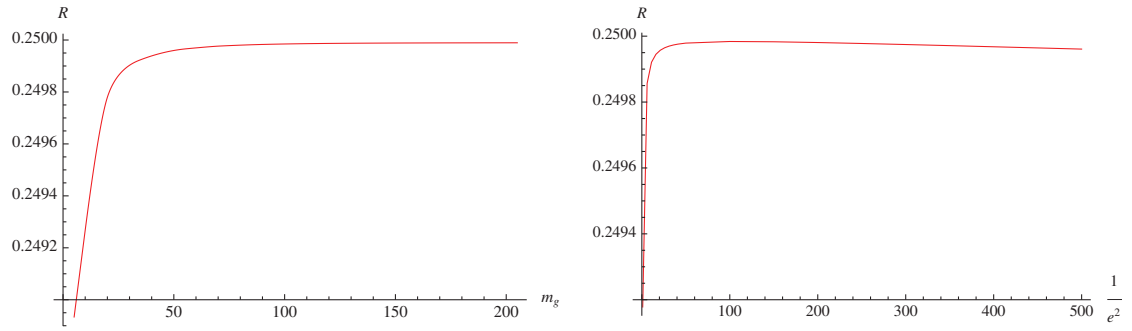

Fig. 18. The numerical value of the ratio R of Eq. (5.56). In the left panel, we plot it as a function of the mass $m_{\rm g}$, fixing the value of the electromagnetic gauge coupling to its realistic value $e^2 = 1/137$. In the right panel, we plot the same quantity as a function of e, fixing the value of the mass $m_{\rm g}$ to a typical value: $m_{\rm g} = 92\,\text{MeV}$. Notice that the value of the ratio R is always of order 1 for the wide range of physical parameter values chosen.

Eq. (5.51), for a special value of the couplings. The decay probability is then:

$$P \sim e^{-\beta R}, \quad R \equiv \frac{\mathcal{T}_{\rm pure} - \mathcal{T}_{\mathbb{C}P^1}}{\mathcal{T}_{\rm pure} - \mathcal{T}_{\rm BDM}}. \tag{5.58}$$

Substituting the numerical values of Eq. (5.51), we obtain $R \sim 0.25$. We have also studied the dependence of this decay probability in terms of a more general set of values of the gauge couplings. The numerical results are shown in Fig. 18. In the left panel we have plotted the quantity R as a function of the mass $m_{\rm g}$, which depends on the gauge coupling $g_{\rm s}$, where we have set $e^2 = 1/137$. In the right panel, we show the same quantity as a function of the electromagnetic coupling e, where we have set $m_{\rm g} = 92\,\text{MeV}$. We see that R has a very mild dependence on the value of both $m_{\rm g}$ and e. As shown in Fig. 18, R is always a quantity of order 1. We have limited ourselves to considering large values of the gauge bosons ($m_{\rm g} \gtrsim 10\,\text{MeV}$) and small values of the electromagnetic gauge coupling ($e \lesssim 1$), as expected in realistic settings in the CFL phase. We thus see that, for the range of values of the couplings considered, the ratio R is never small enough to compensate the large "moduli space" factor β. We thus estimate the probability of decay of $\mathbb{C}P^1$ vortices in BDM vortices to be exponentially small in realistic settings.

Notice that the estimate made above is fully justified only in the case in which the size of the kink is negligible as compared to the critical length $L_{\rm crit}$, while in our case the two sizes are comparable. This estimate is very rough, and has to be corrected including possible Coulomb interactions between the kink/anti-kink pair. However, it should correctly capture the order of magnitude of the decay probability. It is an open problem to give a more precise estimate of the decay probability of $\mathbb{C}P^1$ vortices in the CFL with electromagnetic coupling and vanishing quark masses. However, as we shall see in the next section, the effects of a non-vanishing strange quark mass overshadow the effects of the potential induced by electromagnetic interactions in more realistic settings.

5.3.7. Comparison with other potential terms. In this subsection, we compare the potential generated semiclassically by the electromagnetic interactions with the other potentials, i.e., the quantum mechanically induced potential and the potential induced by the strange quark mass.

First, the quantum potentials in Eqs. (5.76) and (5.64) are exponentially small and negligible as compared to the semiclassical potential induced by electromagnetic interactions.

Second, the potential induced by electromagnetic interactions is comparable with the effects of the strange quark mass discussed in Sect. 5.2 only when the strange quark mass is very negligible as

compared to the chemical potential ($\epsilon \ll m^2$). These densities are not realistic in, e.g., neutron star cores. We then conclude that $\mathbb{C}P^1_+$ is the most relevant in realistic densities, for instance in the inner core of neutron stars. This is interesting because Balachandran, Digal, and Matsuura concluded that the BDM vortex is the most stable [35].

5.4. *Quantum monopoles and the quark–hadron duality*

Understanding the confinement of quarks and gluons is one of the most important questions in QCD. One plausible scenario is the dual superconducting picture of the QCD vacuum [227,245,387]: Assuming the condensation of putative magnetic monopoles, the color electric flux is squeezed and the quarks would be confined. Although this dual picture can explain a number of properties in the QCD vacuum (see, e.g., [208,340]) and is shown to be realized in $\mathcal{N} = 2$ supersymmetric QCD [310,311], the condensation or even the existence of magnetic monopoles have not been justified in real QCD without dramatic assumptions [154]. If the magnetic monopoles indeed exist in real QCD, it is natural to expect that they would also appear in QCD at finite temperature T and finite quark chemical potential μ. In the quark–gluon plasma phase at high T, a number of instances for evidence of the existence of monopoles were suggested in the model calculation in conjunction with the lattice QCD simulations (for reviews, see Refs. [73,324]).

In this subsection, we ask whether the monopole exists or not in QCD at large μ. It is indeed an ideal situation to investigate this question because of the following two reasons: Firstly, the physics is under theoretical control in this regime because the QCD coupling constant g_s is weak according to the asymptotic freedom. Secondly, the ground state is the most symmetric three-flavor CFL phase in the color superconductivity. By making use of these two advantages, we will show that mesonic bound states of confined monopoles appear inside the non-Abelian vortices in the CFL phase.

We start with solving $\mathbb{C}P^{N_C-1}$ model in $1+1$ dimensions, taking the quantum effects into account. The case with $N_C = 3$ corresponds to the low energy effective theory on the non-Abelian vortex. Unfortunately, the solution to the $\mathbb{C}P^2$ nonlinear sigma model is not known so far. Thus, we solve the model to leading order of $1/N_C$ expansion following [81,370]. Owing to the qualitative similarity of the solutions to the $\mathbb{C}P^1$ and $\mathbb{C}P^{N_C-1}$ models, the solution to the $\mathbb{C}P^2$ model should be well approximated by taking $N_C = 3$ at the end.

Let us first rescale the variables as

$$t \to \sqrt{C^0}t, \quad z \to \sqrt{C^3}z, \quad \phi \to \sqrt{C^0C^3}\phi. \tag{5.59}$$

Then the low energy effective Lagrangian given in Eqs. (5.8)–(5.12) can be rewritten in the following form:

$$S = \int d^2x \left[|(\partial_\alpha - iA_\alpha)\phi|^2 - \sigma \left(|\phi|^2 - \frac{N_C}{3}\sqrt{C^0C^3} \right) \right]. \tag{5.60}$$

Here we have performed the Hubbard–Stratonovich transformation by introducing the auxiliary gauge field A_α and also the Lagrange multiplier σ. After the rescaling, the partition function has the standard normalization as

$$Z = \int \left[d\phi d\phi^\dagger d\sigma dA_\alpha \right] e^{iS}. \tag{5.61}$$

Integrating out ϕ and $\phi^\dagger$, one obtains

$$Z = \int [d\sigma A_\alpha] \exp\left\{ -N_C \mathrm{Tr}\, \log\left[-(\partial_\alpha + iA_\alpha)^2 - \sigma \right] + \frac{iN_C}{3}\sqrt{C^0C^3} \int d^2x\, \sigma \right\}. \tag{5.62}$$

Following [370], we solve this in a stationary phase approximation. From the "Lorentz" symmetry, the saddle point should be a point with $A_\alpha = 0$ and $\sigma =$ constant. Then, we vary the partition function in terms of σ leading to the following gap equation:

$$i\frac{\sqrt{C^0C^3}}{3} + \int^{\Lambda=\Delta_{\rm CFL}} \frac{d^2k}{(2\pi)^2}\frac{1}{k^2-\sigma+i\epsilon} = 0. \tag{5.63}$$

Note here that we have introduced the cutoff scale $\Lambda = \Delta_{\rm CFL}$, which is not a dynamical cutoff of the $\mathbb{C}P^2$ model but is a physical cutoff $\Delta_{\rm CFL}$ below which the description in the low energy effective theory does make sense. After integration, we get

$$M^2 \equiv \sigma = \Delta_{\rm CFL}^2 e^{-4\pi\frac{\sqrt{C^0C^3}}{3}} \sim \Delta_{\rm CFL}^2 e^{-\gamma\left(\frac{\mu}{\Delta_{\rm CFL}}\right)^2} > 0, \tag{5.64}$$

where γ is a certain positive constant and we have used $C^0 \sim C^3 \sim (\mu/\Delta_{\rm CFL})^2$ under the assumption $\lambda_3 \sim \varepsilon_3 \sim 1$. Looking back to the original action Eq. (5.60), one sees that a positive expectation value of σ is a mass of ϕ and $\phi^\dagger$.

Let us next consider fluctuations of σ and A_α around the saddle point. It was shown [370] that higher order terms in σ and A_α are suppressed in the large-$N_{\rm C}$ limit; only the quadratic terms are relevant. It turns out that the relevant Feynman diagrams are the propagator of A_α at the one-loop level [370]. Thus the effective world-sheet theory including the quantum effects to leading order of $1/N_{\rm C}$ is

$$\mathcal{L}_{\rm eff}^{\rm quant} = |(\partial_\alpha - iA_\alpha)\phi|^2 - M^2|\phi|^2 - \frac{N_{\rm C}}{48\pi M^2}F_{\alpha\beta}^2. \tag{5.65}$$

By rescaling A_α so that the kinetic terms of A_α are canonically normalized,

$$A_\alpha \to \sqrt{\frac{12\pi M^2}{N_{\rm C}}}\,A_\alpha, \tag{5.66}$$

the final form of the quantum effective theory reads

$$\mathcal{L}_{\rm eff}^{\rm quant} = |(\partial_\alpha - ieA_\alpha)\phi|^2 - M^2|\phi|^2 - \frac{1}{4}F_{\alpha\beta}^2, \quad e \equiv \sqrt{\frac{12\pi}{N_{\rm C}}}\,M. \tag{5.67}$$

In summary, taking the quantum effects into account, the auxiliary gauge fields become dynamical and ϕ acquires the $U(1)$ charge e and a non-zero mass, which is consistent with the Coleman–Mermin–Wagner theorem in $1+1$ dimensions [78,239].

We are now ready to understand the above quantum phenomena in $1+1$ dimensions from the $3+1$ dimensional viewpoint. A clue is that the particles ϕ and $\phi^\dagger$ in $1+1$ dimensions can be interpreted as topological solitons, namely a kink and an anti-kink, as was found by Witten [370]. This might be best seen in a supersymmetric $\mathbb{C}P^{N_{\rm C}-1}$ model, which has $N_{\rm C}$ degenerate quantum vacua with $\mathbb{Z}_{N_{\rm C}}$ symmetry. The kinks interpolate two adjacent vacua among the $N_{\rm C}$ vacua. Remember that, for us, the $\mathbb{C}P^{N_{\rm C}-1}$ fields ϕ and $\phi^\dagger$ are the internal orientational moduli of the non-Abelian vortex in the CFL phase. Therefore, the kink on the vortex is a particle soliton in $3+1$ dimensions and is a junction of two different non-Abelian vortices. Thereby, it is nothing but a magnetic monopole in the Higgs phase; see Fig. 19. The mass of the monopole can be read from Eq. (5.65) as

$$M_{\rm monopole} = M \sim \Delta_{\rm CFL} e^{-\frac{\gamma}{2}\left(\frac{\mu}{\Delta_{\rm CFL}}\right)^2}. \tag{5.68}$$

This is much smaller than the mass $\sim \Delta_{\rm CFL}\log(L/\xi)$ of the non-Abelian vortex of the unit length. Dealing with the monopole as the soliton in the low energy world-sheet theory is justified by this hierarchy in the mass scales.

Fig. 19. A monopole as a kink of the orientational moduli ϕ in supersymmetric models.

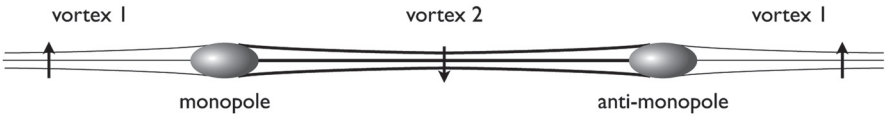

Fig. 20. A confined monopole and anti-monopole in non-supersymmetric models.

Though the kinks on the vortex string are deconfined in the supersymmetric $\mathbb{C}P^{N_C-1}$ model [149, 160], they are confined in the non-supersymmetric case. This is because the particles ϕ and $\phi^\dagger$ have charges $\pm e$ for the dynamical $U(1)$ gauge field as in Eq. (5.67). In one space dimension the Coulomb potential is linear, so that, even if the charges are small, they are confined. This is the reason why Witten referred to ϕ and $\phi^\dagger$ as "quarks" (for us they are magnetic monopoles). The linear potential between a monopole at $z = z_1$ and an anti-monopole at $z = z_2$ is given by

$$V_{\rm conf} = e^2|z_1 - z_2|. \tag{5.69}$$

We illustrate the situation where the monopole and the anti-monopole are confined on the non-Abelian vortex in Fig. 20. The monopole and the anti-monopole are accompanied by semi-infinite long strings (vortex 1 in Fig. 20). The tension of vortex 1 is given by

$$T_1 = T_{\rm classical} - \frac{N_C}{3}M^2 \sim T_{\rm classical} - \frac{N_C}{3}\Delta_{\rm CFL}^2 e^{-\gamma\left(\frac{\mu}{\Delta_{\rm CFL}}\right)^2}. \tag{5.70}$$

From Eq. (5.69) we see that the vortex string (vortex 2 in Fig. 20) has a tension T_2 bigger than that of vortex 1 by

$$T_2 - T_1 = e^2 = \frac{12\pi}{N_C}M^2 \sim \frac{12\pi}{N_C}\Delta_{\rm CFL}^2 e^{-\gamma\left(\frac{\mu}{\Delta_{\rm CFL}}\right)^2}. \tag{5.71}$$

There is another perspective for understanding this phenomenon [149]. The vacuum structure of the non-supersymmetric $\mathbb{C}P^{N_C-1}$ model can be realized by looking at the ϑ dependence of the theory [149,322,373] by adding the ϑ term

$$\mathcal{L}_\vartheta = \frac{\vartheta}{2\pi}\epsilon^{\alpha\beta}\partial_\beta A_\alpha, \tag{5.72}$$

where A_α is that before rescaling (5.66). Recalling that the vacuum energy $E(\vartheta)$ is of order N_C in the large N_C limit, $E(\vartheta)$ is expressed as [149,373]

$$E(\vartheta) = N_C M^2 f\left(\frac{\vartheta}{N_C}\right). \tag{5.73}$$

Here $f(\vartheta)$ is an even function of ϑ due to the CP symmetry under which ϑ transforms as $\vartheta \to -\vartheta$. Furthermore, $E(\vartheta)$ is a periodic function as

$$E(\vartheta + 2\pi) = E(\vartheta). \tag{5.74}$$

One might suspect that these two conditions are incompatible at first sight. However, there is a way out: both of them can be satisfied when $E(\vartheta)$ is a multibranched function as

$$E(\vartheta) = N_C M^2 \min_k \left\{ f\left(\frac{\vartheta + 2\pi(k-1)}{N_C}\right)\right\}, \quad k = 1, 2, \cdots, N_C. \tag{5.75}$$

Expanding $f(\vartheta) = f_0 + f_2\vartheta^2 + \cdots$ and considering that higher order terms in ϑ are suppressed at large N_C, the vacuum energy at $\vartheta = 0$ is given by

$$E_k(0) = -\frac{N_C}{3}M^2 + \frac{12\pi}{N_C}M^2(k-1)^2, \quad k = 1, 2, \cdots, N_C, \tag{5.76}$$

where we have set $f_0 = -1/3$ and $f_2 = 12\pi$ in such a way that Eqs. (5.70) and (5.71) are reproduced. Therefore, there exist N_C local minima among which only one ($k = 1$) is a genuine ground state while the others are quasi vacua. Each local minimum corresponds to a quantum vortex state. Namely, the genuine ground state ($k = 1$) is the stable vortex with $T_1 = T_{\text{classical}} + E_1(0)$, and the quasi vacua with $k \geq 2$ are the metastable string with the tension $T_k = T_{\text{classical}} + E_k(0)$.

It is now natural to interpret ϕ and $\phi^\dagger$ as a kink and an anti-kink interpolating the adjacent local minima on a vortex, respectively [149]; taking into account the codimension, this bound state neutral to the $U(1)$ charge can be identified as the bound state of a monopole and an anti-monopole in terms of the original 3+1 dimensions, as illustrated in Fig. 21: a monopole and an anti-monopole with the mass M are confined into the mesonic bound state by the linear potential. A similar understanding has been demonstrated in Ref. [234] based on a comparison with SUSY QCD.

Let us discuss the representations of the bound state of the monopole and anti-monopole. The physical degrees of freedom of ϕ are $2(N_C - 1)$ after fixing $U(1)$ gauge symmetry. For example, the inhomogeneous coordinates are

$$\phi = \frac{1}{\sqrt{1+|b_1|^2}}\begin{pmatrix}1\\ b_1\end{pmatrix}, \quad \phi = \frac{1}{\sqrt{1+|b_1|^2+|b_2|^2}}\begin{pmatrix}1\\ b_1\\ b_2\end{pmatrix}, \tag{5.77}$$

for $N_C = 2$ and $N_C = 3$, respectively. For $N_C = 2$, ϕ ($\phi^\dagger$) represents one (anti-)kink, as can be seen in Fig. 21(a). Each of them corresponds to one (anti-)monopole. For the case of the CFL phase with $N_C = 3$, one (anti-)monopole is a composite state of $N_C - 1 = 2$ (anti-)kinks, each of which has one complex moduli (position and phase), as seen in Fig. 21(b). Since the fields ϕ and $\phi^\dagger$ transform as (anti-)fundamental representations under $SU(N_C)$, respectively, these (anti-)monopoles belong to $\mathbf{N}_C$ ($\mathbf{N}_C^*$) fundamental representations of $SU(N_C)$. The (anti-)monopoles are not free particles but appear as a mesonic bound state that belongs to the $\mathbf{N}_C \otimes \mathbf{N}_C^* = \mathbf{1} \oplus \mathbf{N}_C^2 - 1$ representation. Note that it was shown in Refs. [384,385] that the singlet in this decomposition does not appear in the spectrum in the $\mathbb{C}P^1$ model ($N_C = 2$). This was interpreted in Ref. [234] as indicating that the singlet

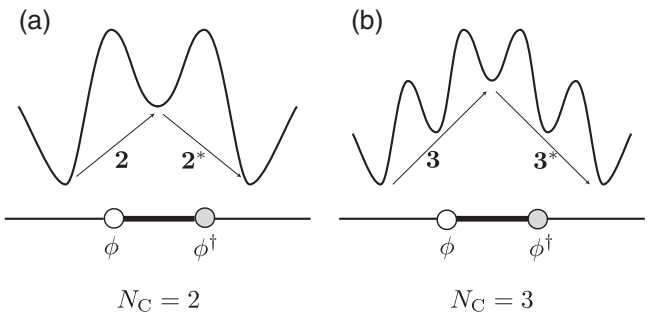

Fig. 21. A schematic illustration of the non-perturbative potential and kinks interpolating between the ground state and the metastable states, in the cases of (a) $N_C = 2$ and (b) $N_C = 3$. Kinks (ϕ and $\phi^\dagger$) can be identified with monopoles (M and $\bar{M}$) from the bulk $3 + 1$ dimensional point of view. The total configuration is a bound state of a monopole and an anti-monopole.

Table 2. Comparisons of the physics between the hadron phase and the CFL phase in massless three-flavor QCD: symmetry breaking patterns [the $U(1)_{\rm A}$ and discrete symmetries are suppressed here] and the elementary excitations. There is still one missing piece in the table: the properties of monopoles in the hadron phase, for which we speculate that the condensation of monopoles corresponds to the condensation of quarks in the CFL phase. See text for further explanations.

Phases	Hadron phase	Color–flavor-locked phase
	Confinement	Higgs
Quarks	Confined	Condensed
Monopoles	*Condensed?*	*Confined*
Coupling constant	Strong	Weak
Order parameters	Chiral condensate $\langle \bar{q}q \rangle$	Diquark condensate $\langle qq \rangle$
Symmetry	$SU(3)_{\rm L} \times SU(3)_{\rm R} \times U(1)_{\rm B}$ $\to SU(3)_{\rm L+R}$	$SU(3)_{\rm C} \times SU(3)_{\rm L} \times SU(3)_{\rm R} \times U(1)_{\rm B}$ $\to SU(3)_{\rm C+L+R}$
Fermions	**8** baryons	$\mathbf{8}+\mathbf{1}$ quarks
Vectors	$\mathbf{8}+\mathbf{1}$ vector mesons	**8** gluons
NG modes	**8** pions $(\bar{q}q)$	$\mathbf{8}+\mathbf{1}$ pions $(\bar{q}\bar{q}qq)$
	H boson	H boson

corresponds to a set of a monopole and an anti-monopole with opposite charges, which is unstable to decay. Although there is no such calculation for $N_{\rm C} \geq 3$, we expect that the same holds.

Next, we would like to discuss the implications of the color-octet of the magnetic-mesonic bound states. Because they live in the CFL phase, they are also flavor-octet under $SU(3)_{\rm C+L+R}$. Clearly, these bound states resemble the flavor-octet mesons formed by quark–antiquark pairs in the hadron phase. Thus we are naturally led to speculation on the idea of the "quark–monopole duality": the roles played by quarks and monopoles are interchanged between the hadron phase (at low density) and the CFL phase (at high density). If this is indeed the case, our results in the CFL phase would imply the condensation of monopoles in the hadron phase; namely, it embodies the dual superconducting scenario for the quark confinement in the hadron phase [227,245,387].

The possible quark–monopole duality may have some relevance to "hadron–quark continuity," which is the one-to-one correspondence without any phase transitions between the hadron phase and the CFL phase conjectured by Schäfer and Wilczek [305]. The hadron–quark continuity may be realized in the QCD phase structure in the three-flavor limit, as explicitly shown in Refs. [165,376]. In Table 2 we summarize the correspondence in the quark–monopole duality and the hadron–quark continuity. A number of pieces of nontrivial evidence that support the hadron–quark continuity have been identified: the same symmetry breaking patterns; the fact that the confinement phase is indistinguishable from the Higgs phase [37,129]; the one-to-one correspondence of elementary excitations such as baryons, vector mesons [164], and pions [376]; and the equivalence of the form of the partition functions in a finite volume called the ϵ-regime [375], between the hadron phase and the CFL phase.

So far, we have considered mesonic bound sates. What is the counterpart of baryonic states in the CFL phase? It has been found in Ref. [36] by lattice QCD simulations that three quarks are connected by a Y-shaped junction of color electric flux tubes. It is a natural expectation that a junction of three non-Abelian vortices with total color fluxes canceled out at the junction point forms; see Fig. 22. We note that they carry the correct baryon number; each non-Abelian vortex carries the $U(1)_{\rm B}$ winding number 1/3, and all of them join together to constitute one $U(1)_{\rm B}$ vortex with a $U(1)_{\rm B}$ winding number one. However, we have not specified the electromagnetic charges of fluxes at this stage because we have ignored the electromagnetic coupling of vortices in this section.

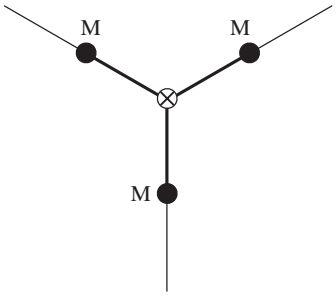

Fig. 22. Baryonic bound state of three monopoles (dark discs M indicate the monopoles). They are connected by a junction of color magnetic flux tubes. The total color is canceled out and a $U(1)_{\rm B}$ vortex represented by $\otimes$ forms at the junction point.

Finally, some comments are in order. The first is on the relation between classical treatments of the orientational zero modes in other sections and the quantum treatment explained in this subsection. First of all, in order for the $\mathbb{C}P^2$ nonlinear sigma model to work as a low energy effective field theory, the energy scale of the orientational modes must be sufficiently smaller than the cutoff scale $\Delta_{\rm CFL}$. Furthermore, since the $1+1$ dimensional $\mathbb{C}P^N$ nonlinear sigma model is asymptotic-free, the low energy physics of the low energy effective theory is highly quantum mechanical. The typical quantum mass scale is of the quantum monopole mass M given in Eq. (5.68). Therefore, the orientational modes can be dealt with classically within an energy scale smaller than $\Delta_{\rm CFL}$ and larger than M, which is very small at the high density limit.

Next, let us make a comment on the effect of the strange quark mass $m_{\rm s}$ with electric charge neutrality and β-equilibrium conditions, as is expected in the physical dense matter like inside neutron stars. This situation was considered previously without the quantum effects in Sect. 5.2. Firstly, note that without the quantum effects there are no monopoles in the CFL phase [115]. This is because the effective potential without the quantum effect does not have any local minima but has only one global minima, as was obtained in Eq. (5.20), so that no metastable kinks can form. Even if we take into account the quantum effects, they are negligibly small: the scale of the effective potential $\sim m_{\rm s}^2/g_{\rm s}$ is much larger than that induced by the quantum effects $\sim \Delta_{\rm CFL}^2 e^{-\gamma\mu^2/\Delta_{\rm CFL}^2}$ for realistic values of the parameters, $m_{\rm s}\sim 100\,\text{MeV}$, $\mu\sim 500\,\text{MeV}$, and $\Delta_{\rm CFL}\sim 50\,\text{MeV}$. Hence, the confined monopoles will be washed out by $m_{\rm s}$. We expect that the notion of quark–monopole duality works well close to the three-flavor limit. It is also a dynamical question whether the hadron–quark continuity survives when one turns on $m_{\rm s}$; there are other candidates for the ground state at intermediate μ other than the CFL phase under the stress of $m_{\rm s}$, such as the meson condensed phase, the crystalline Fulde–Ferrell–Larkin–Ovchinikov phase [140,214], the gluon condensed phase, etc [13].

5.5. Yang–Mills instantons trapped inside a non-Abelian vortex

In this subsection, we discuss Yang–Mills instantons [48], classified by the third homotopy group of the gauge symmetry

$$\pi_3[SU(3)_{\rm C}]\simeq\mathbb{Z}. \tag{5.78}$$

The instanton number is $k=(8\pi^2/g_{\rm s}^2)\int F\wedge F\in\pi_3[SU(3)_{\rm C}]$.

At asymptotic large μ, bulk instanton effects with the energy $\sim 1/g_{\rm s}^2\gg 1$ are highly suppressed due to the asymptotic freedom of QCD and the screening of Yang–Mills instantons [302,374]. As classical solutions, Yang–Mills instantons are unstable against shrinkage in the CFL ground state, which can be understood from Derrick's scaling argument [88]. Instead, Yang–Mills instantons can

exist stably inside a non-Abelian vortex [104,107,133]. They are lumps or sigma model instantons [276] supported by the second homotopy group

$$\pi_2(\mathbb{C}P^2) \simeq \mathbb{Z} \tag{5.79}$$

in the $\mathbb{C}P^2$ model as the low-energy effective theory of a non-Abelian vortex.

Lump solutions exist inside a $\mathbb{C}P^1$ submanifold of the whole $\mathbb{C}P^2$. Let $z \in \mathbb{C}$ be the complex coordinate made of Wick-rotated coordinates of the vortex world-sheet. By using the projective coordinate w of $\mathbb{C}P^1$, the lump solution can be written as

$$w(z) = \sum_{a=1}^{k} \frac{\lambda_a}{z - z_a} \tag{5.80}$$

with the size and phase moduli $\lambda_a \in \mathbb{C}^*$ and the position moduli $z_a \in \mathbb{C}$ of the ath instanton among k instantons where $k \in \pi_2(\mathbb{C}P^2) \simeq \mathbb{Z}$. The instanton energy in the vortex world-sheet is $C^{0,3} \sim (\mu/\Delta_{\rm CFL})^2 \gg 1/g_{\rm s}^2$ [see Eq. (5.18)], which is further suppressed more than the bulk instantons, consistent with the result in the last subsection. The fact that the instanton energy $C^{0,3} \sim (\mu/\Delta_{\rm CFL})^2$ inside the vortex is larger than the one $1/g_{\rm s}^2$ in the bulk implies that instantons are repulsive from vortices.

In the case of SUSY QCD, quantum effects in the $d = 1 + 1$ dimensional vortex world-sheet can be explained by instanton effects in the original $d = 3 + 1$ dimensional theory [160,318,319]. As in SUSY QCD, the quantum effects inside the vortex may be explained by instantons trapped in it, which remains a problem for the future.

6. Interactions of non-Abelian vortices with quasiparticles

In this section, we discuss the interaction of non-Abelian vortices with quasiparticles in the color-superconducting medium. It is necessary to determine the interaction to discuss physical phenomena such as scattering or radiation of quasiparticles by vortices. We can also investigate the interaction between vortices using vortex–quasiparticle interaction, since the intervortex force is mediated by quasiparticles.

In the first subsection, we discuss the interaction of vortices with phonons, which are the Nambu–Goldstone mode associated with the breaking of the $U(1)_{\rm B}$ symmetry, and gluons. In particular, the interaction with gluons is dependent on the orientation of a vortex. This gives rise to an orientation-dependent interaction energy between two vortices.

In the second subsection, we discuss the interaction of vortices with CFL mesons. The CFL mesons are the Nambu–Goldstone bosons for the breaking of chiral symmetry.

In the third subsection, we investigate the interaction of vortices with photons and its phenomenological consequences. The orientational zero modes localized on vortices are charged with respect to $U(1)_{\rm EM}$ symmetry. The interaction Lagrangian is determined by the symmetry consideration. Based on the interaction, we discuss the scattering of photons off a vortex. We also discuss the optical property of a vortex lattice (see Sect. 4.4), which is expected to be formed if CFL matter exists inside the core of a rotating dense star. We show that a lattice of vortices serves as a polarizer of photons.

6.1. Interaction with phonons and gluons

Here we discuss the interaction of vortices with gluons and phonons. For this purpose, we use a method called dual transformation. Dual transformation relates theories that have different

Lagrangians and variables but possess equivalent equations of motion. This method is useful in dealing with topological defects, since topological defects in an original theory are described as particles in its dual theory. After a dual transformation, we can deal with the interaction of topological defects by the methods of the ordinary field theory. The action of the dual theory is derived by using the method of path integration. For example, let us take phonons in three spatial dimensions, which are described by a massless scalar field. In the dual action, phonons are described by a massless antisymmetric tensor field $B_{\mu\nu}$ [130,193]. Antisymmetric tensor fields have been utilized in describing vortices in superfluids or perfect fluids [163,216,297]. In a dual formulation, the field $B_{\mu\nu}$ is introduced via the method of path integration. On the other hand, the gluons, which are massive because of the Higgs mechanism, are described by massive antisymmetric tensor fields in the dual theory [314].

6.1.1. Dual action and vortex–quasiparticle interaction. Starting from the time-dependent Ginzburg–Landau effective Lagrangian in the CFL phase (2.56), a dual Lagrangian can be derived via the method of path integration. The derivation is given in Appendix (D). In the dual theory, gluons and phonons are described by antisymmetric tensors, $B^a_{\mu\nu}$ and $B^0_{\mu\nu}$, respectively. The low-energy action for phonons and gluons interacting with vortices is given by [170]

$$\mathcal{S} = \mathcal{S}_0 + \mathcal{S}_{\rm int}, \tag{6.1}$$

where the free part $\mathcal{S}_0$ is defined as

$$\mathcal{S}_0 = \int d^4x \left[-\frac{1}{12\tilde{K}_{\mu\nu\sigma}} \left(H^a_{\mu\nu\sigma} H^{a,\mu\nu\sigma} + H^0_{\mu\nu\sigma} H^{0,\mu\nu\sigma} \right) - \frac{1}{4} {m_{\rm g}}^2 \left(B^a_{\mu\nu} \right)^2 \right]. \tag{6.2}$$

In the above equation, $H^a_{\mu\nu\sigma} \equiv \partial_\mu B^a_{\nu\sigma} + \partial_\nu B^a_{\sigma\mu} + \partial_\sigma B^a_{\mu\nu}$ and $H^0_{\mu\nu\sigma} \equiv \partial_\mu B^0_{\nu\sigma} + \partial_\nu B^0_{\sigma\mu} + \partial_\sigma B^0_{\mu\nu}$ are field strength tensors of gluons and phonons, and $m_{\rm g}$ is the mass of the gluons. The factor $\tilde{K}_{\mu\nu\sigma} \equiv \epsilon_{\rho\mu\nu\sigma} K^\rho$ comes from the lack of Lorentz invariance, where we have defined $K_\mu = (K_0, K_3, K_3, K_3)^T$. The first (second) terms are kinetic term for gluons (phonons). The third one is the mass term for gluon fields, which is induced via the Higgs mechanism. In the presence of a vortex, the mass of gluons is dependent on the distance from the center of the vortex according to the change of the values of diquark condensates.

The interaction part $\mathcal{S}_{\rm int}$ is written as

$$\mathcal{S}_{\rm int} = -\int d^4x \left[2\pi m^0 B^0_{\mu\nu} \omega^{0,\mu\nu} + \frac{m_{\rm g}}{g_{\rm s}} B^a_{\mu\nu} \omega^{a,\mu\nu} \right], \tag{6.3}$$

where $\omega^0_{\mu\nu}$ and $\omega^a_{\mu\nu}$ are vorticity tensors, which depend on the vortex configuration, and m^0 is a space-dependent function given by the vortex profile functions. Their specific forms are discussed later. The vorticity tensors have finite values only around the core of a vortex. Thus, although gluons and phonons propagate in the four-dimensional spacetime the interaction is localized around the vortex.

Now we discuss the properties of the interaction (6.3). First, let us look at the interaction of vortices with $U(1)_{\rm B}$ phonons. This part is essentially the same as a vortex in a superfluid. For a general vortex configuration we can write the Abelian component of the vorticity tensor as

$$\left(\omega^0\right)_{\rho\sigma}(x) \equiv \frac{1}{2\pi} \epsilon_{\mu\nu\rho\sigma} \partial^\nu \partial^\mu \pi_{\rm MV}(x), \tag{6.4}$$

where $\pi_{\rm MV}(x)$ is the multivalued part of the phase of the order parameter fields. The multivalued part is in general allowed, since it is a phase. Equation (6.4) appears to automatically vanish, but in fact it

does not, since the two derivatives do not commute, which reflects the multivaluedness of $\pi_{\rm MV}(x)$. For a general vortex configuration, the vorticity tensor can be written as

$$(\omega^0)^{\mu\nu}(x) = \frac{1}{N_{\rm C}} \int d\tau d\sigma \frac{\partial(X^\mu, X^\nu)}{\partial(\tau,\sigma)} \delta^{(4)}(x - X^\mu(\tau,\sigma)), \tag{6.5}$$

where $N_{\rm C}$ is the number of colors ($N_{\rm C} = 3$) and $X^\mu(\tau,\sigma)$ is the the space-time position of the vortex parametrized by world-sheet coordinates τ and σ. The interaction of vortices with $U(1)_{\rm B}$ phonons is rewritten as

$$\mathcal{S}^{\rm Ph}_{\rm int} = -\frac{2\pi m^0}{N_{\rm C}} \int d\sigma^{\mu\nu} B^0_{\mu\nu}, \tag{6.6}$$

where $d\sigma^{\mu\nu} \equiv \frac{\partial(X^\mu, X^\nu)}{\partial(\tau,\sigma)} d\tau d\sigma$ is an area element of the vortex world-sheet. The interaction (6.6) is a natural generalization of the gauge interaction of a point particle,

$$\mathcal{S} = \int dx^\mu A_\mu. \tag{6.7}$$

The factor $1/N_{\rm C}$, which is equal to the $U(1)_{\rm B}$ winding number of vortices with the lowest energy, reflects the fact that the strength of the interaction is proportional to the winding number with respect to $U(1)_{\rm B}$ symmetry. We also note that $U(1)_{\rm B}$ phonons $B^0_{\mu\nu}$ do not couple to the orientational zero modes. Phonons are blind to the orientation of a vortex.

Next, let us look at the interaction of vortices with gluons. The non-Abelian vorticity tensor $\omega^a_{\mu\nu}$ is written as

$$\begin{aligned}
\omega^a_{\lambda\sigma} = \epsilon_{\lambda\sigma\mu\nu} \Bigg\{ & \partial_\nu \Bigg\{ -\frac{16}{N_{\rm C}} \gamma(r) \left(\partial_\mu\theta + 2N_{\rm C}\gamma\delta_{\mu 0}\right) \phi^\dagger T^a \phi \\
& + i\alpha(r)(1+\beta(r)) \left(\phi^\dagger T^a \partial_\mu \phi - \partial_\mu \phi^\dagger T^a \phi + 2\phi^\dagger T^a \phi \partial_\mu \phi^\dagger \phi \right) \Bigg\} \\
& - \frac{4}{N_{\rm C}} \alpha(r)\gamma(r)(1+\beta(r)) \left(\partial_{[\mu}\phi^\dagger T^a \phi + \phi^\dagger T^a \partial_{[\mu}\phi \right) \left(\partial_{\nu]}\theta + \frac{N_{\rm C} K_0'}{2K_0} \delta_{\nu]0} \right) \\
& - \frac{i}{2} \alpha(r)^2 (1+\beta(r)^2) \\
& \times \left[\phi^\dagger T^a \phi \partial_{[\mu}\phi^\dagger \partial_{\nu]}\phi + \partial_{[\mu}\phi^\dagger T^a \partial_{\nu]}\phi + \phi^\dagger T^a \partial_{[\mu}\phi \partial_{\nu]}\phi^\dagger \phi + \partial_{[\mu}\phi^\dagger T^a \phi \partial_{\nu]}\phi^\dagger \phi \right] \Bigg\},
\end{aligned} \tag{6.8}$$

where $\alpha(r)$, $\beta(r)$, and $\gamma(r)$ are functions of the distance from the vortex core and are written in terms of vortex solutions, and the parameter γ is the coefficient of the term with one time derivative in Eq. (2.56). The leading-order part in the deviation of the order parameter from the ground-state value is given by

$$\omega^a_{\lambda\sigma} = \epsilon_{\lambda\sigma\mu\nu} \partial^\nu \left[-\frac{16}{N_{\rm C}} \gamma(r) \left\{ \partial^\mu\theta + 2N_{\rm C}\gamma\delta^{\mu 0} \right\} \phi^\dagger T^a \phi \right]. \tag{6.9}$$

As can be seen in Eq. (6.8), gluons actually couple to the orientational zero modes on the vortex. As a result, gluons are emitted through the interaction (6.8) when a wave of the $\mathbb{C}P^2$ orientational modes propagates along a vortex-line. By using the interaction derived above (6.8), we can estimate the amount of radiated gluons from a propagating wave in $\mathbb{C}P^2$ orientational space.

6.1.2. Orientation dependence of the vortex–vortex interaction. As an application of the dual Lagrangian obtained above, let us discuss the orientation dependence of the interaction energy of

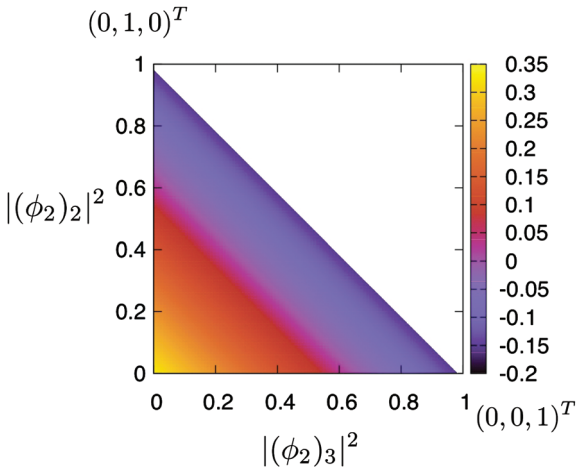

Fig. 23. The value of $G(\phi_1, \phi_2)$ as a function of $|(\phi_2)_2|^2$ and $|(\phi_2)_3|^2$. If the orientation ϕ_2 is in the red zone the interaction is repulsive, while in the blue zone the interaction is attractive.

two vortices placed in parallel. We assume that the orientation of each vortex is constant along the vortex. The interaction energy due to the gluon exchange is proportional to

$$G(\phi_1, \phi_2) \equiv \phi_1^\dagger T^a \phi_1 \phi_2^\dagger T^a \phi_2, \tag{6.10}$$

where ϕ_1 and ϕ_2 denote the orientations of the first and second vortices, respectively. We have shown in Fig. 23 the value of $G(\phi_1, \phi_2)$ as a function of ϕ_2. We have taken ϕ_1 as $\phi_1 = (1, 0, 0)^T$ without loss of generality. Figure 23 indicates that, if the two orientations are close in the $\mathbb{C}P^2$ space, the interaction through gluon exchanges is repulsive, while if the orientations are far apart, the interaction is attractive. This orientation-dependent interaction is expected to be important when the distance between two vortices is small, e.g. when two vortices cross.

6.2. Interaction with mesons

The interactions with phonons and gluons are topological, in the sense that the interaction term does not involve the metric. In contrast, the interaction with photons is not topological. Here, we discuss the interaction with mesons studied in Sect. 2.2.2, which is also non-topological. In this case, one cannot use a dual transformation to obtain the interaction Lagrangian.

First, let us remind ourselves of the effective action of mesons discussed in Sect. 2.2.2. The gauge invariant $\Sigma = \Phi_{\rm L}^\dagger \Phi_{\rm R}$ defined in Eq. (2.82) transforms under the flavor symmetry $U(1)_{\rm A} \times SU(3)_{\rm L} \times SU(3)_{\rm R}$ as

$$\Sigma \to e^{i\alpha} g_{\rm L}^\dagger \Sigma g_{\rm R}, \quad e^{i\alpha} \in U(1)_{\rm A}, \quad g_{\rm L} \in SU(3)_{\rm L}, \quad g_{\rm R} \in SU(3)_{\rm R}. \tag{6.11}$$

The chiral symmetry is broken to the vector symmetry $SU(3)_{\rm L+R}$ with $g_{\rm L} = g_{\rm R}$ in the CFL ground state $\Sigma = \Delta_{\rm CFL} \mathbf{1}_3$. The mesons are $\Sigma = \Delta_{\rm CFL}^2 g_{\rm L}^\dagger g_{\rm R} = \Delta_{\rm CFL}^2 g^2(x) = \Delta_{\rm CFL}^2 U(x)$ with $g_{\rm L}^\dagger = g_{\rm R} = g(x)$.

In a non-Abelian vortex background, $\Phi_{\rm L} = -\Phi_{\rm R} = {\rm diag}(f(r)e^{i\theta}, g(r), g(r))$, the gauge invariant Σ takes the form

$$\Sigma_v = {\rm diag}(f^2(r), g^2(r), g^2(r)) \quad [\to {\rm diag}(0, g_0^2, g_0^2) \text{ at } r = 0], \tag{6.12}$$

with a constant $g_0 = g(r = 0)$. In the presence of the vortex, the gauge invariant Σ becomes

$$\Sigma = \sqrt{U}^\dagger \Sigma_v \sqrt{U}. \tag{6.13}$$

Then, the chiral Lagrangian can be written as

$$\mathcal{L} = \sum_{\mu} f_{\mu} \mathrm{Tr}\,(\partial_{\mu}\Sigma^{\dagger}\partial^{\mu}\Sigma) = \sum_{\mu} f_{\mu} \mathrm{Tr}\,[2\alpha_{\mathrm{L}}\Sigma_{v}\alpha_{\mathrm{R}}\Sigma_{v} - (\alpha_{\mathrm{L}}^{2} + \alpha_{\mathrm{R}}^{2})\Sigma_{v}^{2}] \tag{6.14}$$

with the decay constants $f_{\mu} = (1/2)(f_{\pi}, f_{\pi} v_{\pi})$ in Eq. (2.86), and the left and right Maurer–Cartan forms

$$\alpha_{\mathrm{R}} \equiv \sqrt{U}^{\dagger}\partial_{\mu}\sqrt{U}, \quad \alpha_{\mathrm{L}} \equiv \sqrt{U}\partial_{\mu}\sqrt{U}^{\dagger}. \tag{6.15}$$

Far away from the vortex core, it reduces to

$$\mathcal{L} = -\Delta_{\mathrm{CFL}}^{2} \sum_{\mu} K_{\mu} \mathrm{Tr}\,(U^{\dagger}\partial_{\mu}U)^{2} \tag{6.16}$$

as expected. The Lagrangian in Eq. (6.14) describes the mesons in the vortex background.

6.3. *Interaction with electromagnetic fields*

Here we discuss the electromagnetic properties of non-Abelian vortices in the CFL phase, and their phenomenological consequences. Although the bulk CFL matter is electromagnetically neutral, the orientational zero modes are charged, as discussed later. Thus the vortices interact with photons. For this purpose we consider the low-energy effective action of orientational zero modes interacting with photons. Using the action, we discuss the scattering of photons by a vortex.

In the following analysis, we neglect the mixing of photons and gluons. The gauge field, A'_{μ}, which remains massless in the CFL phase, is a mixture of the photon A_{μ} and a gluon part A_{μ}^{8}, $A'_{\mu} = -\sin\zeta A_{\mu} + \cos\zeta A_{\mu}^{8}$. Here, the mixing angle ζ is given by $\tan\zeta = \sqrt{3}g_{\mathrm{s}}/2e$ [12], where g_{s} and e are the strong and electromagnetic coupling constants. At accessible densities ($\mu \sim 1\,\mathrm{GeV}$), the fraction of the photon is given by $\sin\zeta \sim 0.999$, and so the massless field A'_{μ} consists mostly of the ordinary photon and includes a small amount of the gluon. As a first approximation, we neglect the mixing of the gluon to the massless field.

We denote the orientational zero modes by a complex three-component vector $\phi \in \mathbb{C}P^{2}$, which satisfies $\phi^{\dagger}\phi = 1$. When we neglect the electromagnetic interaction, the low-energy effective theory on the vortex that is placed along the z axis is described by the following $\mathbb{C}P^{2}$ nonlinear sigma model [110]:

$$\mathcal{L}_{\mathbb{C}P^{2}} = \sum_{\alpha=0,3} C_{\alpha}\left[\partial^{\alpha}\phi^{\dagger}\partial_{\alpha}\phi + (\phi^{\dagger}\partial^{\alpha}\phi)(\phi^{\dagger}\partial_{\alpha}\phi)\right], \tag{6.17}$$

where the orientational moduli ϕ are promoted to dynamical fields, and C_{α} are numerical constants. Under the color–flavor-locked transformation, the $\mathbb{C}P^{2}$ fields ϕ transform as

$$\phi \to U\phi, \tag{6.18}$$

with $U \in SU(3)_{\mathrm{C+F}}$.

6.3.1. Coupling of orientation modes with electromagnetic fields. Now, let us consider the electromagnetic interactions. The electromagnetic $U(1)_{\mathrm{EM}}$ group is a subgroup of the flavor group $SU(3)_{\mathrm{F}}$. The generator of $U(1)_{\mathrm{EM}}$ is $T_{8} = \frac{1}{\sqrt{6}}\mathrm{diag}(-2, 1, 1)$ in our choice of basis. The effect of the electromagnetic interaction is incorporated by gauging the corresponding symmetry. The low-energy

effective action on the vortex should be modified to the following gauged $\mathbb{C}P^2$ model:

$$\mathcal{L}_{g\mathbb{C}P^2} = \sum_{\alpha=0,3} C_\alpha \left[\mathcal{D}^\alpha \phi^\dagger \mathcal{D}_\alpha \phi + (\phi^\dagger \mathcal{D}^\alpha \phi)(\phi^\dagger \mathcal{D}_\alpha \phi) \right], \tag{6.19}$$

where the covariant derivative is defined by

$$\mathcal{D}_\alpha \phi = \left(\partial_\alpha - ie\sqrt{6} A_\alpha T_8 \right) \phi. \tag{6.20}$$

Thus the low-energy behavior is described by the $\mathbb{C}P^2$ modes localized on the vortex and photons propagating in three-dimensional space. Hence, the effective action is given by

$$S = \int \left(\frac{\varepsilon_0}{2} \boldsymbol{E}^2 - \frac{1}{2\lambda_0} \boldsymbol{B}^2 \right) d^4x + \int \mathcal{L}_{g\mathbb{C}P^2} dz dt, \tag{6.21}$$

where ε_0 and λ_0 are the dielectric constant and permeability of the CFL matter, respectively. We can formally recover the Lorentz invariance in the kinetic terms of the photons by the following rescaling:

$$A'_0 = \sqrt{\varepsilon_0} A_0, \quad A'_i = \frac{1}{\sqrt{\lambda_0}} A_i, \quad t' = vt, \tag{6.22}$$

where $v \equiv 1/\sqrt{\varepsilon_0 \lambda_0}$. By further rescaling the parameters as

$$e' = \sqrt{\lambda_0} e, \quad C'_0 = C_0 v, \quad C'_3 = \frac{C_3}{v}, \tag{6.23}$$

we can write the Lagrangian in the following form:

$$vS = -\frac{1}{4} \int F_{\mu\nu} F^{\mu\nu} d^4x + \int \mathcal{L}'_{g\mathbb{C}P^2} dz dt, \tag{6.24}$$

where

$$\begin{aligned} \mathcal{L}'_{g\mathbb{C}P^2} &= \sum_{\alpha=0,3} C'_\alpha \left[\mathcal{D}'^\alpha \phi^\dagger \mathcal{D}'_\alpha \phi + (\phi^\dagger \mathcal{D}'^\alpha \phi)(\phi^\dagger \mathcal{D}'_\alpha \phi) \right], \\ \mathcal{D}'_\alpha \phi &= \left(\partial_\alpha - ie'\sqrt{6} A_\alpha T_8 \right) \phi. \end{aligned} \tag{6.25}$$

In the discussions below, primes are omitted for notational simplicity.

6.3.2. Scattering of photons off a vortex. We can discuss the consequences of the charged degrees of freedom on the vortex using the low-energy action (6.24). For example, let us consider the photon scattering off a vortex. The equation of motion of the photon field derived from the effective action is given by

$$\begin{aligned} \partial^\mu F_{\mu\nu} = &-C_\nu ie\sqrt{6}\, \delta(x_\perp)(\delta_{0\nu} + \delta_{3\nu}) \\ &\times \left\{ \phi^\dagger T_8 \mathcal{D}_\nu \phi - (\mathcal{D}_\nu \phi)^\dagger T_8 \phi - 2\phi^\dagger \mathcal{D}_\nu \phi \phi^\dagger T_8 \phi \right\}, \end{aligned} \tag{6.26}$$

where $\delta(x_\perp) \equiv \delta(x)\delta(y)$ is the delta function in the transverse plane. We consider a situation where a linearly polarized photon is normally incident on the vortex. We assume that the electric field of the photon is parallel to the vortex. Then, the problem is z-independent and we can set $\theta = \theta(t)$,

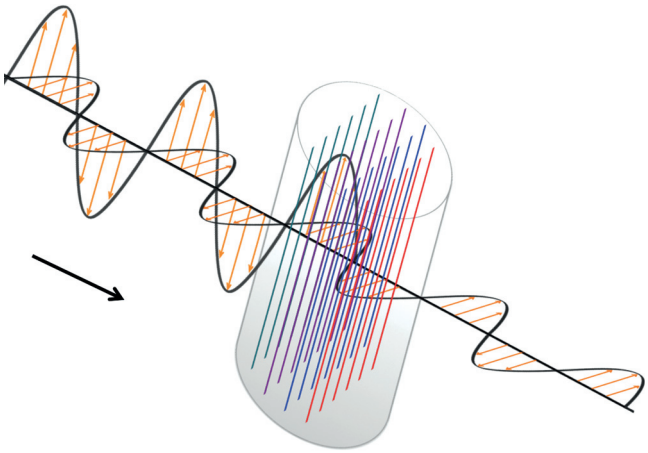

Fig. 24. Schematic figure of two linearly polarized photons entering a vortex lattice. Photons propagate in the direction of the big arrow. The small arrows indicate the electric field vector. The waves whose electric fields are parallel to the vortices are attenuated inside the lattice, while those with perpendicular electric fields pass through it.

$A_t = A_x = A_y = 0$, and $A_z = A_z(t, x, y)$. The equation of motion is rewritten as

$$\begin{aligned}
&(\partial_t^2 - \partial_x^2 - \partial_y^2) A_z(t, x, y) \\
&= 12 C_3 e^2 \left\{ \phi^\dagger (T_8)^2 \phi + (\phi^\dagger T_8 \phi)^2 \right\} A_z(t, x, y)\, \delta(x_\perp) \\
&\equiv 12 C_3 e^2 f(\phi) A_z(t, x, y)\, \delta(x_\perp),
\end{aligned} \tag{6.27}$$

where we have defined

$$f(\phi) \equiv \phi^\dagger (T_8)^2 \phi + (\phi^\dagger T_8 \phi)^2. \tag{6.28}$$

Equation (6.27) is the same as the one discussed by Witten in the context of superconducting strings [371], except for the orientation-dependent factor, $f(\phi)$. The cross section per unit length of a vortex, $d\sigma/dz$, is calculated as

$$\frac{d\sigma}{dz} = \frac{\left(12 C_3 e^2 f(\phi)\right)^2 \eta^2}{8\pi} \lambda = 288\pi \left(C_3 \alpha \eta f(\phi)\right)^2 \lambda, \tag{6.29}$$

where λ is the wavelength of the incident photon, η is a numerical factor of order unity, and α is the fine structure constant. On the other hand, if the electric field of the wave is perpendicular to the vortex, the photon is not scattered, since current can flow only along the vortex.

6.3.3. Vortex lattice as cosmic polarizer. The electromagnetic property of vortices can be phenomenologically important as it may lead to some observable effects. As an illustration of such an effect, we show that a lattice of vortices works as a polarizer of photons. The rotating CFL matter is expected to be threaded with quantum vortices along the axis of rotation, resulting in the formation of a vortex lattice, as discussed in Sect. 4.4 [242,309,315]. This is basically the same phenomenon as when one rotates atomic superfluids. Suppose that a linearly polarized photon is incident on a vortex lattice, as shown in Fig. 24. If the electric field of the photon is parallel to the vortices, it induces currents along the vortices, which results in the attenuation of the photon. On the other hand, waves with electric fields perpendicular to the vortices are not affected. This is exactly what a polarizer does. A lattice passes electromagnetic waves of a specific polarization and blocks waves of other

polarizations. This phenomenon, resulting from the electromagnetic interaction of vortices, may be useful for finding observational evidence of the existence of CFL matter.

We consider a situation where electromagnetic waves of some intensity normally enter the vortex lattice. We first assume that the electric fields of the waves are parallel to the vortices. The fraction of the loss of intensity when the wave passes through the lattice for distance dx is

$$\left\langle \frac{d\sigma}{dz} \right\rangle n_v dx \equiv \frac{dx}{L}, \tag{6.30}$$

where n_v is the number of vortices per unit area. We defined the length L by

$$L \equiv 1/\left(n_v \left\langle \frac{d\sigma}{dz} \right\rangle \right) = \ell^2 / \left\langle \frac{d\sigma}{dz} \right\rangle, \tag{6.31}$$

with the intervortex spacing ℓ. As the cross section depends on the internal state (value of ϕ) of the vortex, we have introduced the averaged scattering cross section $\langle d\sigma/dz \rangle$ over the ensemble of the vortices. Let us denote the intensity of waves at a distance x from the surface of the lattice as $I(x)$. $I(x)$ satisfies

$$\frac{I(x+dx)}{I(x)} = 1 - \frac{dx}{L}. \tag{6.32}$$

Therefore, the x dependence of $I(x)$ is characterized by the following equation:

$$\frac{I'(x)}{I(x)} = -\frac{1}{L}. \tag{6.33}$$

This equation is immediately solved as $I(x) = I_0 e^{-x/L}$, where I_0 is the initial intensity. Hence, the waves are attenuated with the characteristic length L.

Let us make a rough estimate of the attenuation length. The total number of vortices can be estimated, as in Ref. [183], as

$$N_v \simeq 1.9 \times 10^{19} \left(\frac{1\,\mathrm{ms}}{P_{\mathrm{rot}}} \right) \left(\frac{\mu/3}{300\,\mathrm{MeV}} \right) \left(\frac{R}{10\,\mathrm{km}} \right)^2, \tag{6.34}$$

where P_{rot} is the rotation period, μ is the baryon chemical potential, and R is the radius of the CFL matter inside dense stars. We have normalized these quantities by typical values. The intervortex spacing is then written as

$$\ell \equiv \left(\frac{\pi R^2}{N_v} \right)^{1/2} \simeq 4.0 \times 10^{-6}\,\mathrm{m} \left(\frac{P_{\mathrm{rot}}}{1\,\mathrm{ms}} \right)^{1/2} \left(\frac{300\,\mathrm{MeV}}{\mu/3} \right)^{1/2}. \tag{6.35}$$

Therefore, the characteristic decay length of the electromagnetic waves is estimated as

$$L = \frac{\ell^2}{288\pi\,(C_3 \alpha \eta)^2\,\langle f(\phi)^2 \rangle \lambda} \simeq \frac{1.2 \times 10^{-11}\,\mathrm{m}^2}{\lambda}. \tag{6.36}$$

Here we have determined the value of $f(\phi)$ by considering the effect of a finite strange quark mass m_{s}. The finite strange quark mass breaks the flavor $SU(3)$ symmetry and gives rise to a potential in the $\mathbb{C}P^2$ space, as discussed in Ref. [115]. When m_{s} is larger than the typical kinetic energy of the $\mathbb{C}P^2$ modes, which is given by the temperature $T \leq T_{\mathrm{c}} \sim 10^1\,\mathrm{MeV}$, and is small enough that the description by the Ginzburg–Landau theory based on chiral symmetry is valid, the orientation of vortices falls into $\phi_0^T = (0, 1, 0)$. This assumption is valid for the realistic value of $m_{\mathrm{s}} \sim 10^2\,\mathrm{MeV}$. The orientation dependence of the cross section is encapsulated in the function $f(\phi)$ defined in Eq. (6.28). Since $f(\phi_0) = 1/3 \neq 0$, photons interact with a vortex with this orientation. Therefore,

we have taken $\langle f(\phi)^2 \rangle = f(\phi_0)^2 = 1/9$. We have also taken $\eta = 1$, $\mu = 900\,\mathrm{MeV}$, and $\Delta_{\mathrm{CFL}} = 100\,\mathrm{MeV}$, from which the values of C_3 are determined [115].

If we adopt $R \sim 1\,\mathrm{km}$ for the radius of the CFL core, the condition that the intensity is significantly decreased within the core is written as $L \leq 1\,\mathrm{km}$. The condition can also be stated in terms of the wavelength of the photon as

$$\lambda \geq 1.2 \times 10^{-14}\,\mathrm{m} \equiv \lambda_{\mathrm{c}}. \tag{6.37}$$

Hence, a lattice of vortices serves as a wavelength-dependent filter of photons. It filters out the waves with electric fields parallel to the vortices, if the wavelength λ is larger than λ_{c}. The waves that pass through the lattice are linearly polarized ones with the direction of their electric fields perpendicular to the vortices, as shown schematically in Fig. 24.

One may wonder why a vortex lattice with a mean vortex distance ℓ can block photons with wavelengths many orders smaller than ℓ. It is true that the probability that a photon is scattered during its propagation for a small distance (e.g. $\sim \ell$) is small. However, while the photon travels through the lattice, the scattering probability is accumulated and the probability that a photon remains unscattered decreases exponentially. Namely, the small scattering probability is compensated by the large number of vortices through which a photon passes. This is why the vortex mean distance and the wavelength of the attenuated photons can be different.

7. Colorful boojums at a CFL interface

7.1. What are boojums?

When vortices cross or end on an interface between two distinct superfluid phases or on a boundary, they may form interesting structures called "boojums" [238,361]. Boojums are composite topological objects consisting of vortices, an interface, and possibly monopoles at endpoints of vortices, and are topologically characterized in terms of the relative homotopy group [361]. Various types of boojums have been studied in nematic liquids [360], superfluids at the edge of a container filled with ^{4}He, at the A–B phase boundary of ^{3}He [53,161], and in multi-component or spinor Bose–Einstein condensates [56,57,196–198,259,342] in condensed matter physics. Such boojums are also considered in field theories such as nonlinear sigma models [142], Abelian gauge theories [317], and non-Abelian gauge theories [24,94,103,184]; see Refs. [107,319,320] for reviews.

Here we discuss "colorful boojums" [76] appearing at the interface [8,10,144] of a color superconductor. It is most likely that the *npe* phase exists in the core of neutron stars, where neutrons and protons are superfluid and superconducting, respectively. In the high density region of nuclear matter, a spin triplet (p-wave) pairing of neutrons is energetically favored compared to an s-wave pairing [341]. The inner region may be characterized by the presence of hyperons or of the CFL phase. We consider the interface of a hadron phase and a color superconductor [8,10,144].[10] Since neutron stars are rotating rapidly and are accompanied by large magnetic fields, both superfluid and superconducting vortices exist in the *npe* phase [42]. Such vortices are expected to explain the pulsar glitch phenomenon [19]. On the other hand, when the matter in the CFL phase is rotating, such as

[10] The system we describe is the simplest configuration in the pure CFL phase, which is realized at very high densities $\mu \gg m_{\mathrm{s}}^2/\Delta_{\mathrm{CFL}}$. However, in a more realistic setting, the strange quark mass stresses the CFL phase and other phases have to be considered. For example, when the chemical potential is low enough that $m_{\mathrm{s}} \gtrsim m_{\mathrm{u,d}}^{1/3}\Delta_{\mathrm{CFL}}^{2/3}$, kaons can condense, leading to the so-called CFL-K^0 phase [44,47,195,300], where other kinds of vortices arise [62,194]. However, in the high density regime, the boojum can be modified only in the vicinity of the interface, while the overall structure of the junction is kept unchanged.

in the cores of neutron stars, superfluid vortices [128,183] are inevitably created and are expected to constitute a vortex lattice. However, the simplest superfluid vortex carrying integer circulation is unstable and decays [128,183,242] into a set of three non-Abelian vortices, each of which carries a color-magnetic flux and 1/3 quantized circulation [35,112], as discussed in Sect. 4.3. Non-Abelian vortices constitute a colorful vortex lattice in the CFL phase side, as discussed in Sect. 4.4.

It was discussed in Ref. [76] that boojum structures are created when superfluid and superconducting vortices of the *npe* phase penetrate into the CFL core. The shape of the neutron boojum was shown to split into three color magnetic vortices. The colorful boojum is accompanied by confined color-magnetic monopoles of two different kinds, Dirac monopoles and surface superconducting currents.

We first study the structure of a colorful boojum in the CFL phase side in Sect. 7.2 followed by the structure in the *npe* phase in Sect. 7.3.

7.2. *Colorful boojums at the CFL phase side*

7.2.1. The shape of boojums. When a non-Abelian vortex hits the boundary of the CFL phase, it cannot go out from the CFL phase since it carries a color magnetic flux. Since $U(1)_{\rm B}$ vortices do not have fluxes, they can go out. One $U(1)_{\rm B}$ vortex decays into three non-Abelian vortices with total color fluxes canceled out, as discussed in Sect. 4.3. In other words, non-Abelian vortices can go out only when three of them meet to cancel the total color fluxes as imposed by color neutrality. Such connected points form "colorful boojums." Including the electromagnetic interactions, the only possibility is the formation of a BDM, a $\mathbb{C}P^1_+$, and a $\mathbb{C}P^1_-$ vortex. In fact, as explained in Eq. (5.53), the BDM vortex carries a $U(1)_{\rm EM}$ magnetic flux $\Phi^{\rm EM}_{\rm BDM} = \frac{\delta^2}{1+\delta^2}\frac{2\pi}{e}$ with $\delta^2 = \frac{2}{3}\frac{e^2}{g_{\rm s}^2}$, while the $\mathbb{C}P^1_\pm$ vortex flux is $\Phi^{\rm EM}_{\mathbb{C}P^1_\pm} = -\frac{1}{2}\Phi^{\rm BDM}_{\rm EM}$. Then, $U(1)_{\rm EM}$ magnetic fluxes are canceled out.

In order to present a structure of the boojum in the CFL phase side, one can model the system as a regular lattices of boojums where the relative separation between vortices in a single boojum is denoted by $y(z)$ as a function of the distance z from the interface. The center of the ith boojum at the interface is indicated by $\vec{x}_i$. We use the Nambu–Goto action and approximate the interaction of vortices with that of global parallel vortices, given in Eq. (4.22). The energy, per unit length, of the lattice is then:

$$\begin{aligned} E_{\rm tot}(y) &= 3\mathcal{N}\mathcal{T}\sqrt{1+(dy/dz)^2} + V_{\rm int}(y), \\ V_{\rm int}(y) &= -3\mathcal{N}\mathcal{T}\log|y| - 9\mathcal{T}\sum_{i>j}\log|\vec{x}_i - \vec{x}_j|, \end{aligned} \tag{7.1}$$

where $\mathcal{N}$ is the number of boojums and $\mathcal{T}$ is the tension of a color-magnetic vortex. The first term in the potential above is the interaction energy between vortices in the same boojum, while the second term represents the one between boojums, where the shape of the boojum has been neglected. Notice that the first term in the potential has to be regularized in the limit $y \to 0$.

The numerical shape of the boojum is shown in Fig. 25, where we have evaluated the interaction potential for a one dimensional lattice for simplicity. The most important property of the boojum that can be inferred from this very simplified numerical analysis is that the longitudinal size scales proportionally to the transverse lattice spacing. We have also checked that this property and the shape of the boojum also do not depend on the choice of regularization of the interaction potential for coincident vortices.

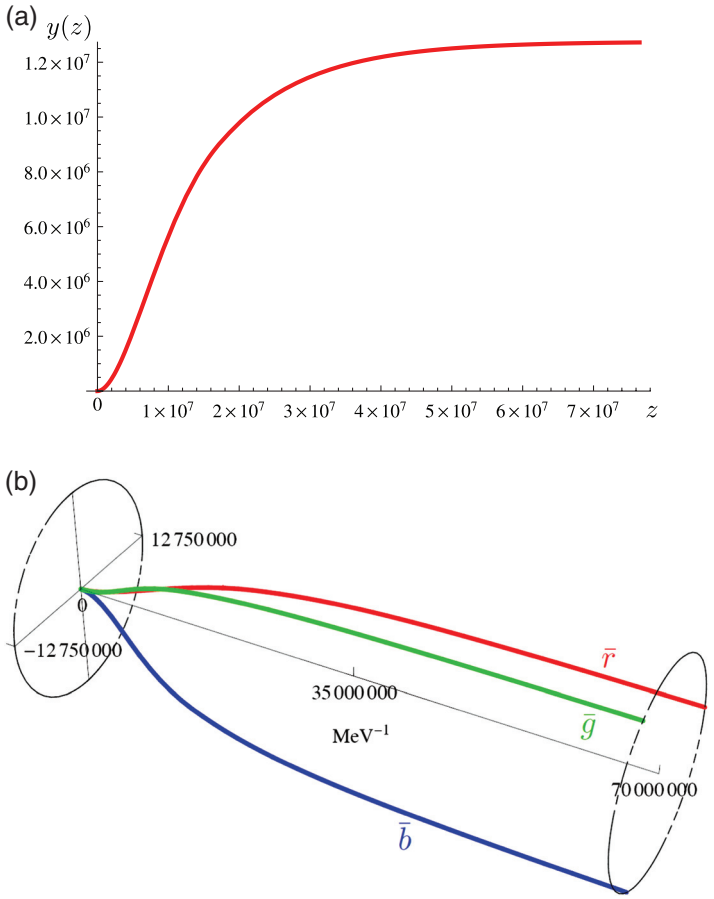

Fig. 25. (a) Transverse shape and (b) three dimensional shape of a colorful boojum. The *npe*–CFL interface is on the left, where three color vortices originate from the boojum. We have used typical values of the GL parameters as done, e.g., in Ref. [356]. In (b), we have ignored the effect of the strange quark mass.

7.2.2. Formation of colorful monopoles with strange quark mass. At a typical distance ξ from the interface, though, the BDM and the $\mathbb{C}P^1_-$ solutions will "decay" to the $\mathbb{C}P^1_+$ vortex, due to their instability. We can estimate the length scale ξ by referring to the low-energy effective Lagrangian (5.11) with (5.12). Following the steps of Eq. (5.24), we obtain

$$\xi \sim m_{\rm s}^{-1}\left(\frac{\mu}{\Delta_\varepsilon}\right)^2 \log\left(\frac{\mu}{\Delta_\varepsilon}\right)^{-1/2} \sim 131\,{\rm GeV}^{-1}, \tag{7.2}$$

with the physical quantities being $\mu \sim 1\,{\rm GeV}$, $\Delta_\varepsilon \sim 100\,{\rm MeV}$, $K_3 = 9$. This length has to be compared with the thickness d of the interface, which can be seen as a domain wall between the two different phases [144]. Using the same values for physical parameters, we get

$$d \simeq 0.1\xi. \tag{7.3}$$

Then the vortices decay at large distances from the interface.

Since vortices decay into others with different fluxes, each junction corresponds in fact to a monopole. Unlike the Dirac monopole at the endpoint of a proton vortex, this is a confined *color magnetic* monopole attached by vortices from both sides. The monopole connecting the $\mathbb{C}P^1_-$ and $\mathbb{C}P^1_+$ vortices is a pure color magnetic monopole, because the two vortices have the same $U(1)_{\rm EM}$ magnetic flux but different color-magnetic fluxes; the junction between BDM and $\mathbb{C}P^1_+$ is instead realized

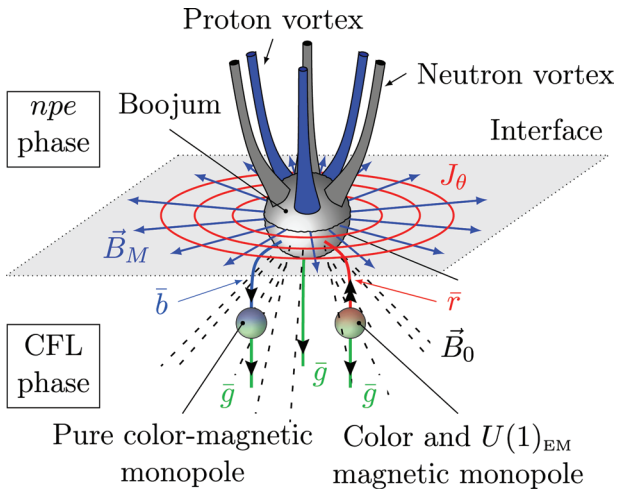

Fig. 26. Colorful boojum. Three neutron vortices and three proton vortices end on a boojum at the interface in the *npe* phase side, and the three BDM ($\bar{r}$), $\mathbb{C}P^1_+$ ($\bar{g}$), and $\mathbb{C}P^1_+$ ($\bar{b}$) vortices end on it in the CFL phase side. The black arrows along the three vortices represent $U(1)_{\rm EM}$ magnetic flux. The two colorful monopole junctions that exist in the presence of the strange quark mass are also depicted. The pure magnetic fluxes split into a massive $\vec{B}^{\rm M}$ component, which is screened by a surface current and bent along the interface, and a massless $\vec{B}^0$ component emanating from the boojum, which looks like a Dirac monopole.

by a color-magnetic and $U(1)_{\rm EM}$ magnetic monopole, because for these vortices both the $U(1)_{\rm EM}$ magnetic and color-magnetic fluxes are different. The colorful boojum is qualitatively depicted in Fig. 26.

7.3. Colorful boojums at the npe phase side

7.3.1. Matching condition. The question of what are formed at a boojum point outside the CFL phase now arises. The CFL phase may be connected with the kaon condensed (CFL + K) phase, 2SC phase, or hyperon phase. However, in a realistic situation for the cores of neutron stars, there is the *npe* phase. Here, we discuss what are connected to the colorful boojums in the *npe* phase. Note that, in the following discussion, we do not assume that the CFL phase is directly connected to the *npe* phase, but that the other phases mentioned above can be sandwiched between the CFL and *npe* phases.

When quarks travel around a vortex, they acquire an Aharonov–Bohm phase in general. Such phases have to match across the interface. In the CFL phase, the order parameter is $\langle qq \rangle$, which behaves as

$$\langle qq \rangle \sim e^{i\theta} : U(1)_{\rm B} \text{ vortex} \tag{7.4}$$

for the endpoint of a $U(1)_{\rm B}$ vortex or a triplet of non-Abelian semi-superfluid vortices, indicating that the quark fields obtain a phase

$$\Delta\theta|_{U(1)_{\rm B}} = \frac{2\pi}{2} = \pi \tag{7.5}$$

corresponding to $1/2$ $U(1)_{\rm B}$ winding, when they travel around a $U(1)_{\rm B}$ vortex or a triplet of semi-superfluid vortices. In particular, all quark fields including u and d quarks relevant in hadronic matter obtain a phase in Eq. (7.5) around the $U(1)_{\rm B}$ vortex.

The order parameters in the *npe* phase are $\langle nn\rangle \sim \langle (udd)(udd)\rangle$ for neutron condensation and $\langle pp\rangle \sim \langle (uud)(uud)\rangle$ for proton condensation.[11] We label the winding numbers of the order parameters $\langle nn\rangle$ and $\langle pp\rangle$ in the presence of a vortex by (p, q). In the presence of a neutron vortex $(1, 0)$, these order parameters behave as

$$(1,0): \quad \langle nn\rangle \sim \langle (udd)(udd)\rangle \sim e^{i\theta}, \quad \langle pp\rangle \sim \langle (uud)(uud)\rangle \sim 1. \tag{7.6}$$

From these behaviors, we find that the u and d quark wave functions are of the form

$$(1,0): \quad (u,d) \sim (e^{-i(1/6)\theta}, e^{i(2/6)\theta}) \tag{7.7}$$

in the presence of a neutron vortex. In the same way, the winding of the order parameters in the presence of a proton vortex $(0, 1)$,

$$(0,1): \quad \langle nn\rangle \sim \langle (udd)(udd)\rangle \sim 1, \quad \langle pp\rangle \sim \langle (uud)(uud)\rangle \sim e^{i\theta}, \tag{7.8}$$

leads the wave functions of u and d quarks to be

$$(0,1): \quad (u,d) \sim (e^{i(2/6)\theta}, e^{-i(1/6)\theta}). \tag{7.9}$$

From Eqs. (7.7) and (7.9), a composite of neutron and proton vortices has the winding numbers of the order parameters and quarks

$$(1,1): \quad \langle nn\rangle \sim \langle (udd)(udd)\rangle \sim e^{i\theta}, \quad \langle pp\rangle \sim \langle (uud)(uud)\rangle \sim e^{i\theta}, \tag{7.10}$$

$$(1,1): \quad (u,d) \sim (e^{i(1/6)\theta}, e^{i(1/6)\theta}), \tag{7.11}$$

respectively. From this, we see that u and d quarks get a phase

$$\Delta\theta|_{(1,1)} = \frac{2\pi}{6} = \frac{\pi}{3}, \tag{7.12}$$

corresponding to $1/6$ $U(1)_{\rm B}$ winding, when they encircle a composite $(1, 1)$ of neutron and proton vortices in the *npe* phase.

From Eqs. (7.5) and (7.12), we have a relation

$$\Delta\theta|_{(3,3)} (= 3\Delta\theta|_{(1,1)}) = \Delta\theta|_{U(1)_{\rm B}}. \tag{7.13}$$

This implies that u and d quarks have continuous wave functions only when three neutron vortices *and* three proton vortices join at a colorful boojum point in the *npe* phase.

7.3.2. Magnetic fluxes. The proton condensation is electrically charged. Therefore, the lowest energy configuration of a proton vortex is accompanied by a magnetic flux, which must be quantized

$$\Phi_0 = \pi/e \tag{7.14}$$

as Abrikosov–Nielsen–Olesen (ANO) vortices in metallic superconductors. When this flux penetrates into the CFL phase, the $U(1)_{\rm EM}$ magnetic flux is converted into both the fluxes corresponding to the massive and massless combinations $A^{\rm M}$ and A^0. This is due to conservation of flux and to the mixing in Eqs. (2.48) and (2.49), respectively. The massive combination $A^{\rm M}$ is screened by a surface

[11] At high density, a spin triplet (p-wave) pairing is favored for neutron condensation more than s-wave pairing [341]. In this case, half-quantized vortices are possible, but here we count neutron vortices as integer vortices for simplicity.

color-magnetic current circulating around the contact point. Unlike metallic superconductors, this is completely screened and cannot enter the CFL phase, even if the flux is larger than the quantized flux of the non-Abelian vortex, because the non-Abelian vortex also has to carry the 1/3 quantized circulation. A rough estimate of the behavior of the current in the proximity of the vortex endpoint can be obtained by using the London equation valid for an ordinary superconductor. Then we obtain

$$J_\theta \simeq \frac{\Phi_0}{2\pi r}, \tag{7.15}$$

where θ and r are the planar polar coordinates centered at the contact point. On the other hand, the massless combination A^0 can spread freely into the CFL phase, there being no superconducting currents that can screen it. This object looks like a Dirac monopole, as is common in boojums in other systems, such as helium superfluids. This boojum is qualitatively depicted in Fig. 26.

One may wonder whether the formation of vortices under rotation would lead to the generation of magnetic fields inside neutron stars. However, it turns out that the magnetic fields induced at colorful boojums are in fact quite small, and are estimated as

$$B \sim \frac{N_v \times \Phi_0}{(10\,\mathrm{km})^2} = 10^{19} \times 10^{-7}\mathrm{G\,cm^2} \times 10^{-8}\,\mathrm{m^2} \simeq 1\mathrm{G} = 10^{-4}\mathrm{T}, \tag{7.16}$$

where N_v is the total number of vortices Eq. (4.41), and parameters like the rotational period, baryon chemical potential, and the core radius are set to typical values.

8. Fermions in vortices

We here discuss fermionic structures inside non-Abelian vortices. Inside a vortex, fermions are important degrees of freedom at low energies, since some of the superconducting gaps vanish in the core and fermions become massless. We can investigate the fermion states by the Bogoliubov–de Gennes (BdG) equation. In Sect. 8.1, we introduce the BdG equation for an *Abelian* vortex, and find the solution of a zero-mode fermion, which is called a Majorana fermion. In Sect. 8.2, we discuss the BdG equation for a *non-Abelian* vortex in the CFL phase, and find Majorana fermions that belong to the triplet or singlet representation of the $SU(2)_{\mathrm{C+F}} \times U(1)_{\mathrm{C+F}}$ symmetry. In Sect. 8.3, we discuss the 1+1 dimensional effective theory for Majorana fermions propagating along a vortex axis. In Sect. 8.4, as a new result in this paper, we show the absence of supercurrent by fermions along a vortex, unlike the case of Witten's superconducting string. In Sect. 8.5, we discuss the index theorem to count the number of zero-mode fermions, and show that the result from the index theorem is consistent with that obtained by directly solving the BdG equation.

8.1. The Bogoliubov–de Gennes equations and Majorana fermions for Abelian vortices

Here we analyze the internal fermionic structures of vortices in terms of the BdG equations. So far we have discussed the structures of non-Abelian vortices based on the GL equation, where the diquarks are dynamical degrees of freedom. Such a description is valid only at distances larger than the coherence length. At short-distance scales, fermionic degrees of freedom become important. The Bogoliubov–de Gennes (BdG) equation describes the dynamics of the fermions as well as the gap functions. The BdG equation gives a self-consistent solution for the wave functions of the fermion and the gap profile function. Note that the BdG equation is different from the Bogoliubov equation or the Bardeen–Cooper–Schrieffer (BCS) equation. The Bogoliubov or BCS equations describe only the plane wave for the fermion, while the BdG equation allows more general wave functions, unlike the plane wave. This property is quite important for the analysis of vortices. Inside vortices, the gap

profile function $\Delta(r)$ is zero at the center of the vortex ($\Delta(0) = 0$), while it becomes the bulk gap (the gap in the bulk space) at a position infinitely far from the vortex core ($\Delta(\infty) = \Delta_{\rm bulk}$). Namely, the gap profile function for a vortex is position-dependent. So we need to use the BdG equation in order to take the position dependence of the gap of a vortex into account and to analyze the fermion structure inside a vortex.

Let us comment on the previous studies on vortices in superconductors using the BdG equations. The BdG equation was first applied to a vortex inside an s-wave superconductor in Refs. [69,86] in which fermions are non-relativistic. In these first studies, the order parameter (the superconducting gap) was treated as a background field. Successive studies were devoted to finding self-consistent solutions of the BdG equation [157,323]. A complete self-consistent description was achieved by considering both quasibound and scattering fermions in the vortex [158,225]. The description reviewed here is very similar to that of the vortex–(relativistic) fermion system discussed in Refs. [189,365,371]. The difference from these studies is that we here consider a fermionic matter at *finite densities* (otherwise color superconductivity does not take place). The previous studies [189,365,371] were formulated only in the vacuum. The analysis of vortices in condensed matter systems via the BdG equation predicted an enhanced local density of fermion states at the Fermi level around the vortex core, which is experimentally observed in various metals [155,288]. Recently, the analysis of vortices in terms of the BdG equation has also been applied to the BEC–BCS crossover in fermionic cold atom systems [226,313]. For the application of the BdG equation in condensed matter systems, see also Refs. [16,51,166,167,217,220,278,284,296,298,345,359].

We discuss the BdG equation for a superconductor with a vortex. Since a non-Abelian vortex has a complex structure because of the internal degrees of freedom, we first review the results for an Abelian vortex, in which a single component massless fermion is trapped. The fermionic structure of a non-Abelian vortex is discussed in Sect. 8.2.

We here consider a superconducting system made of a single species of fermion. The fermions make pairs and form a Bose condensate. The BdG equation in the Nambu–Gor'kov representation $\Psi = (\varphi, \eta)^{\rm T}$ (particle in the upper component and hole in the lower component) is given by

$$\mathcal{H}\Psi = \mathcal{E}\Psi, \tag{8.1}$$

where $\mathcal{E}$ is the energy measured from the chemical potential μ and $\mathcal{H}$ is the Hamiltonian in the mean-field approximation,

$$\mathcal{H} \equiv \begin{pmatrix} -i\gamma_0\vec{\gamma}\cdot\vec{\nabla} - \mu & \Delta(\vec{x})\gamma_0\gamma_5 \\ -\Delta^*(\vec{x})\gamma_0\gamma_5 & -i\gamma_0\vec{\gamma}\cdot\vec{\nabla} + \mu \end{pmatrix}. \tag{8.2}$$

The gap profile function $\Delta(\vec{x})$ (three dimensional coordinate $\vec{x} = (x, y, z)$) is given as $\Delta(\vec{x}) \propto \langle \Psi^{\rm T}\Psi \rangle$, where the expectation value is given by the sum over all the fermion states in the ground state. This Hamiltonian has the particle–hole symmetry

$$\mathcal{U}^{-1}\mathcal{H}U = -\mathcal{H}^*, \quad \mathcal{U} = \begin{pmatrix} 0 & \gamma_2 \\ \gamma_2 & 0 \end{pmatrix}. \tag{8.3}$$

Thus, $\mathcal{H}\Psi = \mathcal{E}\Psi$ implies $\mathcal{H}(\mathcal{U}\Psi) = -\mathcal{E}(\mathcal{U}\Psi)$ and the spectrum is symmetric above and below the Fermi sea.

If one considers a vortex solution, because of the translational invariance along the vortex (z) axis, the gap is a function of the distance $r = \sqrt{x^2 + y^2}$ from the center of the vortex and θ an angle around the vortex; $\Delta(\vec{x}) = |\Delta(r)|e^{i\theta}$. The gap profile function also satisfies the following boundary

conditions: $|\Delta(r=0)|=0$ at the center of the vortex and $|\Delta(r=\infty)|=|\Delta_{\rm bulk}|$ at a position far from the vortex with a bulk gap $\Delta_{\rm bulk}$. Since the system is translationally invariant along the vortex axis, we can always take the fermion states to be eigenstates of the momentum in the z-direction k_z,

$$\Psi^{k_z}_{\pm,m}(r,\theta,z)=\Psi_{\pm,m}(r,\theta)\,{\rm e}^{ik_z z}, \tag{8.4}$$

where $\Psi_{\pm,m}(r,\theta)$ is the wave function on the x–y plane. Here $\pm$ is for the chirality, left and right, of the fermion and an integer m is related to the z component of the total angular momentum J_z. In the Nambu–Gor'kov formalism, the wave function $\Psi_{\pm,m}(r,\theta)$ is given as

$$\Psi_{\pm,m}(r,\theta)=\begin{pmatrix}\varphi_{\pm,m}(r,\theta)\\ \eta_{\mp,m-1}(r,\theta)\end{pmatrix}, \tag{8.5}$$

with the particle component $\varphi_{\pm,m}(r,\theta)$ and the hole component $\eta_{\mp,m-1}(r,\theta)$. The z component of J_z is $m+1/2$ for the particle and $(m-1)+1/2$ for the hole, respectively. Note that the chirality $\pm$ of the particle is assigned opposite to that of the hole.

The solution of the BdG equation (8.1) gives all the fermion modes in the vortex. They include the scattering states with energies $|\mathcal{E}|>|\Delta_{\rm bulk}|$ as well as the bound states with energies $|\mathcal{E}|<|\Delta_{\rm bulk}|$. It is a nontrivial problem to obtain all the fermion solutions. In the present discussion, we concentrate on the fermion states with the lowest energy inside the vortex, which are the most important degrees of freedom at low energies. Furthermore, we here regard the gap profile function $|\Delta(r)|$ as a background field and do not analyze the self-consistent solution for the gap profile function and the fermion wave functions. Such study will be left for future work.

As a result of the particle–hole symmetry, we find that the state with $\mathcal{E}=0$ is a "Majorana fermion", which has the special property that a particle and a hole are equivalent. The explicit solution of the wave function of the Majorana fermion is given as, for the right mode (+ for a particle, − for a hole),

$$\varphi_{+,0}(r,\theta)=C\,{\rm e}^{-\int_0^r|\Delta(r')|\,dr'}\begin{pmatrix}J_0(\mu r)\\ i\,J_1(\mu r)\,{\rm e}^{i\theta}\end{pmatrix}, \tag{8.6}$$

$$\eta_{-,-1}(r,\theta)=C\,{\rm e}^{-\int_0^r|\Delta(r')|\,dr'}\begin{pmatrix}-J_1(\mu r)\,{\rm e}^{-i\theta}\\ i\,J_0(\mu r)\end{pmatrix}, \tag{8.7}$$

and, for the left mode (− for a particle, + for a hole),

$$\varphi_{-,0}(r,\theta)=C'\,{\rm e}^{-\int_0^r|\Delta(r')|\,dr'}\begin{pmatrix}J_0(\mu r)\\ -i\,J_1(\mu r)\,{\rm e}^{i\theta}\end{pmatrix}, \tag{8.8}$$

$$\eta_{+,-1}(r,\theta)=C'\,{\rm e}^{-\int_0^r|\Delta(r')|\,dr'}\begin{pmatrix}J_1(\mu r)\,{\rm e}^{-i\theta}\\ i\,J_0(\mu r)\end{pmatrix}, \tag{8.9}$$

where C and C' are normalization constants, and $J_n(x)$ is the Bessel function. We have represented the solutions in the Weyl (2-component) spinors. The derivation is described in detail in Appendix E.

The solutions above satisfy a "Majorana-like" condition ($\kappa=\pm1$)[12]

$$\Psi=\kappa\mathcal{U}\Psi^*, \tag{8.10}$$

which physically implies the equivalence between a particle and a hole. We note that the Majorana fermion is localized around the center of the vortex. This can be seen by setting $|\Delta(r)|$ as a constant $|\Delta_{\rm bulk}|$, because the exponential functions in Eqs. (8.6) and (8.7) or Eqs. (8.8) and (8.9) exhibit

[12] $\kappa=1$ is for the right mode and $\kappa=-1$ is for the left mode.

behavior like $e^{-|\Delta_{\rm bulk}|r}$. Fermion zero modes (Majorana fermions) in relativistic theories were found in the (Abelian) vortex in the vacuum [189], where the number of zero modes is determined by the index theorem to be $2n$ for vortices with winding number n [365]. The Majorana-fermion solution in a vortex in a p-wave superconductor was first found by Fukui [136] for non-relativistic fermions, and later in Refs. [253,378] for relativistic fermions. Although there exist Majorana-like solutions in vortices in p-wave superconductors both for non-relativistic and relativistic fermions, they are absent for non-relativistic fermions in vortices in s-wave superconductors [69]. We comment that the fermions bound in the vortex are also intuitively understood in view of the Andreev reflection. When the fermions meet the interface between the normal phase (inside of the vortex) and the superconducting phase (outside of the vortex), there appear Cooper pairs created in the superconducting phase and holes reflected in the normal phase. This is called the Andreev reflection [21]. The Andreev reflection was also considered in the CFL phase [289]. The multiple number of reflections of the fermions (particle and holes) at the interface causes the bound state inside the vortex.

8.2. Bogoliubov–de Gennes formalism and Majorana fermions for non-Abelian vortices

Now let us investigate the fermion structure of a non-Abelian vortex in the CFL phase. Because of the internal symmetry, the BdG equation is a multi-component equation with 3(color) $\times$ 3(flavor) $=$ 9 degrees of freedom whose subspaces belong to multiplets of $U(1)_{\rm C+F} \times SU(2)_{\rm C+F}$ symmetry. The gap structure of a non-Abelian vortex is given as [378]

$$\Phi(r,\theta) = \begin{pmatrix} \Delta_0(r) & 0 & 0 \\ 0 & \Delta_0(r) & 0 \\ 0 & 0 & \Delta_1(r,\theta) \end{pmatrix}, \tag{8.11}$$

with the basis spanned by $\bar{\rm u}(\bar{\rm r}) = {\rm ds(gb)}$, $\bar{\rm d}(\bar{\rm g}) = {\rm su(br)}$ and $\bar{\rm s}(\bar{\rm b}) = {\rm ud(rg)}$, where $\Delta_1(r,\theta) = |\Delta_1(r)|\, e^{i\theta}$ corresponds to the vortex configuration with winding number one, and $\Delta_0(r)$ does not have a winding number (though it is not necessarily spatially constant). We remember that $\Delta_1(r)$ satisfies the boundary conditions, $\Delta_1(r=0)=0$ and $\Delta_1(r=\infty) = |\Delta_{\rm CFL}|$, with the gap $\Delta_{\rm CFL}$ in bulk space, while $\Delta_0(r)$ satisfies only $\Delta_0(r=\infty) = |\Delta_{\rm CFL}|$. The value of $\Delta_0(r=0)$ depends the details of the equation of the gap profile function. In the configuration in Eq. (8.11), the ud diquark pair with green and blue has a nontrivial winding number, while the other pairs, i.e. the ds diquark pair with blue and red and the su diquark pair with red and green, have no winding. Correspondingly, the explicit form of the BdG equation is (for a similar representation in the homogeneous CFL phase, see Refs. [7,289])

$$\begin{pmatrix} \hat{\mathcal{H}}_0 & \hat{\Delta}_1 & \hat{\Delta}_0 & 0 & 0 & 0 & 0 & 0 & 0 \\ \hat{\Delta}_1 & \hat{\mathcal{H}}_0 & \hat{\Delta}_0 & 0 & 0 & 0 & 0 & 0 & 0 \\ \hat{\Delta}_0 & \hat{\Delta}_0 & \hat{\mathcal{H}}_0 & 0 & 0 & 0 & 0 & 0 & 0 \\ 0 & 0 & 0 & \hat{\mathcal{H}}_0 & -\hat{\Delta}_1 & 0 & 0 & 0 & 0 \\ 0 & 0 & 0 & -\hat{\Delta}_1 & \hat{\mathcal{H}}_0 & 0 & 0 & 0 & 0 \\ 0 & 0 & 0 & 0 & 0 & \hat{\mathcal{H}}_0 & -\hat{\Delta}_0 & 0 & 0 \\ 0 & 0 & 0 & 0 & 0 & -\hat{\Delta}_0 & \hat{\mathcal{H}}_0 & 0 & 0 \\ 0 & 0 & 0 & 0 & 0 & 0 & 0 & \hat{\mathcal{H}}_0 & -\hat{\Delta}_0 \\ 0 & 0 & 0 & 0 & 0 & 0 & 0 & -\hat{\Delta}_0 & \hat{\mathcal{H}}_0 \end{pmatrix} \begin{pmatrix} u_r \\ d_g \\ s_b \\ d_r \\ u_g \\ s_r \\ u_b \\ s_g \\ d_b \end{pmatrix} = \mathcal{E} \begin{pmatrix} u_r \\ d_g \\ s_b \\ d_r \\ u_g \\ s_r \\ u_b \\ s_g \\ d_b \end{pmatrix}, \tag{8.12}$$

where we introduce the notation, e.g., u_r for a quark with flavor "up" and color "red" in the Nambu–Gor'kov representation. The matrices $\hat{\mathcal{H}}_0$ and $\hat{\Delta}_i$ ($i = 0$ and 1) are given as follows:

$$\hat{\mathcal{H}}_0 = \begin{pmatrix} -i\gamma_0\vec{\gamma}\cdot\vec{\nabla} - \mu & 0 \\ 0 & -i\gamma_0\vec{\gamma}\cdot\vec{\nabla} + \mu \end{pmatrix}, \tag{8.13}$$

$$\hat{\Delta}_i = \begin{pmatrix} 0 & \Delta_i\gamma_0\gamma_5 \\ -\Delta_i^\dagger\gamma_0\gamma_5 & 0 \end{pmatrix}. \tag{8.14}$$

To find the solutions in the BdG equation (8.12), it is useful to express the quark state as

$$\begin{pmatrix} u_r & u_g & u_b \\ d_r & d_g & d_b \\ s_r & s_g & s_b \end{pmatrix} = \sum_{A=1}^{9} \Psi^{(A)} \frac{\lambda_A}{\sqrt{2}}, \tag{8.15}$$

where λ_A ($A = 1, \cdots, 8$) are Gell-Mann matrices normalized as $\mathrm{Tr}\,(\lambda_A\lambda_B) = 2\delta_{AB}$ and $\lambda_9 = \sqrt{2/3}\cdot\mathbf{1}$. We note that, because the non-Abelian vortex has $SU(2)_{\mathrm{C+R+L}}$ symmetry only, the quark state should belong to the representation of $SU(2)_{\mathrm{C+R+L}}$ symmetry. To clarify this, we define

$$\Psi_{\mathrm{t}} \equiv \Psi^{(1)}\lambda_1 + \Psi^{(2)}\lambda_2 + \Psi^{(3)}\lambda_3, \tag{8.16}$$

$$\Psi_{\mathrm{s}} \equiv \Psi^{(8)}\lambda_8 + \Psi^{(9)}\lambda_9 \tag{8.17}$$

for triplet and singlet states, respectively. Explicitly, $\Psi^{(i)}$ ($i = 1, 2, 3, 8, 9$) are given as

$$\Psi^{(1)} = (d_r + u_g)/\sqrt{2}, \tag{8.18}$$

$$\Psi^{(2)} = (d_r - u_g)/(\sqrt{2}i), \tag{8.19}$$

$$\Psi^{(3)} = (u_r - d_g)/\sqrt{2}, \tag{8.20}$$

for triplet, and

$$\Psi^{(8)} = (u_r + d_g - 2s_b)/\sqrt{6}, \tag{8.21}$$

$$\Psi^{(9)} = (u_r + d_g + s_b)/\sqrt{3}, \tag{8.22}$$

for singlet. The doublet states (u_b, d_b) and $(s_r, s_g)^{\mathrm{T}}$ do not couple to $\hat{\Delta}_1$, so they are irrelevant modes for the Majorana fermion.

Let us consider the transformation properties of the quark state $\Psi^{(i)}$ ($i = 1, 2, 3, 8, 9$). Under the $SU(2)_{\mathrm{C+R+L}}$ rotation, the quark state is transformed as

$$\Psi \to \Psi' = U_{\mathrm{F}}\,\Psi\,U_{\mathrm{C}}^{\mathrm{T}} \tag{8.23}$$

where $U_{\mathrm{F}} = \mathrm{e}^{i\vec{\theta}\cdot\vec{\lambda}/2}$ and $U_{\mathrm{C}} = \mathrm{e}^{i\vec{\phi}\cdot\vec{\lambda}/2}$ are the $SU(2)_{\mathrm{L+R}}$ and $SU(2)_{\mathrm{C}}$ rotations, respectively. Since we used the vector $\vec{\lambda} = (\lambda_1, \cdots, \lambda_8)$, the parameters $\vec{\theta}$ and $\vec{\phi}$ are defined only for the first three components $\vec{\theta} = (\theta_1, \theta_2, \theta_3, 0, 0, 0, 0, 0)$ and $\vec{\phi} = (\phi_1, \phi_2, \phi_3, 0, 0, 0, 0, 0)$. For the locking for rotation in color and flavor space under $SU(2)_{\mathrm{C+R+L}}$ symmetry, the color and flavor rotations may be locked

as $\phi_1 = -\theta_1$, $\phi_2 = \theta_2$, and $\phi_3 = -\theta_3$ as the simplest choice. We define

$$\theta_1 = \tilde{\theta}_1 \begin{pmatrix} 1 & 0 \\ 0 & -1 \end{pmatrix}, \quad \theta_2 = \tilde{\theta}_2 \begin{pmatrix} 1 & 0 \\ 0 & 1 \end{pmatrix}, \quad \theta_3 = \tilde{\theta}_3 \begin{pmatrix} 1 & 0 \\ 0 & -1 \end{pmatrix}, \tag{8.24}$$

with $\tilde{\theta}_i$ $(i = 1, 2, 3)$ being real numbers. For infinitesimal $\tilde{\theta}_i$, we find that the quark state $\Psi_{\rm t}$ is transformed as a triplet,

$$\begin{aligned} \delta\Psi^{(1)} &= \theta_3 \Psi^{(2)} - \theta_2 \Psi^{(3)}, \\ \delta\Psi^{(2)} &= \theta_1 \Psi^{(3)} - \theta_3 \Psi^{(1)}, \\ \delta\Psi^{(3)} &= \theta_2 \Psi^{(1)} - \theta_1 \Psi^{(2)}, \end{aligned} \tag{8.25}$$

and the singlet $\Psi_{\rm s}$ is invariant,

$$\delta\Psi^{(8)} = \delta\Psi^{(9)} = 0. \tag{8.26}$$

With the setup for the BdG equation for a non-Abelian vortex with $SU(2)_{\rm C+R+L}$, we can find a fermion solution with $\mathcal{E} = 0$. Among several representations of the quark state in $SU(2)_{\rm C+R+L}$ symmetry, the Majorana fermion is found only in the triplet sector. The wave functions of the Majorana fermion (for right-handed ones) is given in an analytic form as

$$\Psi^{(1)}(r,\theta) = C_1 \begin{pmatrix} \varphi(r,\theta) \\ \eta(r,\theta) \end{pmatrix}, \ \Psi^{(2)}(r,\theta) = C_2 \begin{pmatrix} \varphi(r,\theta) \\ -\eta(r,\theta) \end{pmatrix}, \ \Psi^{(3)}(r,\theta) = C_3 \begin{pmatrix} \varphi(r,\theta) \\ \eta(r,\theta) \end{pmatrix}, \tag{8.27}$$

where C_i are normalization constants and the particle (φ) and hole (η) components are

$$\varphi(r,\theta) = \mathrm{e}^{-\int_0^r |\Delta_1(r')| \mathrm{d}r'} \begin{pmatrix} J_0(\mu r) \\ i J_1(\mu r)\, \mathrm{e}^{i\theta} \end{pmatrix}, \ \eta(r,\theta) = \mathrm{e}^{-\int_0^r |\Delta_1(r')| \mathrm{d}r'} \begin{pmatrix} -J_1(\mu r)\, \mathrm{e}^{-i\theta} \\ i J_0(\mu r) \end{pmatrix}, \tag{8.28}$$

for the vortex profile $|\Delta_1(r)|$. The wave function is well localized around the center of the vortex, because the wave function damps exponentially by $e^{-|\Delta_{\rm CFL}| r}$ at large distances from the center of the vortex. The wave functions for the triplet Majorana fermion are exactly the same as that for the single component Majorana fermion displayed in Eqs. (8.6) and (8.7), except for the minus sign in the hole in $\Psi^{(2)}$.

Concerning the singlet quark state, we also obtain a solution for $\mathcal{E} = 0$, as the asymptotic form for $r \to \infty$ was found in Ref. [378]. We show the explicit form of the wave functions of the singlet solution for the right mode $(\gamma_5 = +1)$ in the Weyl representation

$$\hat{u}_r = \begin{pmatrix} \varphi_1(r,\theta) \\ \eta_1(r,\theta) \end{pmatrix}, \ \hat{d}_g = \begin{pmatrix} \varphi_2(r,\theta) \\ \eta_2(r,\theta) \end{pmatrix}, \ \hat{s}_b = \begin{pmatrix} \varphi_3(r,\theta) \\ \eta_3(r,\theta) \end{pmatrix}, \tag{8.29}$$

where

$$\varphi_i(r,\theta) = \begin{pmatrix} f_i(r) \\ i g_i(r) e^{i\theta} \\ 0 \\ 0 \end{pmatrix}, \quad \eta_i(r,\theta) = \begin{pmatrix} 0 \\ 0 \\ \bar{f}_i(r) e^{-i\theta} \\ i \bar{g}_i(r) \end{pmatrix}, \tag{8.30}$$

for $\hat{u}_r$ $(i = 1)$ and $\hat{d}_g$ $(i = 2)$, and

$$\varphi_3(r,\theta) = \begin{pmatrix} f_3(r) e^{-i\theta} \\ i g_3(r) \\ 0 \\ 0 \end{pmatrix}, \quad \eta_3(r,\theta) = \begin{pmatrix} 0 \\ 0 \\ \bar{f}_3(r) \\ i \bar{g}_3(r) e^{i\theta} \end{pmatrix}, \tag{8.31}$$

for $\hat{s}_b$. At large r, both $|\Delta_0|$ and $|\Delta_1|$ become a common constant $|\Delta_{\rm CFL}|$ given in the bulk state. Then, with an approximation of small $|\Delta_{\rm CFL}|$ and large μ, we find asymptotic forms of the wave functions with a condition of the convergence at large r. The first solution is

$$f_i(r) = \mathcal{N} e^{-|\Delta_{\rm CFL}|r/2} J_0(\mu r), \tag{8.32}$$

$$g_i(r) = \mathcal{N} e^{-|\Delta_{\rm CFL}|r/2} J_1(\mu r), \tag{8.33}$$

$(i = 1, 2)$ and

$$f_3(r) = -\frac{\mathcal{N}}{2} e^{-|\Delta_{\rm CFL}|r/2} J_0(\mu r), \tag{8.34}$$

$$g_3(r) = -\frac{\mathcal{N}}{2} e^{-|\Delta_{\rm CFL}|r/2} J_1(\mu r), \tag{8.35}$$

with a normalization constant $\mathcal{N}$. This is the solution given in Ref. [378].

As the second solution, we find a new asymptotic solution, which is very different from the solution in the triplet sector

$$f_i'(r) = \mathcal{N}' e^{-|\Delta_{\rm CFL}|r/2} \frac{\pi}{4} (\mu r)^2 J_1(\mu r) \big(J_1(\mu r) N_0(\mu r) - J_0(\mu r) N_1(\mu r) \big), \tag{8.36}$$

$$g_i'(r) = \mathcal{N}' e^{-|\Delta_{\rm CFL}|r/2} \frac{1}{4} \big(-\mu r J_0(\mu r) + J_1(\mu r) \big), \tag{8.37}$$

$(i = 1, 2)$ and

$$\begin{aligned} f_3'(r) = \mathcal{N}' e^{-|\Delta_{\rm CFL}|r/2} \frac{\mu}{8|\Delta|} \Big\{ & 4 (\mu r J_0(\mu r) - J_1(\mu r)) - \pi (\mu r)^2 \\ & \times \left(2 J_0(\mu r) + \frac{|\Delta_{\rm CFL}|}{\mu} J_1(\mu r) \right) \big(J_1(\mu r) N_0(\mu r) - J_0(\mu r) N_1(\mu r) \big) \Big\}, \end{aligned} \tag{8.38}$$

$$\begin{aligned} g_3'(r) = \mathcal{N}' e^{-|\Delta_{\rm CFL}|r/2} \frac{\mu}{4|\Delta_{\rm CFL}|} \Big\{ & (2 + |\Delta_{\rm CFL}| r)\, J_0(\mu r) - \left(\frac{|\Delta_{\rm CFL}|}{\mu} + 2\mu r \right) J_1(\mu r) \\ & + \pi (\mu r)^2 J_1(\mu r) \big(J_1(\mu r) N_0(\mu r) - J_0(\mu r) N_1(\mu r) \big) \Big\}, \end{aligned} \tag{8.39}$$

with a normalization constant $\mathcal{N}'$. It should be emphasized that these asymptotic solutions are correct only at large r, at which $|\Delta_0|$ and $|\Delta_1|$ are constant. However, these solutions may be divergent at small r in general, because $|\Delta_1|$ becomes zero at $r = 0$, and we find that this is the case. The result that there is no normalizable zero mode fermion in the singlet is consistent with that of the index theorem, as discussed in Sect. 8.5. Although non-normalizable modes having a singular peak at the vortex core are usually considered to be unphysical, there is also a discussion in the context of cosmic strings that they may play some interesting roles, such as in baryogenesis [9].

8.3. Effective theory in $1 + 1$ *dimensions along a vortex string*

In the previous subsection, we considered the transverse motion of the quark on the plane perpendicular to the vortex axis. Now we discuss the longitudinal motion of the quark along the vortex. Let us consider the case of a single flavor for an illustration. The Hamiltonian is written as a sum of the

perpendicular part (with subscript $\perp$) and the longitudinal part (with subscript z):

$$\mathcal{H} = \begin{pmatrix} -i\vec{\alpha}_\perp \cdot \vec{\nabla}_\perp - \mu & |\Delta| e^{i\theta}\gamma_0\gamma_5 \\ -|\Delta| e^{-i\theta}\gamma_0\gamma_5 & -i\vec{\alpha}_\perp \cdot \vec{\nabla}_\perp + \mu \end{pmatrix} + \begin{pmatrix} -i\alpha_z \frac{\partial}{\partial z} & 0 \\ 0 & -i\alpha_z \frac{\partial}{\partial z} \end{pmatrix}$$
$$\equiv \mathcal{H}_\perp + \mathcal{H}_z. \tag{8.40}$$

Because the Hamiltonian is a sum of the contributions from the transverse and longitudinal directions, we separate the wave function as

$$\Psi(t, z, r, \theta) = a(t, z)\Psi_0(r, \theta), \tag{8.41}$$

where $a(t, z)$ is a function with variables of time t and the coordinate z in the longitudinal direction, and $\Psi_0(r, \theta)$ is a function with variables of (r, θ) on the transverse plane. Concerning the transverse plane, we have found the solution of the Majorana fermion as the lowest mode in the Hamiltonian $\mathcal{H}_\perp$, as shown in Eqs. (8.6)–(8.9). Since we are interested in the low-energy dynamics, we can take $\Psi_0(r, \theta)$ to be the state of the transverse zero mode. We can identify the field $a(t, z)$ with the low-energy degree of freedom on the vortex. The equation of motion for $a(t, z)$ can be derived in the following way. We start with the original equation of motion, $i\partial/\partial t\Psi = \mathcal{H}\Psi$. By integrating the transverse degree of freedom, namely by multiplying $\Psi_0^\dagger$ from the left in the equation of motion $i\partial/\partial t\Psi = \mathcal{H}\Psi$ and integrating over the transverse coordinates r and θ, we obtain the equation of motion for $a(t, z)$ as

$$i\frac{\partial}{\partial t}a(t, z) = \int \Psi_0^\dagger(r, \theta)\mathcal{H}_z\Psi_0(r, \theta) r dr d\theta a(t, z), \tag{8.42}$$

where we have used the normalization $\int \Psi_0^\dagger\Psi_0 r dr d\theta = 1$. On the right-hand side, $\int \Psi_0^\dagger(r, \theta)\mathcal{H}_z \Psi_0(r, \theta) r dr d\theta$ may be regarded as an effective Hamiltonian for $a(t, z)$. We can rewrite this equation as

$$i\left\{\frac{\partial}{\partial t} + v_+(\mu, |\Delta|)\frac{\partial}{\partial z}\right\} a(t, z) = 0, \tag{8.43}$$

with the "velocity" $v_+(\mu, |\Delta|)$ defined by

$$v_+(\mu, |\Delta|) \equiv \int \Psi_0^\dagger(r, \theta) \begin{pmatrix} \alpha_z & 0 \\ 0 & \alpha_z \end{pmatrix} \Psi_0(r, \theta)\, r dr d\theta. \tag{8.44}$$

The solution to Eq. (8.43) is given by $a(t, z) \propto e^{i\mathcal{E}t - ik_z z}$ with a linear (gapless) dispersion with respect to k_z:

$$\mathcal{E} = v_+(\mu, |\Delta|)\, k_z, \tag{8.45}$$

where

$$v_+(\mu, |\Delta|) = \frac{\mu^2}{|\Delta|^2 + \mu^2} \frac{E\left(-\frac{\mu^2}{|\Delta|^2}\right)}{E\left(-\frac{\mu^2}{|\Delta|^2}\right) - K\left(-\frac{\mu^2}{|\Delta|^2}\right)} - 1, \tag{8.46}$$

where $K(x)$ and $E(x)$ are the complete elliptic integrals of the first and second kinds, respectively;

$$K(x) = \int_0^{\pi/2} \frac{1}{\sqrt{1 - x^2 \sin^2\theta}} d\theta, \tag{8.47}$$

$$E(x) = \int_0^{\pi/2} \sqrt{1 - x^2 \sin^2\theta}\, d\theta. \tag{8.48}$$

We plot $v_+(\mu, |\Delta|)$ as a function of $\mu/|\Delta|$ in Fig. 27 ($v_+ = 1$ is the speed of light). As a consequence, low-energy excitations inside the vortex are gapless (massless) fermions described by Eqs. (8.43) and

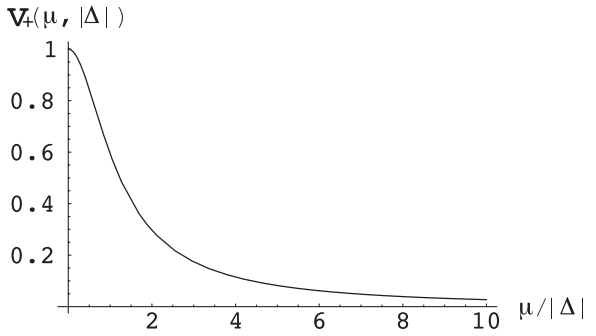

Fig. 27. Velocity of a zero mode fermion propagating along the vortex axis (Ref. [378].)

(8.44). One can indeed express these fermions in terms of spinors in $1+1$ dimensions, and write down an equation similar to the Dirac equation.

The effective theory is obtained also for the triplet Majorana fermion in the CFL phase. The effective field with t and z has three components, each of which follows Eq. (8.44). The only change is to replace $|\Delta|$ with $|\Delta_{\rm CFL}|$. The dispersion relation is not modified from Eq. (8.45).

8.4. The absence of supercurrent along a vortex

We here comment on the absence of electromagnetic supercurrents induced by fermions along vortices, even if we start from charged fermions in $3+1$ dimensions. This is anticipated from the "Majorana" nature of the zero-mode fermions. We start with a single-component charged fermion described by the following Hamiltonian:

$$\begin{aligned}\mathcal{H} &= \begin{pmatrix} -i\vec{\alpha}_\perp\cdot\vec{\nabla}_\perp - \mu & |\Delta|e^{i\theta}\gamma_0\gamma_5 \\ -|\Delta|e^{-i\theta}\gamma_0\gamma_5 & -i\vec{\alpha}_\perp\cdot\vec{\nabla}_\perp + \mu \end{pmatrix} \\ &\quad + \begin{pmatrix} -i\alpha_z\left(\frac{\partial}{\partial z} - ieA_z\right) & 0 \\ 0 & -i\left(\alpha_z\frac{\partial}{\partial z} + ieA_z\right) \end{pmatrix} \\ &\equiv \mathcal{H}_\perp + \mathcal{H}_z^{A_z}, \end{aligned} \tag{8.49}$$

where the fermion is coupled to an electromagnetic gauge field $A^\mu(t,z) = (0,0,0,A_z(t,z))$. As we are interested in the low-energy dynamics, we can take the wave function as

$$\Psi(t,\vec{x}) = a(t,z)\Psi_0(r,\theta), \tag{8.50}$$

where $\Psi_0(r,\theta)$ is the transverse zero-mode wave function that satisfies

$$\mathcal{H}_\perp\Psi_0(r,\theta) = 0. \tag{8.51}$$

Then, the dynamical equation for the effective dynamics along the vortex axis is derived in exactly the same way as Eq. (8.43),

$$\begin{aligned}\frac{\partial}{\partial t}a(t,z) &= -i\int rdrd\theta\Psi_0^\dagger(r,\theta)\mathcal{H}_z^{A_z}(t,z)\Psi_0(r,\theta) \\ &= \mp\left[v_\pm a(t,z) - ie'A_z(t,z)a(t,z)\right], \end{aligned} \tag{8.52}$$

where we have defined the "effective velocity" as

$$v = \varphi_\pm^\dagger\sigma_3\varphi_\pm - \eta_\mp^\dagger\sigma_3\eta_\mp, \tag{8.53}$$

and the "effective charge" as

$$e' = e\left(\varphi_{\pm}^{\dagger}\sigma_3\varphi_{\pm} + \eta_{\mp}^{\dagger}\sigma_3\eta_{\mp}\right) = 0. \tag{8.54}$$

The final equation is obtained by substituting the wave function of the transverse zero mode. Because the effective charge is zero, the Majorana fermion propagating along the vortex axis is neutral and does not couple to electromagnetic fields. Therefore, there is no electromagnetic current induced by the Majorana fermions in vortices. The same is true for the triplet Majorana fermions in non-Abelian vortices, where the $SU(2)_{\rm C+F}$ non-Abelian gauge field is switched on along the vortex axis as $A^{i,\mu}(t,z) = (0,0,0,A^i_z(t,z))$ with $i = 1,2,3$ for indices of the adjoint representation (triplet) in $SU(2)_{\rm C+F}$ symmetry.

8.5. Index theorem

So far we have discussed zero mode fermions by explicitly solving the BdG equation based on the mean-field Hamiltonian with a gap profile function. In fact, the existence of zero modes is robust and does not depend on the details of the system, since the massless modes on the edge of a superconductor are closely related to the "topology" of the bulk matter. A manifestation of this fact is the index theorem [67,134,136,365], which relates the number of zero modes and a topological invariant. (A detailed description is given in Refs. [134,136].) The index theorem has a long history and has elucidated topological characteristics of anomalies in gauge fields [91]. The index theorem has also been applied to condensed matter systems by many researchers [135–137,176,285,292,293,299]. We here review the application of the index theorem to the non-Abelian vortices in the CFL phase.

Let us first review the index theorem in the case of Euclidean Dirac operators, $H = i\not{D}$. We consider normalized eigenstates of this operator $\{u_i(x)\}$, which satisfy

$$\not{D}u_i(x) = \lambda_i u_i(x). \tag{8.55}$$

Suppose we have an operator γ_5 that anticommutes with $\not{D}$:

$$\gamma_5\not{D} + \not{D}\gamma_5 = 0, \quad (\gamma_5)^2 = 1. \tag{8.56}$$

The zero modes, which are the eigenfunctions of $\lambda_i = 0$, can always be taken as the eigenstates of chirality,

$$\gamma_5 u_i(x) = u_i(x) \ \text{ or } \ \gamma_5 u_i(x) = -u_i(x). \tag{8.57}$$

Let us consider the analytical index of the operator H, which is defined as the difference between the dimensions of the kernel and co-kernel of the operator. The analytical index can be written as the difference of the number of zero mode solutions for positive and negative chiralities,

$$\text{ind}\, H \equiv N_+ - N_-, \tag{8.58}$$

where N_+ and N_- are the numbers of zero modes for positive and negative chiralities. The index theorem relates the analytical index to the topological index. To see this, we rewrite ind H as

$$\text{ind}\, H = \lim_{m\to 0} \text{Tr}\,\gamma_5 \frac{m^2}{H^2 + m^2}. \tag{8.59}$$

As m tends to zero, only the contribution of the zero eigenvalues survives, and $+$ $(-)$ states are accounted with plus (minus) signs due to γ_5. Furthermore, we introduce the current

defined by

$$J^k = \lim_{y\to x} \mathrm{Tr}\,\gamma_5\gamma^k \left(\frac{1}{\not{D}+m} - \frac{1}{\not{D}+M}\right)\delta(x-y), \tag{8.60}$$

where k indicates the spatial component and the second term is a regulator with large mass M, which is eventually taken to infinity. By taking the divergence of the current, one can show the following relation [365]:

$$\mathrm{ind}\, H = -\frac{1}{2}\int dS_k J^k + c_d, \tag{8.61}$$

where dS_k is the infinitesimal surface element on the boundary of the space. It can be shown that the constant c_d is the Chern number for even d,

$$c_d \equiv \lim_{M\to\infty} \mathrm{Tr}\,\gamma_5 \frac{M^2}{H^2+M^2}. \tag{8.62}$$

Thus, the analytical index is related to the topological index defined on the right-hand side of Eq. (8.61).

We apply the index theorem to count the number of zero mode Majorana fermions in non-Abelian vortices. In non-Abelian vortices, the analytical index of the operator $\mathcal{H}_\perp$ is defined by

$$\mathrm{ind}\,\mathcal{H}_\perp = N_+(\mathcal{H}_\perp) - N_-(\mathcal{H}_\perp), \tag{8.63}$$

where $N_\pm(\mathcal{H}_\perp)$ are the numbers of zero-energy states of $\mathcal{H}_\perp$ with definite Γ^3 chiralities, $\Gamma^3 = \pm 1$ (corresponding to $\gamma_5 = \pm 1$ in Eq. (8.57)). Here Γ^3 is defined as

$$\Gamma^3 = \begin{pmatrix} \alpha_z & 0 \\ 0 & \alpha_z \end{pmatrix}. \tag{8.64}$$

Let us review the derivation of the index theorem. We note that the index is rewritten as

$$\mathrm{ind}\,\mathcal{H}_\perp = \lim_{m\to 0} \mathrm{Tr}\,\Gamma^3 \frac{m^2}{\mathcal{H}_\perp^2 + m^2}, \tag{8.65}$$

where Tr stands for the trace over two-dimensional space as well as the Dirac indices. For $\mu = 0$, $\mathrm{ind}\,\mathcal{H}_\perp$ is equal to the number of Majorana fermions. For $\mu \neq 0$, the relation does not hold, since the chiral symmetry is broken ($\{\Gamma_3, \mathcal{H}_\perp\} \neq 0$). When μ is small, we can naturally assume that the states at finite μ are smoothly connected to the states in vacuum (see Fig. 28). Note that the particle–hole symmetry is intact even at finite densities, $\mu \neq 0$. Then we can expect that the zero modes can always appear or disappear in pairs, as one increases the chemical potential μ. Thus, in the case of $\mu \neq 0$, $\mathrm{ind}\,\mathcal{H}_\perp$ gives the number of zero mode fermions modulo 2. Here we introduce the axial current

$$\begin{aligned} J^j(x,m,M) &= \lim_{y\to x} \mathrm{Tr}\,\Gamma^3\Gamma^j \left(\frac{1}{-i\mathcal{H}_\perp + m} - \frac{1}{-i\mathcal{H}_\perp + M}\right)\delta^{(2)}(x-y) \\ &= \lim_{y\to x} \mathrm{Tr}\,\Gamma^3\Gamma^j i\mathcal{H}_\perp \left(\frac{1}{\mathcal{H}_\perp^2 + m^2} - \frac{1}{\mathcal{H}_\perp^2 + M^2}\right)\delta^{(2)}(x-y), \end{aligned} \tag{8.66}$$

with $j = 1, 2$ for the coordinate on the two dimensional plane, where M is a large mass parameter for the Pauli–Villars regulator. Then, the divergence of the current is written as

$$\partial_j J^j(x,m,M) = 2\lim_{y\to x} \mathrm{Tr}\,\Gamma^3\Gamma^j i\mathcal{H}_\perp \left(\frac{m^2}{\mathcal{H}_\perp^2 + m^2} - \frac{M^2}{\mathcal{H}_\perp^2 + M^2}\right)\delta^{(2)}(x-y). \tag{8.67}$$

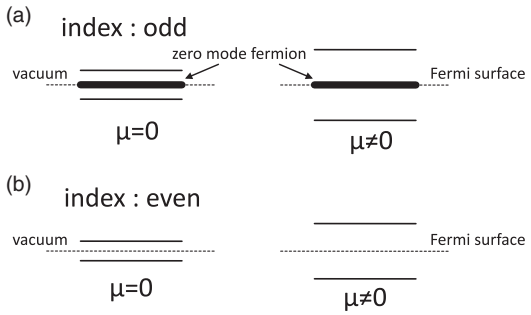

Fig. 28. A schematic picture of energy levels of fermions in vacuum ($\mu = 0$) and in matter ($\mu \neq 0$). (a) When the index is odd, the zero mode fermions in vacuum still exist in matter. (b) When the index is even, however, the zero mode fermions do not exist in either vacuum or matter.

Therefore, we obtain

$$\operatorname{ind} \mathcal{H}_\perp = c + \lim_{m\to 0,\, M\to\infty} \frac{1}{2} \oint_{|\vec{x}|\to\infty} \epsilon_{ij} J^i(x, m, M) dx^j, \tag{8.68}$$

where we have defined

$$c = \lim_{M\to\infty} \operatorname{Tr} \Gamma^3 \frac{M^2}{\mathcal{H}_\perp^2 + M^2}. \tag{8.69}$$

It is known that c is the Chern number associated with the gauge field. In the present discussion, we do not consider the gauge field and hence we neglect c. We note that the second term in the above equation is a topological invariant. Thus, we have shown the index theorem; the index $\operatorname{ind} \mathcal{H}_\perp$ is related to the topologically invariant quantity. We can know whether the number of zero mode fermions is even or odd when the index is even or odd, respectively. In most cases, the number of zero mode fermions is 0 or 1, and other numbers can happen by chance.

The calculation of Eq. (8.65) is performed by supplying the basis of the plane wave, as explicitly given in Ref. [134]. We use the basis of the plane wave and give the axial current as

$$J^j(x, m, M) = \int \frac{d^2k}{(2\pi)^2} e^{-ik\cdot x} \operatorname{Tr} \Gamma^3 \Gamma^j i\mathcal{H}_\perp \frac{1}{\mathcal{H}_\perp^2 + m^2} e^{ik\cdot x}, \tag{8.70}$$

where the regularization of the current is neglected, because the above current is well defined in the present discussion. Indeed, the index theorem needs the current only at $|\vec{x}| \to \infty$, where $|\Delta| \to \Delta_{\mathrm{CFL}}$ and $\partial_j \Delta \sim \mathcal{O}(r^{-1})$. The result is

$$\operatorname{ind} \mathcal{H}_\perp = \frac{1}{2\pi} \oint d\theta \partial_\theta \Theta_k(\theta) = \begin{cases} 2Q & \text{(singlet)} \\ Q & \text{(doublet)} \\ q & \text{(triplet)} \end{cases} \tag{8.71}$$

for the generalized gap profile $\Delta(r, \theta) = \operatorname{diag}(\Delta_Q, \Delta_Q, \Delta_q)$ with $\Delta_k(r, \theta) = |\Delta_k(r)| e^{i\Theta_k(\theta)}$ and the condition $\Theta_k(2\pi) = \Theta_k(0) + 2\pi k$. The case of $Q = 0$ and $q = 1$ corresponds to the vortex configuration in Eq. (8.11). Therefore, the zero mode exists only in the triplet sector.

From the result of the index theorem, we find that the doublet zero-mode does not exist, and the singlet zero-mode does not exist either. Although an asymptotic form of the wave function can be found at large $r \to \infty$, as shown in Eqs. (8.32)–(8.39), it turns out that the wave function is divergent at the origin ($r = 0$). Because the index theorem counts the number of the zero mode (precisely, the

difference between N_+ and N_-), which is normalizable over the space, the result does not contradict that from the analysis of the BdG equation.

The index of the Hamiltonian $\mathcal{H}_\perp$ is also calculated by the analytical method [188,189], as presented in Refs. [134,136]. We consider the equation of motion

$$\mathcal{H}_\perp(r,\theta)\Psi(r,\theta) = 0 \tag{8.72}$$

and analyze the eigenwave function $\Psi(r,\theta)$. The advantage of this method is that it gives us the number of zero-energy states for each Γ^3-chirality ($\Gamma^3 = \pm 1$), namely N_+ and N_-.

Let us see the doublet and triplet states. We rewrite the Hamiltonian as

$$\begin{pmatrix} 0 & \mathcal{H}_{\perp,-} \\ \mathcal{H}_{\perp,+} & 0 \end{pmatrix} \begin{pmatrix} \Psi_+ \\ \Psi_- \end{pmatrix} = 0, \tag{8.73}$$

where $\pm$ denotes Γ^3-chirality, and

$$\mathcal{H}_{\perp,\pm} = \begin{pmatrix} -i\partial_\pm & -|\Delta_q(r)|e^{iq\theta} \\ -|\Delta_q(r)|e^{iq\theta} & i\partial_\mp \end{pmatrix}, \tag{8.74}$$

with $\partial_\pm = e^{\pm i\theta}(\partial_r \pm i\partial_\theta/r)$. This is the equation for the triplet. If q is replaced with Q, then we obtain the equation for the doublet. We set the wave function with the variables r and θ as

$$\Psi_{m,\pm}(r,\theta) = \begin{pmatrix} \alpha_m(r)e^{\pm im\theta} \\ i\beta_m(r)e^{i(\pm m - q \pm 1)\theta} \end{pmatrix}, \tag{8.75}$$

where m is the quantum number associated with the angular momentum, and $\alpha_m(r)$ and $\beta_m(r)$ are radial components. The equation for the radial components is given as

$$\left(\frac{d}{dr} - \frac{M_\pm}{r} + \Omega\right)\psi_m(r) = 0, \tag{8.76}$$

for $\psi_m(r) = (\alpha_m(r), \beta_m(r))^{\mathrm{T}}$, $M_\pm = \mathrm{diag}(m, -m-1 \pm q)$, and

$$\Omega = \begin{pmatrix} 0 & |\Delta_q| \\ |\Delta_q| & 0 \end{pmatrix}. \tag{8.77}$$

The solutions of this equation were studied in Ref. [189]. Following their analysis, we naturally assume the asymptotic behavior of the gap profile function; $|\Delta_q| \sim r^{|q|}$ at $r \to 0$. We also assume generically that Ω is expanded as

$$\Omega = \sum_{n=0}^{\infty} \Omega_n r^n, \tag{8.78}$$

where $\Omega_0 = 0$ if $q \neq 0$. From a mathematical point of view, we can assume that $|\Delta_q| \sim r$ at $r \to 0$. However, it turns out that this behavior gives a logarithmic term ($\log r$) in the wave function. Therefore, we neglect the case of $|\Delta_q| \sim r$ and consider the case of $|\Delta_q| \sim r^{|q|}$ only.

With this setup, we expand the wave function as

$$\psi_m^{(i)}(r) = \psi_{m,n_i}^{(i)} r^{n_i} + \psi_{m,n_i+1}^{(i)} r^{n_i+1} + \cdots, \tag{8.79}$$

for $i = 1, 2$. The leading power n_i is one of the diagonal elements of M; $n_1 = m$ and $n_2 = -m - 1 + q$ for $\Gamma^3 = +1$, and $n_1 = m$ and $n_2 = -m - 1 - q$ for $\Gamma^3 = -1$. The normalizability of $\psi_m^{(i)}(r)$ at $r \to 0$ is guaranteed by $n_i \geq 0$. It means that $0 \leq m \leq q - 1$ for $\Gamma^3 = +1$, and $0 \leq m \leq -q - 1$

for $\Gamma^3 = -1$. Then, we obtain (1) $N_+ = q$ and $N_- = 0$ for $1 \leq q$, (2) $N_+ = N_- = 0$ for $q = 0$, and (3) $N_+ = 0$ and $N_- = -q$ for $q \leq -1$. We finally conclude that $\mathrm{ind}\mathcal{H}_\perp = N_+ - N_- = q$ in any case. This result is consistent with that from the topological discussion.

As a final remark, we notice that another gap configuration $\Delta(r, \theta) = \mathrm{diag}(\Delta_1, \Delta_1, \Delta_0)$ ($Q = 1$ and $q = 0$) corresponds to the M_2 vortex. As discussed in Sect. 5, this is an unstable configuration, decaying to two M_1 vortices. Nevertheless, it will be interesting to consider the zero mode fermions (two zero modes in singlet and one zero mode in doublet), if the M_2 vortex could exist as a quasi-stable state. In particular, zero mode fermions in a doublet form a Dirac fermion, which is still zero mode, inside the single vortex. As the Majorana fermion in the M_1 vortex contributes to the non-Abelian statistics, the Dirac fermion in the M_2 vortex provides us with non-Abelian statistics, as discussed in Sect. 9.

8.6. Topological superconductor

Topological phases have recently been attracting much attention in condensed matter physics. Topological superconductors are characterized by a full pairing gap in the bulk, and gapless surface states that consist of Majorana fermions. A state with a nontrivial topological number is called a topological state. When there is a boundary between two states with different topological numbers, the energy gap should be closed on the boundary so that the topological number can change. This assures the existence of gapless surface states.

We now come to the question: is a color superconductor topological? This question is addressed and discussed by Nishida [253]. Whether a superconductor is topological or not is determined only by discrete symmetries of the Hamiltonian and spatial dimensionality according to the periodic table of topological superconductors [307], at least for non-interacting Hamiltonians. As already discussed, the mean-field Hamiltonian of a color superconductor has a charge-conjugation symmetry. We can also define a time-reversal symmetry for this Hamiltonian. Then the Hamiltonian belongs to the symmetry class DIII, which is topological in three spatial dimensions.

We can define topological charges N_R and N_L for right-handed and left-handed sectors independently in the chiral limit, in which the two sectors are independent. For an even (odd)-parity pairing[13], $N_\mathrm{R} = \mp N_\mathrm{L}$. Because of these non-zero topological charges, surface states exist. For example, a vortex in the superconductor supports right-handed and left-handed massless fermions propagating in opposite directions[14]

At finite quark masses, right-handed and left-handed sectors mix and only the total topological charge $N = N_\mathrm{R} + N_\mathrm{L}$ is well defined. What becomes of the surface states at finite quark masses? The results are qualitatively different depending on the parity of the pairing. For the even-parity pairing case, the total topological charge is zero, $N = 0$. In this case, the presence of the fermion mass immediately opens up a gap for localized fermions on a vortex. When the pairing gap is parity odd, the topological charge is unchanged for small fermion masses, since the system remains gapped as long as $m^2 < \mu^2 + |\Delta|^2$. If the fermion mass is increased further, there will be a topological phase transition at $m^2 = \mu^2 + |\Delta|^2$ and the fermions would acquire a mass gap.

[13] For an even-parity pairing, the order parameter is given by $\Phi \sim \langle q^T C\gamma_5 q\rangle$, and by $\Phi \sim \langle q^T C q\rangle$ for an odd-parity pairing.

[14] The vortex state discussed in Ref. [253] is not the lowest-energy vortex solution, so it would be unstable against decay.

9. Non-Abelian exchange statistics of non-Abelian vortices

The exchange statistics in the system of multiple numbers of quantum vortices with zero mode Majorana fermions provides a novel statistics, which is different from the conventional statistics, such as the Fermi–Dirac statistics for fermions, the Bose–Einstein statistics for bosons and the (Abelian) anyon statistics for anyons. The exchange statistics of vortices with Majorana fermions obeys the non-Abelian statistics. This is the subject of this section. In Sect. 9.1, we discuss general properties of exchanging vortices. In Sect. 9.2, we review the non-Abelian statistics for *Abelian* vortices with Majorana fermions. In Sect. 9.3, we discuss the non-Abelian statistics for *non-Abelian* vortices with Majorana fermions. In Sect. 9.4, we comment on the case of (non-)Abelian vortices with Dirac fermions.

9.1. Exchange of vortices

Let us suppose that there are multiple numbers of non-Abelian vortices. The motion of the parallel vortices in $d = 3 + 1$ dimensional space is regarded as the motion of the particles on a $d = 2 + 1$ dimensional space, because the vortex has translational invariance along the vortex axis. Generally speaking, the exchange of two particles on a plane obeys the braid group. We introduce an operation T_k that exchanges the kth and $(k + 1)$th vortices, where the former vortex rotates around the latter vortex in a counterclockwise direction. The braid group is given by two rules:

$$\text{(i) } T_k T_{k+1} T_k = T_{k+1} T_k T_{k+1}, \tag{9.1}$$

$$\text{(ii) } T_k T_\ell = T_\ell T_k \ \ (|k - \ell| > 1). \tag{9.2}$$

It should be noted that the inverse of T_k is not necessarily identical to T_k ($(T_k)^{-1} \neq T_k$) because the operation is directed. This property of the braid group leads to the non-Abelian statistics [82,156, 185,281,339,348].

We consider that the vortices are exchanged adiabatically as shown in Fig. 9.1. Then, the Majorana fermion plays an important role because it is the most stable state protected topologically by perturbation from outside. The wave function of the Majorana fermion is a double-valued function for the angle around the vortex axis. This can be inferred from the form of the BdG equations (8.12); when we shift the phase winding of a vortex as $\theta \to \theta + \alpha$, it can be canceled if the phases of the particle and hole wave functions are shifted by $\alpha/2$ and $-\alpha/2$, respectively. This implies that, when quasiparticles travel around a vortex at $\alpha = 2\pi$, both particle and hole wave functions receive a minus sign. In order to regard the wave function as a single-valued function, we need to introduce a cut from the center of the vortex to infinitely far from the vortex. The directions of cuts are arbitrary and gauge dependent. This means that the wave function acquires a minus sign when the Majorana fermion goes across the cut. Let us pick up the kth and $(k + 1)$th vortices among the multiple numbers of vortices, and consider the exchange operation T_k for these two vortices as in Fig. 29. By the operation T_k, the positions of the kth and $(k + 1)$th vortices are exchanged, where the kth vortex goes across the cut from the $(k + 1)$th vortex. Then, the wave function of the Majorana fermion in the $(k + 1)$th vortex acquires a minus sign, while that in the kth vortex does not change. The resulting exchange is expressed by the Majorana fermion operators γ_k^a and γ_{k+1}^a for the kth and $(k + 1)$th vortices. Here a indicates the component of the Majorana fermion with internal symmetry. The fermion operators γ_ℓ^a satisfy the anticommutation relation

$$\{\gamma_k^a, \gamma_\ell^b\} = 2\delta_{k\ell}\delta^{ab}. \tag{9.3}$$

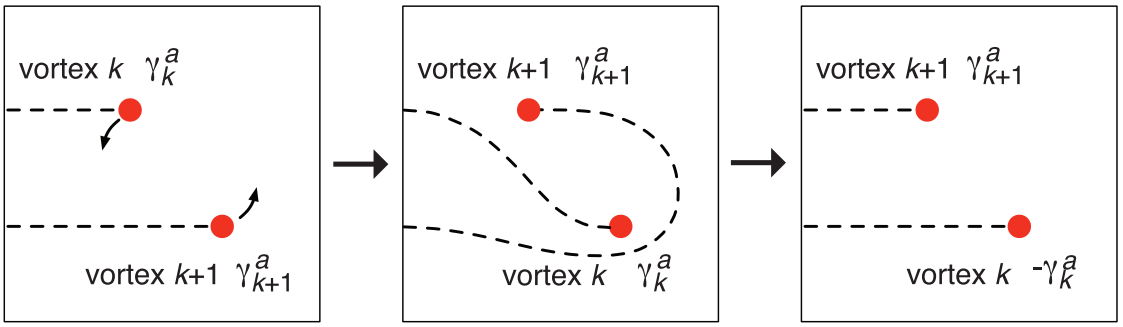

Fig. 29. Exchange of two vortices k and $k+1$ with Majorana fermions described by γ_k^a and γ_{k+1}^a ($a = 1, 2, 3$), respectively. The dashed lines are cut from the vortex to an infinitely distant point. (Ref. [379].)

We note the relation

$$(\gamma_\ell^a)^\dagger = \gamma_\ell^a \tag{9.4}$$

because the particle state is equal to the hole state as the property of the Majorana fermion.

We find that the operation T_k gives the following exchange rule:

$$T_k : \begin{cases} \gamma_k^a & \to \gamma_{k+1}^a \\ \gamma_{k+1}^a & \to -\gamma_k^a \end{cases} . \tag{9.5}$$

Here $a = 1, 2, 3$ denote the components in the triplet state, because the Majorana fermions belong to the triplet of $SU(2)_{\mathrm{C+F}} \simeq O(3)_{\mathrm{C+F}}$. In the present discussion, we do not consider the singlet component.

From Eq. (9.5), we find that the operation by two-time exchanges does not give the initial state; $T_k^2 \neq 1$. This means that the exchange of vortices is different from neither the Fermi–Dirac statistics nor the Bose–Einstein statistics.

9.2. *Abelian vortices with Majorana fermions*

The explicit expression of the operation T_k in terms of Majorana fermions was first found by Ivanov in the case of "Abelian" vortices with single component Majorana fermions ($a = 1$ only) [185] in chiral p-wave superconductors. See also the early discussions on other systems in Ref. [295]. The non-Abelian statistics by Majorana fermions in (Abelian) vortices, explicit forms of which will be shown below, is attracting many researchers as devices for quantum computing [204,205,246,369]. They can be realized not only in the core of half-quantized vortices in chiral p-wave superconductors or p-wave superfluids [361], but also in the edge of topological superconductors and insulators [131], and even in the three dimensional systems in which Majorana fermions are trapped on monopole-like objects [347]. Before moving on to the detailed discussion about the exchange in Eq. (9.5) for a multiple number of Majorana fermions, in this subsection, let us study the case of the single fermion component found by Ivanov [185]. In this case, we have the Majorana fermion operators γ_k and γ_{k+1} at the vortex k and $k+1$, respectively. Under the exchange of vortices, γ_k and γ_{k+1} are transformed as

$$T_k : \begin{cases} \gamma_k & \to \gamma_{k+1} \\ \gamma_{k+1} & \to -\gamma_k \end{cases} . \tag{9.6}$$

If we define the operator

$$\hat{\tau}_k = \frac{1}{\sqrt{2}}(1 + \gamma_{k+1}\gamma_k), \tag{9.7}$$

up to an overall phase, it is easy to confirm that the transformation in Eq. (9.6) can be reproduced by

$$\gamma_\ell \to \hat{\tau}_k \gamma_\ell \hat{\tau}_k^{-1}. \tag{9.8}$$

Hence, the operator $\hat{\tau}_k$ represents the operation T_k.

Next, let us define the Hilbert (Fock) space. It should be noted that the annihilation of the Majorana fermion is identical to the creation of the Majorana fermion ($\gamma_k = \gamma_k^\dagger$). Hence it is not possible to construct the Hilbert space on a single vortex. When preparing a pair of vortices, we define the Dirac operator by

$$\hat{\Psi}_k \equiv \frac{1}{2}\left(\gamma_{2k-1} + i\gamma_{2k}\right). \tag{9.9}$$

The Dirac operator satisfies the usual anticommutation relations for the creation ($\Psi_k^\dagger$) and annihilation (Ψ_k) operators:

$$\left\{\hat{\Psi}_k, \hat{\Psi}_\ell^\dagger\right\} = \delta_{kl}, \quad \left\{\hat{\Psi}_k, \hat{\Psi}_\ell\right\} = \left\{\hat{\Psi}_k^\dagger, \hat{\Psi}_\ell^\dagger\right\} = 0. \tag{9.10}$$

We then define the Fock vacuum $|0\rangle$ as $\Psi_k|0\rangle = 0$ for all k. We can build the Hilbert space by acting the creation operators on the Fock vacuum.

In the case of $n = 2$ vortices, the Hilbert space can be constructed as $\{|0\rangle, \Psi_1^\dagger|0\rangle\}$. With these bases, the operator $\hat{\tau}_1$ can be expressed by a matrix form as

$$\tau_1 = \begin{pmatrix} e^{-i\pi/4} & 0 \\ 0 & e^{i\pi/4} \end{pmatrix}. \tag{9.11}$$

Because of a nontrivial phase factor, this gives rise to an Abelian anyon statistics.

The non-Abelian statistics can be found in the case of $n \geq 4$ vortices. For the case of $n = 4$ vortices, we define the Hilbert space $\{|0\rangle, i\Psi_2^\dagger\Psi_1^\dagger|0\rangle, \Psi_1^\dagger|0\rangle, i\Psi_2^\dagger|0\rangle\}$. With these bases, $\hat{\tau}_k$ ($k = 1, 2, 3$) can be expressed by matrix forms

$$\tau_1 = \begin{pmatrix} \omega^* & 0 & 0 & 0 \\ 0 & \omega & 0 & 0 \\ 0 & 0 & \omega & 0 \\ 0 & 0 & 0 & \omega^* \end{pmatrix}, \quad \tau_2 = \frac{1}{\sqrt{2}} \begin{pmatrix} 1 & -1 & 0 & 0 \\ 1 & 1 & 0 & 0 \\ 0 & 0 & 1 & -1 \\ 0 & 0 & 1 & 1 \end{pmatrix}, \quad \tau_3 = \begin{pmatrix} \omega^* & 0 & 0 & 0 \\ 0 & \omega & 0 & 0 \\ 0 & 0 & \omega^* & 0 \\ 0 & 0 & 0 & \omega \end{pmatrix}, \tag{9.12}$$

with $\omega = e^{i\pi/4}$ and $\omega^* = e^{-i\pi/4}$. In these bases, τ_1, τ_3 are diagonal but τ_2 is non-diagonal. One cannot diagonalize all of these at the same time. We find the non-Abelian nature; $\tau_1\tau_2 \neq \tau_2\tau_1$ and $\tau_2\tau_3 \neq \tau_3\tau_2$. This implies that the order of exchanging the kth and $k+1$th vortices is not commutative. It is straightforward to show the non-Abelian property

$$\tau_k\tau_{k+1} \neq \tau_{k+1}\tau_k \tag{9.13}$$

for any even number n. This is very different from conventional statistics, such as the Fermi–Dirac statistics, the Bose–Einstein statistics, and even the (Abelian) anyon statistics. In these conventional statistics, the state after the exchange does not depend on the choice of which particles are exchanged.

9.3. *Non-Abelian vortices with Majorana fermions*

Now, let us discuss the property of the exchange of non-Abelian vortices. For this purpose, we introduce an operator $\hat{\tau}_k$ that represents the operation T_k by

$$\hat{\tau}_k \equiv \prod_{a=1,2,3} \hat{\tau}_k^a, \quad \text{with } \hat{\tau}_k^a \equiv \frac{1}{\sqrt{2}}(1 + \gamma_{k+1}^a \gamma_k^a). \tag{9.14}$$

This is invariant under the $SO(3)$ symmetry. The operator $\hat{\tau}_k$ represents the operation T_k, because $\hat{\tau}_k \gamma_\ell^a \hat{\tau}_k^{-1}$ reproduces the exchange rule in Eq. (9.5). We also introduce the non-local Dirac operators by

$$\hat{\Psi}_k^a \equiv \frac{1}{2}\left(\gamma_{2k-1}^a + i\gamma_{2k}^a\right), \tag{9.15}$$

satisfying the anticommutation relations

$$\left\{\hat{\Psi}_k^a, \hat{\Psi}_\ell^{b\,\dagger}\right\} = \delta_{kl}\delta^{ab}, \quad \left\{\hat{\Psi}_k^a, \hat{\Psi}_\ell^b\right\} = \left\{\hat{\Psi}_k^{a\,\dagger}, \hat{\Psi}_\ell^{b\,\dagger}\right\} = 0. \tag{9.16}$$

Then, we can define the Hilbert (Fock) space. The Fock vacuum state $|0\rangle$ is defined by $\hat{\Psi}_k^a|0\rangle = 0$ for all k and $a = 1, 2, 3$, and multiparticle states are defined by operating successively $\hat{\Psi}_k^{a\,\dagger}$ to the vacuum state.

As an example, we consider the *four* non-Abelian vortices ($n = 4$). Noting that the Dirac fermion is a triplet state, we obtain the Hilbert space with $\mathcal{M}$-plet ($\mathcal{M} = \mathbf{1}, \mathbf{3}, \mathbf{5}$). Furthermore, each $\mathcal{M}$-plet is classified by even or odd numbers of the Dirac fermions ($\mathcal{P} = \mathcal{E}, \mathcal{O}$). Thus, the basis of the Hilbert space can be classified according to the representations $(\mathcal{M}, \mathcal{P})$. Their explicit forms are given as

$$|\mathbf{1}_{00}\rangle = |0\rangle, \tag{9.17}$$

$$|\mathbf{1}_{33}\rangle = i\frac{1}{3!}\epsilon^{abc}\frac{1}{3!}\epsilon^{def}\hat{\Psi}_1^{a\dagger}\hat{\Psi}_1^{b\dagger}\hat{\Psi}_1^{c\dagger}\hat{\Psi}_2^{d\dagger}\hat{\Psi}_2^{e\dagger}\hat{\Psi}_2^{f\dagger}|0\rangle, \tag{9.18}$$

$$|\mathbf{1}_{11}\rangle = i\frac{1}{\sqrt{3}}\hat{\Psi}_1^{a\dagger}\hat{\Psi}_2^{a\dagger}|0\rangle, \tag{9.19}$$

$$|\mathbf{1}_{22}\rangle = \frac{1}{\sqrt{3}}\frac{1}{2!}\epsilon^{abc}\frac{1}{2!}\epsilon^{ade}\hat{\Psi}_1^{b\dagger}\hat{\Psi}_1^{c\dagger}\hat{\Psi}_2^{d\dagger}\hat{\Psi}_2^{e\dagger}|0\rangle, \tag{9.20}$$

for the singlet-even $(\mathbf{1}, \mathcal{E})$ states and

$$|\mathbf{1}_{03}\rangle = \frac{1}{3!}\epsilon^{abc}\hat{\Psi}_2^{a\dagger}\hat{\Psi}_2^{b\dagger}\hat{\Psi}_2^{c\dagger}|0\rangle, \tag{9.21}$$

$$|\mathbf{1}_{30}\rangle = -i\frac{1}{3!}\epsilon^{abc}\hat{\Psi}_1^{a\dagger}\hat{\Psi}_1^{b\dagger}\hat{\Psi}_1^{c\dagger}|0\rangle, \tag{9.22}$$

$$|\mathbf{1}_{21}\rangle = -\frac{1}{\sqrt{3}}\frac{1}{2!}\epsilon^{abc}\hat{\Psi}_1^{a\dagger}\hat{\Psi}_1^{b\dagger}\hat{\Psi}_2^{c\dagger}|0\rangle, \tag{9.23}$$

$$|\mathbf{1}_{12}\rangle = i\frac{1}{\sqrt{3}}\frac{1}{2!}\epsilon^{abc}\hat{\Psi}_1^{a\dagger}\hat{\Psi}_2^{b\dagger}\hat{\Psi}_2^{c\dagger}|0\rangle, \tag{9.24}$$

for the singlet-odd $(\mathbf{1}, \mathcal{O})$ states.

There are six bases,

$$|\mathbf{3}_{02}\rangle = \frac{1}{2!}\epsilon^{abc}\hat{\Psi}_2^{b\dagger}\hat{\Psi}_2^{c\dagger}|0\rangle, \tag{9.25}$$

$$|\mathbf{3}_{31}\rangle = -i\frac{1}{3!}\epsilon^{bcd}\hat{\Psi}_1^{b\dagger}\hat{\Psi}_1^{c\dagger}\hat{\Psi}_1^{d\dagger}\hat{\Psi}_2^{a\dagger}|0\rangle, \tag{9.26}$$

$$|\mathbf{3}_{22}\rangle = \frac{1}{\sqrt{2}}\epsilon^{abc}\frac{1}{2!}\epsilon^{bde}\frac{1}{2!}\epsilon^{cfg}\hat{\Psi}_1^{d\dagger}\hat{\Psi}_1^{e\dagger}\hat{\Psi}_2^{f\dagger}\hat{\Psi}_2^{g\dagger}|0\rangle, \tag{9.27}$$

$$|\mathbf{3}_{11}\rangle = i\frac{1}{\sqrt{2}}\epsilon^{abc}\hat{\Psi}_1^{b\dagger}\hat{\Psi}_2^{c\dagger}|0\rangle, \tag{9.28}$$

$$|\mathbf{3}_{20}\rangle = -\frac{1}{2!}\epsilon^{abc}\hat{\Psi}_1^{b\dagger}\hat{\Psi}_1^{c\dagger}|0\rangle, \tag{9.29}$$

$$|\mathbf{3}_{13}\rangle = i\frac{1}{3!}\epsilon^{bcd}\hat{\Psi}_1^{a\dagger}\hat{\Psi}_2^{b\dagger}\hat{\Psi}_2^{c\dagger}\hat{\Psi}_2^{d\dagger}|0\rangle, \tag{9.30}$$

for the triplet-even $(\mathbf{3}, \mathcal{E})$ states and

$$|\mathbf{3}_{01}\rangle = \hat{\Psi}_2^{a\dagger}|0\rangle, \tag{9.31}$$

$$|\mathbf{3}_{32}\rangle = i\frac{1}{3!}\epsilon^{bcd}\hat{\Psi}_1^{b\dagger}\hat{\Psi}_1^{c\dagger}\hat{\Psi}_1^{d\dagger}\frac{1}{2!}\epsilon^{aef}\hat{\Psi}_2^{e\dagger}\hat{\Psi}_2^{f\dagger}|0\rangle, \tag{9.32}$$

$$|\mathbf{3}_{21}\rangle = \frac{1}{\sqrt{2}}\epsilon^{abc}\frac{1}{2!}\epsilon^{bde}\hat{\Psi}_1^{d\dagger}\hat{\Psi}_1^{e\dagger}\hat{\Psi}_2^{c\dagger}|0\rangle, \tag{9.33}$$

$$|\mathbf{3}_{12}\rangle = -i\frac{1}{\sqrt{3}}\epsilon^{abc}\frac{1}{2!}\epsilon^{cde}\hat{\Psi}_1^{b\dagger}\hat{\Psi}_2^{d\dagger}\hat{\Psi}_2^{e\dagger}|0\rangle, \tag{9.34}$$

$$|\mathbf{3}_{23}\rangle = \frac{1}{2!}\epsilon^{abc}\hat{\Psi}_1^{b\dagger}\hat{\Psi}_1^{c\dagger}\frac{1}{3!}\epsilon^{def}\hat{\Psi}_2^{d\dagger}\hat{\Psi}_2^{e\dagger}\hat{\Psi}_2^{f\dagger}|0\rangle, \tag{9.35}$$

$$|\mathbf{3}_{10}\rangle = i\hat{\Psi}_1^{a\dagger}|0\rangle, \tag{9.36}$$

for the triplet-odd $(\mathbf{3}, \mathcal{O})$ states. There are two bases,

$$\begin{aligned}|\mathbf{5}_{22}\rangle = i\mathcal{N}\Bigg\{&\frac{1}{2}\Bigg(\frac{1}{2!}\epsilon^{acd}\hat{\Psi}_1^{c\dagger}\hat{\Psi}_1^{d\dagger}\frac{1}{2!}\epsilon^{bef}\hat{\Psi}_2^{e\dagger}\hat{\Psi}_2^{f\dagger}\\ &+\frac{1}{2!}\epsilon^{bcd}\hat{\Psi}_1^{c\dagger}\hat{\Psi}_1^{d\dagger}\frac{1}{2!}\epsilon^{aef}\hat{\Psi}_2^{e\dagger}\hat{\Psi}_2^{f\dagger}\Bigg)\\ &-\frac{\delta^{ab}}{3}\frac{1}{2!}\epsilon^{cde}\hat{\Psi}_1^{d\dagger}\hat{\Psi}_1^{e\dagger}\frac{1}{2!}\epsilon^{cfg}\hat{\Psi}_2^{f\dagger}\hat{\Psi}_2^{g\dagger}\Bigg\}|0\rangle,\end{aligned} \tag{9.37}$$

$$|\mathbf{5}_{11}\rangle = -\mathcal{N}\left\{\frac{1}{2}\left(\hat{\Psi}_1^{a\dagger}\hat{\Psi}_2^{b\dagger}+\hat{\Psi}_1^{b\dagger}\hat{\Psi}_2^{a\dagger}\right)-\frac{\delta^{ab}}{3}\hat{\Psi}_1^{c\dagger}\hat{\Psi}_2^{c\dagger}\right\}|0\rangle, \tag{9.38}$$

for the quintet-even $(\mathbf{5}, \mathcal{E})$ states and

$$\begin{aligned}|\mathbf{5}_{21}\rangle = -i\mathcal{N}\Bigg\{&\frac{1}{2}\Bigg(\frac{1}{2!}\epsilon^{acd}\hat{\Psi}_1^{c\dagger}\hat{\Psi}_1^{d\dagger}\hat{\Psi}_2^{b\dagger}+\frac{1}{2!}\epsilon^{bcd}\hat{\Psi}_1^{c\dagger}\hat{\Psi}_1^{d\dagger}\hat{\Psi}_2^{a\dagger}\Bigg)\\ &-\frac{\delta^{ab}}{3}\frac{1}{2!}\epsilon^{cde}\hat{\Psi}_1^{c\dagger}\hat{\Psi}_1^{d\dagger}\hat{\Psi}_2^{e\dagger}\Bigg\}|0\rangle,\end{aligned} \tag{9.39}$$

$$\begin{aligned}|\mathbf{5}_{12}\rangle = -\mathcal{N}\Bigg\{&\frac{1}{2}\Bigg(\hat{\Psi}_1^{a\dagger}\frac{1}{2!}\epsilon^{bcd}\hat{\Psi}_2^{c\dagger}\hat{\Psi}_2^{d\dagger}+\hat{\Psi}_1^{b\dagger}\frac{1}{2!}\epsilon^{acd}\hat{\Psi}_2^{c\dagger}\hat{\Psi}_2^{d\dagger}\Bigg)\\ &-\frac{\delta^{ab}}{3}\frac{1}{2!}\epsilon^{cde}\hat{\Psi}_1^{c\dagger}\hat{\Psi}_2^{d\dagger}\hat{\Psi}_2^{e\dagger}\Bigg\}|0\rangle,\end{aligned} \tag{9.40}$$

for the quintet-odd (**5**, $\mathcal{O}$) states with $\mathcal{N} = \sqrt{3/2}$ for $a = b$ and $\mathcal{N} = \sqrt{2}$ for $a \neq b$.

According to the classification by $(\mathcal{M}, \mathcal{P})$, the operator $\hat{\tau}_k$ is given as matrices with the bases of the Hilbert space. We find that the matrix representations of the operators $\hat{\tau}_k$ are

$$\tau_k^{\mathcal{M},\mathcal{P}} = \sigma_k^{\mathcal{M}} \otimes h_k^{\mathcal{P}}, \tag{9.41}$$

i.e. a tensor product of the $\mathcal{M}$-dependent term $\sigma_k^{\mathcal{M}}$ and the $\mathcal{P}$-dependent term $h_k^{\mathcal{P}}$. Their matrix forms are

$$\sigma_1^{\mathbf{1}} = \begin{pmatrix} -1 & 0 \\ 0 & 1 \end{pmatrix}, \quad \sigma_2^{\mathbf{1}} = \frac{1}{2}\begin{pmatrix} 1 & \sqrt{3} \\ \sqrt{3} & -1 \end{pmatrix}, \quad \sigma_3^{\mathbf{1}} = \sigma_1^{\mathbf{1}}, \tag{9.42}$$

for $\mathcal{M} = \mathbf{1}$,

$$\sigma_1^{\mathbf{3}} = \begin{pmatrix} -1 & 0 & 0 \\ 0 & 1 & 0 \\ 0 & 0 & 1 \end{pmatrix}, \sigma_2^{\mathbf{3}} = \frac{1}{2}\begin{pmatrix} 1 & \sqrt{2} & 1 \\ \sqrt{2} & 0 & -\sqrt{2} \\ 1 & -\sqrt{2} & 1 \end{pmatrix}, \sigma_3^{\mathbf{3}} = \begin{pmatrix} 1 & 0 & 0 \\ 0 & 1 & 0 \\ 0 & 0 & -1 \end{pmatrix}, \tag{9.43}$$

for $\mathcal{M} = \mathbf{3}$, and

$$\sigma_1^{\mathbf{5}} = \sigma_2^{\mathbf{5}} = \sigma_3^{\mathbf{5}} = 1, \tag{9.44}$$

for $\mathcal{M} = \mathbf{5}$. On the other hand, $h_k^{\mathcal{P}}$ are common to all the $\mathcal{M}$-plets, and are given as

$$h_1^{\mathcal{E}} = h_1^{\mathcal{O}} = \begin{pmatrix} e^{i\frac{\pi}{4}} & 0 \\ 0 & e^{-i\frac{\pi}{4}} \end{pmatrix}, \quad h_2^{\mathcal{E}} = h_2^{\mathcal{O}} = \frac{1}{\sqrt{2}}\begin{pmatrix} 1 & -1 \\ 1 & 1 \end{pmatrix}, \quad h_3^{\mathcal{E}} = h_3^{\mathcal{O}\dagger} = h_1^{\mathcal{E}}. \tag{9.45}$$

Those matrices give the mixing of the wave functions of the Dirac fermions in exchanging the vortices. We note that they are non-Abelian matrices;

$$\hat{\tau}_\ell^{\mathcal{M},\mathcal{P}} \hat{\tau}_{\ell+1}^{\mathcal{M},\mathcal{P}} \neq \hat{\tau}_{\ell+1}^{\mathcal{M},\mathcal{P}} \hat{\tau}_\ell^{\mathcal{M},\mathcal{P}}. \tag{9.46}$$

This is confirmed by $\hat{\sigma}_\ell^{\mathcal{M}} \hat{\sigma}_{\ell+1}^{\mathcal{M}} \neq \hat{\sigma}_{\ell+1}^{\mathcal{M}} \hat{\sigma}_\ell^{\mathcal{M}}$ and $\hat{h}_\ell^{\mathcal{P}} \hat{h}_{\ell+1}^{\mathcal{P}} \neq \hat{h}_{\ell+1}^{\mathcal{P}} \hat{h}_\ell^{\mathcal{P}}$. This means that simultaneous diagonalization is not possible. In other words, different exchanges of neighboring vortices can lead to different states. Therefore, it obeys the non-Abelian statistics.

An important remark is in order. We note that $h_k^{\mathcal{P}}$ is nothing but the matrices in the non-Abelian statistics for "Abelian" vortices that contain a single component Majorana fermion found by Ivanov. What is new for "non-Abelian" vortices is the existence of the multiple component Majorana fermions with $SO(3)$ symmetry. Then, the non-Abelian statistics of the non-Abelian vortices have been obtained as a tensor product of $\sigma_k^{\mathcal{M}}$ and $h_k^{\mathcal{P}}$, where $\sigma_k^{\mathcal{M}}$ is a new ingredient from the $SO(3)$ symmetry. Interestingly, it is found that $\sigma_k^{\mathcal{M}}$ obeys the Coxeter group [80,177]. The Coxeter group gives a symmetry of the polytopes in high-dimensional space. The Coxeter group was studied by Harold Scott MacDonald ("Donald") Coxeter, one of the great mathematicians of the 20th century. The generators s_i $(i = 1, 2, ...)$ of the Coxeter group are given by two conditions;

$$\text{(a) } s_i^2 = 1, \tag{9.47}$$

$$\text{(b) } (s_i s_j)^{m_{ij}} = 1, \tag{9.48}$$

with positive integers $m_{ij} \geq 2$. The conditions (a) and (b) represent the mirror reflection and the rotation of the polytopes, respectively. In our present case, it is confirmed that $\sigma_k^{\mathcal{M}}$ satisfies these two relations; (a) $\sigma_i^2 = 1$ and (b) $(\sigma_i \sigma_j)^{m_{ij}} = 1$ with $m_{ij} = 3$ for $|i - j| = 1$ and $m_{ij} = 2$ for $|i - j| > 1$. The matrices $\sigma_k^{\mathbf{1}}$ for $\mathcal{M} = \mathbf{1}$ in Eq. (9.42) represent the symmetry for a triangle, and the matrices $\sigma_k^{\mathbf{3}}$

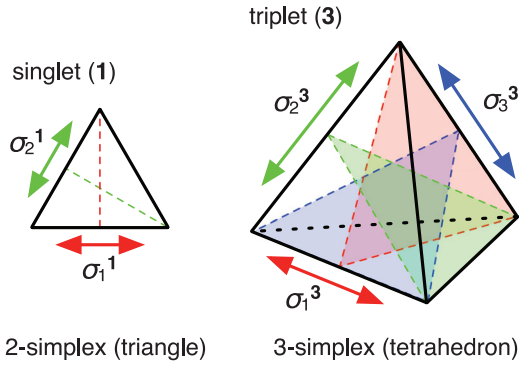

Fig. 30. The triangle for $\mathcal{M} = \mathbf{1}$ and the tetrahedron for $\mathcal{M} = \mathbf{3}$ are shown. (Ref. [379].)

for $\mathcal{M} = \mathbf{3}$ in Eq. (9.43) represent the symmetry for a tetrahedron in Fig. 30. As a result, it is found that the structure of high dimensional polytopes exists in the Hilbert space for non-Abelian vortices.

Finally, we comment that the decomposition in Eq. (9.41) can be obtained for the operator $\hat{\tau}_k$ itself. The operator $\hat{\tau}_k$ is expressed as a product of two $SO(3)$ invariant unitary operators,

$$\hat{\tau}_k = \hat{\sigma}_k \hat{h}_k, \tag{9.49}$$

where

$$\hat{\sigma}_k = \frac{1}{2}\left(1 - \gamma_{k+1}^1 \gamma_{k+1}^2 \gamma_k^1 \gamma_k^2 - \gamma_{k+1}^2 \gamma_{k+1}^3 \gamma_k^2 \gamma_k^3 - \gamma_{k+1}^3 \gamma_{k+1}^1 \gamma_k^3 \gamma_k^1\right) \tag{9.50}$$

and

$$\hat{h}_k = \frac{1}{\sqrt{2}}\left(1 - \gamma_{k+1}^1 \gamma_{k+1}^2 \gamma_{k+1}^3 \gamma_k^1 \gamma_k^2 \gamma_k^3\right). \tag{9.51}$$

It is easily verified that operators $\hat{\sigma}_k$ satisfy relations (a) and (b) of the Coxeter group, such that

$$\begin{aligned} \hat{\sigma}_k^2 &= 1, \\ (\hat{\sigma}_k \hat{\sigma}_l)^3 &= 1 \quad \text{for} \quad |k-l| = 1, \\ (\hat{\sigma}_k \hat{\sigma}_l)^2 &= 1 \quad \text{for} \quad |k-l| > 1. \end{aligned} \tag{9.52}$$

We confirm that $\hat{\sigma}_k$ obeys the Coxeter group for an arbitrary number of non-Abelian vortices. Therefore, for an arbitrary large number of non-Abelian vortices, the non-Abelian statistics contains the polytope structures in high dimensional space. This is a useful method, because it can be applied to vortices with $SO(N)$ symmetry (N: odd number), as demonstrated in Ref. [172].

9.4. Abelian/non-Abelian vortices with Dirac fermions

So far we have discussed the exchange statistics of vortices, where either a single Majorana fermion or three Majorana fermions are contained. They are called Majorana vortices. There, the Dirac fermion is defined by picking up two Majorana fermions that are located in different vortices. In this sense, the Dirac fermions are defined *non-locally*.

However, the situation is very different when there is an even number of Majorana fermions [377, 380]. In this case, we can construct the Dirac operators by picking up two Majorana fermions at the same vortex. Namely, the Dirac fermions are defined *locally* at the single vortex. Vortices containing the Dirac fermions can be called Dirac vortices.

In the CFL phase, an M_1 vortex contains three Majorana fermions and can be regarded as a Majorana vortex as discussed above, while an M_2 vortex contains two Dirac fermions [134] and can be

regarded as a Dirac vortex. Although M_2 vortices are energetically unstable against decay into two M_1, as illustrated in Fig. 11, there is a possibility that the M_2 vortices might be metastable when gluons are much heavier than other scalar fields. As shown for the Majorana vortex, we can consider the exchange of Dirac vortices. The Dirac fermions in the M_2 vortices can have internal degrees of freedom from $U(2)$ symmetry [377]. It was found that, while exchanges of vortices with a single Dirac fermion do *not* give non-Abelian statistics [380], exchanges of vortices with multiple Dirac fermions such as the M_2 vortices do give non-Abelian statistics [377]. We also note that non-Abelian vortices in supersymmetric $U(N)$ QCD contain $N-1$ Dirac fermions in their cores, as summarized in Appendix A.

10. Topological objects associated with chiral symmetry breaking

In the previous sections, we have studied the (non-)topological solitons in the order parameter manifold $U(3)_{\mathrm{C}-(\mathrm{L}+\mathrm{R})+\mathrm{B}} \simeq [SU(3)_{\mathrm{C}} \times SU(3)_{\mathrm{L}+\mathrm{R}} \times U(1)_{\mathrm{B}}]/[SU(3)_{\mathrm{C}+\mathrm{L}+\mathrm{R}} \times \mathbb{Z}_3]$. In this section, we study topological objects in the chiral symmetry breaking sector $U(3)_{\mathrm{L}-\mathrm{R}+\mathrm{A}} \simeq [SU(3)_{\mathrm{L}} \times SU(3)_{\mathrm{R}} \times U(1)_{\mathrm{A}}]/[SU(3)_{\mathrm{L}+\mathrm{R}} \times \mathbb{Z}_3]$. The $U(1)_{\mathrm{A}}$ symmetry is explicitly broken by the instanton effect (the chiral anomaly) and the corresponding $U(1)_{\mathrm{A}}$ Nambu–Goldstone mode, the η' meson, acquires a potential term. In Sect. 10.1, we first discuss $U(1)_{\mathrm{A}}$ axial domain walls interpolating ground states of the instanton-induced potential, with massless and massive quarks. After giving a linear sigma model in Sect. 10.2, we discuss $U(1)_{\mathrm{A}}$ Abelian axial vortices and non-Abelian axial vortices in the absence of the instanton-induced potentials in Sect. 10.3. In Sect. 10.4, we discuss composite states of axial domain walls and axial vortices in the presence of the instanton-induced potentials. In Sect. 10.5, we discuss the quantum decay of axial domain walls. Skyrmions as qualitons are briefly discussed in Sect. 10.7.

10.1. Axial domain walls

10.1.1. Fractional axial domain walls in the chiral limit. Instantons flip the chiralities of quarks and thus break the $U(1)_{\mathrm{A}}$ symmetry (the chiral anomaly). Instanton effects in the CFL phase are parametrically small at asymptotically high densities and controlled calculations are possible. In the chiral limit with massless quarks, the leading contribution to the mass of the η' meson arises from two-instanton diagrams [302]. As shown in Eq. (2.92), the instanton-induced potential takes the form

$$V_{\text{2-inst}} = -2C\cos 3\varphi_{\mathrm{A}}. \tag{10.1}$$

Here the $U(1)_{\mathrm{A}}$ phase mode φ_{A} is $\arg(\det \Sigma)$ in terms of the gauge invariant field Σ in Eq. (2.72). Thus, the effective Lagrangian for the η' meson is given by

$$\mathcal{L} = \frac{3f_{\eta'}^2}{4}\left((\partial_0\varphi_{\mathrm{A}})^2 - v_{\eta'}^2(\partial_i\varphi_{\mathrm{A}})^2\right) + 2C\cos 3\varphi_{\mathrm{A}}, \tag{10.2}$$

where the elementary meson field is defined as $\varphi_{\mathrm{A}} = 2\eta'/\sqrt{6}f_{\eta'}$. The decay constant $f_{\eta'}$ and the velocity $v_{\eta'}$ were found as [333]

$$f_{\eta'} = \frac{3\mu^2}{2\pi^2}, \quad v_{\eta'} = \frac{1}{\sqrt{3}}. \tag{10.3}$$

The above Lagrangian is the sine-Gordon model with a period $\varphi_{\mathrm{A}} \sim \varphi_{\mathrm{A}} + 2\pi/3$, which allows sine-Gordon domain wall solutions [327]. Since the potential is periodic in φ_{A} with the period $2\pi/3$, there are three different minima $\varphi_{\mathrm{A}} = 0, 2\pi/3, 4\pi/3$ in the period $\varphi_{\mathrm{A}} \in [0, 2\pi)$. One of the minimal

configurations is a domain wall, which interpolates between $\varphi_{\rm A} = 0$ at $x = -\infty$ and $\varphi_{\rm A} = 2\pi/3$ at $x = \infty$. Assuming that the field depends only on one space direction, say x, an exact solution of a single static domain wall can be available:

$$\varphi_{\rm A}(x) = \frac{4}{3} \arctan e^{\frac{m_{\eta'}}{v_{\eta'}}(x-x_0)}, \tag{10.4}$$

where

$$m_{\eta'} = \frac{2\sqrt{3C}}{f_{\eta'}} \tag{10.5}$$

is the mass of the η' meson, and x_0 denotes the position of the domain wall. The tension of the domain wall is given by

$$T = \frac{8\sqrt{C} f_{\eta'} v_{\eta'}}{\sqrt{3}}. \tag{10.6}$$

The other two domain walls interpolating between $\varphi_{\rm A} = 2\pi/3$ and $\varphi_{\rm A} = 4\pi/3$, and between $\varphi_{\rm A} = 4\pi/3$ and 2π are simply obtained by phase shifts. All three domain walls wind the $U(1)_{\rm A}$ phase $1/3$ times, unlike the unit winding for the usual sine-Gordon domain walls. Therefore, these domain walls can be called *fractional* axial (sine-Gordon) domain walls.

Two fractional sine-Gordon domain walls repel each other (the repulsion $\sim e^{-2R}$ with distance $2R$) [272]. If one considers an integer sine-Gordon domain wall winding $U(1)_{\rm A}$ once, it splits into three fractional sine-Gordon domain walls.

Note that, if we include the amplitude mode $|\det \Sigma|$ in addition to the effective theory for $\varphi_{\rm A}$ in Eq. (10.1), it is similar to the so-called $N = 3$ axion model [89,268,269], which is an elegant extension of the standard model for solving the strong CP problem [268,269,366,368]. The domain walls in the axion models were first studied in Ref. [325]. Domain walls in the $N > 1$ axion models are stable because they connect two vacua with different phases $\varphi_{\rm A}$. Consequently, the domain wall energy dominates the energy density of the universe, causing the cosmological domain wall problem. Only the $N = 1$ case is known to be cosmologically viable, in which the domain wall can decay, as is explained in Sect. 10.5.1, and the domain wall energy does not dominate the energy density of the universe. In our case of dense QCD, one might think that the axial domain walls would be stable because they interpolate between two disconnected points among $\varphi_{\rm A} = 0, 2\pi/3, 4\pi/3$. This is, however, not the case. The axial domain walls in dense QCD are metastable as we discuss in Sect. 10.5.2.

10.1.2. Integer axial domain walls with massive quarks. Let us next consider an axial domain wall in the case that the quark masses are not all zero [335]. Here, we assume $m_{\rm u} = m_{\rm d} = m_{\rm s} = m$ for simplicity, so that the mixing in the neutral mesons (π^0, η, η') simply vanishes [47,233,302,303]. As shown in Eq. (2.92), the potential for the η' meson receives two additional contributions to the one in Eq. (10.1). One is from the quark mass term [333] and the other is the one-instanton contribution [302,335],

$$V = -6mA\cos\varphi_{\rm A} - 12Bm^2\cos\varphi_{\rm A} - 2C\cos 3\varphi_{\rm A}, \tag{10.7}$$

where the first term stands for the one-instanton contribution, which is a contribution from the chiral condensates. The coefficients A, B were obtained in Ref. [302].

In the limit where the chemical potential is infinite while keeping the quark masses fixed, we have $m^2 B \gg mA \gg C$. So we can omit the terms whose coefficients are A and C, then the effective

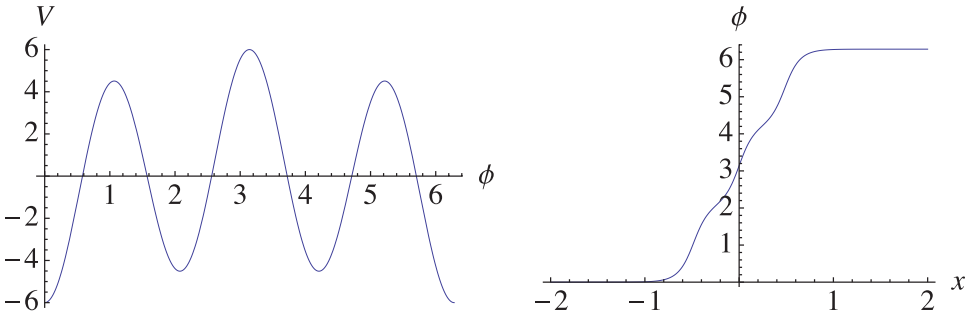

Fig. 31. A composite of fractional axial domain walls. An example of a numerical solution for a generic sine-Gordon potential $V = -\alpha \cos\varphi_{\rm A} - \beta \cos 3\varphi_{\rm A}$ is shown in the left panel. We set $\alpha = 1$, $\beta = 5$, and $f'_\eta = 1$ to show a typical configuration. The domain wall solution is shown in the right panel. The integer axial domain wall consists of three fractional axial domain walls.

theory becomes

$$\mathcal{L} = \frac{3f_{\eta'}^2}{4}\left((\partial_0\varphi_{\rm A})^2 - v_{\eta'}^2(\partial_i\varphi_{\rm A})^2\right) + 12Bm^2\cos\varphi_{\rm A}. \tag{10.8}$$

This is the conventional sine-Gordon model. A single static domain wall solution is known to be [325,335]

$$\varphi_{\rm A}(x) = 4\arctan e^{\frac{\tilde{m}_{\eta'}}{v_{\eta'}}(x-x_0)}, \tag{10.9}$$

with $\tilde{m}_{\eta'} = 2m\sqrt{2B}/f_{\eta'}$. The tension of the domain wall is given by

$$T = 24\sqrt{2B}f_{\eta'}v_{\eta'}m. \tag{10.10}$$

The difference between the axial domain walls in Eqs. (10.2) and (10.9) is only the coefficients; In contrast to the fractional axial domain wall in Eq. (10.2), the domain wall in Eq. (10.9) winds the $U(1)_{\rm A}$ once; therefore it can be referred to as an *integer* axial (sine-Gordon) domain wall characterized by the first homotopy group[15]

$$\pi_1[U(1)_{\rm A}] \simeq \mathbb{Z}. \tag{10.11}$$

The classical stability of the integer axial domain walls was studied in Ref. [60].

Finally, let us consider the most generic potential in Eq. (10.7). If we include the two-instanton contributions, the potential includes $\cos\varphi_{\rm A}$ and $\cos 3\varphi_{\rm A}$ as in Eq. (10.7). This potential is known as that of the triple sine-Gordon model. For generic parameter choices, the minimum of the potential is unique, $\varphi_{\rm A} = 0$, and only an integer axial domain wall winding the $U(1)_{\rm A}$ phase once is allowed. A numerical solution is shown in Fig. 31. The figure shows substructures of three peaks, and this integer axial domain wall can be interpreted as a composite of three fractional axial domain walls with 1/3 $U(1)_{\rm A}$ windings in Eq. (10.9). Without the two-instanton contribution $\cos\varphi_{\rm A}$, these three fractional axial domain walls repel each other and the integer axial domain wall decays completely into three fractional axial domain walls, as mentioned above. On the other hand, the two-instanton-induced

[15] Sine-Gordon kinks should be regarded as textures more like defects. So they are classified by an approximate order parameter manifold in the absence of the potential, while the exact order parameter is lifted by the potential. When the spatial infinities are identified as a point, topological textures in $\mathbb{R}^d$ are classified by a map from S^d to the (approximate) order parameter manifold M, and the corresponding homotopy group is $\pi_d(M)$. Fractional sine-Gordon domain walls discussed in the last subsection cannot be characterized by the first homotopy group.

potential $\cos\varphi_{\rm A}$ introduces the energy between domain walls, resulting in a constant attractive force between them. Therefore, the linear confinement of domain walls occurs.

10.2. Linear sigma model

As discussed above, instanton effects are parametrically small in the asymptotically high density limit. Then the $U(1)_{\rm A}$ symmetry becomes an exact symmetry of the system. In the CFL phase, the diquarks are condensed and the $U(1)_{\rm A}$ is spontaneously broken. As explained in Sect. 3.1.2, therefore, there exist topologically stable global vortices, $U(1)_{\rm A}$ global vortices. However, this is not the whole story. One should be careful that not only the $U(1)_{\rm A}$ symmetry, but also the full axial symmetry $[SU(3)_{\rm L-R} \times U(1)_{\rm A}]/\mathbb{Z}_3$ of QCD is spontaneously broken completely in the CFL phase. As we have seen, this kind of spontaneously broken non-Abelian symmetry gives rise to non-Abelian vortices. One crucial difference from the previous sections is that no local symmetries take part in here. Thus, the $U(1)_{\rm A}$ vortices that we study in this section are *global* non-Abelian vortices.

We start with a generic linear sigma model in the chiral limit:

$$\mathcal{L} = {\rm Tr}\left[\partial_0\Sigma^\dagger\partial^0\Sigma + u^2\partial_i\Sigma^\dagger\partial^i\Sigma - \lambda_2(\Sigma^\dagger\Sigma)^2 + \eta^2\Sigma^\dagger\Sigma\right] - \lambda_1\left({\rm Tr}\left[\Sigma^\dagger\Sigma\right]\right)^2 - \kappa(\det\Sigma + {\rm c.c.}) - \frac{3\eta^4}{4\,(3\lambda_1+\lambda_2)}, \tag{10.12}$$

where Σ is a 3×3 complex matrix scalar field without any constraints, as is defined in Eq. (2.72). The speed of the modes is taken to be $u \sim v_\pi \sim v_{\eta'}$. The coefficient κ of the anomaly term is related to the C of the chiral Lagrangian as $\kappa\langle\Sigma\rangle^3 = C$. The field Σ is invariant under $SU(3)_{\rm C}$ and $U(1)_{\rm B}$, while it transforms under $SU(3)_{\rm L}\times SU(3)_{\rm R}\times U(1)_{\rm A}$ as

$$\Sigma \to e^{i\theta_{\rm A}} g_{\rm L}^\dagger \Sigma g_{\rm R}, \quad \left(e^{i\theta_{\rm A}}, g_{\rm L}, g_{\rm R}\right) \in U(1)_{\rm A}\times SU(3)_{\rm L}\times SU(3)_{\rm R}. \tag{10.13}$$

Here, we have used different notation for $\theta_{\rm A}$ from Eq. (2.73). Since we are interested in topological vortices in this model, we do not specify values of the coupling constants $\lambda_{1,2}$, η but leave them as the parameters of the model. By taking the heavy mass limit, one can relate this linear sigma model with the chiral Lagrangian of the light fields in Eq. (2.83) with the anomaly term in Eq. (2.92). We also ignore the electromagnetic interaction here.

Taking into account discrete symmetries, the full chiral symmetry of the Lagrangian in Eq. (10.12) is $G_{\rm F}$, given in Eq. (2.74). Let us consider the case in which the anomaly effect is absent, $\kappa = 0$. The ground states are stable when the coupling constants in Eq. (10.12) satisfy

$$\eta^2 > 0, \quad 3\lambda_1 + \lambda_2 > 0. \tag{10.14}$$

Up to the flavor rotation, one can choose the ground state value as

$$\langle\Sigma\rangle = v\mathbf{1}_3, \quad v = \sqrt{\frac{\eta^2}{2(3\lambda_1+\lambda_2)}}. \tag{10.15}$$

The vacuum expectation value v should be identified with $v \sim f_\pi \sim f_{\eta'}$. In the ground state, the chiral symmetry $G_{\rm F}$ breaks down to its diagonal subgroup $H_{\rm F} = SU(3)_{\rm V}/\mathbb{Z}_{3{\rm V}}$, given in Eq. (2.79). Then, the order parameter manifold is $G_{\rm F}/H_{\rm F} \simeq U(3)_{\rm L-R+A}$, given in Eq. (2.80).

The mass spectra are as follows: there are $8+1$ NG bosons associated with the spontaneously broken $U(3)_{\mathrm{L-R+A}}$ and the same number of massive bosons, whose masses are

$$m_1^2 = 2\eta^2, \quad m_8^2 = 4\lambda_2 v^2. \tag{10.16}$$

Note that the linear sigma model (10.12) can be regarded as that for the chiral symmetry breaking in the low density hadronic phase. There are a number of works studying various topological solitons in the hadronic phase. For example, η' strings, which are the $U(1)_{\mathrm{A}}$ global vortices, were studied in Refs. [34,386]. Non-topological vortices called pion strings with a trivial topology $\pi_1[SU(2)] = 0$ were studied in Refs. [59,386].

Non-Abelian global vortices in the hadronic phase were first found by Balachandran and Digal in Ref. [33]. Various aspects of the non-Abelian global vortices were studied in the subsequent papers [111,244,261]. Since the linear sigma model for the chiral symmetry breaking in the CFL phase shares many similar properties with that for the hadronic phase, there should exist the same kind of non-Abelian global vortices in dense QCD.

10.3. Abelian and non-Abelian axial vortices

10.3.1. Abelian axial vortices. Since the order parameter manifold $G_{\mathrm{F}}/H_{\mathrm{F}} \simeq U(3)_{\mathrm{L-R+A}}$ is not simply connected, the first homotopy group is nontrivial:

$$\pi_1[U(1)_{\mathrm{A}}] \simeq \mathbb{Z}. \tag{10.17}$$

Therefore, there exist topologically stable vortices. In order to generate a nontrivial loop in the order parameter manifold, one may use only a T_0 generator. Such a loop corresponds to the η' string [34, 386] for which the order parameter Σ behaves as

$$\Sigma(r,\theta) = v f(r) e^{i\theta} \mathbf{1}_3. \tag{10.18}$$

The equation of motion for the amplitude function $f(r)$ is of the form

$$u^2 \left(f'' + \frac{f'}{r} - \frac{f}{r^2} \right) - \frac{m_1^2}{2} f(f^2 - 1) = 0. \tag{10.19}$$

This is exactly the same equation as the equation of motion for the familiar $U(1)$ global vortices. Solutions can be numerically obtained with the suitable boundary condition $f(0) = 0$ and $f(\infty) = 1$; see e.g. Ref. [355]. The tension of the Abelian global string is [261]

$$T_{U(1)_{\mathrm{A}}} = 3 \times 2\pi v^2 u^2 \log \frac{L}{\xi} + \text{const.} \tag{10.20}$$

with the size of the system L and the size of the axial vortex $\xi = m_1^{-1}$.

10.3.2. Non-Abelian axial vortices. One can construct a smaller loop inside the order parameter manifold by combining the $U(1)_{\mathrm{A}}$ generator $T_0 \sim \mathbf{1}_3$ and non-Abelian generators T_a ($a = 1, 2, \cdots, 8$) of $SU(3)$ [33]. They correspond to non-Abelian axial vortices characterized by the

homotopy group

$$\pi_1[U(3)_{\rm L-R+A}] \simeq \mathbb{Z}. \tag{10.21}$$

The three typical configurations are given by

$$\begin{aligned}
\Sigma &= v\,\mathrm{diag}\left(e^{i\theta} f(r), g(r), g(r)\right) \xrightarrow{r\to\infty} v\,\mathrm{diag}\left(e^{i\theta}, 1, 1\right) \\
&= v\, e^{i\frac{\theta}{3}} \mathrm{diag}\left(e^{i\frac{2\theta}{3}}, e^{-i\frac{\theta}{3}}, e^{-i\frac{\theta}{3}}\right), \\
\Sigma &= v\,\mathrm{diag}\left(g(r), e^{i\theta} f(r), g(r)\right) \xrightarrow{r\to\infty} v\,\mathrm{diag}\left(1, e^{i\theta}, 1\right) \\
&= v\, e^{i\frac{\theta}{3}} \mathrm{diag}\left(e^{-i\frac{\theta}{3}}, e^{i\frac{2\theta}{3}}, e^{-i\frac{\theta}{3}}\right), \\
\Sigma &= v\,\mathrm{diag}\left(g(r), g(r), e^{i\theta} f(r)\right) \xrightarrow{r\to\infty} v\,\mathrm{diag}\left(1, 1, e^{i\theta}\right) \\
&= v\, e^{i\frac{\theta}{3}} \mathrm{diag}\left(e^{-i\frac{\theta}{3}}, e^{-i\frac{\theta}{3}}, e^{i\frac{2\theta}{3}}\right),
\end{aligned} \tag{10.22}$$

with the profile functions $f(r)$ and $g(r)$ satisfying the boundary conditions

$$f(r\to\infty) = g(r\to\infty) = 1, \quad f(0) = g'(0) = 0. \tag{10.23}$$

The boundary condition at spatial infinities in Eqs. (10.22) clearly shows that the corresponding loops wind 1/3 of the $U(1)_{\rm A}$ phase, and are generated by non-Abelian generators of $SU(3)_{\rm L-R}$ at the same time. They are called fractional vortices because of the fractional winding of the $U(1)_{\rm A}$ phase and non-Abelian vortices because of the contribution of the non-Abelian generators. Because of the fractionality of the $U(1)_{\rm A}$ winding, the tension of a single non-Abelian axial vortex is one-third of that for an Abelian axial vortex [261]:

$$T_{U(3)_{\rm L-R+A}} = 2\pi v^2 u^2 \log\frac{L}{\xi} + \text{const.}, \tag{10.24}$$

with $\xi \sim \max(m_8^{-1}, m_1^{-1})$.

The equations of motion for the amplitudes $f(r)$ and $g(r)$ are

$$u^2\left(f'' + \frac{f'}{r} - \frac{f}{r^2}\right) - \frac{m_1}{6} f(f^2 + 2g^2 - 3) - \frac{m_8^2}{3} f(f^2 - g^2) = 0, \tag{10.25}$$

$$u^2\left(g'' + \frac{g'}{r}\right) - \frac{m_1^2}{6} g(f^2 + 2g^2 - 3) + \frac{m_8^2}{6} g(f^2 - g^2) = 0, \tag{10.26}$$

where $\tau \equiv m_8/m_1$. These should be solved with the boundary conditions $f(0) = g'(0) = 0$. The asymptotic behavior of a profile function of a $U(1)$ global vortex is established; see e.g. Ref. [355]. On the other hand, the profile functions for a non-Abelian axial vortex were studied in Refs. [111,261] in detail. Typical profile functions for the cases with $m_1 < m_8$ and $m_1 > m_8$ are shown in Fig. 32.

The asymptotic behaviors depend on the two mass scales m_1 and m_8. For instance, the profile functions near the center of the vortex and far from the vortex were found [111,261] to be

$$f(r) = c_1 r + c_3 r^3 + \cdots, \quad g(r) = d_0 + d_2 r^2 + \cdots, \qquad \left(r \ll \min\{m_1^{-1}, m_8^{-1}\}\right), \tag{10.27}$$

and

$$f(r) = 1 + \frac{a_2}{r^2} + \frac{a_4}{r^4} + \cdots, \quad g(r) = 1 + \frac{b_2}{r^2} + \frac{b_4}{r^4} + \cdots, \quad \left(r \gg \min\{m_1^{-1}, m_8^{-1}\}\right). \tag{10.28}$$

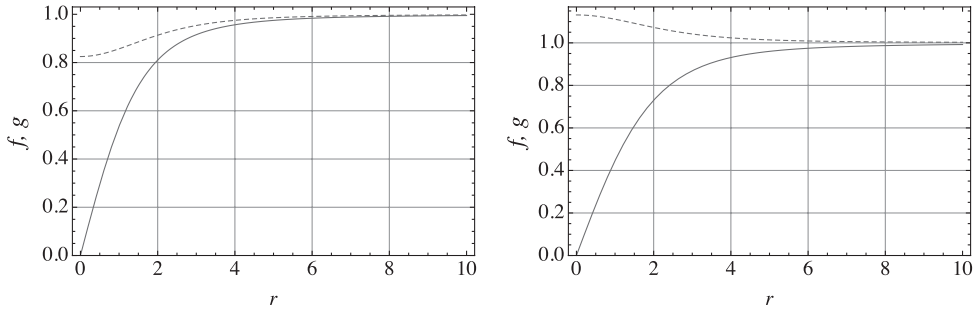

Fig. 32. Typical profile functions of $f(r)$ (solid line) and $g(r)$ (broken line). The parameters are set to $m_1 = 1$ and $m_8 = 2$ for the left panel and $m_1 = 2$ and $m_8 = 1$ for the right panel.

While numerical study is needed to determine the coefficients c_i and d_i, the coefficients a_i and b_i are analytically determined [111] as

$$a_2 = -\frac{1}{3}\left(\frac{1}{m_1^2} + \frac{2}{m_8^2}\right), \quad b_2 = -\frac{1}{3}\left(\frac{1}{m_1^2} - \frac{1}{m_8^2}\right). \tag{10.29}$$

Full numerical profile functions were also obtained in Refs. [111,261].

The configurations in Eq. (10.22) are connected by the flavor rotation $SU(3)_{\rm L+R}$ and all of them form an infinitely degenerate family [261]. Since the configurations in Eq. (10.22) are invariant under the little group $U(2)_{\rm L+R}$, the physically independent solutions are labeled by

$$\frac{SU(3)_{\rm L+R}}{U(1)_{\rm L+R} \times SU(2)_{\rm L+R}} \simeq \mathbb{C}P^2. \tag{10.30}$$

Therefore, $\mathbb{C}P^2$ Nambu–Goldstone modes appear as semi-superfluid non-Abelian vortices. However, these $\mathbb{C}P^2$ Nambu–Goldstone modes are *not* localized around a vortex. Instead, the wave functions of the $\mathbb{C}P^2$ modes extend to spatial infinity, because $SU(3)_{\rm L+R}$ transformations change the boundary conditions at spatial infinities, as can be seen in Eq. (10.22). They are non-normalizable and should be regarded as more like bulk modes.[16]

The intervortex force between two well separated non-Abelian axial vortices was obtained in Ref. [244]. The details of the calculations are quite similar to those in Sect. 4.2. As explained in Sect. 4.2, as far as two string interaction is concerned, only an $SU(2)_{\rm L+R}$ rotation is enough to set up two strings whose relative orientation is generic. In the following, we fix the amplitudes $f(r)$ and $g(r)$ at one, which is valid for a vortex distance $2R$ much larger than the mass scales m_1^{-1}, m_8^{-1}. Thus, we take two well separated strings parallel to the z-axis separated with the distance $2R$ into the x-axis as in Fig. 8:

$$\Sigma_1 = v\,\mathrm{diag}(e^{i\theta_1}, 1, 1), \tag{10.31}$$

and

$$\Sigma_2 = v \begin{pmatrix} g \begin{pmatrix} e^{i\theta_2} & & \\ & 1 & \\ & 0 & \end{pmatrix} g^{-1} & 0 \\ 0 & 1 \end{pmatrix}, \tag{10.32}$$

where g is an element of $SU(2)_{\rm L+R}$:

$$g = \cos\frac{\alpha}{2} + i\vec{n}\cdot\vec{\sigma}\,\sin\frac{\alpha}{2}. \tag{10.33}$$

[16] If $g_{\rm L}$ were the gauge transformation, as is the case in Sect. 3 ($g_{\rm L} \to g_{\rm C} \in SU(3)_{\rm C}$), the boundary conditions are physically identical, because they can be transformed to each other by a suitable gauge transformation in Eq. (4.19). Consequently, the $\mathbb{C}P^2$ modes would become normalizable.

The interaction energy density of the two strings is obtained by subtracting two individual string energies from the total configuration energy for the Abrikosov ansatz $\Sigma_{\rm tot} = \Sigma_1 \Sigma_2$ as

$$\begin{aligned} F(r, \theta, R, \alpha) &= \mathrm{Tr}\left(|\partial \Sigma_{\rm tot}|^2 - |\partial \Sigma_1|^2 - |\partial \Sigma_2|^2 \right) \\ &= \pm(1 + \cos\alpha) \left(\frac{-R^2 + r^2}{R^4 + r^4 - 2R^2 r^2 \cos 2\theta} \right), \end{aligned} \tag{10.34}$$

where the sign $\pm$ is for the vortex–vortex and vortex–anti-vortex pairs. Integrating this over the x–y plane, one gets the interaction energy

$$E(a, \alpha, L) = \pm\pi(1 + \cos\alpha) \left[-\ln 4 - 2\ln R + \ln(R^2 + L^2) \right]. \tag{10.35}$$

Finally, the intervortex force can be obtained by differentiating E by the interval $2R$ as

$$f(R, \alpha, L) = \pm\pi(1 + \cos\alpha) \left(\frac{1}{R} - \frac{R}{R^2 + L^2} \right) \simeq \pm(1 + \cos\alpha) \frac{\pi}{R}. \tag{10.36}$$

Although the calculations here are quite similar to those in Sect. 4.2, there is a sharp contrast in comparison with the intervortex forces. While the intervortex force of the semi-superfluid vortices is independent of the orientation at the leading order, one of the non-Abelian axial vortices depends on the relative orientation α at the leading order. This difference reflects the fact that the orientational modes $\mathbb{C}P^2$ are normalizable or non-normalizable for semi-superfluid vortices or non-Abelian axial vortices, respectively.

The intervortex force at the leading order in Eq. (10.36) vanishes at $\alpha = \pi/2$. For instance, the three configurations in Eq. (10.22) do not interact at this order. A $U(1)_{\rm A}$ vortex can be marginally separated to three non-Abelian axial vortices as

$$\mathrm{diag}\,(e^{i\theta}, e^{i\theta}, e^{i\theta}) \to \mathrm{diag}\,(e^{i\theta_1}, 1, 1) \times \mathrm{diag}\,(1, e^{i\theta_2}, 1) \times \mathrm{diag}\,(1, 1, e^{i\theta_3}) \tag{10.37}$$

at this order, where $\theta_{1,2,3}$ denotes an angle coordinate at each vortex center.

However, when the leading order term vanishes in general, one needs to consider the next-leading order. The next-leading order of interaction between two vortices winding around different components was obtained in the context of two-component Bose–Einstein condensates in Ref. [108]. In terms of the parameters in Eq. (10.12), the interaction energy and force between vortices at a distance $2R$ much larger than m_1^{-1}, m_8^{-1} are

$$\begin{aligned} E_{\rm next} &\sim \lambda_2 \frac{\log(2R/\xi)}{(2R)^2}, \\ f_{\rm next} &\sim \lambda_2 \frac{1}{(2R)^3} \left(\log\frac{2R}{\xi} - \frac{1}{2} \right), \end{aligned} \tag{10.38}$$

respectively, which is repulsive.

10.4. Composites of axial domain walls and axial vortices

Let us next take into account the instanton effects in the presence of vortices. We first consider the chiral limit with massless quarks in Sect. 10.4.1, followed by the case with massive quarks in Sect. 10.4.2.

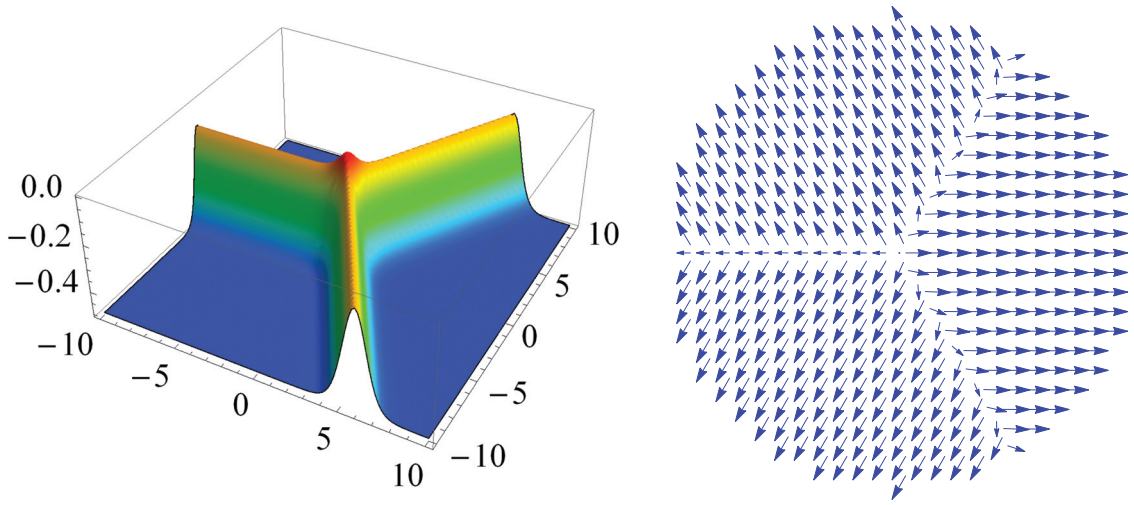

Fig. 33. A three-pronged fractional axial domain wall junction is formed in the presence of an Abelian axial vortex in the chiral limit. The effective potential is $V_{\eta'} = -C\cos 3\varphi_A$, which is generated by the two-instanton effect. The energy density is shown in the left panel and the $U(1)_{\rm A}$ phase $(\cos\varphi_{\rm A}, \sin\varphi_{\rm A})$ is shown in the right panel.

10.4.1. Abelian and non-Abelian axial vortices attached by fractional axial domain walls in the chiral limit. In the chiral limit, the instanton-induced potential for the η'-boson is given in Eq. (10.1). While we have studied domain walls in the chiral Lagrangian in Sect. 10.1, they remain almost the same with slight modifications in the linear sigma model introduced in Sect. 10.2. Similarly to axion strings, Abelian axial vortices are attached by axial domain walls in the presence of the instanton-induced potential $\sim \cos 3\varphi_{\rm A}$. Since the phase changes from $\varphi_{\rm A} = 0$ to $\varphi_{\rm A} = 2\pi$ around a single Abelian axial vortex, three different domain walls forming a three-pronged junction attach to it, as illustrated in Fig. 33. Since the domain walls repel each other, the configuration becomes a $\mathbb{Z}_3$ symmetric domain wall junction. A numerical solution for this configuration was first obtained in the chiral phase transition in the low baryon density region in Ref. [34].

Next, let us consider non-Abelian axial vortices in the presence of the instanton-induced potential $\sim \cos 3\varphi_{\rm A}$ [102]. The $U(1)_{\rm A}$ phase changes by $2\pi/3$ around a non-Abelian axial vortex. Therefore, one fractional axial wall attaches to one non-Abelian axial vortex, as illustrated in Fig. 34. Let us consider it in more detail, focusing on the configuration of the type $\mathrm{diag}(e^{i\theta}, 1, 1)$. In the vicinity of the vortex, let us divide a closed loop encircling the vortex to the paths b_1 and b_2, as in Fig. 34. Then, along the path b_1 and b_2, the order parameter receives the transformation by the group elements

$$g(\theta) = \begin{cases} \exp\left[\frac{2i}{3}\left(\theta + \frac{\pi}{2}\right)\mathrm{diag}(1,1,1)\right] \in U(1)_{\rm A}, & b_1 : -\frac{\pi}{2} \le \theta \le \frac{\pi}{2} \\ \exp\left[\frac{2i}{3}\left(\theta - \frac{\pi}{2}\right)\mathrm{diag}(2,-1,-1)\right]\omega \in SU(3)_{\rm L-R}, & b_2 : \frac{\pi}{2} \le \theta \le \frac{3}{2}\pi. \end{cases} \tag{10.39}$$

Only the $U(1)_{\rm A}$ phase is rotated in the path b_1 while only the $SU(3)_{\rm L-R}$ transformation acts along the path b_2. This configuration was discussed in the chiral phase transition in the low baryon density region in Ref. [33]. This is of course unstable because it is pulled by the domain wall tension to spatial infinity [102].

As for non-Abelian semi-superfluid vortices, there is an M_2 non-Abelian vortex, which is

$$\begin{aligned} \Sigma &= v\,\mathrm{diag}\left(g(r), e^{i\theta}f(r), e^{i\theta}f(r)\right) \\ &\xrightarrow{r\to\infty} v\,\mathrm{diag}\left(1, e^{i\theta}, e^{i\theta}\right) = v\,e^{i\frac{2\theta}{3}}\mathrm{diag}\left(e^{-i\frac{2\theta}{3}}, e^{i\frac{\theta}{3}}, e^{i\frac{\theta}{3}}\right), \end{aligned} \tag{10.40}$$

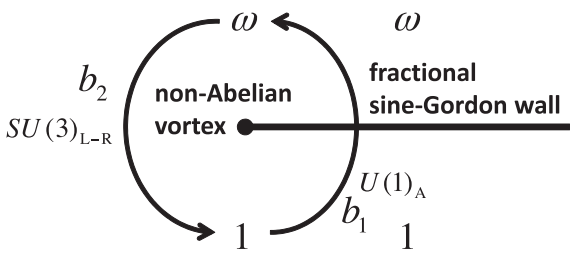

Fig. 34. A non-Abelian axial vortex attached by a fractional axial domain wall with the instanton-induced potential $V_{\eta'} = -C\cos 3\varphi_A$. Along the path b_1, only the $U(1)_{\rm A}$ phase is rotated by $2\pi/3$. Then, the $SU(3)_{\rm L-R}$ transformation $\exp[(i/3)(\theta - \pi/2)\mathrm{diag}(2, -1, -1)]$ is performed along the path b_2, where θ $(\pi/2 \le \theta \le 3\pi/2)$ is the angle of the polar coordinates at the black point.

Fig. 35. An M_2 non-Abelian axial vortex attached by two fractional axial domain walls with the instanton-induced potential $V_{\eta'} = -C\cos 3\varphi_A$.

in the absence of the instanton-induced potential. In the presence of the instanton-induced potential, the $U(1)_{\rm A}$ phase rotates by $-2\pi/3$. Therefore, two axial domain walls are attached, as illustrated in Fig. 35. A numerical solution was constructed in Ref. [33] with an approximation.

Let us point out that an axial vortex attached by three fractional axial domain walls decays into a set of three non-Abelian axial vortices, each of which is attached by a fractional axial domain wall [102]. Let us remember that, in the absence of the instanton-induced potential, an axial vortex can be separated into three non-Abelian axial vortices without binding force at the leading order as in Eq. (10.37), since the force in Eq. (10.36) vanishes at $\alpha = \pi$. Therefore, the configuration of the single Abelian axial vortex attached by three domain walls is unstable to decay, as illustrated in the right of Fig. 36, because each non-Abelian axial vortex is pulled by the tension of a semi-infinitely long domain wall. The $U(1)_{\rm A}$ phase changes by $2\pi/3$ around each of the non-Abelian axial vortices attached by fractional axial domain walls. We show a detailed configuration of this decaying configuration in Fig. 37. The Abelian axial vortex initially located at the origin O decays into three non-Abelian axial vortices, denoted by the red, green, and blue dots. The three fractional axial domain walls denoted by the red, blue, and green dotted lines initially separate $\Sigma \sim \mathbf{1}_3$ and $\omega\mathbf{1}_3$, $\omega\mathbf{1}_3$ and $\omega^{-1}\mathbf{1}_3$, and $\omega^{-1}\mathbf{1}_3$ and $\mathbf{1}_3$, respectively. The red, blue, and green non-Abelian axial vortices are encircled by the paths

$$b_1 - r_3 + r_2, \quad b_2 - r_1 + r_3, \quad b_3 - r_2 + r_1 \tag{10.41}$$

respectively, as in Eq. (4.27) for non-Abelian semi-superfluid vortices. At the boundary of the spatial infinity, the $U(1)_{\rm A}$ phase is rotated by $\exp[i\theta\mathrm{diag}(1, 1, 1)]$ with the angle θ of the polar coordinates from the origin O. Therefore, the $U(1)_{\rm A}$ phase is rotated by $2\pi/3$ along each of the paths b_1, b_2, and b_3. Let us suppose that the three paths in Eq. (10.41) enclose the three configurations in Eq. (10.22), respectively. Then, we find that the transformations $g(r) \in SU(3)_{\rm L-R}$ occur along the paths r_1, r_2,

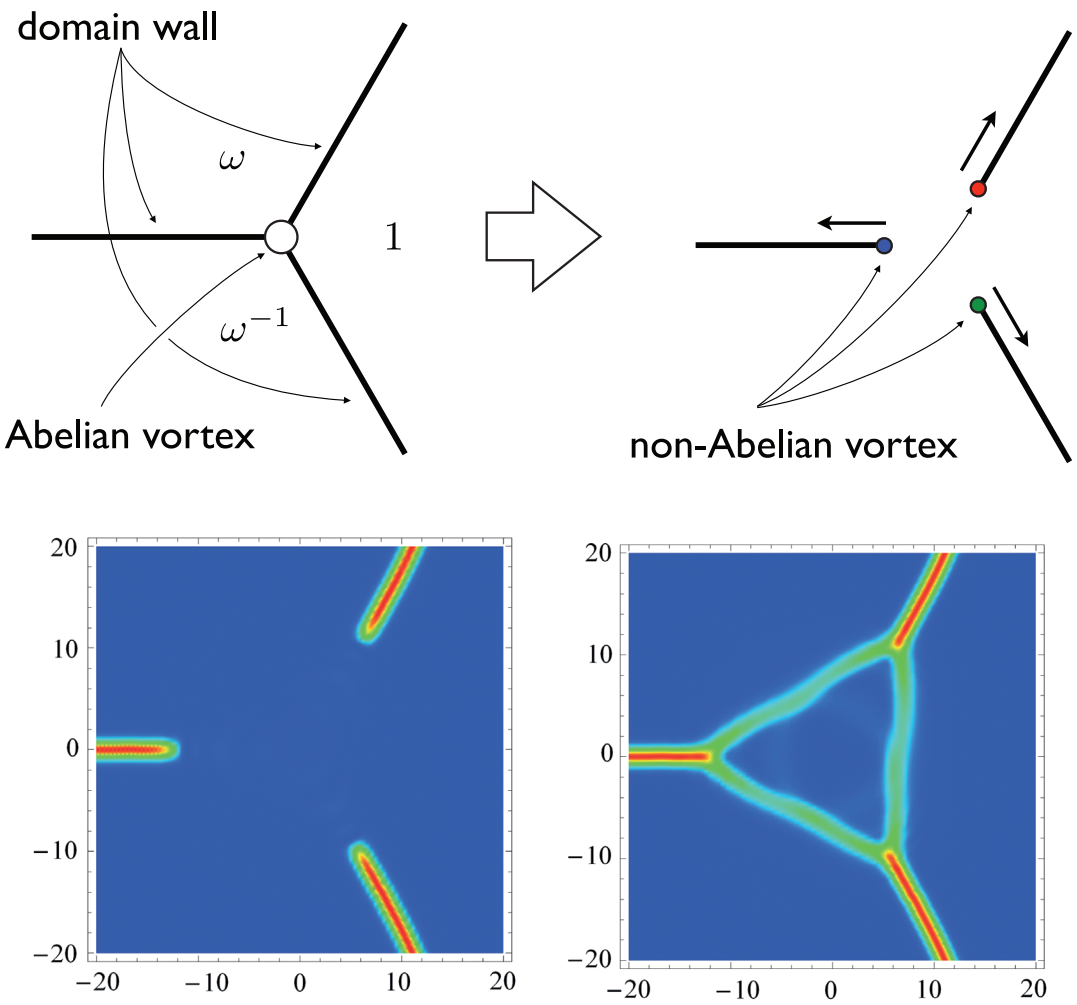

Fig. 36. Decay of a three-prolonged fractional axial domain wall junction in the chiral limit. The junction is three unstable to decay non-Abelian axial vortices that are pulled by three semi-infinitely long fractional axial domain walls. The figures (the potential energy density in the left panel and the total energy density in the right panel) in the second line are snapshots taken at an instant. These figures clearly show three domain walls torn off from the junction point. An initial configuration is the junction solution given in Fig. 33.

and r_3 as

$$
\begin{aligned}
r_1: \quad & g(r) = \exp[iu(r)\mathrm{diag}(0,-1,1)] = \begin{cases} \mathrm{diag}(1,1,1), & r=0 \\ \mathrm{diag}(1,\omega^{-1},\omega), & r=\infty \end{cases}, \\
r_2: \quad & g(r) = \exp[iu(r)\mathrm{diag}(1,0,-1)] = \begin{cases} \mathrm{diag}(1,1,1), & r=0 \\ \mathrm{diag}(\omega,1,\omega^{-1}), & r=\infty \end{cases}, \\
r_3: \quad & g(r) = \exp[iu(r)\mathrm{diag}(-1,1,0)] = \begin{cases} \mathrm{diag}(1,1,1), & r=0 \\ \mathrm{diag}(\omega^{-1},\omega,1), & r=\infty \end{cases},
\end{aligned}
\tag{10.42}
$$

respectively, as in Eq. (4.28) for non-Abelian semi-superfluid vortices, where $u(r)$ is a monotonically increasing function with the boundary conditions $u(r=0)=0$ and $u(r=\infty)=2\pi/3$. We find that

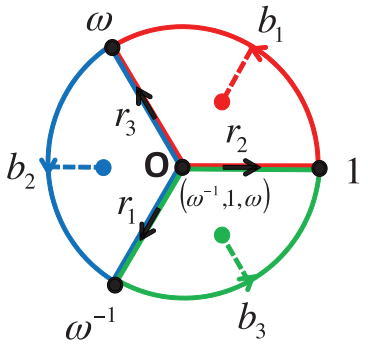

Fig. 37. Classical decay of an axial domain wall junction. The three ground states are $\Sigma = \mathbf{1}_3$, $\omega\mathbf{1}_3$, and $\omega^{-1}\mathbf{1}_3 = \omega^2\mathbf{1}_3$, and the origin O is $\Sigma = \mathrm{diag}(\omega^{-1}, 1, \omega)$. The Abelian axial vortex initially located at the origin O decays into three non-Abelian axial vortices, denoted by the red, green, and blue dots. The three fractional axial domain walls denoted by the red, blue, and green dotted lines initially separate $\mathbf{1}_3$ and $\omega\mathbf{1}_3$, $\omega\mathbf{1}_3$ and $\omega^{-1}\mathbf{1}_3$, and $\omega^{-1}\mathbf{1}_3$ and $\mathbf{1}_3$, respectively. b_1, b_2, and b_3 are the paths with angles $2\pi/3$ at the boundary at spatial infinity, and r_1, r_2, r_3 denote the paths from the origin O to spatial infinities. For b_1, b_2, and b_3, the $U(1)_{\mathrm{A}}$ phase is rotated by $\exp[i\theta\,\mathrm{diag}(1, 1, 1)]$ with the angle θ of the polar coordinates. Along the paths r_1, r_2, and r_3, $SU(3)_{\mathrm{L-R}}$ group transformations occur: $\exp[iu(r)\mathrm{diag}(0, -1, 1)]$, $\exp[iu(r)\mathrm{diag}(1, 0, -1)]$, and $\exp[iu(r)\mathrm{diag}(-1, 1, 0)]$, respectively, with a monotonically increasing function $u(r)$ with the boundary conditions $u(r = 0) = 0$ and $u(r = \infty) = 2\pi/3$.

the origin O is consistently given by

$$\Sigma = v\,\mathrm{diag}(\omega^{-1}, 1, \omega). \tag{10.43}$$

From a symmetry, permutations of each component are equally possible as the case of decay of a $U(1)_{\mathrm{B}}$ vortex.

The M_2 non-Abelian axial vortex in Fig. 35 also decays into two non-Abelian axial vortices for the same reason.

Note that there is a sharp contrast to the axion string. Though an axion string in the $N = 3$ axion model also gets attached by three domain walls, the domain walls cannot tear off the axion string into three fractional strings [355].

10.4.2. Abelian axial vortices attached by a composite axial domain wall with massive quarks. What happens when we include an effect caused by the quark masses? The dominant contribution to the potential for the η' meson in the high density limit is $\sim \cos\varphi_{\mathrm{A}}$, as in Eq. (10.8). One interesting consequence is that this potential does not allow the existence of a non-Abelian axial vortex alone. For the single-valuedness of φ_{A}, a set of three non-Abelian axial vortices must appear at the same time as an integer Abelian axial vortex, and a single integer axial domain wall attaches to it, as illustrated in the left panel of Fig. 38.

When both $\cos\varphi_{\mathrm{A}}$ and $\cos 3\varphi_{\mathrm{A}}$ exist, there appears an integer axial domain wall as a composite of three fractional axial domain walls, as discussed in Sect. 10.1.2. Again, only an Abelian axial vortex can exist, which is attached by an integer axial domain wall as a composite of three fractional axial domain walls, as illustrated in the right panel of Fig. 38.

10.5. Quantum decays of axial domain walls

10.5.1. Decay of integer axial domain walls. In the $U(1)_{\mathrm{A}}$ model with the potential $V \sim \cos\varphi_{\mathrm{A}}$, the minimum domain wall is an integer axial domain wall interpolating between $\varphi_{\mathrm{A}} = 0$ and $\varphi_{\mathrm{A}} = 2\pi$, given in Eq. (10.9). While this domain wall is classically stable [60], it is metastable if one takes

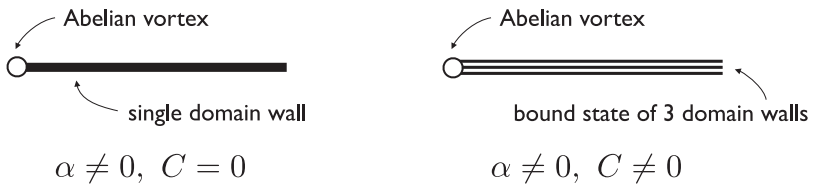

Fig. 38. An Abelian axial vortex attached by axial domain walls for the effective potential $V_{\eta'} = -\alpha \cos\varphi_A - C\cos 3\varphi_A$ with $\alpha \equiv 6Am + 12Bm^2$. When $C = 0$, a fat single axial domain wall attaches to an axial vortex. When neither α nor C are zero, three thin domain walls are bounded as in Fig. 31 and attach to a vortex. The case with $\alpha = 0$ and $C \neq 0$ is shown in Fig. 33.

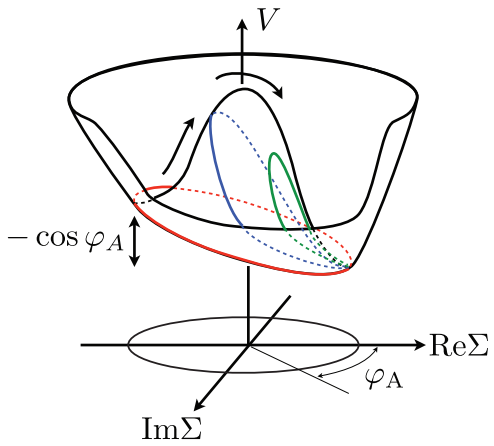

Fig. 39. Unwinding an integer axial domain wall. The potential is composed of a Mexican hat potential plus a linear potential. A metastable axial domain wall is represented by a red loop. This can be unwound through the blue and green loops by quantum tunneling.

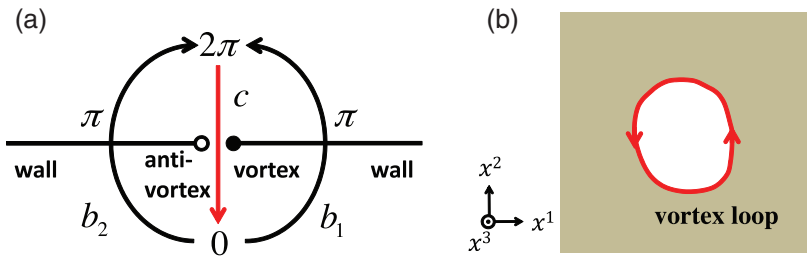

Fig. 40. Quantum decay of an integer axial domain wall. (a) A hole bounded by a pair of an Abelian axial vortex and an Abelian axial anti-vortex is created in $d = 2 + 1$. The numbers denote the phase of φ_A. (b) A two-dimensional hole bounded by a closed Abelian axial vortex is created in $d = 3 + 1$.

into account the quantum tunneling effect, and it can decay into the ground state quantum mechanically (or thermally), as illustrated in Fig. 39. This is also discussed in Ref. [30], where it is called a ribbon soliton. Since the axial domain wall separates $\varphi_\mathrm{A} = 0$ and $\varphi_\mathrm{A} = 2\pi$, which are equivalent, a hole can be created as in Fig. 40(a), where the order parameter remains the same along the path c through the hole. The $U(1)_\mathrm{A}$ phase is rotated counterclockwise along the closed counterclockwise loop $b_1 + c$; it encloses an Abelian axial vortex, denoted by the black point in Fig. 40(a). On the other hand, the $U(1)_\mathrm{A}$ phase is rotated clockwise along the counterclockwise loop $-c - b_2$, which encloses a $U(1)$ anti-vortex, denoted by the white point in Fig. 40(a). Therefore, the hole is bounded by a pair of a vortex and an anti-vortex. In $d = 3 + 1$ dimensions, a two dimensional hole bounded

by a closed Abelian axial vortex loop is created, as illustrated in Fig. 40(b). The energy of the axial domain wall turns to the radiation of the η' mesons.

Let us calculate the decay probability of axial domain walls. Similar calculations were done for the $U(1)_{\rm A}$ axial domain wall in the 2SC phase in Ref. [335] and an application of their calculations to the CFL phase was also pointed out there. Once the hole is created on the integer axial wall, it will expand if the size of this hole is larger than a critical value, and the axial domain wall decays. The quantum tunneling probability of this process can be calculated following Ref. [277]. Let R be the initial radius of the hole created on the axial domain wall. Then, the bounce action of this tunneling process is

$$B = 4\pi R^2 T_{\rm v} - \frac{4}{3}\pi R^3 T_{\rm w}, \tag{10.44}$$

where $T_{\rm v}$ and $T_{\rm w}$ stand for the tensions of the vortex and the axial domain wall, respectively. The critical radius $R_{\rm c}$ is the one that minimizes this bounce action, given by

$$R_{\rm c} = \frac{2T_{\rm v}}{T_{\rm w}}. \tag{10.45}$$

Thus, the decay probability is

$$P \sim e^{-B}\big|_{R=R_{\rm c}} = \exp\left(-\frac{16\pi}{3}\frac{T_{\rm v}^3}{v_{\eta'}T_{\rm w}^2}\right). \tag{10.46}$$

The factor $1/v_{\eta'}$ in the exponent reflects the fact that $v_{\eta'}$ is the speed of the modes in this system [335]. Since we have $T_{\rm v} \sim f_{\eta'}^2 \log L/\Delta_{\rm CFL} \sim \mu^2 \log L/\Delta_{\rm CFL}$ and $T_{\rm w} \sim \sqrt{B} f_{\eta'} m \sim \Delta_{\rm CFL}\mu m$, the decay probability is roughly estimated as $P \sim \exp[-(\mu \log L/\Delta_{\rm CFL})^4/(\Delta_{\rm CFL}\mu)^2]$. Here, L is an IR cutoff scale and we choose $\Delta_{\rm CFL}$ as a UV cutoff. Thus, at the high baryon density limit, the decay probability becomes parametrically small and the integer axial domain walls have a long lifetime.

10.5.2. Decay of fractional axial domain walls. The $U(1)_{\rm A}$ model with the potential $V \sim \cos 3\varphi_{\rm A}$ allows the ground states $\varphi_{\rm A} = 0$, $\varphi_{\rm A} = 2\pi/3$, and $\varphi_{\rm A} = 4\pi/3$, and the minimum domain wall is a fractional axial domain wall interpolating between two of them, say $\varphi_{\rm A} = 0$ and $\varphi_{\rm A} = 2\pi/3$, as given in Eq. (10.4). As described in Sect. 10.1.1, minimum axion domain walls in the $N = 3$ axion models are stable because they connect the vacua with different phases $\varphi_{\rm A}$.

On the other hand, fractional axial domain walls in the CFL phase also interpolate between two different ground states, say $\varphi_{\rm A} = 0$ and $\varphi_{\rm A} = 2\pi/3$, separated by the potential term $V \sim \cos 3\varphi_{\rm A}$ for the phase $\varphi_{\rm A}$. However, they are not stable, unlike the case of the $N = 3$ axion model, but they are metastable and can decay quantum mechanically or thermally [102]. The point is that these ground states can be connected by a path in the $SU(3)_{\rm L-R}$ group without a potential inside the whole order parameter space $U(3)_{\rm L-R+A} = [SU(3)_{\rm L-R} \times U(1)_{\rm A}]/\mathbb{Z}_3$. To see this, we note that the ground states $\varphi_{\rm A} = 0$, $2\pi/3$, and $4\pi/3$ are $\Sigma \sim \mathbf{1}_3$, $\omega\mathbf{1}_3$, and $\omega^2\mathbf{1}_3 = \omega^{-1}\mathbf{1}_3$, respectively, with $\omega = e^{2\pi i/3}$. Let us first consider $d = 2 + 1$ dimensions for simplicity. For example, let us consider an axial domain wall interpolating between $\Sigma \sim \mathbf{1}_3$ and $\Sigma \sim \omega\mathbf{1}_3$, as in the left panel of Fig. 41. This wall can decay by creating the path c in the right panel of Fig. 41, along which the two ground states 1 and ω are connected by

$$\exp\left[\frac{i}{3}\left(\theta - \frac{\pi}{2}\right)\mathrm{diag}(2,-1,-1)\right]\omega = \begin{cases} \omega, & \theta = \dfrac{\pi}{2} \\ 1, & \theta = \dfrac{3}{2}\pi \end{cases} \quad \left(\frac{\pi}{2} \le \theta \le \frac{3}{2}\pi\right) \tag{10.47}$$

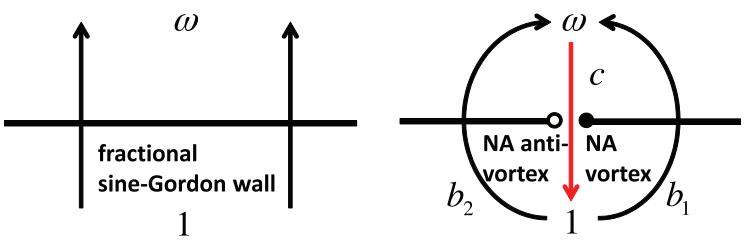

Fig. 41. Quantum decay of a fractional axial domain wall. A pair of a non-Abelian axial vortex and a non-Abelian axial anti-vortex is created.

in the $SU(3)_{\mathrm{L-R}}$ group. Here θ represents the angle from the black point. Then, one finds that the counterclockwise loop $b_1 + c$ encloses a non-Abelian axial vortex of the type diag $(e^{i\theta}, 1, 1)$ (represented by the black point). This is nothing but the configuration in Fig. 34. The clockwise closed loop $-b_2 + c$ also encloses a non-Abelian axial vortex (denoted by the white point), which implies that it is a non-Abelian axial anti-vortex. Therefore, a hole bounded by a pair of a non-Abelian axial vortex and a non-Abelian axial anti-vortex is created.

In $d = 3 + 1$ dimensions, a two dimensional hole bounded by a closed non-Abelian axial vortex loop is created as the Abelian case. When one deforms the path b_1 to $-c$ in Fig. 41, one must create a non-Abelian vortex, implying an energy barrier between these two paths. Therefore, the calculation of the decaying probability is the same as Eqs. (10.44)–(10.46) in the case of an integer axial domain wall, replacing the tension of vortices and domain walls with non-Abelian ones. Through this decaying process, the domain wall energy turns to radiation of the $U(3)_{\mathrm{L-R+A}}$ Nambu–Goldstone modes (the η' meson and the CFL pions).

We conclude this subsection by noting that, while integer axial domain walls can decay without $SU(3)_{\mathrm{L-R}}$ degrees of freedom, fractional axial domain walls can decay once $SU(3)_{\mathrm{L-R}}$ degrees of freedom are taken into account, unlike the case of the $N = 3$ axion model, in which domain walls are stable.

10.6. Quantum anomalies and transport effects on topological defects

It is well known that the axial $U(1)_{\mathrm{A}}$ symmetry is explicitly broken by the quantum anomaly in the QCD vacuum. Even at finite density, it was found that the anomaly plays important roles, especially in the presence of topological solitons [332,337]. Because the effective theory has to reproduce the anomaly relation of QCD, the effective theory given in Sect. 2.2.2 should be corrected. The additional terms were found in Ref. [337] as

$$\mathcal{L}_{\mathrm{anom}} = \frac{1}{16\pi^2}\partial_\mu\varphi_{\mathrm{A}}\Bigg[e^2 C_{\mathrm{A}\gamma\gamma} A_\nu \tilde{F}^{\mu\nu} - 2eC_{\mathrm{AB}\gamma}\left(\mu n_\nu - \frac{1}{2}\partial_\nu\varphi_{\mathrm{B}}\right)\tilde{F}^{\mu\nu} - \frac{1}{2}C_{\mathrm{ABB}}\epsilon^{\mu\nu\alpha\beta}\left(\mu n_\nu - \frac{1}{2}\partial_\nu\varphi_{\mathrm{B}}\right)\partial_\alpha\partial_\beta\varphi_{\mathrm{B}}\Bigg], \tag{10.48}$$

with $n_\nu = (\mu, 0, 0, 0)$. The first term describes two-photon decay like $\eta' \to 2\gamma$. For the CFL phase, the coefficients were found as

$$C_{\mathrm{A}\gamma\gamma} = \frac{4}{3}, \quad C_{\mathrm{AB}\gamma} = \frac{2}{3}, \quad C_{\mathrm{ABB}} = \frac{1}{3}. \tag{10.49}$$

Although the anomalous terms do not contribute to the equations of motion since they are total derivatives, they give extraordinary effects if a topological soliton exists. According to Ref. [337], here we review two phenomena below. The first anomalous phenomenon is axial current on a $U(1)_{\mathrm{B}}$

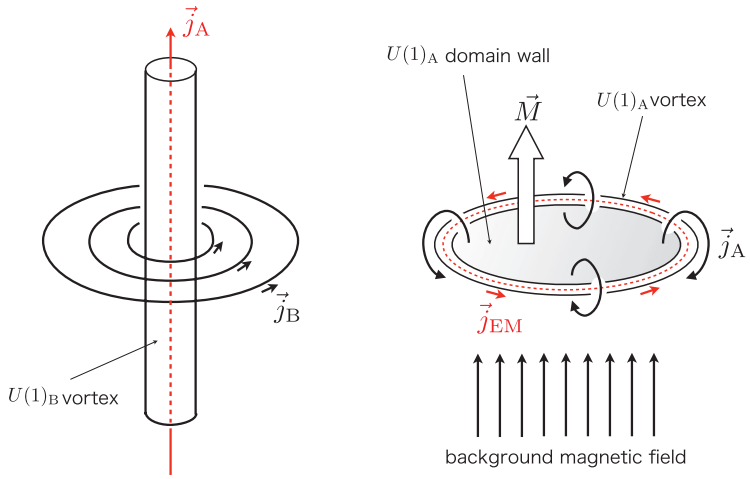

Fig. 42. Schematic pictures of the anomaly effects on a $U(1)_{\rm B}$ superfluid vortex, an axial domain wall, and an axial vortex (drum vorton) [337].

superfluid vortex. Let us consider a straight $U(1)_{\rm B}$ superfluid vortex extending along the z-axis. Then, rotation of the $U(1)_{\rm B}$ phase is $j^3_{\rm B} = (\partial_x\partial_y - \partial_y\partial_x)\varphi_{\rm B} = 2\pi\delta(x)\delta(y)$; see Eqs. (2.63) and (3.5). Therefore, in the presence of a $U(1)_{\rm B}$ superfluid vortex, the anomaly term reduces to

$$\mathcal{L}_{\rm anom} = \frac{\mu}{12\pi}\int dt\, dz\, \partial_z\varphi_{\rm A}. \tag{10.50}$$

From Noether's theorem, this anomalous term gives the non-zero axial current

$$j^{\rm A}_\mu = \frac{\mu}{12\pi}(0,0,0,1). \tag{10.51}$$

Thus, there is an axial current running on the superfluid vortex; see Fig. 42.

The second anomalous phenomenon is magnetization of axial domain walls under a background magnetic field $\vec{B}$. Let us consider an axial domain wall perpendicular to the z-axis. Since the $U(1)_{\rm A}$ phase $\varphi_{\rm A}$ changes from 0 to 2π along the z-axis, we have non-zero $\partial_z\varphi_{\rm A}$. Then the anomaly term reduces to

$$\mathcal{L}_{\rm anom} = \frac{e\mu}{12\pi^2}\vec{B}\cdot\vec{\nabla}\varphi_{\rm A}. \tag{10.52}$$

This equation implies that the axial domain wall is magnetized with a finite magnetic moment per unit area equal to

$$M = \frac{e\mu}{6\pi}. \tag{10.53}$$

The magnetic moment is oriented perpendicular to the axial domain wall.

This phenomenon can be understood in a different way. Since an axial domain wall is metastable, it is bounded by an axial vortex; see Fig. 42. It is called a drum vorton [70], which was first found in a nonlinear sigma model at finite temperature. Since $\epsilon_{ijk}\partial_j\partial_k\varphi_{\rm A} = 2\pi\delta^2(x_\perp)$ on the axial vortex, the anomalous action can be written as a line integral along the vortex as

$$S_{\rm anom} = \frac{e\mu}{3\pi}\int d\vec{\ell}\cdot\vec{A}. \tag{10.54}$$

This means that an electric current runs along the core of the axial vortex equal to

$$j^{\rm EM} = \frac{e\mu}{3\pi}. \tag{10.55}$$

When the axial vortex surrounds an axial domain wall, it gives rise to a magnetic moment per unit area equal to $j^{\rm EM}/2 = e\mu/(6\pi)$, which is exactly the same as Eq. (10.53).

These anomalous effects were further investigated in Ref. [332], in which it was found that a strong magnetic field of order 10^{17}–10^{18} [G] transforms the CFL phase into a new phase containing multiple η (or η') domain walls, which are magnetized due to the anomalous effects. It was also proposed in Ref. [332] that enormously strong magnetic fields of magnetars (10^{14-15} [G]) are due to ferromagnetism (spontaneous magnetization) by the non-zero gradient of the chiral field in the meson current (Goldstone boson current) phase [213,304]. There are also a number of works studying anomalous phenomena. The so-called chiral magnetic effects [139,201] are similar phenomena that occur when a system with a non-zero chiral chemical potential is under a strong magnetic field. Electric charge separation of Q-balls by the chiral magnetic effect was studied in Ref. [100], and seemingly anomaly induced electric charges on a baryon as a Skyrmion under a strong background magnetic field were discussed in Refs. [99,202,362]. It was found in Ref. [151] that fermions escape during the decay process of metastable defects through the anomaly term. It was found for low-density nuclear matter that a stack of magnetized pionic domain walls is energetically more favorable than nuclear matter [332]. The relation between the ferromagnetism of neutron stars and a stack of magnetized pionic walls was also discussed in Ref. [98]. It has also been proposed that an anomalous global vortex may generate primordial magnetic fields in galaxies [59].

10.7. Skyrmions as qualitons

As discussed in Sect. 2.2.2, there are Nambu–Goldstone boson modes (CFL mesons), namely $SU(3)_{\mathrm{C+L+R}}$ octet and singlet modes, in the ground state of the CFL phase. The nonlinear realization of the Nambu–Goldstone bosons gives the effective Lagrangian whose forms are restricted by $SU(3)_{\mathrm{C+L+R}}$ symmetry. The simplest form of the effective Lagrangian for the pion field is constituted by the kinetic term, the four-derivative term (the Skyrme term), and the Wess–Zumino–Witten term from the chiral anomaly:

$$\mathcal{L}_{\mathrm{eff}} = \frac{F^2}{4}\mathrm{Tr}\left(\mathcal{D}_0\Phi_{\mathrm{L}}\mathcal{D}_0\Phi_{\mathrm{L}}^\dagger\right) - \frac{F'^2}{4}\mathrm{Tr}\left(\mathcal{D}_i\Phi_{\mathrm{L}}\mathcal{D}_i\Phi_{\mathrm{L}}^\dagger\right) + \mathcal{L}_{\mathrm{Skyrme}} + n_{\mathrm{L}}\mathcal{L}_{\mathrm{WZW}} + (\mathrm{L}\leftrightarrow\mathrm{R}) + \cdots, \tag{10.56}$$

where $\Phi_{\mathrm{L,R}}$ is restricted by $|\det\Phi_{\mathrm{L,R}}| = 1$, $n_{\mathrm{L}} = 1$, and the ellipsis denotes the terms with the higher order derivative.[17] F is the "pion decay constant" in the CFL phase. Because of the nontrivial third homotopy group of the order parameter manifold,

$$\pi_3[U(3)_{\mathrm{L-R+A}}] \simeq \mathbb{Z}, \tag{10.57}$$

one expects the existence of Skrmions [326,328] as three-dimensional textures, as explained in footnote 15. As the solution, there is a "hedgehog" configuration as the most stable (soliton) state from the energy balance between the kinetic term and the Skyrme term [175]. The Wess–Zumino–Witten term guarantees the correct quantization of the soliton as a spin 1/2 object. The winding number in Eq. (10.57) carries the baryon charge $(1 \bmod 2)/3$. We note that $U(1)_{\mathrm{B}}$ symmetry for baryon number conservation in the QCD Lagrangian is broken to $\mathbb{Z}_2$ symmetry in the CFL phase, because the transformation $q \to -q$ for the quark field q leaves the condensate invariant. This stable object is called a "qualiton" (or "superqualiton") [175]. Since the low-energy constants as the coefficients in the effective Lagrangian in the CFL phase are calculable by matching with QCD in high density

[17] The Skyrme term that stabilizes the hedgehog solution was given in Ref. [190].

limit, we obtain the hedgehog configuration and hence the mass of the qualiton. They were given as $\alpha\, 4\pi F$ [174,175], with $\alpha = \mathcal{O}(0.1 - 1)$ and the pion decay constant F in the CFL phase. We note that the mass $\alpha\, 4\pi F$ is proportional to the chemical potential μ because $F \sim \mu$ (see Eq. (2.86)). However, this is different from the quark mass (2.29) in the CFL phase. This discrepancy will be an interesting problem. The mass of the qualiton is important, because the qualiton can be produced easily in the ground state and can cause the rearrangement of the ground state, if the mass is smaller than the gap [175].

We make a comment that the word "qualiton" was originally used in the quark soliton model to analyze the properties of hadrons in vacuum at zero chemical potential. We have to be careful to strictly distinguish the "qualiton" in the CFL phase from that in vacuum. The qualiton in the CFL phase corresponds rather to the Skyrmion in vacuum. Thus we observe that the state of "qualiton" in the CFL phase corresponds to the baryon state in vacuum. In fact, there is a discussion that the qualiton is identical to the quark [175]. This may support the idea of the "quark–hadron duality", which indicates the correspondence of the low-energy modes in the CFL phase and those in vacuum [190,215].

11. Topological objects in other phases

We review topological solitons in phases other than the CFL phase in this section. The CFL phase discussed so far is the ground state at high densities where masses of the three flavors are small compared to the baryon chemical potential. If one lowers the density gradually, the effect of finite strange quark mass comes in. Then it is expected that kaons form a condensate in addition to the CFL condensates. This is called the CFL+K phase [47]. If the density is further decreased, only the light flavors (u and d) contribute to the condensate, which is called the 2SC phase [32]. In Sect. 11.1, we discuss the domain walls and color magnetic fluxes in the 2SC phase. In Sect. 11.2, we review the strings, vortons, domain walls, and drum vortons in the CFL+K phase.

11.1. 2SC phase

11.1.1. $U(1)_{\rm A}$ domain walls. The CFL phase changes into the so-called 2SC phase at a lower density [11,31,32,280]. Due to asymmetry among the strange quark mass and the masses of the up and down quarks, only up and down quarks form Cooper pairs in the 2SC phase. The 2SC pairing pattern is thus given by

$$(\Phi_{\rm L,R})^A_a \sim \delta^A_3 \delta^3_a, \tag{11.1}$$

where the symmetry breaking pattern is

$$\begin{aligned} &SU(3)_{\rm C} \times SU(2)_{\rm L} \times SU(2)_{\rm R} \times U(1)_{\rm B} \times U(1)_{\rm S} \times U(1)_{\rm A} \\ &\quad \to SU(2)_{\rm C} \times SU(2)_{\rm L} \times SU(2)_{\rm R} \times \tilde{U}(1)_{\rm B} \times U(1)_{\rm S}. \end{aligned} \tag{11.2}$$

Here we assume that the up and down quarks are massless. The axial $U(1)_{\rm A}$ symmetry is not an exact symmetry but it is explicitly broken by instanton effects. $\tilde{U}(1)_{\rm B}$ is a linear combination of the original $U(1)_{\rm B}$ and the broken $U(1)_8 \in SU(3)_{\rm C}$ generated by T_8. The $U(1)_{\rm S}$ is the phase rotation of the strange quark. The order parameter space is of the form

$$\mathcal{M}_{\rm 2SC} = \frac{SU(3)_{\rm C} \times U(1)_{\rm B}}{SU(2)_{\rm C} \times \tilde{U}(1)_{\rm B}} \times U(1)_{\rm A}. \tag{11.3}$$

It was observed that metastable $U(1)_{\rm A}$ domain walls [335] also exist in the 2SC phase. Although domain walls are very familiar in field theory, it is widely believed that the standard model has no

domain walls. It was pointed out that metastable domain walls could exist in QCD at zero temperature and density [127], but no definite statement can be made because the theory is not under theoretical control. In contrast, QCD at high density is a weakly coupled theory due to asymptotic freedom, so that the relevant physics are under theoretical control. In Ref. [335], it was found that QCD at high density, especially in the 2SC phase, must have domain walls.

The domain walls in the 2SC phase are similar to those explained in Sect. 10.1.2. In the 2SC phase, the chiral symmetry is not broken but the $U(1)_{\rm A}$ is spontaneously broken by the diquark condensate. Then the relevant order parameter manifold is $U(1)_{\rm A}$. The corresponding mode $\varphi_{\rm A}$ is a pseudo Nambu–Goldstone field, which gets a finite mass by instanton effects. The effective Lagrangian is

$$\mathcal{L} = f^2 \left[(\partial_0 \varphi_{\rm A})^2 - v^2 (\partial_i \varphi_{\rm A})^2 \right] - V_{\rm inst}, \tag{11.4}$$

where the constants f and v were determined [43] as $f^2 = \mu^2/8\pi^2$ and $v^2 = 1/3$. $V_{\rm inst}$ stands for an instanton-induced effective potential that was calculated [335] as

$$V_{\rm inst} = -a\mu^2 \Delta_{\rm CFL}^2 \cos\varphi_{\rm A}. \tag{11.5}$$

The dimensionless coefficient a that vanishes at $\mu \to \infty$ is given by

$$a = 5 \times 10^4 \left(\log \frac{\mu}{\Lambda_{\rm QCD}} \right)^7 \left(\frac{\Lambda_{\rm QCD}}{\mu} \right)^{\frac{29}{3}}. \tag{11.6}$$

The Lagrangian (11.4) is in the same form as Eq. (10.8), so that integer sine-Gordon domain walls exist. The domain wall tension was found to be

$$T_{\rm w}^{\rm 2SC} = 8\sqrt{2a} v f \mu \Delta_{\rm CFL}. \tag{11.7}$$

Its decay probability was also calculated [335] as

$$\Gamma \sim \exp\left\{ -\frac{\pi^4}{3} \frac{v^3}{a} \frac{\mu^2}{\Delta_{\rm CFL}^2} \left(\log \frac{1}{\sqrt{a}} \right)^3 \right\}. \tag{11.8}$$

Since a decreases with increasing μ, the decay rate is suppressed and the domain walls are long-lived [335].

11.1.2. Color magnetic flux tubes. The interesting problem of the color Aharonov–Bohm scattering of fermions off the color magnetic flux tubes[18] in the 2SC phase and forces exerted on vortices are studied in Ref. [14]. The authors calculated the cross section for Aharonov–Bohm scattering of gapless fermions off the flux tubes, and the associated collision time and frictional force on a moving flux tube. Since the CFL phase has no gapless quarks, a color magnetic flux tube in the 2SC phase is considered where several massless fermions are present and the effect would be more significant than in the CFL phase.

The Aharonov–Bohm effect turns out to lead to a strong interaction between a charged particle and a magnetic flux tube. In the case of a single $U(1)$ gauge group, the cross section per unit length is

[18] Since they are non-topological solitons and their stability is not ensured by the symmetry, they would be unstable against decay.

given by [15]

$$\frac{d\sigma}{d\theta} = \frac{\sin^2(\pi\tilde{\beta})}{2\pi k \sin^2(\theta/2)}, \quad \tilde{\beta} = \frac{q_p}{q_c}, \tag{11.9}$$

where q_p and q_c are the charges of the scattering particle and condensed field respectively, k is the momentum in the plane perpendicular to the vortex, and θ is the scattering angle. The Aharonov–Bohm interaction has several important characteristics:

- The cross section vanishes if $\tilde{\beta}$ is an integer.
- The cross section is independent of the thickness of the flux tube. The scattering occurs even at energies much smaller than the symmetry breaking scale.
- The cross section diverges for small k and forward scattering $\theta \sim 0$.

Thus, it is important to determine the values of $\tilde{\beta}$ for gapless fermions in the 2SC phase, which is done in Ref. [14].

The authors also calculated the characteristic timescale for a perturbation from equilibrium to relax, due to scattering of the fermions off the color magnetic flux tubes. The timescale is roughly the mean free time of collisions of fermions off fluxes, which is evaluated for a fermion species i as

$$\tau_{if}^{-1} = \frac{n_v}{p_{Fi}} \sin^2(\pi\tilde{\beta}_i), \tag{11.10}$$

where n_v is the vortex area density and p_{Fi} is the Fermi momentum of the fermion denoted by i. The timescale are compared with the relaxation time due to Coulomb interactions,

$$\tau_{qq}^{-1} = \frac{6\zeta(3)}{\pi^2}\tilde{\alpha}T, \tag{11.11}$$

where $\zeta(3) = 1.202$, T is the temperature, and $\tilde{\alpha}$ is the fine structure constant for the rotated electromagnetism. The temperature T_f below which flux tubes dominate the relaxation of deviations from thermal equilibrium is determined as

$$T_f = \frac{\pi^2}{6\zeta(3)} \frac{\sin^2(\pi\beta_{bu})}{\tilde{\alpha}} \frac{n_v}{\mu_q}, \tag{11.12}$$

where β_{bu} is the β for the up blue quark (which is the most abundant) and μ_q is the quark chemical potential. Below the temperature (11.12), the Aharonov–Bohm scattering plays the main role in thermal relaxation.

11.2. CFL + K

In this section, we will review solitons in the CFL+K phase. We will ignore instanton effects in Sect. 11.2.1 and take them into account in Sect. 11.2.2.

11.2.1. Superconducting strings and vortons. The CFL phase is the ground state in the massless three-flavor limit in high-density QCD. If one considers a finite strange quark mass, it puts a stress on the ground state to reduce the strange quark density compared to up and down quarks. As long as the strange quark mass is small, it cannot overcome the diquark pairing energy and the ground state is in the CFL phase. At sufficiently large strange quark masses, a kaon condensate would be formed [44,47,300], since kaons K^0 ($d\bar{s}$) and K^+ ($u\bar{s}$) are the lightest mesons [333] that can reduce the strange quark content of the ground state. Kaon condensation is characterized by the spontaneous breaking

of $U(1)_{\rm Y}$ symmetry or $U(1)_{\rm EM}$ symmetry, or both. Let us denote the kaon field as $K = (K^+, K^0)^T$. The field K is transformed under $U(1)_{\rm Y}$ and $U(1)_{\rm EM}$ symmetry as

$$\begin{pmatrix} K^+ \\ K^0 \end{pmatrix} \to e^{i\alpha} \begin{pmatrix} K^+ \\ K^0 \end{pmatrix}, \quad \begin{pmatrix} K^+ \\ K^0 \end{pmatrix} \to \begin{pmatrix} e^{i\beta(x)} K^+ \\ K^0 \end{pmatrix}, \tag{11.13}$$

respectively, where α and $\beta(x)$ are parameters characterizing $U(1)_{\rm Y}$ and $U(1)_{\rm EM}$ transformations. We here consider the phase in which $U(1)_{\rm Y}$ symmetry is broken in the bulk. The diquark condensate takes the form

$$\Sigma_{K^0} = \begin{pmatrix} 1 & 0 & 0 \\ 0 & \cos\theta_0 & e^{-i\psi}\sin\theta_0 \\ 0 & -e^{i\psi}\sin\theta_0 & \cos\theta_0 \end{pmatrix}, \tag{11.14}$$

where θ_0 represents the strength of the K^0 condensation and the phase ψ corresponds to the Nambu–Goldstone mode associated with the spontaneous breaking of the hypercharge symmetry $U(1)_{\rm Y}$. The strength of condensation was found [47] as

$$\cos\theta_0 = \frac{m_0^2}{\mu_{\rm eff}^2}, \quad m_0^2 = \frac{3\Delta_{\rm CFL}^2}{\pi^2 f_\pi^2} m_{\rm u}(m_{\rm d} + m_{\rm s}), \quad \mu_{\rm eff} = \frac{m_{\rm s}^2}{2p_F}. \tag{11.15}$$

We can expect the appearance of topological vortices that are characterized by $U(1)_{\rm Y}$ winding numbers [128,330]. Furthermore, a particularly interesting possibility is pointed out: the cores of $U(1)_{\rm Y}$ vortices can be electromagnetically charged and superconducting [194]. Namely, $U(1)_{\rm EM}$ symmetry is broken only inside vortices. We here briefly review these topological vortices following the argument given in Ref. [61]: Firstly, we expand the chiral Lagrangian (2.83) to the fourth order in the lightest fields $K = (K^+, K^0)$ as

$$\mathcal{L}_K = |\partial_0 K|^2 - v^2 |\partial_i K|^2 - \lambda \left(|K|^2 - \frac{\eta^2}{2} \right)^2 - \delta m^2 K^\dagger \sigma_3 K, \tag{11.16}$$

with

$$\lambda \simeq \frac{4\mu_{\rm eff}^2 - m_0^2}{6 f_\pi^2}, \quad \lambda\eta^2 = \mu_{\rm eff} - \frac{m_0^2 + m_+^2}{2}, \quad \delta m^2 = \frac{m_+^2 - m_0^2}{2}, \tag{11.17}$$

$$m_0^2 = \frac{3\Delta_{\rm CFL}^2}{\pi^2 f_\pi^2} m_{\rm u}(m_{\rm d} + m_{\rm s}), \quad m_+^2 = \frac{3\Delta_{\rm CFL}^2}{\pi^2 f_\pi^2} m_{\rm d}(m_{\rm s} + m_{\rm u}). \tag{11.18}$$

The reduced theory (11.16) has a stable topological vortex solution whose profile is described by the standard ansatz [61]

$$K^0(r,\theta) = \sqrt{\frac{\mu_{\rm eff}^2 - m_0^2}{2\lambda}}\, f(r) e^{i\theta}, \quad K^+(r,\theta) = \sigma g(r), \tag{11.19}$$

where the profile functions $f(r)$ and $g(r)$ satisfy the boundary conditions $f(\infty) = 1$, $f(0) = 0$, $g(\infty) = 0$ and $g'(0) = 0$. At the center of the vortex core, there is a non-zero K^+ condensate. Since K^+ is charged, the vortex is a superconducting string: A persistent electromagnetic current can flow on a $U(1)_{\rm Y}$ vortex. In contrast, $U(1)_{\rm Y}$ symmetry is restored inside vortices since the K^0 condensate vanishes. Such vortices are dense-QCD realizations of the superconducting cosmic strings, that have been studied for a long time [372].

Vortex loops that carry persistent currents are called "vortons" in the context of cosmic strings [84]. The vortons may exist in the CFL+K^0 phase [45,46,61,62,194]. For the vortons, we should add a time and z dependence in the phase of K^+ as

$$K^0 = K^0_{\rm string}(r,\theta), \quad K^+ = K^+_{\rm cond}(r,\theta)e^{-i\omega t+ikz}, \tag{11.20}$$

where z is the coordinate along the vortex loop. Substituting this into the original Lagrangian (2.83) and picking up all the terms to fourth order in the fields, one finds [61]

$$\begin{aligned}\tilde{\mathcal{L}}_K =& -v_\pi^2|\partial_i K^0|^2 - v_\pi^2|\partial_i K^+|^2 \\ &+ M_0^2|K^0|^2 + M_+^2|K^+|^2 - \lambda|K^0|^4 - \lambda_+|K^+|^4 - \zeta|K^0|^2|K^+|^2,\end{aligned} \tag{11.21}$$

with the parameters defined by

$$\omega_{\rm eff} = \omega + \mu_{\rm eff}, \quad M_0^2 = \mu_{\rm eff}^2 - m_0^2, \quad M_+^2 = \omega_{\rm eff}^2 - v_\pi^2 k^2 - m_+^2, \tag{11.22}$$

$$\lambda_+ = \frac{4(\omega_{\rm eff}^2 - v_\pi^2 k^2) - m_+^2}{6f_\pi^2}, \quad \zeta = \frac{(\omega_{\rm eff}+\mu_{\rm eff})^2 + 4\omega_{\rm eff}\mu_{\rm eff} - v_\pi^2 k^2 - m_+^2 - m_0^2}{6f_\pi^2}. \tag{11.23}$$

The vorton is characterized by two additional conserved changes; a topological charge and a Noether charge

$$N = \oint_C \frac{dz}{2\pi} \arg\log K^+ = kR, \tag{11.24}$$

$$Q = \int d^3x\, j_+^0 \sim R\omega_{\rm eff} S, \tag{11.25}$$

with R being the radius of the vorton and $S \equiv \int d^2x\, |K^+|^2$. The stability of the vorton can be seen by finding the R dependence of the energy of the vorton

$$E_{\rm vorton}(R) \simeq \left\{ \frac{2\pi^2(\mu_{\rm eff}^2 - m_0^2)}{\lambda} v^2 \log\frac{L}{\xi} \right\} R + \left(\frac{1}{2\pi S} + 2\pi v_\pi^2 N^2 S \right) \frac{1}{R}. \tag{11.26}$$

The existence of a global minimum implies that the vorton is stable and its size is given by

$$2\pi R = \sqrt{\frac{Q^2 + (2\pi)^2 v_\pi^2 N^2 S^2}{\pi S v^2 (\log L/\xi)(\mu_{\rm eff}^2 - m_0^2)/\lambda}}. \tag{11.27}$$

Note that there are no constraints on the size of vortons. The vortons can be any size as can cosmic string vortons.

11.2.2. Domain walls and drum vortons. It was pointed out in Ref. [330] that the CFL+K phase may have metastable domain walls. When weak interactions are taken into account, $U(1)_{\rm Y}$ symmetry is explicitly broken. So the $U(1)_{\rm Y}$ Nambu–Goldstone mode ψ gets a small mass. This is seen in the effective theory in Eq. (11.16) by adding an effective potential [330]

$$V(\psi) = f_\pi^2 m^2 \cos\psi, \tag{11.28}$$

$$m^2 = \frac{162\sqrt{2}\,\pi}{21 - 8\log 2} \frac{G_{\rm F}}{g_{\rm s}} \cos\theta_{\rm C} \sin\theta_{\rm C} m_{\rm u} m_{\rm s} \Delta_{\rm CFL}^2, \tag{11.29}$$

where $G_{\rm F}$ is the Fermi constant and $\theta_{\rm C}$ is the Cabbibo angle. Thus the effective theory for the quasi Nambu–Goldstone particle ψ is the sine-Gordon model, and there exists a metastable domain wall

solution that we call the kaon domain wall

$$\psi(z) = 4 \arctan e^{mz/v_\pi}, \tag{11.30}$$

where z is a coordinate perpendicular to the domain wall. The tension of the domain wall was calculated [330] as

$$T_{\rm dw}^K = 8 v_\pi f_\pi^2 m. \tag{11.31}$$

It was also found that the decay rate of the kaon domain wall with respect to hole nucleation is parametrically small at high density and zero temperature:

$$\Gamma \sim \exp\left(-\frac{\pi^4 v_\pi^3}{12} \frac{f_\pi^2}{m^2} \log \frac{m_K}{m} \right), \tag{11.32}$$

with $f_\pi^2/m^2 \sim \mu^2/m^2$.

Let us next consider the superconducting vortices explained in Sect. 11.2.2 in the presence of the instanton-induced potential. As we have seen in Sect. 10, a kaon domain wall must be attached to a kaon superconducting string due to the potential in Eq. (11.28). When a kaon domain wall decays with a hole nucleation, a kaon superconducting string attaches to the edge of the hole.

Let us next turn to kaon vortons in the presence of the potential (11.28). Since any kaon superconducting strings are attached by the kaon domain walls, the kaon vortons also have domain walls stretched across their surfaces as drums [61]. They are called drum vortons [70], and were first found in a nonlinear sigma model at finite temperature. It has been argued that the domain wall gives an upper bound on the size of vortons, in contrast to the vortons without domain walls [61].

12. Summary and discussions

Quark matter at extremely high density becomes a color superconductor due to the formation of diquark pairings. It exhibits superfluidity as well as color superconductivity because of the spontaneously broken baryon symmetry as well as color symmetry. When a color superconductor is rotating, as is the case if it is realized in the core of a neutron star, non-Abelian vortices are created along the rotation axis. Non-Abelian vortices are superfluid vortices carrying 1/3 quantized circulation and a color magnetic flux. Corresponding to the color of the magnetic flux, a non-Abelian vortex carries orientational zero modes $\mathbb{C}P^2$. The properties of non-Abelian vortices have been studied in the time-dependent GL effective theory for high density QCD and the BdG equation. A superfluid $U(1)_{\rm B}$ vortex decays into a set of three non-Abelian vortices, because the interaction between two non-Abelian vortices at large distance is repulsive, independent of orientational modes. Two kinds of bosonic gapless modes propagate along a non-Abelian vortex string. One is a translational or Kelvin mode with a quadratic dissipation (of the type II Nambu–Goldstone mode), and the other is an orientational $\mathbb{C}P^2$ zero mode with a linear dissipation (of the type I Nambu–Goldstone mode). The dynamics of these modes can be described by the low-energy effective theories on the $1+1$ dimensional vortex world-sheet, a free complex scalar field with the first derivative with respect to time and a $\mathbb{C}P^2$ model, respectively in $d = 1+1$ dimensions. The $SU(3)$ isometry of the $\mathbb{C}P^2$ space is exact, neglecting quark masses and electromagnetic interactions. The effect of strange quark mass can be taken into account as an effective potential in the $\mathbb{C}P^2$ vortex effective theory, which shows that all vortices decay into one kind immediately. On the other hand, the electromagnetic interaction contributes a finite correction to the tension of the non-Abelian vortex, which also induces an effective potential in the $\mathbb{C}P^2$ vortex effective theory. As stationary solutions of the effective potential, there exist the BDM vortex as the ground state in the absence of strange quark masses, metastable

$\mathbb{C}P^1$ vortices, and unstable pure color vortices. Metastable $\mathbb{C}P^1$ vortices decay into the BDM vortex through quantum tunneling. Another effect of the electromagnetic interactions is that the vortex effective theory becomes a $U(1)$ gauged $\mathbb{C}P^2$ model.

Neutron vortices and proton vortices exist in the *npe* phase because of neutron superfluidity and proton superconductivity under rotation and magnetic field, respectively. The existence of colorful boojums has been predicted in the interface between the CFL phase and the *npe* phase, between which there may be other phases, such as the CFL + K, 2SC phases, and so on. At a colorful boojum, three non-Abelian vortices with the total color flux canceled out join in the CFL phase, and three neutron vortices and three proton vortices meet in the *npe* phase. There appear a Dirac monopole of the massless gauge field and a surface current of the massive gauge field. Two kinds of colored monopoles appear at non-Abelian vortices when strange quark mass is taken into account.

At the extremely high density limit in which the strange quark mass can be neglected, there appears a quantum mechanically induced potential in the low-energy $\mathbb{C}P^2$ vortex effective theory through non-perturbative effects. Consequently, there appear quantum monopoles confined by non-Abelian vortices as kinks on the vortex, which are relevant to show a duality between the confining phase, where quarks are confined and monopoles are condensed, and the CFL phase, where monopoles are confined and quarks are condensed. Yang–Mills instantons are trapped inside a non-Abelian vortex and stably exist as lumps or sigma model instantons in the $d = 1 + 1$ dimensional $\mathbb{C}P^2$ model in the vortex world-sheet.

The interactions between a non-Abelian vortex and phonons and gluons have been obtained by a dual transformation in which the phonon field and the gluon field are dualized into an Abelian two-form field and a non-Abelian massive two-form field, respectively. On the other hand, the interaction between the mesons and a non-Abelian vortex can be described in the chiral Lagrangian. The interaction between a non-Abelian vortex and photons can be described by a $U(1)$ gauged $\mathbb{C}P^2$ model. One interesting consequence of the electromagnetic interactions is that a lattice of non-Abelian vortices behaves as a polarizer.

It has been shown in the BdG equations that there exist localized and normalizable triplet Majorana fermion zero modes and a localized but non-normalizable singlet Majorana fermion zero mode in the core of a non-Abelian vortex. The low-energy effective theory of the localized gapless fermions propagating along the vortex string has been constructed and the chemical potential dependence of the velocity of gapless modes has been obtained. The index theorem for the fermion zero modes in the background of a non-Abelian vortex ensures the existence of such fermion zero modes. As a result of the Majorana property, localized fermions do not carry a current along a vortex string. A characterization of color superconductors as topological superconductors has also been discussed. As a novel application of Majorana fermion zero modes trapped inside a non-Abelian vortex, the exchange statistics of non-Abelian vortices in $d = 2 + 1$ dimensions has been studied and a new non-Abelian statistics has been found.

In the CFL phase, the chiral symmetry is also spontaneously broken, and there appear various kinds of topological objects, such as axial domain walls, Abelian and non-Abelian axial strings, and Skyrmions. In the chiral limit with massless quarks, the instanton-induced potential shows that a non-Abelian axial string is attached by an axial domain wall. An Abelian axial string is attached by three axial domain walls and decays into three non-Abelian axial vortices, each of which is attached by an axial domain wall. In the presence of quark masses, three axial domain walls attract each other to be combined as a composite wall. Consequently, three axial domain walls attached to an Abelian axial string are also combined. While integer and fractional axial domain walls are metastable classically,

they decay by quantum tunnelings. The quantum anomaly induces an axial current along $U(1)_B$ superfluid vortices, and an electric current along $U(1)_A$ axial strings and magnetic field perpendicular to axial domain walls in the presence of a background magnetic field.

Finally, we have reviewed topological solitons in phases other than the CFL phase. The CFL phase is the ground state at high densities where the masses of the three flavors are small compared to the baryon chemical potential. If one lowers the density gradually, the effect of finite strange quark mass comes in. Then it is expected that kaons form a condensate in addition to the CFL condensates (CFL+K phase). If the density is further decreased, only the light flavors (u and d) contribute to the condensate, which is called the 2SC phase. We have discussed the domain walls and color magnetic fluxes in the 2SC phase, and the K-strings, vortons, domain walls, and drum vortons in the CFL+K phase.

Here we make comments on the other phases that we did not discuss in the last section. The magnetic CFL (MCFL) phase was proposed as the CFL phase under a strong magnetic field [117,121, 122]; it may be relevant in the cores of neutron stars. At moderate densities, charged gluons are condensed due to the chromomagnetic instability in the ground state, known as the Nielsen–Olesen instability [252]. Gluon vortices can be formed inducing a magnetic field of a rotated magnetic field inside a superconductor [118]. The gluon vortices are different from the non-Abelian vortices discussed in this paper. When gluon vortices are generated in dense quark matter under a strong magnetic field, anti-screening occurs, boosting the magnetic field to values higher than the applied one [118], a phenomenon similar to that in magnetized electroweak theory [17,18]. See also Refs. [119,120,123,124].

The different type of vortices for the gluonic phase in dense two-flavor QCD was discussed in Ref. [147].

The gap function of metallic superconductors is proposed to have a spatial modulation under strong magnetic field [224], i.e., in the Fulde–Ferrell–Larkin–Ovchinnikov (FFLO) states [140,214]. Recently, exact self-consistent solutions of the FFLO states have been found [39–41] (see also Ref. [383]). A similar modulation was discussed in color superconductors of dense QCD [248]. The crystalline superconducting phase has been proposed in dense QCD matter; see Refs. [22,72] for a review. In this case, the modulation is not only along one spatial direction but also along three dimensions, forming a crystal. If this is realized, for instance in dense stars, it should significantly affect various dynamics. For instance, vortices created by a rotation should be trapped in nodes of the modulations. It is an interesting problem whether the coexistence of a vortex lattice and a crystalline structure is possible.

Before closing this review paper, let us summarize future problems. We first make a list of problems and explain each of them subsequently.

(1) Dynamics of vortices.
   (a) What does the $U(1)_A$ anomaly do for non-Abelian semi-superfluid vortices?
   (b) The stability of vortex rings.
   (c) Nonlinear/higher order effects on the low-energy effective theory.
   (d) The vortex–vortex interaction at short distances.
   (e) The metastability of $U(1)_B$ (and M_2) vortices.
   (f) The reconnection of non-Abelian semi-superfluid vortices.

(2) Generation of vortices.
   (a) Rotation of the CFL matter.
   (b) The Kibble–Zurek mechanism at phase transitions.

(3) Vortex lattices, vortex phase diagram, and vortex states.
   (a) Transitions from a colorful vortex lattice to a colorless $U(1)_{\rm B}$ vortex lattice.
   (b) Disordered colorful vortex lattices.
   (c) Vortex matter/vortex phase diagram.
   (d) Quantum turbulence. Kolmogorov's law.
(4) Dynamics of orientational modes.
   (a) Quantum monopoles, instantons, and the quark–hadron duality.
(5) Interaction between vortices and quasiparticles.
   (a) Effects on the transportation properties of various quasiparticles.
(6) Fermions.
   (a) Coupling between bosonic and fermionic zero modes.
   (b) Fermions scattering off vortices. The Callan–Rubakov effect.
   (c) The use of the non-normalizable singlet Majorana fermion.
   (d) Self-consistent solutions of vortices.
   (e) Vortex core structures in the BEC/BCS crossover.
   (f) Do the non-Abelian statistics affect the state of matter?
   (g) Topological quantum computation.
(7) Chiral symmetry breaking.
   (a) The interaction between non-Abelian axial vortices and CFL pions.
   (b) The interaction between Skyrmions and non-Abelian axial vortices and axial domain walls.
   (c) The interaction between non-Abelian axial vortices and non-Abelian semi-superfluid vortices.
(8) How do we detect the CFL phase? Hadron colliders and neutron stars.
   (a) Heavy-ion collisions.
   (b) Physics of neutron stars such as pulsar glitch phenomena, strong magnetic fields (magnetars), cooling of neutron stars, and gravitational waves from neutron stars.

(1a) A production of magnetic field by axial domain walls was studied in Sect. 10.6. However, the anomaly effects on non-Abelian semi-superfluid vortices have not been studied. The $U(1)_{\rm A}$ axial current should exist along non-Abelian semi-superfluid vortices as for $U(1)_{\rm B}$ superfluid vortices. There should be a significant role of such a current in a colorful vortex lattice in rotating CFL matter in Sect. 4.4.

(1b) In the absence of dissipation at zero temperature, a superfluid vortex ring moving at constant velocity is stable because of the inertial force. A non-Abelian semi-superfluid vortex ring is also stable. In the presence of dissipation, the size of the ring decreases in time because of the Magnus force. However, due to (1a), the $U(1)_{\rm A}$ current is present along the vortex ring and would make it stable. The stability of vortex rings should be important for states of superfluids such as quantum turbulence. In the case of a superfluid vortex ring, the dynamics can be described by the sine-Gordon model [223]. This may be extended to the case of non-Abelian vortex rings.

(1c) For translational zero (Kelvin) modes X and Y of a vortex, a higher order term for X and Y in the low-energy effective Lagrangian was studied in the context of fluid mechanics [162], and a nonlinear Schrödinger equation was found. Nonlinear soliton waves, called Hasimoto solitons, were studied extensively. While higher derivative correction terms should be in the form of the Nambu–Goto action in the case of relativistic field theories, it is not clear whether such action is relevant for non-relativistic cases. On the other hand, higher derivative corrections were found for the $\mathbb{C}P^2$

orientational zero modes in the context of supersymmetric theories [97]. A more general form of the possible higher derivative correction was given in Ref. [221] by using nonlinear realizations. A similar term should be present for non-Abelian semi-superfluid vortices in the CFL phase.

(1d) The interaction between two non-Abelian semi-superfluid vortices is essentially the same as that between Abelian superfluid vortices, at large distances much larger than the core size. The interaction is mediated by the massless $U(1)_{\rm B}$ Nambu–Goldstone boson (phonon), giving a long-range force. At short distances, two vortices begin to exchange massive modes such as gluons and massive scalar (Higgs) fields. In Sect. 6.1.2, the contribution from gluons was found to depend on relative $\mathbb{C}P^2$ orientations, or color fluxes. It is attractive when the two vortices have different colors. There remains an open question of what is the contribution from the Higgs fields. Full numerical calculations or an analytic estimation from asymptotic forms are needed, as was done for a related model [26].

(1e) A $U(1)_{\rm B}$ vortex has been suggested to decay into three non-Abelian vortices because of being energetic at large distances and repulsion between non-Abelian vortices. However, the interaction at short distances is not known thus far, as explained in (1d). In fact, $U(1)_{\rm B}$ vortices do not carry fluxes while non-Abelian vortices do. Therefore, the gauge field gives an attraction among non-Abelian vortices with different colors and a binding energy among them so that there is a possibility of metastability of $U(1)_{\rm B}$ vortices. Metastability was found for vortices in a three component BEC, which is the same as the diagonal configuration of dense QCD except for the absence of gauge fields [75].

(1f) When two vortices collide in superfluids such as helium superfluids or atomic BECs, they reconnect with each other [211,247], as was confirmed numerically by the Gross–Pitaevskii equation [68] and experimentally by direct observations in helium superfluids [52]. The reconnection process is very important in quantum turbulence [267,351,353,357] where vortices reduce their length through the reconnection. In the case of CFL matter, it is quite nontrivial whether two non-Abelian semi-superfluid vortices reconnect when they collide because they have internal orientations in the $\mathbb{C}P^2$ space; when two vortices have different $\mathbb{C}P^2$ modes, they may pass through without reconnection because the two different orientations could not be connected if they reconnected. This question was addressed in the context of cosmic strings; whether two cosmic strings produced at a phase transition in the early universe can reconnect or not is important for how many strings remain in our universe. This problem was solved for relativistic non-Abelian strings [101]; even when two non-Abelian vortices have two different orientations (color fluxes) in the internal space, they always reconnect at least when the colliding speed is not large, in which two different orientations are smoothly connected at the collision point, as in Fig. 43. Although this result was shown for relativistic strings, we expect that the same holds for semi-superfluid vortices in the non-relativistic case, because the $\mathbb{C}P^2$ effective theory is relativistic (of the type I NG modes). After a reconnection, Kelvin modes are induced and propagate along the two strings as in the case of the usual superfluid vortices. In addition, the $\mathbb{C}P^2$ modes are also induced and propagate along the two strings. Strings would emit phonons and gluons through the interactions studied in Sect. 6.1.

(2a) As for creation vortices, one mechanism is rotation. Since dense stars rotate rapidly, this is the more plausible scenario if CFL matter is realized in their core. However, the minimum vortices in the CFL phase are non-Abelian semi-superfluid vortices carrying color magnetic fluxes. Since it is unlikely to be the case that color fluxes are created from nothing, one plausible scenario is that $U(1)_{\rm B}$ superfluid vortices are created at first as usual and they decay into non-Abelian vortices with total fluxes canceled out (however, see (1e)). A simulation for the formation of non-Abelian vortices

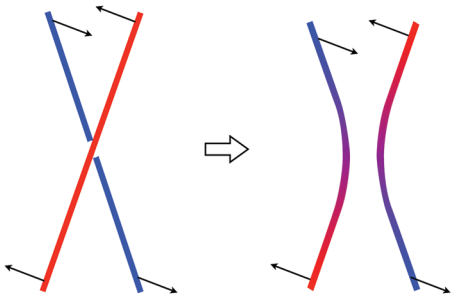

Fig. 43. Reconnection of two non-Abelian vortices.

in rotation is one important future problem. As a similar simulation, creation of superfluid vortices with formation of Abrikosov lattices and splitting into fractional vortices with formation of colorful vortex lattices was simulated in a three-component BEC [75].

(2b) The other scenario of a creation of vortices is the Kibble–Zurek mechanism at the phase transition [169,203,388,389]. In cosmology, this is an almost unique mechanism of a creation of cosmic strings and other defects [169]. The Kibble–Zurek mechanism has been experimentally confirmed in various condensed matter systems. An estimation of the number of non-Abelian vortices produced at phase transitions should be made.

(3a) We have introduced colorful vortex lattices in Sect. 4.4. As the rotation speed is larger, the distance between the vortices becomes shorter. At some point, there may be a transition to a $U(1)_{\rm B}$ vortex lattice because there should be attraction between vortices with different colors, as discussed in (1d), and $U(1)_{\rm B}$ vortices may be metastable (1e).

(3b) Another interesting topic is what happens when a colorful vortex lattice is not ordered in color as in Fig. 13(b). If the colors of a vortex lattice are ordered as in Fig. 13(a), it is easily transformed into a $U(1)_{\rm B}$ vortex lattice and connected to superfluid vortices in the confining phase, as supposed in Sect. 7. However, if the colors of a vortex lattice are disordered as in Fig. 13(b), there should appear an unpaired triplet when the lattice is transformed to a $U(1)_{\rm B}$ vortex lattice or connected to superfluid vortices in the confining phase. There may be characterization of the disordered lattice by frustration or entropy.

(3c) Vortex matter, like vortex-solid or vortex-liquid, is expected to exist in high $T_{\rm c}$ superconductors [55]. Such kinds of vortex matter could also exist in the CFL phase and it is important to determine what kind of vortex state is realized at finite rotation speeds and temperatures. In particular, at finite temperatures, vortices fluctuate and Kelvin modes are induced. When the temperature is further increased, a vortex lattice would eventually melt into a vortex liquid. At even higher temperatures, vortices start to reconnect with each other frequently as in (1f). In this state the CFL condensates vanish and the matter is no longer in the CFL phase. This is a view of the quark-gluon-plasma phase from the vortex point of view.

(3d) The quantum turbulence is a state of superfluids governed by quantized vortices. The energy flows from a larger scale to a smaller scale and Kolmogorov's power law $E \sim k^{-5/3}$ holds. This energy transfer is carried by reconnection of vortices and emission of phonons from Kelvin waves [267,351,353,357]. It is interesting whether such a law holds for CFL matter and whether there is a state that can be called "non-Abelian" quantum turbulence.

(4a) In Sect. 5.4, we constructed quantum monopoles on an infinitely long non-Abelian vortex string. However, we do not want to have a monopole–anti-monopole meson with an infinite string. Therefore, we may consider monopole–anti-monopole mesons in a vortex ring, which may be stable,

as discussed in (1b). Such monopole mesons with finite mass may be more relevant for the quark–hadron duality. It is still unclear whether the quantum potential can be explained by an effect of Yang–Mills instantons trapped in the vortex world-sheet discussed in Sect. 5.5.

(5a) The transportation of phonons was studied in Ref. [228]. Bulk viscosity was studied in Ref. [229]. We may take into account the presence of colorful vortices. Phonons are scattered by vortices through the vortex–phonon interaction studied in Sect. 6.1. In particular, a vortex reconnection (1f) induces Kelvin modes and enhances the dissipation through the phonon–vortex interaction. Interactions of vortices with other quasiparticles such as the CFL mesons and gluons studied in Sect. 6 would also affect the transportation of these quasiparticles.

(6a) Thus far, bosonic zero modes and fermionic zero modes have been studied independently in the GL theory and the BdG equations, respectively. However, we have not discussed a relation between them or if they are coupled to each other. In this regard, fermions cannot be dealt with in the GL theory because fermions are integrated out. Therefore, we should use the BdG equation to study both fermions and bosons in a unified way. It is, however, not easy to deal with bosons in the BdG equation not only technically but also practically. As a compromise, we can use nonlinear realizations [66,79] to construct coupling between the triplet Majorana fermion zero modes and the $\mathbb{C}P^2$ zero modes, since the CFL symmetry $SU(3)_{\mathrm{C+F}}$ is spontaneously broken into $SU(2) \times U(1)$ and fermions belong to the triplet of the unbroken symmetry. The $\mathbb{C}P^2$ zero modes are frozen in the presence of strange quark mass, and therefore this coupling is not relevant for the study of fermions in the energy scale below strange quark mass.

(6b) The Callan–Rubakov effect was first proposed for the scattering of fermions off magnetic monopoles in Refs. [63–65,286], where the s-wave component of the fermion wave function is greatly enhanced, and it was later extended to the fermion scattering off cosmic strings and domain walls [58]. The idea is that when fermions in the bulk interact with topological solitons only fermion zero modes can reach the cores of solitons. The solitons give the boundary condition for scattering fermions and, for instance, enforce the condensates of fermions close to the core. This mechanism was applied for instance to proton decays in grand unified theories and baryogenesis by cosmic strings. The fermion zero modes found in this paper may give a similar effect.

(6c) The singlet fermion zero mode was found to be non-normalizable and cannot be counted by the index theorem as shown in Sect. 8.1. Although non-normalizable modes having a singular peak at the vortex core are usually considered to be unphysical, there is also a discussion in the context of cosmic strings that they may play some interesting roles such as in baryogenesis [9].

(6d) We have constructed only fermion zero modes that are expressed in terms of the gap function. To know the precise form, we need the profiles of the gap function. For this, one needs to construct the gap function and fermion solutions self-consistently. Self-consistent vortex solutions were constructed numerically for s-wave superconductors [157,158]. One also obtains all massive modes trapped inside the core of a vortex. Self-consistent vortex solutions in the CFL phase remain as a future problem.

(6e) Superfluidity of ultracold Fermi gases was established in all the regions of the BEC/BCS crossover by experimentally observing a vortex lattice [390]. Theoretically, for instance, the presence (absence) of fermion modes in the vortex cores in the BCS (BEC) region [226] is one of the interesting phenomena in the BEC/BEC crossover. Crossover of BCS (weak coupling) at high density and BEC (strong coupling) at low density in QCD was also studied in Refs. [5,237,254]. As in ultracold atomic gases, the vortex core structure of the BEC/BCS crossover in dense QCD is an interesting problem.

(6f) Non-Abelian statistics of non-Abelian vortices have been studied [172,379], as reviewed in Sect. 9. This makes vortices non-Abelian anyons when restricted to $d = 2 + 1$ dimensions. When promoted to $d = 3 + 1$ dimensions, vortices are strings. The statistics still remains when one considers adiabatic exchanges of parallel vortices. Another possibility is vortex rings. As discussed in (1b), non-Abelian vortex rings are stable in the absence of dissipations at zero temperature, or they may be stable even at finite temperature once axial anomaly is taken into account. In this case, one may consider exchange of two vortex rings where a smaller one passes through inside a larger one. It is an open question whether such a statistics affects the dynamics of CFL matter.

(6g) Apart from QCD matter, non-Abelian exchange statistics can be used for topological quantum computations [246], which were proposed as a quantum computation robust against perturbations. It is an open question whether triplet Majorana fermions can be useful for it.

(7a) The interaction between a non-Abelian semi-superfluid vortex and gluons was achieved [170] by dualizing gluons to massive two-form fields [314] in Sect. 6.1. In this case, the order parameter space, $U(3)_{\mathrm{C-F+B}}$, around which semi-superfluid vortices wind, is gauged by the $SU(3)_{\mathrm{C}}$ color gauge symmetry, and so we have massive two-form fields. On the other hand, the order parameter space $U(3)_{\mathrm{L-R+A}}$ is not gauged. Accordingly, the interaction between a non-Abelian axial vortex and the $U(3)$ fields, i.e. the CFL pions and the η' meson, should be described by dualizing the $U(3)$ fields to massless two-form fields, known as the Freedman–Townsend model [130] (see also Ref. [141]).

(7b) Skyrmions can interact with axial domain walls and axial vortices. Presumably the interaction is attractive. After a Skyrmion is absorbed into an axial domain wall, it may be stable as a lump ($2 + 1$-dimensional Skyrmion) or unstable depending on the models [255,256]. On the other hand, if a Skyrmion is absorbed into an axial vortex, it may become a kink on the vortex.

(7c) In the CFL phase, two kinds of non-Abelian vortices are present as discussed in this review, non-Abelian semi-superfluid vortices and non-Abelian axial vortices. While the order parameter spaces around which these vortices wind are different, it is an open question whether these two kinds of vortices interact nontrivially.

(8a) In heavy-ion collision experiments, where two relativistically accelerated nuclei are collided, it might be possible that some kinds of superfluid phases are realized, like the neutron superfluid or the CFL matter, especially at low-energy collisions. If a superfluid is produced in heavy-ion collisions, quantum vortices would appear since the created matter would have finite angular momentum at off-central collisions. It is an interesting problem to find the experimental signatures of such phenomena.

(8b) A more plausible candidate for dense QCD matter in nature may be the cores of dense stars such as neutron stars (or quark stars) [146,316]. It has been argued that the recent discovery of a massive neutron star [87] tends to deny the existence of exotic matter such as hyperon or quark matter in their cores because of the equation of state for neutron stars, but there is also an argument that exotic matter is still possible (see e.g. Refs. [235,294,346,367] and Refs. [54,381] for recent and earlier works) and the situation is not conclusive. Although the evidence for the presence of such quark matter is elusive, we may give observation limits to the existence from rotating QCD matter in particular vortices. For reviews of dense matter in compact stars, see Refs. [266,306,382]. Here we make brief comments on this issue.

Pulsar glitch phenomena may be explained by unpinning of pinned vortices, as suggested by Anderson and Itoh [19]. While some unpinning mechanisms were suggested, there has been no agreement thus far. Non-Abelian vortices in the CFL phase may play some role in explaining this mechanism, in particular colorful vortex lattices and boojums.

Strong magnetic fields of neutron stars are still a very important unsolved problem, in particular magnetars. As discussed in Sect. 10.6, magnetic fields are produced from axial domain walls and axial vortices by the axial anomaly. This mechanism may explain the strong magnetic fields of neutron stars.

The emission of neutrinos is the main process of the cooling of compact stars [146,316]. Neutrino emission in the CFL phase was studied in Refs. [191,282]. It turns out that the decays of phonons into neutrinos are the dominant process of cooling (phonons couple to Z^0 weak bosons). The astrophysical implication of the cooling of compact stars in the presence of color superconducting phases was studied; for instance, see Ref. [262]. One should take into account the presence of a colorful vortex lattice, since the phonons interact with vortices. Reheating in the presence of vortices was also studied in Ref. [249], without specifying the kinds of vortices.

Gravitational wave detectors are now one of the hottest topics in astrophysics. Gravitational waves in the presence of vortex lattices in the CFL phase (and the 2SC phase) were studied, assuming vortex lattices of unstable color magnetic fluxes, and compared with neutron star observations in Ref. [145]. The calculation should be revised by considering colorful vortex lattices. Apart from vortices, the r-mode instability of neutron stars and gravitational waves related to this mode were studied assuming the CFL phase [20,230]. This calculation should be modified in the presence of a colorful vortex lattice.

Sole observations of gravitational waves will tell us only the stiffness of the equation of state of neutron stars, while these observations combined with observations of neutrinos, gamma rays, and X rays will give us more detailed information on the cooling process of neutron stars, which should contain information on the presence or absence of exotic matter and vortices in such matter.

We believe that the problems listed above are important and should be investigated in the future. We hope that this list is useful for those who are interested in this field.

Acknowledgements

We would like to thank our collaborators, Mattia Cipriani, Takanori Fujiwara, Takahiro Fukui, Noriko Shiiki, Kazunori Itakura, Takuya Kanazawa, Michikazu Kobayashi, Taeko Matsuura, Eiji Nakano, Walter Vinci, and Naoki Yamamoto for extensive discussions and collaborations. Many parts of this review result from these collaborations. M.N. is especially grateful to Taeko Matsuura and Eiji Nakano, who introduced him to this subject. Without them, this review paper would have been impossible. We further thank Eiji Nakano, Motoi Tachibana, and Naoki Yamamoto for careful reading of the manuscript and crucial comments, and Kei Iida and Nobutoshi Yasutake for useful comments.

This work is supported in part by a Grant-in-Aid for Scientific Research (Grants No. 23740198 (M.E.), No. 23740198 and No. 25400268 (M.N.)). The work of Y.H. is partially supported by the Japan Society for the Promotion of Science for Young Scientists and partially by the JSPS Strategic Young Researcher Overseas Visits Program for Accelerating Brain Circulation (No. R2411). The work of M.N. is also supported in part by the "Topological Quantum Phenomena" Grant-in-Aid for Scientific Research on Innovative Areas (Grants No. 23103515 and No. 25103720) from the Ministry of Education, Culture, Sports, Science and Technology (MEXT) of Japan. The work of S.Y. is supported by a Grant-in-Aid for Scientific Research on Priority Areas "Elucidation of New Hadrons with a Variety of Flavors (E01: 21105006)."

Appendix A. Non-Abelian vortices in supersymmetric QCD

In the context of supersymmetric (SUSY) QCD, non-Abelian vortices were discovered independently in Refs. [25,159] as a generalization of Abrikosov–Nielsen–Olesen (ANO) vortices [3,251] in the Abelian–Higgs model. Since then, much progress has been made in recent years; see Refs. [103, 107,209,210,319,320,349,350] for a review. They are topologically the same objects as non-Abelian

vortices in dense QCD, discussed in this review paper. It is interesting that such similar objects were found in different contexts, dense QCD and SUSY QCD, almost at the same time. Here, we summarize the differences and similarities of non-Abelian vortices in dense QCD and SUSY QCD, and summarize the properties of non-Abelian vortices in SUSY QCD, which may be useful in the study of those in dense QCD. One of the most important common features is the existence of bosonic orientational gapless modes $\mathbb{C}P^2$ and $\mathbb{C}P^{N-1}$ in the core of a non-Abelian vortex in dense QCD and SUSY $U(N)$ QCD, respectively.

Three crucial differences are present between non-Abelian vortices in dense QCD and SUSY QCD, as summarized in the following:

(1) The overall $U(1)$ symmetry is global $U(1)_{\rm B}$ symmetry in dense QCD, while it is gauged in SUSY QCD. Consequently,
   (a) vortices are global vortices in dense QCD, while they are local vortices in SUSY QCD,
   (b) the energy of vortices in dense QCD is logarithmically divergent with the infinite system size, while that of local vortices in SUSY QCD is finite,
   (c) the interaction between two vortices at a distance R is $1/R$ for dense QCD, while it is zero for two local BPS vortices in SUSY QCD, and $\pm e^{-cR}$ for two local vortices in non-SUSY QCD.

(2) Dense QCD matter is non-relativistic while SUSY QCD is relativistic. Consequently,
   (a) Two translational zero modes are not independent of each other, one is the momentum conjugate to the other, and there exists only one Kelvin mode (Kelvon) for vortices in dense QCD, as shown in Sect. 4. On the other hand, two translational zero modes are independent in vortices in SUSY QCD. The former are so-called type II Nambu–Goldstone modes and the latter are so-called type I Nambu–Goldstone modes [168,260,363], as summarized in footnote 8.

(3) The bosons are not independent degrees of freedom, and fermions couple to bosons (with the order parameter Δ) in the BdG equation in dense QCD, while bosons and fermions are degrees of freedom independent of each other in SUSY QCD, and they are related by SUSY transformations. Consequently,
   (a) *Majorana* fermions belonging to *triplet (the adjoint representation)* of the unbroken $SU(2)$ symmetry in the vortex core are localized in a non-Abelian vortex in dense QCD, while *Dirac* fermions in the *fundamental* representation of the unbroken $SU(N-1)$ symmetry in the vortex core are localized in a non-Abelian vortex in SUSY QCD.
   (b) Fermion zero modes and bosonic zero modes are not related to each other in dense QCD, while fermion zero modes are "tangent bundle" to bosonic zero modes. On the other hand, in SUSY QCD, linearized equations of motion of the bosonic fields coincide with the equation of motion of the fermions, and therefore the index theorems for fermions and bosons coincide [159].

Although these are major differences, both vortices have many common features.

Unlike ANO vortices in the Abelian–Higgs model, non-Abelian vortices have non-Abelian internal orientations and associated conserved charges. In the case of $U(N)$ gauge theory with N flavors of Higgs fields in the fundamental representation, the internal orientation is the complex projective space $\mathbb{C}P^{N-1}$, which corresponds to Nambu–Goldstone modes associated with the $SU(N)_{\rm C+F}$ color–flavor-locked global symmetry spontaneously broken in the presence of vortices. Because of

non-Abelian internal orientations, we can expect that the dynamics of the non-Abelian vortices is much richer and more interesting compared to the ANO vortices.

Since there exists no net force between multiple BPS vortices, a space of the whole solutions is characterized by multiple collective coordinates called moduli. The number of the moduli parameters was determined to be $2kN$ for k vortices in $U(N)$ gauge theory [159]. The moduli space of multiple vortices with full moduli parameters was completely determined without metric by partially solving the BPS vortex equations [106,107,109,184]. The moduli space for k separated vortices is a k-symmetric product

$$\mathcal{M}_k^{\rm sep} \simeq (\mathbb{C} \times \mathbb{C}P^{N-1})^k / \mathcal{S}_k \subset \mathcal{M}_k \tag{A1}$$

of the single vortex moduli space [106], while the whole space $\mathcal{M}_k$ is regular.

First, let us consider vortex particles in $d = 2 + 1$ dimensions or parallel vortices in $d = 3 + 1$ dimensions. Although there is no force between BPS vortices at rest, vortices scatter nontrivially when they are moving. The low-energy dynamics of BPS solitons can be described as geodesics of a proper metric on the moduli space [232]. By using a general formula for the moduli space metric given in Ref. [105], the explicit moduli space metric was obtained for the moduli subspace $\mathcal{M}_k^{\rm sep}$ of k well separated vortices, which is valid when the separation of vortices is much larger than the length scale of the vortices, i.e., the Compton wavelength of massive vector bosons [132]. This metric describes low-energy scattering of two slowly moving vortices [96]. The moduli space metric of the moduli subspace for two coincident vortices [92,93,101], which is supplementary to $\mathcal{M}_{k=2}^{\rm sep}$ inside the whole space $\mathcal{M}_{k=2}$, was also found, which shows that two non-Abelian vortices scatter at 90 degrees in head-on collisions, even though they have different internal orientations $\mathbb{C}P^{N-1}$ as the initial conditions [101].

Going back to $d = 3 + 1$ dimensions, one nontrivial and important dynamics is the reconnection of two vortex strings colliding at an angle. It was shown in Ref. [101] that when two vortex strings collide at an angle, they always reconnect each other.

There exists a static force between non-BPS vortices. Static force between two non-BPS non-Abelian local vortices was shown to depend on internal orientations [26]. The dynamics of non-BPS vortices can be described by the moduli space approximation plus the potential term corresponding to the static force. Therefore, the dynamics of non-Abelian vortices in dense QCD is also expected to be described by the moduli approximation and the potential term of the static interaction $1/r$ studied in Sect. 4.2. In particular, the reconnection dynamics should hold for non-Abelian vortices in dense QCD, because its possibility depends only on topology. Since the reconnection dynamics is an essential process, for instance in quantum turbulence in superfluids and ultracold atomic gases, it should be important if the CFL phase is realized in the cores of dense stars.

Non-BPS non-Abelian vortices were studied for instance in Refs. [26,148,149]. It was also claimed that vortices in Ref. [148] describe those in dense QCD but this is not the case because the $U(1)_{\rm B}$ symmetry is gauged there.

Appendix B. Toric diagram

Here we would like to explain a geometrical aspect of the complex projective space $\mathbb{C}P^{N-1}$, which is a complex manifold of the complex dimension $N - 1$. The $\mathbb{C}P^{N-1}$ manifold is known as a toric geometry, on which there is a $U(1)^{N-1}$ action allowing several fixed points. One can find a good explanation of the toric geometry in Ref. [218].

The simplest example of toric geometry is the complex plane $\mathbb{C}$. Let z be a coordinate on $\mathbb{C}$. There exists a $U(1)$ action

$$z \to e^{i\theta} z. \tag{B1}$$

A fixed point of $U(1)$ is the origin $z = 0$. The complex plane can be seen as a half-line with a circle on top. The circle shrinks at the fixed point; see Fig. B1.

The next example is $\mathbb{C}P^1$. As is well known, $\mathbb{C}P^1$ is the space of two complex numbers (ϕ_1, ϕ_2), which are not all zero. The two complex numbers are themselves identified up to multiplying by a non-zero complex number

$$(\phi_1, \phi_2) \sim \lambda(\phi_1, \phi_2), \quad \lambda \in \mathbb{C}^*. \tag{B2}$$

One can fix the equivalence relation by setting

$$(\phi_1, \phi_2) \to (1, z) \qquad \text{for} \quad \phi_1 \neq 0, \tag{B3}$$

$$(\phi_1, \phi_2) \to (z', 1) \qquad \text{for} \quad \phi_2 \neq 0. \tag{B4}$$

z and z' are complex numbers, which are related by $zz' = 1$, except for the $z = 0$ and $z' = 0$ cases. There is again a $U(1)$ action

$$(1, z) \to (1, e^{i\theta} z), \quad (z', 1) \to (e^{-i\theta} z', 1). \tag{B5}$$

The fixed points are $z = 0$ and $z' = 0$. Let us take a real basis that is invariant under the $U(1)$ action

$$X = \frac{|z|^2}{1 + |z|^2} = \frac{1}{1 + |z'|^2}. \tag{B6}$$

This X takes values in the segment $[0, 1]$: $X = 0$ and $X = 1$ correspond to $z = 0$ and $z' = 0$, respectively. Thus, $\mathbb{C}P^1$ can be viewed as the interval with a circle on top, as shown in Fig. B2.

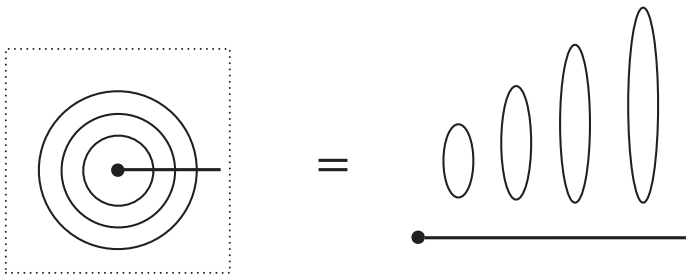

Fig. B1. A toric diagram for the complex plane $\mathbb{C}$.

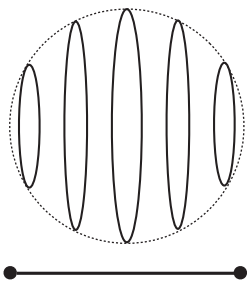

Fig. B2. A toric diagram for the complex plane $\mathbb{C}P^1$.

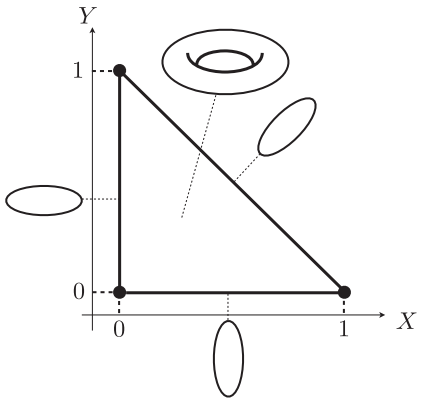

Fig. B3. A toric diagram for the complex plane $\mathbb{C}P^2$.

$\mathbb{C}P^2$ is a straightforward extension of $\mathbb{C}P^1$. It is defined as the space of three complex numbers (ϕ_1, ϕ_2, ϕ_3), not all zeros, with the following identification:

$$(\phi_1, \phi_2, \phi_3) \sim \lambda(\phi_1, \phi_2, \phi_3), \quad \lambda \in \mathbb{C}^*. \tag{B7}$$

One can fix this equivalence relation by setting the first component $\phi_1 = 1$ when $\phi_1 \neq 0$ as

$$(\phi_1, \phi_2, \phi_3) \to (1, z, w). \tag{B8}$$

There is a $U(1)^2$ action except for the trivial $U(1)$. Without loss of generality, one can take the basis of $U(1)^2$ as

$$(1, z, w) \to (1, e^{i\theta} z, e^{i\phi} w). \tag{B9}$$

As in the case of $\mathbb{C}P^1$, let us take a real basis that is invariant under $U(1)^2$. It is of the form

$$X = \frac{|z|^2}{1 + |z|^2 + |w|^2}, \quad Y = \frac{|w|^2}{1 + |z|^2 + |w|^2}. \tag{B10}$$

Both X and Y take their value in the segment $[0, 1]$ and $X + Y \leq 1$ holds. Therefore, $\mathbb{C}P^2$ is expressed as a rectangular equilateral triangle, as shown in Fig. B3. At a generic point, we have a T^2 fiber (θ, ϕ) since the action of $U(1)^2$ is not free. The T^2 fiber shrinks to a T^2 at the edges of the triangle. For instance, $Y = 0$ $(w = 0)$ is the fixed point of ϕ. Therefore, the T^1 fiber of ϕ shrinks there. Note that the submanifold at $Y = 0$ is $\mathbb{C}P^1$, which can be easily understood by setting $\phi_3 = 0$ in Eq. (B7). The other edges correspond to the other $\mathbb{C}P^1$s. At the vertices of the triangle, the $U(1)^2$ action becomes completely free. Therefore, the T^2 fiber shrinks.

Appendix C. Derivation of the low-energy effective theory of orientational zero modes

Here we explain how to derive the low-energy effective field theory (5.8) of the unit winding non-Abelian vortex. The effective action consists of a linear combination of $\mathrm{Tr}[F_{\alpha i} F^{\alpha i}]$ and $\mathrm{Tr}[\mathcal{D}_\alpha \Phi \mathcal{D}^\alpha \Phi^\dagger]$ $(\alpha = 0, 3)$. Therefore, we only need to calculate these terms one by one in terms of the orientational moduli field $\phi(t, x^3)$, which appears via the gauge field A_α given in Eq. (5.7). To this end, it will turn out that it is convenient to introduce a 3×3 matrix valued function $\mathcal{F}_\alpha(a, b)$ of

two complex variables (a, b) by

$$\mathcal{F}_\alpha(a,b) \equiv a\phi\partial_\alpha\phi^\dagger + b\partial_\alpha\phi\phi^\dagger + (a-b)\phi^\dagger\phi\partial_\alpha\phi\phi^\dagger. \tag{C1}$$

One finds that this function $\mathcal{F}_\alpha(a,b)$ satisfies the following relations:

$$\mathcal{F}_\alpha(a,b)^\dagger = \mathcal{F}(b^*,a^*), \tag{C2}$$

$$\mathrm{Tr}\mathcal{F}_\alpha(a,b) = 0, \tag{C3}$$

$$\alpha\mathcal{F}_\alpha(a,b) = \mathcal{F}_\alpha(\alpha a, \alpha b), \tag{C4}$$

$$\mathcal{F}_\alpha(a,b) + \mathcal{F}_\alpha(a',b') = \mathcal{F}_\alpha(a+a', b+b'). \tag{C5}$$

Then the gauge field given in Eq. (5.7) can be expressed as

$$A_\alpha = \frac{i\rho_\alpha}{g_\mathrm{s}}\mathcal{F}_\alpha(1,-1). \tag{C6}$$

One can easily check the following equation by making use of the constraint $\phi^\dagger\phi = 1$

$$\mathrm{Tr}[\mathcal{F}_\alpha(a,b)^\dagger\mathcal{F}^\alpha(a,b)] = (|a|^2+|b|^2)\mathcal{L}^{(\alpha)}_{\mathbb{C}P^2}, \tag{C7}$$

where no summation is taken over α and $\mathcal{L}^{(\alpha)}_{\mathbb{C}P^2}$ is given in Eq. (5.12). In terms of the function $\mathcal{F}_\alpha$, the covariant derivative and the field strength are expressed by

$$\mathcal{D}_\alpha\Phi = e^{\frac{i\theta}{3}}\Delta_{\mathrm{CFL}}\mathcal{F}_\alpha(f-g+\rho_\alpha g, f-g-\rho_\alpha f), \tag{C8}$$

$$F_{\alpha i} = \frac{1}{g_\mathrm{s}}\epsilon_{ij}\frac{x_j}{r^2}(1-\rho_\alpha)\mathcal{F}_\alpha(1,1) - \frac{i}{g_\mathrm{s}}\frac{x_j}{r}\rho'_\alpha\mathcal{F}_\alpha(1,-1). \tag{C9}$$

With these expressions at hand, we can now calculate the effective Lagrangian. Let us first calculate the F^2 term

$$\begin{aligned}\mathrm{Tr}[F_{i\alpha}F^{i\alpha}] &= \frac{1}{g_\mathrm{s}^2}\frac{x_i x^i}{r^4}h^2 g(1-\rho_\alpha)^2\mathcal{G}_\alpha(1,1|1,1) - \frac{1}{g_\mathrm{s}^2}\frac{x_i x^i}{r^2}(\rho'_\alpha)^2\mathcal{G}_\alpha(1,-1|1,-1)\\ &= -\frac{2}{g_\mathrm{s}^2}\left[\rho_\alpha'^2 + \frac{h^2(1-\rho_\alpha)^2}{r^2}\right]\mathcal{L}^{(\alpha)}_{\mathbb{C}P^2},\end{aligned} \tag{C10}$$

where we have defined

$$\mathcal{G}_\alpha(k,l|m,n) \equiv \mathrm{Tr}[\mathcal{F}_\alpha(k,l)^\dagger\mathcal{F}^\alpha(m,n)], \tag{C11}$$

with no summation for α. Note that we have eliminated the term proportional to $\mathcal{G}_\alpha(1,1|1,-1)$ in Eq. (C10) because $\mathcal{G}_\alpha(1,1|1,-1)$ is zero. Let us next calculate the $|\mathcal{D}_\alpha\Phi|^2$ term. To this end, let us rewrite $\mathcal{D}_\alpha\Phi$ as

$$\begin{aligned}\mathcal{D}_\alpha\Phi &= -\mathcal{F}_\alpha\left(\frac{(f-g)\rho_\alpha}{2}, \frac{(f-g)\rho_\alpha}{2}\right)\\ &\quad + \mathcal{F}_\alpha\left(f-g+\rho_\alpha g + \frac{(f-g)\rho_\alpha}{2}, f-g-\rho_\alpha f + \frac{(f-g)\rho_\alpha}{2}\right)\\ &= -\mathcal{F}_\alpha\left(\frac{(f-g)\rho_\alpha}{2}, \frac{(f-g)\rho_\alpha}{2}\right) + \mathcal{F}_\alpha\left(f-g+\frac{(f+g)\rho_\alpha}{2}, f-g-\frac{(f+g)\rho_\alpha}{2}\right)\\ &= -\frac{(f-g)\rho_\alpha}{2}\mathcal{F}_\alpha(1,1) + \mathcal{F}_\alpha(f-g, f-g) + \mathcal{F}_\alpha\left(\frac{(f+g)\rho_\alpha}{2}, -\frac{(f+g)\rho_\alpha}{2}\right)\\ &= \left(1-\frac{\rho_\alpha}{2}\right)(f-g)\mathcal{F}_\alpha(1,1) + \frac{(f+g)\rho_\alpha}{2}\mathcal{F}_\alpha(1,-1).\end{aligned} \tag{C12}$$

Then we have

$$\begin{aligned}\mathrm{Tr}[\mathcal{D}_\alpha\Phi^\dagger\mathcal{D}^\alpha\Phi] &= \left(1-\frac{\rho_\alpha}{2}\right)^2(f-g)^2\mathcal{G}_\alpha(1,1|1,1)+\frac{(f+g)^2\rho_\alpha^2}{4}\mathcal{G}_\alpha(1,1|1,-1)\\ &= 2\Delta_{\mathrm{CFL}}^2\left[(1-\rho_\alpha)(f-g)^2+\frac{\rho_\alpha^2}{2}(f^2+g^2)\right]\mathcal{L}^{(\alpha)}_{\mathbb{C}P^2}. \end{aligned} \tag{C13}$$

Plugging Eqs. (C10) and (C13) into Eqs. (5.9) and (5.10), it is straightforward to find the Kähler classes $C^{0,3}$ given in Eqs. (5.13) and (5.14).

Appendix D. Derivation of the dual Lagrangians for phonons and gluons

In this appendix, we derive the dual Lagrangians for phonons and gluons. After a dual transformation, massive gluons are described by massive non-Abelian antisymmetric tensor fields [314] and $U(1)_{\mathrm{B}}$ phonons are described by massless antisymmetric tensor fields. In the dual description, vortices appear as sources that can absorb or emit these particles.

Appendix D.1 Low-energy effective theory of the CFL phase

We start with a time-dependent Ginzburg–Landau (GL) effective Lagrangian for the CFL phase, which is given in Eq. (2.56):

$$\begin{aligned}\mathcal{L}(x) = &\frac{\varepsilon_3}{2}\left(\mathbf{E}^a\right)^2-\frac{1}{2\lambda_3}\left(\mathbf{B}^a\right)^2+K_0\mathrm{Tr}\left[(D_0\Phi)^\dagger D^0\Phi\right]+K_3\mathrm{Tr}\left[(D_i\Phi)^\dagger D^i\Phi\right]\\ &-4i\gamma\mathrm{Tr}\left[\Phi^\dagger D_0\Phi\right]-V(\Phi),\end{aligned} \tag{D1}$$

where $E_i^a=F_{0i}^a$, $B_i^a=\frac{1}{2}\epsilon_{ijk}F_{jk}^a$. The effect of $U(1)_{\mathrm{EM}}$ electromagnetism is neglected here. The parameters ε_3 and λ_3 are the color dielectric constant and the color magnetic permeability. The Lorentz symmetry does not have to be maintained in general since superconducting matter exists. However, the kinetic term of the gluons has a modified Lorentz symmetry in which the speed of light is replaced by $1/\sqrt{\varepsilon_3\lambda_3}$. It is always possible to restore the Lorentz invariance of the kinetic term of the gauge fields by rescaling x^0, A_0^a, K_0, γ, and K_3. Therefore, we can start with the Lagrangian in which ϵ and λ are taken to be unity. For notational convenience, we introduce a vector $K_\mu\equiv(K_0,K_3,K_3,K_3)$. Thus our starting point is the following GL Lagrangian:

$$\mathcal{L}(x)=-\frac{1}{4}\left(F_{\mu\nu}^a\right)^2+K_\mu\mathrm{Tr}\left[\left(D_\mu\Phi\right)^\dagger D^\mu\Phi\right]-4i\gamma\mathrm{Tr}\left[\Phi^\dagger D_0\Phi\right]-V(\Phi). \tag{D2}$$

Appendix D.2 The dual transformation

Here we perform dual transformations within the path integral formalism to derive a dual Lagrangian for the CFL phase. After the transformation, massive gluons are described by massive non-Abelian antisymmetric tensor fields [314] and $U(1)_{\mathrm{B}}$ phonons are described by massless antisymmetric tensor fields. We show that in the dual description vortices appear as sources that can absorb or emit these particles.

Appendix D.2.1 The dual transformation of massive gluons The partition function of the CFL phase can be written as

$$Z=\int\mathcal{D}A_\mu^a(x)\mathcal{D}\Phi(x)\exp\left\{i\int d^4x\mathcal{L}(x)\right\}, \tag{D3}$$

with the Lagrangian defined in Eq. (D2). We shall impose the gauge fixing condition on the field Φ rather than on the gauge fields since they are integrated out in the end. The gauge fixing condition is taken care of when we consider a concrete vortex solution.

We introduce non-Abelian antisymmetric tensor fields $B^a_{\mu\nu}$ by a Hubbard–Stratonovich transformation,

$$\begin{aligned}&\exp\left[i\int \mathrm{d}^4x\left\{-\frac{1}{4}(F^a_{\mu\nu})^2\right\}\right]\\&\quad\propto\int\mathcal{D}B^a_{\mu\nu}\exp\left[i\int\mathrm{d}^4x\left\{-\frac{1}{4}\left[m^2(B^a_{\mu\nu})^2-2m\tilde{B}^a_{\mu\nu}F^{a,\mu\nu}\right]\right\}\right],\end{aligned}\tag{D4}$$

where $\tilde{B}^a_{\mu\nu}\equiv\frac{1}{2}\epsilon_{\mu\nu\rho\sigma}B^{a,\rho\sigma}$. The parameter m introduced above is a free parameter at this stage. We will choose m later so that the kinetic term of $B^a_{\mu\nu}$ is canonically normalized.

Substituting (D4) into (D3), we can now perform the integration over the gauge fields A^a_μ. The degrees of freedom of gluons are expressed by $B^a_{\mu\nu}$ after this transformation. Each term in the Lagrangian is transformed as follows:

$$\begin{aligned}&K_\mu\mathrm{Tr}\{(D_\mu\Phi)^\dagger(D^\mu\Phi)\}-4i\gamma\mathrm{Tr}\left[\Phi^\dagger D_0\Phi\right]\\&\quad=K_\mu\mathrm{Tr}\left\{\Phi^\dagger(\overleftarrow{\partial}_\mu+ig_sA^a_\mu T^a)(\overrightarrow{\partial}^\mu-ig_sA^{b,\mu}T^b)\Phi\right\}-4i\gamma\mathrm{Tr}\left[\Phi^\dagger(\partial_0-ig_sA^a_\mu T^a)\Phi\right]\\&\quad=K_\mu\mathrm{Tr}\{(\partial_\mu\Phi)^\dagger(\partial^\mu\Phi)\}-4i\gamma\mathrm{Tr}\left[\Phi^\dagger\partial_0\Phi\right]+g_sA^a_\mu J^{a,\mu}\\&\qquad+g_s^2g_{\mu\nu}\sqrt{K_\mu K_\nu}A^{a,\mu}A^{b,\nu}\mathrm{Tr}\left[\Phi^\dagger T^aT^b\Phi\right],\end{aligned}\tag{D5}$$

with $J^a_\mu\equiv-iK_\mu\mathrm{Tr}\left[\Phi^\dagger(\overleftarrow{\partial}_\mu-\overrightarrow{\partial}_\mu)T^a\Phi\right]+4\gamma\mathrm{Tr}\left[\Phi^\dagger T^a\Phi\right]$, and

$$\begin{aligned}-\frac{1}{2}m\tilde{B}^a_{\mu\nu}F^{a,\mu\nu}&=-\frac{1}{2}m\tilde{B}^a_{\mu\nu}(2\partial_\nu A^a_\mu+g_sf^{abc}A^b_\mu A^c_\nu)\\&=mA^a_\mu\partial_\nu\tilde{B}^a_{\mu\nu}+\frac{1}{2}mg_sf^{abc}A^a_\mu A^b_\nu\tilde{B}^c_{\mu\nu}.\end{aligned}\tag{D6}$$

Performing the integration over A^a_μ, the following part of the partition function is rewritten as

$$\begin{aligned}&\int\mathcal{D}A^a_\mu\exp\left\{i\int\mathrm{d}^4x\left[\frac{1}{2}g_s^2A^{a,\mu}K^{ab}_{\mu\nu}A^{b,\nu}-m\left(\partial^\nu\tilde{B}^a_{\mu\nu}-\frac{g_s}{m}J^a_\mu\right)A^{a,\mu}\right]\right\}\\&\quad\propto(\det K^{ab}_{\mu\nu})^{-1/2}\\&\quad\exp\left\{i\int\mathrm{d}^4x\left[-\frac{1}{2}\left(\frac{m}{g_s}\right)^2\left(\partial_\rho\tilde{B}^{a,\mu\rho}-\frac{g_s}{m}J^{a,\mu}\right)\left(K^{-1}\right)^{ab}_{\mu\nu}\left(\partial_\sigma\tilde{B}^{b,\nu\sigma}-\frac{g_s}{m}J^{b,\nu}\right)\right]\right\},\end{aligned}\tag{D7}$$

where $K^{ab}_{\mu\nu}$ is defined by

$$\begin{aligned}K^{ab}_{\mu\nu}&=\frac{1}{2}g_{\mu\nu}\sqrt{K_\mu K_\nu}\mathrm{Tr}\left[\Phi^\dagger T^aT^b\Phi\right]-\frac{m}{g_s}f^{abc}\tilde{B}^c_{\mu\nu}\\&\equiv\mathbf{\Phi}^{ab}_{\mu\nu}-\frac{m}{g_s}\hat{B}^{ab}_{\mu\nu},\end{aligned}\tag{D8}$$

with $\mathbf{\Phi}^{ab}_{\mu\nu}\equiv\frac{1}{2}g_{\mu\nu}\sqrt{K_\mu K_\nu}\mathrm{Tr}\left[\Phi^\dagger T^aT^b\Phi\right]$ and $\hat{B}^{ab}_{\mu\nu}\equiv f^{abc}\tilde{B}^c_{\mu\nu}$. We define the inverse of $K^{ab}_{\mu\nu}$ by the power-series expansion in $1/g$:

$$K^{-1}=\left(\mathbf{\Phi}-\frac{m}{g_s}\hat{B}\right)^{-1}=\mathbf{\Phi}^{-1}\sum_{n=0}^{\infty}\left(\frac{m}{g_s}\hat{B}\mathbf{\Phi}^{-1}\right)^n.\tag{D9}$$

As a result, we obtain the following partition function:

$$Z \propto \int \mathcal{D}B^a_{\mu\nu} (\det K^{ab}_{\mu\nu})^{-1/2} \exp\left\{ i \int \mathrm{d}^4 x \mathcal{L}^*_{\mathrm{G}}(x) \right\}, \tag{D10}$$

where $\mathcal{L}^*_{\mathrm{G}}$ denotes the gluonic part of the dual Lagrangian:

$$\mathcal{L}^*_{\mathrm{G}} = -\frac{1}{2}\left(\frac{m}{g_{\mathrm{s}}}\right)^2 \left(\partial_\rho \tilde{B}^{a,\mu\rho} - \frac{g_{\mathrm{s}}}{m} J^{a,\mu}\right) \left(K^{-1}\right)^{ab}_{\mu\nu} \left(\partial_\sigma \tilde{B}^{b,\nu\sigma} - \frac{g_{\mathrm{s}}}{m} J^{b,\nu}\right) - \frac{1}{4} m^2 (B^a_{\mu\nu})^2. \tag{D11}$$

Now we define the non-Abelian vorticity tensor $\omega^a_{\mu\nu}$ as the coefficient of the term linearly proportional to $B^a_{\mu\nu}$. Collecting the relevant terms in the above Lagrangian, the coupling between massive gluons and the vorticity is given by

$$\begin{aligned}
\mathcal{L}^*_{\mathrm{G}} \supset{}& \frac{1}{2}\frac{m}{g_{\mathrm{s}}} \left[\partial_\rho \tilde{B}^{a,\mu\rho} (\boldsymbol{\Phi}^{-1})^{ab}_{\mu\nu} J^{b,\nu} + J^{a,\mu} (\boldsymbol{\Phi}^{-1})^{ab}_{\mu\nu} \partial_\rho \tilde{B}^{b,\nu\rho} \right] \\
& - \frac{1}{2}\left(\frac{m}{g_{\mathrm{s}}}\right) J^{a,\mu} [\boldsymbol{\Phi}^{-1} \hat{B} \boldsymbol{\Phi}^{-1}]^{ab}_{\mu\nu} J^{b,\nu} \\
\equiv{}& -\frac{1}{2}\left(\frac{m}{g_{\mathrm{s}}}\right) B^a_{\lambda\sigma} \omega^{a,\lambda\sigma},
\end{aligned} \tag{D12}$$

where we have defined the vorticity tensor $\omega^a_{\mu\nu}$ as

$$\omega^{a,\lambda\sigma} \equiv \epsilon^{\lambda\sigma\mu\nu} \left[\partial_\nu \left\{ (\boldsymbol{\Phi}^{-1})^{(ab}_{\mu\rho) } J^{b,\rho} \right\} + J^{e,\alpha} (\boldsymbol{\Phi}^{-1})^{ec}_{\alpha\mu} f^{cda} (\boldsymbol{\Phi}^{-1})^{db}_{\nu\beta} J^{b,\beta} \right]. \tag{D13}$$

Here $A^{(ab}_{\mu\nu)}$ is a symmetrized summation defined by $A^{(ab}_{\mu\nu)} \equiv A^{ab}_{\mu\nu} + A^{ba}_{\nu\mu}$. This expression for the non-Abelian vorticity is valid for general vortex configurations. The information on vortex configuration is included in $\boldsymbol{\Phi}$ and J^a_μ.

Appendix D.2.2 The dual transformation of $U(1)_{\mathrm{B}}$ phonons In the following, we perform a dual transformation of the NG boson associated with the breaking of $U(1)_{\mathrm{B}}$ symmetry. This mode corresponds to the fluctuation of the overall phase of Φ, which can be parametrized as $\Phi(x) = \mathrm{e}^{i\pi(x)}\psi(x)$, where $\pi(x)$ is a real scalar field. Substituting this into the following part in the Lagrangian (D2) leads to[19]

$$\begin{aligned}
& K_\mu \mathrm{Tr}\{(\partial_\mu \Phi)^\dagger (\partial^\mu \Phi)\} - 4i\gamma \mathrm{Tr}\{\Phi^\dagger \partial_0 \Phi\} \\
& \quad = K_\mu \left(\partial_\mu \pi\right)^2 M^2 - \partial^\mu \pi J^0_\mu + K_\mu \mathrm{Tr}(\partial_\mu \psi)^2 - 4i\gamma \mathrm{Tr}\{\psi^\dagger \partial_0 \psi\},
\end{aligned} \tag{D14}$$

with $J^0_\mu \equiv -4\delta_{\mu 0}\gamma M^2$ and $M^2 \equiv \mathrm{Tr}\left[\psi^\dagger \psi\right]$. We will transform the $U(1)_{\mathrm{B}}$ phonon field $\pi(x)$ into a massless two-form field $B^0_{\mu\nu}$. Note that the field $\pi(x)$ has a multivalued part in general; since $\pi(x)$ is the phase degree of freedom, $\pi(x)$ can be multivalued without violating the single-valuedness of $\Phi(x)$. In fact the multivalued part of $\pi(x)$ corresponds to a vortex. Let us denote the multivalued part of $\pi(x)$ as $\pi_{\mathrm{MV}}(x)$.

The dual transformation of this $U(1)_{\mathrm{B}}$ phonon field is essentially the same as the case of a superfluid. We basically follow the argument of Ref. [216]. Let us introduce an auxiliary field C_μ by

[19] The term $\mathrm{Tr}\left[\partial_\mu \psi^\dagger \psi - \psi^\dagger \partial_\mu \psi\right]$ automatically vanishes since ψ can be decomposed as $\psi = (\Delta + \rho)\mathbf{1}_N + (\chi^a + i\zeta^a)T^a$ and the modes ζ^a are absorbed by gluons.

linearizing the kinetic term of $\pi(x)$ in the partition function as follows:

$$\begin{aligned} Z &\propto \int \mathcal{D}\pi \mathcal{D}\pi_{\rm MV} \exp i \left[\int {\rm d}^4x \left(M^2 K_\mu \left\{ \partial_\mu (\pi + \pi_{\rm MV}) \right\}^2 - \partial^\mu (\pi + \pi_{\rm MV}) J^0_\mu \right) \right] \\ &\propto \int \mathcal{D}\pi \mathcal{D}\pi_{\rm MV} \mathcal{D}C_\mu \exp i \left[\int {\rm d}^4x \left(-\frac{C_\mu^2}{M^2} - 2C_\mu \sqrt{K_\mu} \partial^\mu (\pi + \pi_{\rm MV}) - \partial^\mu (\pi + \pi_{\rm MV}) J^0_\mu \right) \right]. \end{aligned} \tag{D15}$$

Integration over $\pi(x)$ gives a delta function

$$\int \mathcal{D}\pi \exp i \left[\int {\rm d}^4x \left(-2C_\mu \sqrt{K_\mu} \partial^\mu \pi + \pi \partial^\mu J^0_\mu \right) \right] = \delta \left\{ \partial^\mu \left(2C_\mu \sqrt{K_\mu} + J^0_\mu \right) \right\}. \tag{D16}$$

Then let us introduce the dual antisymmetric tensor field $B^0_{\mu\nu}$ by

$$\int \mathcal{D}C_\mu \delta \left\{ \partial^\mu \left(2C_\mu \sqrt{K_\mu} + J^0_\mu \right) \right\} \cdots = \int \mathcal{D}C_\mu \mathcal{D}B^0_{\mu\nu} \delta \left(2C_\mu \sqrt{K_\mu} + J^0_\mu - m^0 \partial^\nu \tilde{B}^0_{\mu\nu} \right) \cdots, \tag{D17}$$

where the dots denote the rest of the integrand and m^0 is a parameter. By this change of variables we have introduced an infinite gauge volume, corresponding to the transformation $\delta B^0_{\mu\nu} = \partial_\mu \Lambda_\nu - \partial_\nu \Lambda_\mu$ with a massless vector field Λ_μ. This can be taken care of by fixing the gauge later. There is no nontrivial Jacobian factor as the change of variables is linear. We integrating over C_μ, and transform a resultant term in the Lagrangian as

$$\begin{aligned} m^0 \partial^\nu \tilde{B}^0_{\mu\nu} \partial^\mu \pi_{\rm MV} &= -m^0 B^{0,\rho\sigma} \epsilon_{\mu\nu\rho\sigma} \partial^\nu \partial^\mu \pi_{\rm MV} \\ &\equiv -2\pi m^0 B^{0,\rho\sigma} \omega^0_{\rho\sigma}, \end{aligned} \tag{D18}$$

where the first equality holds up to a total derivative and we have defined

$$\omega^0_{\rho\sigma} \equiv \frac{1}{2\pi} \epsilon_{\mu\nu\rho\sigma} \partial^\nu \partial^\mu \pi_{\rm MV}. \tag{D19}$$

We thus obtain the dual Lagrangian for the $U(1)_{\rm B}$ phonon part

$$\mathcal{L}^*_{\rm Ph} = -\left(\frac{1}{2M} \right)^2 K_\mu (m^0 \partial_\nu \tilde{B}^0_{\mu\nu} - J^0_\mu)^2 - 2\pi m^0 B^{0,\mu\nu} \omega^0_{\mu\nu}. \tag{D20}$$

Note that the term linear in $B^0_{\mu\nu}$ coming from the first term of (D20) is a total derivative and does not contribute to the equation of motion. The partition function is proportional to

$$Z \propto \int \mathcal{D}\pi_{\rm MV} \mathcal{D}B^0_{\mu\nu} \exp i \left[\int {\rm d}^4x \mathcal{L}^*_{\rm Ph} \right]. \tag{D21}$$

The $U(1)_{\rm B}$ phonons are now described by a massless two-form field $B^0_{\mu\nu}$ and vortices appear as sources for $B^0_{\mu\nu}$.

Appendix D.3 The dual Lagrangian

We have shown that the partition function Z of the CFL phase is proportional to Z^* with the dual Lagrangian $\mathcal{L}^*$:

$$Z \propto Z^* = \int \mathcal{D}B^a_{\mu\nu}\mathcal{D}\pi_{\rm MV}\mathcal{D}B^0_{\mu\nu}\mathcal{D}\psi\,(\det K^{ab}_{\mu\nu})^{-1/2}\exp\left\{i\int {\rm d}^4x\mathcal{L}^*(x)\right\}, \tag{D22}$$

where

$$\mathcal{L}^* = \mathcal{L}^*_{\rm G} + \mathcal{L}^*_{\rm Ph} + K_\mu {\rm Tr}(\partial_\mu\psi)^2 - 4i\gamma{\rm Tr}\{\psi^\dagger\partial_0\psi\} - V(\psi). \tag{D23}$$

Here $\mathcal{L}^*_{\rm G}$ and $\mathcal{L}^*_{\rm Ph}$ are given in (D11) and (D20), respectively. The result above is valid for general vortex configurations. We can discuss the interaction between vortices and quasiparticles in terms of the dual Lagrangian. Vortices are expected to appear as a source term for gluons and $U(1)_{\rm B}$ phonons.

Appendix E. Derivation of fermion zero modes

We consider the BdG equation for the single component fermion. The Hamiltonian is given by the particle–hole basis as

$$\mathcal{H} = \begin{pmatrix} H_0 - \mu & |\Delta(r)|e^{i\theta}\gamma_0\gamma_5 \\ -|\Delta(r)|e^{-i\theta}\gamma_0\gamma_5 & H_0 + \mu \end{pmatrix}, \tag{E1}$$

where we define

$$H_0 = \begin{pmatrix} -\mu & -i\vec{\sigma}\cdot\vec{\nabla} \\ -i\vec{\sigma}\cdot\vec{\nabla}\gamma_5 & -\mu \end{pmatrix}. \tag{E2}$$

The BdG equation is then given by

$$\mathcal{H}\Psi_n = E\Psi_n, \tag{E3}$$

with the wave function

$$\Psi_n = \begin{pmatrix} \psi_{n+1} \\ \eta_n \end{pmatrix}, \tag{E4}$$

with the particle component (ψ_{n+1}) and the hole component (η_n). Then, the BdG equation is given explicitly as

$$\begin{pmatrix} H_0 - \mu & |\Delta(r)|e^{i\theta}\gamma_0\gamma_5 \\ -|\Delta(r)|e^{-i\theta}\gamma_0\gamma_5 & H_0 + \mu \end{pmatrix}\begin{pmatrix} \psi_{n+1} \\ \eta_n \end{pmatrix} = E\begin{pmatrix} \psi_{n+1} \\ \eta_n \end{pmatrix}. \tag{E5}$$

The particle and hole components are written as

$$\psi_{n+1} = \begin{pmatrix} f(r)\Phi_n \\ i\,g(r)\Phi_{n+1} \\ \pm f(r)\Phi_n \\ \pm i\,g(r)\Phi_{n+1} \end{pmatrix}e^{-ik_z z},\ \eta_n = \begin{pmatrix} \bar{f}(r)\Phi_n \\ i\,\bar{g}(r)\Phi_{n+1} \\ \mp\bar{f}(r)\Phi_n \\ \mp i\,\bar{g}(r)\Phi_{n+1} \end{pmatrix}e^{ik_z z}, \tag{E6}$$

where we introduce four functions $f(r)$, $g(r)$, $\bar{f}(r)$, and $\bar{g}(r)$, and define $\Phi_n = e^{in\theta}$. Here $\pm$ ($\mp$) refers to the eigenvalue of γ_5. From Eq. (E5), we obtain

$$(-\mu \pm k_z) f \pm \left(\frac{\partial}{\partial r} + \frac{n+2}{r}\right) g \mp |\Delta| \bar{f} = E f, \tag{E7}$$

$$\mp \left(\frac{\partial}{\partial r} - \frac{n+1}{r}\right) f + (-\mu \mp k_z) g \mp |\Delta| \bar{g} = E g, \tag{E8}$$

$$(\mu \mp k_z) \bar{f} \mp \left(\frac{\partial}{\partial r} + \frac{n+1}{r}\right) \bar{g} \mp |\Delta| f = E \bar{f}, \tag{E9}$$

$$\pm \left(\frac{\partial}{\partial r} - \frac{n}{r}\right) \bar{f} + (\mu \pm k_z) \bar{g} \mp |\Delta| g = E \bar{g}. \tag{E10}$$

Now, we consider the solution of the zero-mode fermion with $E = 0$. Here, we impose the "Majorana condition",

$$\Psi = U \Psi^*, \tag{E11}$$

with the unitary matrix

$$U = \begin{pmatrix} 0 & \gamma_2 \\ \gamma_2 & 0 \end{pmatrix}, \tag{E12}$$

which satisfies

$$U^{-1} \mathcal{H} U = -\mathcal{H}^*. \tag{E13}$$

We then find that the Majorana condition leads to the solution with $E = 0$. From the BdG equation, $\mathcal{H}\Psi = E\Psi$, we obtain $\mathcal{H}^*\Psi^* = E\Psi^*$, which in turn gives $\mathcal{H}\Psi = -E\Psi$ from $\Psi = U\Psi^*$ and $U^{-1}\mathcal{H}U = -\mathcal{H}^*$. Therefore, we obtain $E = 0$. The Majorana condition restricts the wave functions, ψ_{n+1} and η_n, as

$$n = -1 \tag{E14}$$

and

$$\bar{f} = \mp g, \tag{E15}$$

$$\bar{g} = f. \tag{E16}$$

Thus, we find the BdG equation simplified to

$$-\mu f \pm \left(\frac{\partial}{\partial r} + \frac{1}{r}\right) g + |\Delta| g = 0, \tag{E17}$$

$$\mp \frac{\partial}{\partial r} f - \mu g - |\Delta| f = 0, \tag{E18}$$

$$\mp \mu g - \frac{\partial}{\partial r} f \mp |\Delta| f = 0, \tag{E19}$$

$$-\left(\frac{\partial}{\partial r} + \frac{1}{r}\right) g \mp \mu f \mp |\Delta| g = 0, \tag{E20}$$

with $k_z = 0$, which turns out to be the two independent equations,

$$\mp \frac{\partial}{\partial r} f - |\Delta| f - \mu g = 0, \tag{E21}$$

$$\pm \left(\frac{\partial}{\partial r} + \frac{1}{r}\right) g + |\Delta| g - \mu f = 0. \tag{E22}$$

When we eliminate $g(r)$, we obtain the equation only for $f(r)$,

$$\frac{\partial^2}{\partial r^2} f + \frac{1}{r}\frac{\partial}{\partial r} \pm 2|\Delta|\frac{\partial}{\partial r} f \pm \frac{|\Delta|}{r} f + (\mu^2 + |\Delta|^2) f = 0. \tag{E23}$$

The solution of this equation is given as

$$f(r) = Ce^{-\int_0^r |\Delta(r')| \mathrm{d}r'} J_0(\mu r), \tag{E24}$$

with the condition that it is regular at $r = 0$ and infinitely large r. As a consequence, we find the other components as

$$g(r) = \pm Ce^{-\int_0^r |\Delta(r')| \mathrm{d}r'} J_1(\mu r), \tag{E25}$$

$$\bar{f}(r) = \mp Ce^{-\int_0^r |\Delta(r')| \mathrm{d}r'} J_1(\mu r), \tag{E26}$$

$$\bar{g}(r) = Ce^{-\int_0^r |\Delta(r')| \mathrm{d}r'} J_0(\mu r). \tag{E27}$$

This is the wave function of the Majorana fermion.

Funding

Open Access funding: SCOAP[3].

References

[1] J. R. Abo-Shaeer, C. Raman, W. Vogels, and J. M. Ketterle, Science **292**, 476 (2001).
[2] E. Abrahams and T. Tsuneto, Phys. Rev. **152**, 416 (1966).
[3] A. A. Abrikosov, Sov. Phys. JETP **5**, 1174 (1957).
[4] H. Abuki, Nucl. Phys. A **791**, 117 (2007).
[5] H. Abuki, T. Hatsuda, and K. Itakura, Phys. Rev. D **65**, 074014 (2002).
[6] M. G. Alford, Annu. Rev. Nucl. Part. Sci. **51**, 131 (2001).
[7] M. G. Alford, J. Berges, and K. Rajagopal, Nucl. Phys. B **558**, 219 (1999).
[8] M. G. Alford, J. Berges, and K. Rajagopal, Nucl. Phys. B **571**, 269 (2000).
[9] M. G. Alford, J. March-Russell, and F. Wilczek, Nucl. Phys. B **328**, 140 (1989).
[10] M. G. Alford, K. Rajagopal, S. Reddy, and F. Wilczek, Phys. Rev. D **64**, 074017 (2001).
[11] M. G. Alford, K. Rajagopal, and F. Wilczek, Phys. Lett. B **422**, 247 (1998).
[12] M. G. Alford, K. Rajagopal, and F. Wilczek, Nucl. Phys. B **537**, 443 (1999).
[13] M. G. Alford, A. Schmitt, K. Rajagopal, and T. Schafer, Rev. Mod. Phys. **80**, 1455 (2008).
[14] M. G. Alford and A. Sedrakian, J. Phys. G **37**, 075202 (2010).
[15] M. G. Alford and F. Wilczek, Phys. Rev. Lett. **62**, 1071, (1989).
[16] J. Alicea, Phys. Rev. B **81**, 125318 (2010).
[17] J. Ambjorn and P. Olesen, Phys. Lett. B **214**, 565 (1988).
[18] J. Ambjorn and P. Olesen, Nucl. Phys. B **315**, 606 (1989).
[19] P. W. Anderson and N. Itoh, Nature **256**, 25 (1975).
[20] N. Andersson, B. Haskell, and G. L. Comer, Phys. Rev. D **82**, 023007 (2010).
[21] A. F. Andreev, Sov. Phys. JETP **20**, 1490 (1965).
[22] R. Anglani et al., arXiv:1302.4264 [hep-ph].
[23] R. Anglani, M. Mannarelli, and M. Ruggieri, New J. Phys. **13**, 055002 (2011).
[24] R. Auzzi, M. Shifman, and A. Yung, Phys. Rev. D **72**, 025002 (2005).
[25] R. Auzzi, S. Bolognesi, J. Evslin, K. Konishi, and A. Yung, Nucl. Phys. B **673**, 187 (2003).
[26] R. Auzzi, M. Eto, and W. Vinci, J. High Energy Phys. **02**, 100 (2008).
[27] E. Babaev, Phys. Rev. Lett. **89**, 067001 (2002).
[28] E. Babaev and N. W. Ashcroft, Nature Phys. **3**, 530 (2007).
[29] E. Babaev, A. Sudbo, and N. W. Ashcroft, Nature **431**, 666 (2004).
[30] C. Bachas and T. N. Tomaras, Nucl. Phys. B **428**, 209 (1994).
[31] D. Bailin and A. Love, J. Phys. A **12**, L283 (1979).

[32] D. Bailin and A. Love, Phys. Rept. **107**, 325 (1984).
[33] A. P. Balachandran and S. Digal, Phys. Rev. D **66**, 034018 (2002).
[34] A. P. Balachandran and S. Digal, Int. J. Mod. Phys. A **17**, 1149 (2002).
[35] A. P. Balachandran, S. Digal, and T. Matsuura, Phys. Rev. D **73**, 074009 (2006).
[36] G. S. Bali, Phys. Rept. **343**, 1 (2001).
[37] T. Banks and E. Rabinovici, Nucl. Phys. B **160**, 349 (1979).
[38] B. C. Barrois, Nucl. Phys. B **129**, 390 (1977).
[39] G. Basar and G. V. Dunne, Phys. Rev. D **78**, 065022 (2008).
[40] G. Basar and G. V. Dunne, Phys. Rev. Lett. **100**, 200404 (2008).
[41] G. Basar, G. V. Dunne, and M. Thies, Phys. Rev. D **79**, 105012 (2009).
[42] G. Baym, C. Pethick, and D. Pines, Nature **224**, 673 (1969).
[43] S. R. Beane, P. F. Bedaque, and M. J. Savage, Phys. Lett. B **483**, 131 (2000).
[44] P. F. Bedaque, Phys. Lett. B **524**, 137 (2002).
[45] P. F. Bedaque, E. Berkowitz, and A. Cherman, Phys. Rev. D **84**, 023006 (2011).
[46] P. F. Bedaque, E. Berkowitz, G. Ji, and N. Ng, Phys. Rev. D **85**, 043008 (2012).
[47] P. F. Bedaque and T. Schafer, Nucl. Phys. A **697**, 802 (2002).
[48] A. A. Belavin, A. M. Polyakov, A. S. Schwartz, and Yu. S. Tyupkin, Phys. Lett. B **59**, 85 (1975).
[49] V. L. Berezinskii, Sov. Phys. JETP **32**, 493 (1971).
[50] V. L. Berezinskii, Sov. Phys. JETP **34**, 610 (1972).
[51] D. L. Bergman and K. Le Hur, Phys. Rev. B **79**, 184520 (2009).
[52] G. P. Bewley, M. S. Paoletti, K. R. Sreenivasan, and D. P. Lathrop, Proc. Nat. Acad. Sci. USA, **105**, 13707 (2008).
[53] R. Blaauwgeers, V. B. Eltsov, G. Eska, A. P. Finne, R. P. Haley, M. Krusius, J. J. Ruohio, L. Skrbek, and G. E. Volovik, Phys. Rev. Lett. **89**, 155301 (2002).
[54] D. B. Blaschke, D. Gomez Dumm, A. G. Grunfeld, T. Klahn, and N. N. Scoccola, Phys. Rev. C **75**, 065804 (2007).
[55] G. Blatter, M. V. Feigel'man, V. B. Geshkenbein, A. I. Larkin, and V. M. Vinokur, Rev. Mod. Phys. **66**, 1125 (1994).
[56] M. O. Borgh and J. Ruostekoski, Phys. Rev. Lett. **109**, 015302 (2012).
[57] M. O. Borgh and J. Ruostekoski, Phys. Rev. A **87**, 033617 (2013).
[58] R. H. Brandenberger, A.-C. Davis, and A. M. Matheson, Nucl. Phys. B **307**, 909 (1988).
[59] R. H. Brandenberger and X.-m. Zhang, Phys. Rev. D **59**, 081301 (1999).
[60] K. B. W. Buckley, Phys. Rev. D **65**, 125011 (2002).
[61] K. B. W. Buckley, M. A. Metlitski, and A. R. Zhitnitsky, Phys. Rev. D **68**, 105006 (2003).
[62] K. B. W. Buckley and A. R. Zhitnitsky, J. High Energy Phys. **08**, 013 (2002).
[63] C. G. Callan Jr., Phys. Rev. D **25**, 2141 (1982).
[64] C. G. Callan Jr., Phys. Rev. D **26**, 2058 (1982).
[65] C. G. Callan Jr., Nucl. Phys. B **212**, 391 (1983).
[66] C. G. Callan Jr., S. R. Coleman, J. Wess, and B. Zumino, Phys. Rev. **177**, 2247 (1969).
[67] C. Callias, Commun. Math. Phys. **62**, 213 (1978).
[68] B. M. Caradoc-Davies, R. J. Ballagh, and P. B. Blakie, Phys. Rev. A **62**, 011602 (2000).
[69] C. Caroli, P. G. De Gennes, and J. Matricon, Phys. Lett. **9**, 307 (1964).
[70] B. Carter, R. H. Brandenberger, and A.-C. Davis, Phys. Rev. D **65**, 103520 (2002).
[71] R. Casalbuoni and R. Gatto, Phys. Lett. B **464**, 111 (1999).
[72] R. Casalbuoni and G. Nardulli, Rev. Mod. Phys. **76**, 263 (2004).
[73] M. N. Chernodub and V. I. Zakharov, Phys. Atom. Nucl. **72**, 2136 (2009).
[74] M. Cipriani and M. Nitta, Phys. Rev. Lett. **111**, 170401 (2013).
[75] M. Cipriani and M. Nitta, Phys. Rev. A **88**, 013634 (2013).
[76] M. Cipriani, W. Vinci, and M. Nitta, Phys. Rev. D **86**, 121704 (2012).
[77] T. E. Clark, M. Nitta, and T. ter Veldhuis, Phys. Rev. D **67**, 085026 (2003).
[78] S. R. Coleman, Commun. Math. Phys. **31**, 259 (1973).
[79] S. R. Coleman, J. Wess, and B. Zumino, Phys. Rev. **177**, 2239 (1969).
[80] H. S. M. Coxeter, Annals Math. **35**, 588 (1934).
[81] A. D'Adda, P. Di Vecchia, and M. Luscher, Nucl. Phys. B **152**, 125 (1979).
[82] S. Das Sarma, C. Nayak, and S. Tewari, Phys. Rev. B **73**, 220502 (2006).
[83] R. L. Davis, Phys. Rev. D **40**, 4033 (1989).

[84] R. L. Davis and E. P. S. Shellard, Nucl. Phys. B **323**, 209 (1989).
[85] R. L. Davis and E. P. S. Shellard, Phys. Rev. Lett. **63**, 2021 (1989).
[86] P. G. De Gennes, *Superconductivity of Metals and Alloys*, (Addison-Wesley, Boston, 1989), Advanced Book Classics.
[87] P. Demorest, T. Pennucci, S. Ransom, M. Roberts, and J. Hessels, Nature **467**, 1081 (2010).
[88] G. H. Derrick, J. Math. Phys. **5**, 1252 (1964).
[89] M. Dine, W. Fischler, and M. Srednicki, Phys. Lett. B **104**, 199 (1981).
[90] R. J. Donnelly, *Quantized Vortices in Helium II* (Cambridge University Press, Cambridge, UK, 1991), 2nd ed. in Cambridge Studies in American Literature and Culture.
[91] T. Eguchi, P. B. Gilkey, and A. J. Hanson, Phys. Rept. **66**, 213 (1980).
[92] M. Eto, L. Ferretti, K. Konishi, G. Marmorini, M. Nitta, K. Ohashi, W. Vinci, and N. Yokoi, Nucl. Phys. B **780**, 161 (2007).
[93] M. Eto, T. Fujimori, S. B. Gudnason, Y. Jiang, K. Konishi, M. Nitta, and K. Ohashi, J. High Energy Phys. **11**, 042 (2010).
[94] M. Eto, T. Fujimori, T. Nagashima, M. Nitta, K. Ohashi, and N. Sakai, Phys. Rev. D **79**, 045015 (2009).
[95] M. Eto, T. Fujimori, T. Nagashima, M. Nitta, K. Ohashi, and N. Sakai, Phys. Lett. B **678**, 254 (2009).
[96] M. Eto, T. Fujimori, M. Nitta, K. Ohashi, and N. Sakai, Phys. Rev. D **84**, 125030 (2011).
[97] M. Eto, T. Fujimori, M. Nitta, K. Ohashi, and N. Sakai, Prog. Theor. Phys. **128**, 67 (2012).
[98] M. Eto, K. Hashimoto, and T. Hatsuda, Phys. Rev. D **88**, 081701 (2013).
[99] M. Eto, K. Hashimoto, H. Iida, Y. Maezawa, and T. Ishii, Phys. Rev. D **85**, 114038 (2012).
[100] M. Eto, K. Hashimoto, H. Iida, and A. Miwa, Phys. Rev. **D83**, 125033 (2011).
[101] M. Eto, K. Hashimoto, G. Marmorini, M. Nitta, K. Ohashi, and W. Vinci, Phys. Rev. Lett. **98**, 091602 (2007).
[102] M. Eto, Y. Hirono, and M. Nitta arXiv:1309.4559 [hep-ph].
[103] M. Eto, Y. Isozumi, M. Nitta, and K. Ohashi, Nucl. Phys. B **752**, 140 (2006).
[104] M. Eto, Y. Isozumi, M. Nitta, K. Ohashi, and N. Sakai, Phys. Rev. D **72**, 025011 (2005).
[105] M. Eto, Y. Isozumi, M. Nitta, K. Ohashi, and N. Sakai, Phys. Rev. D **73**, 125008 (2006).
[106] M. Eto, Y. Isozumi, M. Nitta, K. Ohashi, and N. Sakai, Phys. Rev. Lett. **96**, 161601 (2006).
[107] M. Eto, Y. Isozumi, M. Nitta, K. Ohashi, and N. Sakai, J. Phys. A **39**, R315 (2006).
[108] M. Eto, K. Kasamatsu, M. Nitta, H. Takeuchi, and M. Tsubota, Phys. Rev. A **83**, 063603 (2011).
[109] M. Eto, K. Konishi, G. Marmorini, M. Nitta, K. Ohashi, W. Vinci, and N. Yokoi Phys. Rev. D **74**, 065021 (2006).
[110] M. Eto, E. Nakano, and M. Nitta, Phys. Rev. D **80**, 125011 (2009).
[111] M. Eto, E. Nakano, and M. Nitta, Nucl. Phys. B **821**, 129 (2009).
[112] M. Eto and M. Nitta, Phys. Rev. D **80**, 125007 (2009).
[113] M. Eto and M. Nitta, Phys. Rev. A **85**, 053645 (2012).
[114] M. Eto and M. Nitta, EPL (Europhys. Lett.) **103**, 60006 (2013).
[115] M. Eto, M. Nitta, and N. Yamamoto, Phys. Rev. Lett. **104**, 161601 (2010).
[116] M. Eto, M. Nitta, and N. Yamamoto, Phys. Rev. D **83**, 085005 (2011).
[117] E. J. Ferrer arXiv:1110.2081 [nucl-th].
[118] E. J. Ferrer and V. de la Incera, Phys. Rev. Lett. **97**, 122301 (2006).
[119] E. J. Ferrer and V. de la Incera, Phys. Rev. D **76**, 114012 (2007).
[120] E. J. Ferrer and V. de la Incera, Phys. Rev. D **76**, 045011 (2007).
[121] E. J. Ferrer and V. de la Incera, Lect. Notes Phys. **871**, 399 (2013).
[122] E. J. Ferrer, V. de la Incera, and C. Manuel, Phys. Rev. Lett. **95**, 152002 (2005).
[123] E. J. Ferrer, V. de la Incera, and C. Manuel, Nucl. Phys. B **747**, 88 (2006).
[124] E. J. Ferrer and V. de la Incera, J. Phys. A **40**, 6913 (2007).
[125] A. L. Fetter, Rev. Mod. Phys. **81**, 647 (2009).
[126] A. L Fetter and A. A Svidzinsky, J. Phys.: Condens. Matter **13**, R135 (2001).
[127] M. McNeil Forbes and A. R. Zhitnitsky, J. High Energy Phys. **10**, 013 (2001).
[128] M. McNeil Forbes and A. R. Zhitnitsky, Phys. Rev. D **65**, 085009 (2002).
[129] E. H. Fradkin and S. H. Shenker, Phys. Rev. D **19**, 3682 (1979).
[130] D. Z. Freedman and P. K. Townsend, Nucl. Phys. B **177**, 282 (1981).
[131] L. Fu and C. L. Kane, Phys. Rev. Lett. **100**, 096407 (2008).
[132] T. Fujimori, G. Marmorini, M. Nitta, K. Ohashi, and N. Sakai, Phys. Rev. D **82**, 065005 (2010).

[133] T. Fujimori, M. Nitta, K. Ohta, N. Sakai, and M. Yamazaki, Phys. Rev. D **78**, 105004 (2008).
[134] T. Fujiwara, T. Fukui, M. Nitta, and S. Yasui, Phys. Rev. D **84**, 076002 (2011).
[135] T. Fukui, Phys. Rev. B **81**, 214516 (2010).
[136] T. Fukui and T. Fujiwara, J. Phys. Soc. Jpn. **79**, 033701 (2010).
[137] T. Fukui and T. Fujiwara, Phys. Rev. B **82**, 184536 (2010).
[138] K. Fukushima and T. Hatsuda, Rep. Prog. Phys. **74**, 014001 (2011).
[139] K. Fukushima, D. E. Kharzeev, and H. J. Warringa, Phys. Rev. D **78**, 074033 (2008).
[140] P. Fulde and R. A. Ferrell, Phys. Rev. **135**, A550 (1964).
[141] K. Furuta, T. Inami, H. Nakajima, and M. Nitta, Prog. Theor. Phys. **106**, 851 (2001).
[142] J. P. Gauntlett, R. Portugues, D. Tong, and P. K. Townsend, Phys. Rev. D **63**, 085002 (2001).
[143] I. Giannakis and H.-c. Ren, Phys. Rev. D **65**, 054017 (2002).
[144] I. Giannakis and H.-c. Ren, Nucl. Phys. B **669**, 462 (2003).
[145] K. Glampedakis, D. I. Jones, and L. Samuelsson, Phys. Rev. Lett. **109**, 081103 (2012).
[146] N. K. Glendenning, *Compact Stars: Nuclear Physics, Particle Physics, and General Relativity* (Springer, Berlin, 2000), Astronomy and Astrophysics Library.
[147] E. V. Gorbar, J. Jia, and V. A. Miransky, Phys. Rev. D **73**, 045001 (2006).
[148] A. Gorsky and V. Mikhailov, Phys. Rev. D **76**, 105008 (2007).
[149] A. Gorsky, M. Shifman, and A. Yung, Phys. Rev. D **71**, 045010 (2005).
[150] A. Gorsky, M. Shifman, and A. Yung, Phys. Rev. D **83**, 085027 (2011).
[151] A. Gorsky and M. B. Voloshin, Phys. Rev. D **82**, 086008 (2010).
[152] J. Goryo, S. Soma, and H. Matsukawa, Europhys. Lett. **80**, 17002 (2007).
[153] T. Goto, Prog. Theor. Phys. **46**, 1560 (1971).
[154] J. Greensite, Prog. Part. Nucl. Phys. **51**, 1 (2003).
[155] I. Guillamon, H. Suderow, S. Vieira, L. Cario, P. Diener, and P. Rodiere, Phys. Rev. Lett. **101**, 166407 (2008).
[156] V. Gurarie and L. Radzihovsky, Phys. Rev. B **75**, 212509 (2007).
[157] F. Gygi and M. Schluter, Phys. Rev. B **41**, 822 (1990).
[158] F. Gygi and M. Schluter, Phys. Rev. B **43**, 7609 (1991).
[159] A. Hanany and D. Tong, J. High Energy Phys. **07**, 037 (2003).
[160] A. Hanany and D. Tong, J. High Energy Phys. **04**, 066 (2004).
[161] R. Hanninen, R. Blaauwgeers, V. B. Eltsov, A. P. Finne, M. Krusius, E. V. Thuneberg, and G. E. Volovik, Phys. Rev. Lett. **90**, 225301 (2003).
[162] H. Hasimoto, J. Fluid Mech. **51**, 477 (1972).
[163] M. Hatsuda, S. Yahikozawa, P. Ao, and D. J. Thouless, Phys. Rev. B **49**, 15870 (1994).
[164] T. Hatsuda, M. Tachibana, and N. Yamamoto, Phys. Rev. D **78**, 011501 (2008).
[165] T. Hatsuda, M. Tachibana, N. Yamamoto, and G. Baym, Phys. Rev. Lett. **97**, 122001 (2006).
[166] I. F. Herbut, Phys. Rev. Lett. **104**, 066404 (2010).
[167] I. F. Herbut, Phys. Rev. B **81**, 205429 (2010).
[168] Y. Hidaka, Phys. Rev. Lett. **110**, 091601 (2013).
[169] M. B. Hindmarsh and T. W. B. Kibble, Rep. Prog. Phys. **58**, 477 (1995).
[170] Y. Hirono, T. Kanazawa, and M. Nitta, Phys. Rev. D **83**, 085018 (2011).
[171] Y. Hirono and M. Nitta, Phys. Rev. Lett. **109**, 062501 (2012).
[172] Y. Hirono, S. Yasui, K. Itakura, and M. Nitta, Phys. Rev. B **86**, 014508 (2012).
[173] T. L. Ho, Phys. Rev. Lett. **81**, 742 (1998).
[174] D. K. Hong, S.-T. Hong, and Y.-J. Park, Phys. Lett. B **499**, 125 (2001).
[175] D. K. Hong, M. Rho, and I. Zahed, Phys. Lett. B **468**, 261 (1999).
[176] C.-Y. Hou, C. Chamon, and C. Mudry, Phys. Rev. B **81**, 075427 (2010).
[177] J. E. Humphreys, *Reflection Groups and Coxeter Groups* (Cambridge University Press, Cambridge, UK, 1992), Cambridge Studies in Advanced Mathematics.
[178] K. Iida, T. Matsuura, M. Tachibana, and T. Hatsuda, Phys. Rev. Lett. **93**, 132001 (2004).
[179] K. Iida, T. Matsuura, M. Tachibana, and T. Hatsuda, Phys. Rev. D **71**, 054003 (2005).
[180] K. Iida, Phys. Rev. D **71**, 054011 (2005).
[181] K. Iida and G. Baym, Phys. Rev. D **63**, 074018 (2001).
[182] K. Iida and G. Baym, Phys. Rev. D **65**, 014022 (2002).
[183] K. Iida and G. Baym, Phys. Rev. D **66**, 014015 (2002).
[184] Y. Isozumi, M. Nitta, K. Ohashi, and N. Sakai, Phys. Rev. D **71**, 065018 (2005).

[185] D. A. Ivanov, Phys. Rev. Lett. **86**, 268 (2001).
[186] E. A. Ivanov and V. I. Ogievetsky, Teor. Mat. Fiz. **25**, 164 (1975).
[187] M. Iwasaki and T. Iwado, Phys. Lett. B **350**, 163 (1995).
[188] R. Jackiw and C. Rebbi, Phys. Rev. D **13**, 3398 (1976).
[189] R. Jackiw and P. Rossi, Nucl. Phys. B **190**, 681 (1981).
[190] A. D. Jackson and F. Sannino, Phys. Lett. B **578**, 133 (2004).
[191] P. Jaikumar, M. Prakash, and T. Schafer, Phys. Rev. D **66**, 063003 (2002).
[192] J. Jang, D. G. Ferguson, V. Vakaryuk, R. Budakian, S. B. Chung, P. M. Goldbart, and Y. Maeno, Science **331**, 186 (2011).
[193] M. Kalb and P. Ramond, Phys. Rev. D **9**, 2273 (1974).
[194] D. B. Kaplan and S. Reddy, Phys. Rev. Lett. **88**, 132302 (2002).
[195] D. B. Kaplan and S. Reddy, Phys. Rev. D **65**, 054042 (2002).
[196] K. Kasamatsu, H. Takeuchi, and M. Nitta, J. Phys.: Condens. Matter, **25**, 404213 (2013).
[197] K. Kasamatsu, H. Takeuchi, M. Nitta, and M. Tsubota, J. High Energy Phys. **11**, 068 (2010).
[198] K. Kasamatsu, H. Takeuchi, M. Tsubota, and M. Nitta, Phys. Rev. A **88**, 013620 (2013).
[199] K. Kasamatsu and M. Tsubota, *Progress in Low Temperature Physics: Quantum Turbulence*, **16**, 351 (2009).
[200] K. Kasamatsu, M. Tsubota, and M. Ueda, Int. J. Mod. Phys. B **19**, 1835 (2005).
[201] D. E. Kharzeev, L. D. McLerran, and H. J. Warringa, Nucl. Phys. A **A803**, 227 (2008).
[202] D. E. Kharzeev, H.-U. Yee, and I. Zahed, Phys. Rev. D **84**, 037503 (2011).
[203] T. W. B. Kibble, J. Phys. A **9**, 1387 (1976).
[204] A. Yu. Kitaev, Ann. Phys. (N.Y.) **303**, 2 (2003).
[205] A. Kitaev, Ann. Phys. (N.Y.) **321**, 2 (2006).
[206] M. Kobayashi, Y. Kawaguchi, M. Nitta, and M. Ueda, Phys. Rev. Lett. **103**, 115301 (2009).
[207] M. Kobayashi and M. Nitta, arXiv:1307.6632 [hep-th].
[208] K.-I. Kondo, Phys. Rev. D **57**, 7467 (1998).
[209] K. Konishi, Prog. Theor. Phys. Suppl. **177**, 83 (2009).
[210] K. Konishi, Int. J. Mod. Phys. A **25**, 5025 (2010).
[211] J. Koplik and H. Levine, Phys. Rev. Lett. **71**, 1375 (1993).
[212] J. M. Kosterlitz and D. J. Thouless, J. Phys. C **6**, 1181(1973).
[213] A. Kryjevski, Phys. Rev. D **77**, 014018 (2008).
[214] A. I. Larkin and Y. N. Ovchinnikov, Zh. Eksp. Teor. Fiz. **47**, 1136 (1964).
[215] H. K. Lee and M. Rho, arXiv:0905.0235 [hep-ph].
[216] K.-M. Lee, Phys. Rev. D, **48**, 2493 (1993).
[217] P. A. Lee, arXiv:0907.2681 [cond-mat.str-el].
[218] N. C. Leung and C. Vafa, Adv. Theor. Math. Phys. **2**, 91 (1998).
[219] J. Liao and E. Shuryak, Phys. Rev. C **77**, 064905 (2008).
[220] J. Linder, Y. Tanaka, T. Yokoyama, A. Sudbo, and N. Nagaosa, Phys. Rev. Lett. **104**, 067001 (2010).
[221] L.-X. Liu and M. Nitta, Int. J. Mod. Phys. A **27**, 1250097 (2012).
[222] I. Low and A. V. Manohar, Phys. Rev. Lett. **88**, 101602 (2002).
[223] F. Lund and T. Regge, Phys. Rev. D **14**, 1524 (1976).
[224] K. Machida and H. Nakanishi, Phys. Rev. B **30**, 122 (1984).
[225] M. Machida and T. Koyama, Phys. Rev. Lett. **90**, 077003 (2003).
[226] M. Machida and T. Koyama, Phys. Rev. Lett. **94**, 140401 (2005).
[227] S. Mandelstam, Phys. Rept. **23**, 245 (1976).
[228] M. Mannarelli and C. Manuel, Phys. Rev. D **77**, 103014 (2008).
[229] M. Mannarelli and C. Manuel, Phys. Rev. D **81**, 043002 (2010).
[230] M. Mannarelli, C. Manuel, and B. A. Sa'd, Phys. Rev. Lett. **101**, 241101 (2008).
[231] N. Manton and P. M. Sutcliffe, *Topological Solitons*, (Cambridge University Press, Cambridge, UK, 2007).
[232] N. S. Manton, Phys. Lett. B **110**, 54 (1982).
[233] C. Manuel and M. H. G. Tytgat, Phys. Lett. B **479**, 190 (2000).
[234] V. Markov, A. Marshakov, and A. Yung, Nucl. Phys. B **709**, 267 (2005).
[235] K. Masuda, T. Hatsuda, and T. Takatsuka, Astrophys. J. **764**, 12 (2013).
[236] T. Matsuura, *Ginzburg-Landau Approach to Color Superconductivity*, Tokyo University (2005).
[237] M. Matsuzaki, Phys. Rev. D **62**, 017501 (2000).

[238] N. D. Mermin, *Quantum Fluids and Solids*, eds. S. B. Trickey, E. D. Adams, and J. W. Dufty (Plenum, New York, 1977) pp. 3–22.
[239] N. D. Mermin and H. Wagner, Phys. Rev. Lett. **17**, 1133 (1966).
[240] N. D. Mermin, Rev. Mod. Phys. **51**, 591 (1979).
[241] E. J. Mueller and T. L. Ho, Phys. Rev. Lett. **88**, 180403 (2002).
[242] E. Nakano, M. Nitta, and T. Matsuura, Phys. Rev. D **78**, 045002 (2008).
[243] E. Nakano, M. Nitta, and T. Matsuura, Prog. Theor. Phys. Suppl. **174**, 254 (2008).
[244] E. Nakano, M. Nitta, and T. Matsuura, Phys. Lett. B **672**, 61 (2009).
[245] Y. Nambu, Phys. Rev. D **10**, 4262 (1974).
[246] C. Nayak, S. H. Simon, A. Stern, M. Freedman, and S. Das Sarma, Rev. Mod. Phys. **80**, 1083 (2008).
[247] S. Nazarenko and R. West, J. Low Temp. Phys. **132**, 1 (2003).
[248] D. Nickel and M. Buballa, Phys. Rev. D **79**, 054009 (2009).
[249] B. Niebergal, R. Ouyed, R. Negreiros, and F. Weber, Phys. Rev. D **81**, 043005 (2010).
[250] H. B. Nielsen and S. Chadha, Nucl. Phys. B **105**, 445 (1976).
[251] H. B. Nielsen and P. Olesen, Nucl. Phys. B **61**, 45 (1973).
[252] N. K. Nielsen and P. Olesen, Nucl. Phys. B **144**, 376 (1978).
[253] Y. Nishida, Phys. Rev. D **81**, 074004 (2010).
[254] Y. Nishida and H. Abuki, Phys. Rev. D **72**, 096004 (2005).
[255] M. Nitta, Phys. Rev. D **87**, 025013 (2013).
[256] M. Nitta, Nucl. Phys. B **872**, 62 (2013).
[257] M. Nitta, M. Eto, and M. Cipriani, J. Low Temp. Phys. (to appear) arXiv:1307.4312 [cond-mat.quant-gas].
[258] M. Nitta, M. Eto, T. Fujimori, and K. Ohashi, J. Phys. Soc. Jpn. **81**, 084711 (2012).
[259] M. Nitta, K. Kasamatsu, M. Tsubota, and H. Takeuchi, Phys. Rev. A **85**, 053639 (2012).
[260] M. Nitta, M. Shifman, and W. Vinci, Phys. Rev. D **87**, 081702 (2013).
[261] M. Nitta and N. Shiiki, Phys. Lett. B **658**, 143 (2008).
[262] T. Noda, M. Hashimoto, N. Yasutake, T. Maruyama, T. Tatsumi, and M. Fujimoto, Astrophys. J. **765**, 1 (2013).
[263] J. Noronha and A. Sedrakian, Phys. Rev. D **77**, 023008 (2008).
[264] T. Ohmi and K. Machida, J. Phys. Soc. Jpn. **67**, 1822 (1998).
[265] Yu. N. Ovchinnikov and I. M. Sigal, Nonlinearity **11**, 1277 (1998).
[266] D. Page and S. Reddy, Ann. Rev. Nucl. Part. Sci. **56**, 327 (2006).
[267] M. S. Paoletti and D. P. Lathrop, Ann. Rev. Condens. Matter Phys. **2**, 213 (2011).
[268] R. D. Peccei and H. R. Quinn, Phys. Rev. D **16**, 1791 (1977).
[269] R. D. Peccei and H. R. Quinn, Phys. Rev. Lett. **38**, 1440 (1977).
[270] L. Perivolaropoulos, Nucl. Phys. B **375**, 665 (1992).
[271] L. Perivolaropoulos, Phys. Rev. D **48**, 5961 (1993).
[272] J. K. Perring and T. H. R. Skyrme, Nucl. Phys. **31**, 550 (1962).
[273] C. J Pethick and H. Smith, *Bose–Einstein Condensation in Dilute Gases* (Cambridge University Press, Cambridge, UK, 2002).
[274] L. P. Pitaevskii and S. Stringari, *Bose–Einstein Condensation* (Clarendon, Oxford, UK, 2003), Vol. 116.
[275] B. Plohr, J. Math. Phys. **22**, 2184 (1981).
[276] A. M. Polyakov and A. A. Belavin, JETP Lett. **22**, 245 (1975).
[277] J. Preskill and A. Vilenkin, Phys. Rev. D **47**, 2324 (1993).
[278] X.-L. Qi, T. L. Hughes, S. Raghu, and S.-C. Zhang, Phys. Rev. Lett. **102**, 187001 (2009).
[279] K. Rajagopal and F. Wilczek, in *At the Frontier of Particle Physics* (World Scientific), ed. M. Shifman, **3**, 2061 (2000).
[280] R. Rapp, T. Schafer, E. V. Shuryak, and M. Velkovsky, Phys. Rev. Lett. **81**, 53 (1998).
[281] N. Read and D. Green, Phys. Rev. B **61**, 10267 (2000).
[282] S. Reddy, M. Sadzikowski, and M. Tachibana, Nucl. Phys. A **714**, 337 (2003).
[283] H.-c. Ren, arXiv:hep-ph/0404074.
[284] B. Roy, Phys. Rev. B **85**, 165453 (2012).
[285] B. Roy and P. Goswami, arXiv:1303.2998 [cond-mat.mes-hall].
[286] V. A. Rubakov, Nucl. Phys. B **203**, 311 (1982).
[287] C. A. R. Sa de Melo, M. Randeria, and J. R. Engelbrecht, Phys. Rev. Lett. **71**, 3202 (1993).

[288] B. Sacepe, C. Chapelier, C. Marcenat, J. Kacmarcik, T. Klein, M. Bernard, and E. Bustarret, Phys. Rev. Lett. **96**, 097006 (2006).
[289] M. Sadzikowski and M. Tachibana, Phys. Rev. D **66**, 045024 (2002).
[290] M. M. Salomaa and G. E. Volovik, Phys. Rev. Lett. **55**, 1184 (1985).
[291] M. M. Salomaa and G. E. Volovik, Rev. Mod. Phys. **59**, 533 (1987).
[292] L. Santos, T. Neupert, C. Chamon, and C. Mudry, Phys. Rev. B **81**, 184502 (2010).
[293] L. Santos, S. Ryu, C. Chamon, and C. Mudry, Phys. Rev. B **82**, 165101 (2010).
[294] T. Sasaki, N. Yasutake, M. Kohno, H. Kouno, and M. Yahiro, arXiv:1307.0681 [hep-ph].
[295] M. Sato, Phys. Lett. B **575**, 126 (2003).
[296] M. Sato, Y. Takahashi, and S. Fujimoto, Phys. Rev. Lett. **103**, 020401 (2009).
[297] M. Sato and S. Yahikozawa, Nucl. Phys. B **436**, 100 (1995).
[298] J. D. Sau, R. M. Lutchyn, S. Tewari, and S. Das Sarma, Phys. Rev. Lett. **104**, 040502 (2010).
[299] J. D. Sau, R. M. Lutchyn, S. Tewari, and S. Das Sarma, Phys. Rev. B **82**, 094522 (2010).
[300] T. Schafer, Phys. Rev. Lett. **85**, 5531 (2000).
[301] T. Schafer, Nucl. Phys. B **575**, 269 (2000).
[302] T. Schafer, Phys. Rev. D **65**, 094033 (2002).
[303] T. Schafer, Phys. Rev. D **65**, 074006 (2002).
[304] T. Schafer, Phys. Rev. Lett., **96**, 012305 (2006).
[305] T. Schafer and F. Wilczek, Phys. Rev. Lett. **82**, 3956 (1999).
[306] A. Schmitt, Lect. Notes Phys. **811**, 1 (2010).
[307] A. P. Schnyder, S. Ryu, A. Furusaki, and A. W. W. Ludwig, Phys. Rev. B **78**, 195125 (2008).
[308] A. Sedrakian, PoS, **ConfinementX**, 251 (2012).
[309] D. M. Sedrakian, K. M. Shahabasyan, D. Blaschke, and K. M. Shahabasyan, Astrophys. **51**, 544 (2008).
[310] N. Seiberg and E. Witten, Nucl. Phys. B **426**, 19 (1994).
[311] N. Seiberg and E. Witten, Nucl. Phys. B **431**, 484 (1994).
[312] G. W. Semenoff and F. Zhou, Phys. Rev. Lett. **98**, 100401 (2007).
[313] R. Sensarma, M. Randeria, and T. L. Ho, Phys. Rev. Lett. **96**, 090403 (2006).
[314] K. Seo, M. Okawa, and A. Sugamoto, Phys. Rev. D **19**, 3744 (1979).
[315] M. K. Shahabasyan, Astrophys. **52**, 151 (2009).
[316] S. L. Shapiro and S. A. Teukolsky, *Black Holes, White Dwarfs and Neutron Stars: The Physics of Compact Objects* (Wiley, New York, 2008).
[317] M. Shifman and A. Yung, Phys. Rev. D **67**, 125007 (2003).
[318] M. Shifman and A. Yung, Phys. Rev. D **70**, 045004 (2004).
[319] M. Shifman and A. Yung, Rev. Mod. Phys. **79**, 1139 (2007).
[320] M. Shifman and A. Yung, *Supersymmetric Solitons* (Cambridge University Press, Cambridge, UK, 2009), Cambridge Monographs on Mathematical Physics.
[321] M. Shifman and A. Yung, Phys. Rev. D **66**, 045012 (2002).
[322] M. A. Shifman, Phys. Rev. D **59**, 021501 (1999).
[323] J. D. Shore, M. Huang, A. T. Dorsey, and J. P. Sethna, Phys. Rev. Lett. **62**, 3089 (1989).
[324] E. Shuryak, Prog. Part. Nucl. Phys. **62**, 48 (2009).
[325] P. Sikivie, Phys. Rev. Lett. **48**, 1156 (1982).
[326] T. H. R. Skyrme, Proc. R. Soc. London A **260**, 127 (1961).
[327] T. H. R. Skyrme, Proc. R. Soc. London A **262**, 237 (1961).
[328] T. H. R. Skyrme, Nucl. Phys. **31**, 556 (1962).
[329] J. Smiseth, E. Smorgrav, E. Babaev, and A. Sudbo, Phys. Rev. B **71**, 214509 (2005).
[330] D. T. Son, arXiv:hep-ph/0108260.
[331] D. T. Son, arXiv:hep-ph/0204199.
[332] D. T. Son and M. A. Stephanov, Phys. Rev. D **77**, 014021 (2008).
[333] D. T. Son and M. A. Stephanov, Phys. Rev. D **61**, 074012 (2000).
[334] D. T. Son and M. A. Stephanov, Phys. Rev. D **62**, 059902 (2000).
[335] D. T. Son, M. A. Stephanov, and A. R. Zhitnitsky, Phys. Rev. Lett. **86**, 3955 (2001).
[336] D. T. Son, M. A. Stephanov, and A. R. Zhitnitsky, Phys. Lett. B **510**, 167 (2001).
[337] D. T. Son and A. R. Zhitnitsky, Phys. Rev. D **70**, 074018 (2004).
[338] E. B. Sonin, Rev. Mod. Phys. **59**, 87 (1987).
[339] A. Stern, F. von Oppen, and E. Mariani, Phys. Rev. B **70**, 205338 (2004).

[340] H. Suganuma, S. Sasaki, and H. Toki, Nucl. Phys. B **435**, 207 (1995).
[341] T. Takatsuka and R. Tamagaki, Prog. Theor. Phys. Suppl. **112**, 27 (1993).
[342] H. Takeuchi and M. Tsubota, J. Phys. Soc. Jpn. **75**, 063601 (2006).
[343] Y. Tanaka, Phys. Rev. Lett. **88**, 017002 (2001).
[344] Y. Tanaka, J. Phys. Soc. Jpn. **70**, 2844 (2001).
[345] Y. Tanaka, T. Yokoyama, and N. Nagaosa, Phys. Rev. Lett. **103**, 107002 (2009).
[346] G. Taranto, M. Baldo, and G. F. Burgio, Phys. Rev. C **87**, 045803 (2013).
[347] J. C. Y. Teo and C. L. Kane, Phys. Rev. Lett. **104**, 046401 (2010).
[348] S. Tewari, S. Das Sarma, and D.-H. Lee, Phys. Rev. Lett. **99**, 037001 (2007).
[349] D. Tong, arXiv:hep-th/0509216.
[350] D. Tong, Ann. Phys. (N.Y.) **324**, 30 (2009).
[351] M. Tsubota, J. Phys.: Condens. Matter **21**, 164207 (2009).
[352] M. Tsubota, K. Kasamatsu, and M. Kobayashi, *Quantized Vortices in Superfluid Helium and Atomic Bose–Einstein Condensates* (Oxford University Press, Oxford, UK, 2013), Vol. 1 of *Novel Superfluids*.
[353] M. Tsubota, M. Kobayashi, and H. Takeuchi, Phys. Rept. **522**, 191 (2013).
[354] M. Ueda, *Fundamentals and New Frontiers of Bose–Einstein Condensation* (World Scientific, Singapore, 2010).
[355] A. Vilenkin and E. P. S. Shellard, *Cosmic Strings and other Topological Defects* (Cambridge University Press, Cambridge, UK, 2000).
[356] W. Vinci, M. Cipriani, and M. Nitta, Phys. Rev. D **86**, 085018 (2012).
[357] W. F. Vinen and R. J. Donnelly, Phys. Today **60**, 43 (2007).
[358] M. B. Voloshin, Yad. Fiz. **42**, 1017 (1985).
[359] G. E. Volovik, JETP Lett. **90**, 587 (2009).
[360] G. E. Volovik and O. D. Lavrentovich, Zh. Eksp. Teor. Fiz. **85**, 1997 (1983).
[361] G. E. Volovik, *The Universe in a Helium Droplet* (Oxford University Press, Oxford, UK, 2009), Vol. 117.
[362] M. Wakamatsu, arXiv:1108.1236 [hep-ph].
[363] H. Watanabe and H. Murayama, Phys. Rev. Lett. **108**, 251602 (2012).
[364] H. Watanabe and H. Murayama, Phys. Rev. Lett. **110**, 181601 (2013).
[365] E. J. Weinberg, Phys. Rev. D **24**, 2669 (1981).
[366] S. Weinberg, Phys. Rev. Lett. **40**, 223 (1978).
[367] S. Weissenborn, D. Chatterjee, and J. Schaffner-Bielich, Phys. Rev. C **85**, 065802 (2012).
[368] F. Wilczek, Phys. Rev. Lett. **40**, 279 (1978).
[369] F. Wilczek, Nature Phys. **5**, 614 (2009).
[370] E. Witten, Nucl. Phys. B **149**, 285 (1979).
[371] E. Witten, Nucl. Phys. B **249**, 557 (1985).
[372] E. Witten, Conf. Proc. **C861214**, 606 (1986).
[373] E. Witten, Phys. Rev. Lett. **81**, 2862 (1998).
[374] N. Yamamoto, J. High Energy Phys. **12**, 060 (2008).
[375] N. Yamamoto and T. Kanazawa, Phys. Rev. Lett. **103**, 032001(2009).
[376] N. Yamamoto, M. Tachibana, T. Hatsuda, and G. Baym, Phys. Rev. D **76**, 074001 (2007).
[377] S. Yasui, Y. Hirono, K. Itakura, and M. Nitta, Phys. Rev. E **87**, 052142 (2013).
[378] S. Yasui, K. Itakura, and M. Nitta, Phys. Rev. D **81**, 105003 (2010).
[379] S. Yasui, K. Itakura, and M. Nitta, Phys. Rev. B **83**, 134518 (2011).
[380] S. Yasui, K. Itakura, and M. Nitta, Nucl. Phys. B **859**, 261 (2012).
[381] N. Yasutake and K. Kashiwa, Phys. Rev. D **79**, 043012 (2009).
[382] N. Yasutake, T. Noda, H. Sotani, T. Maruyama, and T. Tatsumi arXiv:1208.0427 [astro-ph.HE].
[383] R. Yoshii, S. Tsuchiya, G. Marmorini, and M. Nitta, Phys. Rev. B **84**, 024503 (2011).
[384] A. B. Zamolodchikov and A. B. Zamolodchikov, Ann. Phys. (N.Y.) **120**, 253 (1979).
[385] A. B. Zamolodchikov and A. B. Zamolodchikov, Nucl. Phys. B **379**, 602 (1992).
[386] X. Zhang, T. Huang, and R. H. Brandenberger, Phys. Rev. D **58**, 027702 (1998).
[387] A. Zichichi, Proc. EPS Int. Conf. High-Energy Physics, p. 1 (1976).
[388] W. H. Zurek, Nature, **317**, 505 (1985).
[389] W. H. Zurek, Phys. Rept. **276**, 177 (1996).
[390] M. W. Zwierlein, J. R. Abo-Shaeer, A. Schirotzek, C. H. Schunck, and W. Ketterle, Nature **435**, 1047 (2005).